Normal cycle models for deformation analysis

Pierre Roussillon

▶ **To cite this version:**

Pierre Roussillon. Normal cycle models for deformation analysis. Discrete Mathematics [cs.DM]. Université Sorbonne Paris Cité, 2017. English. NNT : 2017USPCB073 . tel-02180601

HAL Id: tel-02180601

https://theses.hal.science/tel-02180601v1

Submitted on 11 Jul 2019

HAL is a multi-disciplinary open access archive for the deposit and dissemination of scientific research documents, whether they are published or not. The documents may come from teaching and research institutions in France or abroad, or from public or private research centers.

L'archive ouverte pluridisciplinaire **HAL**, est destinée au dépôt et à la diffusion de documents scientifiques de niveau recherche, publiés ou non, émanant des établissements d'enseignement et de recherche français ou étrangers, des laboratoires publics ou privés.

Université Paris Descartes
Laboratoire MAP5 UMR CNRS 8145
École doctorale 386 : Sciences Mathématiques de Paris Centre

Thèse de doctorat

Présentée par

Pierre Roussillon

Pour obtenir le grade de

Docteur de l'Université Paris Descartes
Spécialité : Mathématiques appliquées

Modèle de Cycles Normaux pour l'Analyse des Déformations

soutenue le 24 novembre 2017 devant le jury composé de :

Julie Delon	Université Paris Descartes	Directrice de thèse
Stanley Durrleman	INRIA	Examinateur
Joan Alexis Glaunès	Université Paris Descartes	Directeur de thèse
Sarang Joshi	University of Utah	Rapporteur
Simon Masnou	Université Lyon 1	Examinateur
Boris Thibert	Université Grenoble Alpes	Rapporteur
Alain Trouvé	ENS Paris-Saclay	Examinateur

RÉSUMÉ

Dans cette thèse, nous développons un modèle du second ordre pour la représentation des formes (courbes et surfaces) grâce à la théorie des cycles normaux. Le cycle normal d'une forme est le courant associé à son fibré normal. En introduisant des métriques à noyaux sur les cycles normaux, nous obtenons une mesure de dissimilarité entre formes qui prend en compte leurs courbures. Cette mesure est ensuite utilisée comme terme d'attache aux données dans une optique d'appariement et d'analyse de formes par les déformations.

Le chapitre 1 est une revue du domaine de l'analyse de formes par les déformations. Nous insistons plus particulièrement sur la mise en place théorique et numérique du modèle de Large Deformation Diffeomorphic Metric Mapping (LDDMM).

Le chapitre 2 se concentre sur la représentation des formes par les cycles normaux dans un cadre unifié qui englobe à la fois les formes continues et discrètes. Nous précisons dans quelle mesure cette représentation contient des informations de courbure. Enfin nous montrons le lien entre le cycle normal d'une forme et son varifold.

Dans le chapitre 3, nous introduisons les métriques à noyaux. Ainsi, nous pouvons considérer les cycles normaux dans un espace de Hilbert avec un produit scalaire explicite. Nous détaillons ce produit scalaire dans le cas des courbes et surfaces discrètes avec certains noyaux, ainsi que le gradient associé. Nous montrons enfin que malgré le choix de noyaux simples, nous ne perdons pas toutes les informations de courbures.

Le chapitre 4 utilise cette nouvelle métrique comme terme d'attache aux données dans le cadre LDDMM. Nous présentons de nombreux appariements et estimations de formes moyennes avec des courbes ou des surfaces. L'objectif de ce chapitre est d'illustrer les différentes propriétés des cycles normaux pour l'analyse des déformations sur des exemples synthétiques et réels.

ABSTRACT

In this thesis, we develop a second order model for the representation of shapes (curves or surfaces) using the theory of normal cycles. The normal cycle of a shape is the current associated with its normal bundle. Introducing kernel metrics on normal cycles, we obtain a dissimilarity measure between shapes which takes into account curvature. This measure is used as a data attachment term for a purpose of registration and shape analysis by deformations.

Chapter 1 is a review of the field of shape analysis. We focus on the setting of the theoretical and numerical model of the Large Deformation Diffeomorphic Metric Mapping (LDDMM).

Chapter 2 focuses on the representation of shapes with normal cycles in a unified framework that encompasses both the continuous and the discrete shapes. We specify to what extend this representation encodes curvature information. Finally, we show the link between the normal cycle of a shape and its varifold.

In Chapter 3, we introduce the kernel metrics, so that we can consider normal cycles in a Hilbert space with an explicit scalar product. We detail this scalar product for discrete curves and surfaces with some kernels, as well as the associated gradient. We show that even with simple kernels, we do not get rid of all the curvature informations.

The Chapter 4 introduce this new metric as a data attachment term in the framework of LDDMM. We present numerous registrations and mean shape estimation for curves and surfaces. The aim of this chapter is to illustrate the different properties of normal cycles for the deformations analysis on synthetic and real examples.

Remerciements

Bien sûr, mes premiers remerciements vont à mes encadrants, Joan Glaunès et Julie Delon. Joan, merci de m'avoir reçu un mois de janvier 2014 alors que tu ne me connaissais pas, et d'avoir pris le temps de discuter longuement d'un choix de sujet de thèse qui me plairait. Cela est, je pense, caractéristique de ta gentillesse et ça a été le début de trois belles années. Ta disponibilité et ton recul scientifique ont été très précieux durant cette thèse. Julie, merci d'avoir bien voulu m'encadrer. C'était un plaisir de t'avoir comme directrice de thèse.

Je remercie chaleureusement Stanley Durrleman, Sarang Joshi, Simon Masnou, Boris Thibert et Alain Trouvé d'avoir accepté de faire partie de mon jury de thèse et plus particulièrement Boris et Sarang pour leur relecture attentive et les remarques pertinentes sur mon manuscrit.

Je ne saurai suffisamment remercier Alain Trouvé qui a accompagné mes années d'étudiant à l'ENS Cachan en tant que directeur bienveillant du département de mathématiques. Merci de m'avoir aidé avec patience lors de mes questionnements sur mon avenir et mon choix de thèse. Enfin, merci pour tout l'apport scientifique, que ce soit en M2 ou lors de mon parcours de doctorant.

Si je garde si peu de mauvais souvenirs de ma thèse, c'est en grande partie grâce au milieu professionnel qui m'a entouré lors de ces trois années (presque quatre maintenant). Merci aux directrices successives du MAP5 Annie Raoult et Fabienne Comte pour leur gestion du laboratoire et leur aide lors des divers déboires administratifs. Merci à Marie-Hélène pour son efficacité et sa bonne humeur communicative, ainsi qu'à Isabelle Valéro et Christophe Catellani. Enfin merci aux maitres de conférence et professeurs du MAP5 de participer activement à la vie du laboratoire. Une pensée particulière pour Lionel et Bruno, qui après avoir encadré mon stage de L3 ont été des collègues très présents lors de mes années à Descartes.

Cette dernière année a été marquée par mon retour à l'ENS Cachan, en tant qu'ATER. C'est un plaisir de revenir sur les lieux qui m'ont fait grandir en tant que mathématicien. Tout d'abord merci au personnel administratif de Cachan pour leur bel accueil. Je pense notamment à Delphine Laverge, Alina Müller et Virginie Pauchont. Merci aussi à Véronique, "copine de ma copine" et donc forcément extraordinaire !

Un grand merci à l'équipe pédagogique du département de mathématiques de Cachan pour ces années en tant que moniteur ou ATER. Merci à Marc Hindry et Thomas Alazard pour qui je donne des TD. Et bien sûr, un merci particulier à Claudine Picarony et Frédéric Pascal pour leur investissement sans faille dans le département et la confiance accordée en me permettant d'intervenir en prépa agreg. C'est pour moi une expérience très enrichissante. Enfin, cette année serait bien plus triste sans mes adorables collègues Sandrine, Loïc, Tuong-Huy et Arthur (que je suis depuis maintenant 4 ans, je m'inquièterais à sa place) . C'est une chance de pouvoir travailler et échanger avec vous.

Au cours de ces années de thèse, j'ai aussi pu profiter d'une communauté scientifique très active. Je garde un excellent souvenir de tous les “Shape Meeting”

qui ont rythmé mon parcours, que ce soit à Londres, Vienne, Munich ou Singapour. Un merci à Martin & Martins de nous avoir accueilli à Vienne. Je pense aussi à la "french team", Nicolas, Benjamin, Giacomo, Irène, Barbara, Sylvain, Jean, Loïc. Benjamin, merci de m'avoir fait découvrir ce merveilleux logiciel qu'est Paraview. Cela a grandement simplifié la fin de ma thèse ! Une pensée particulière pour Irène et Barbara qui ont été des joyeuses compagnes de route. Merci aussi à Jakob, Line et Alice d'avoir partagé cette école d'été à Singapour. Merci à Sergey de l'avoir organisé, et de nous avoir pris sous son aile pour nous faire découvrir toutes les spécialités culinaires de Singapour ! C'est souvent avec nostalgie que je repense à ces trois semaines.

Je ne sais pas ce qu'auraient été ces trois années de thèse sans l'ambiance unique qui règne au sein des doctorants de Descartes. En tant que désormais "vieux" du laboratoire, j'ai eu la chance de connaitre plusieurs promos. Je commence donc par mes "vieux" à moi, merci à Rémy, Charlotte D., Charlotte L., Christèle, Fanny, Gwennaëlle, Laurent, Loïc, Arthur, Anne-Sophie (ça te fera plaisir d'apparaître ici, j'en suis sûr) et Jean pour mes premières années. L'intégration fut rapide à force de GTTJD, pauses café, et soirées. Et que dire des 10 ans du MAP5 ! Rémy, tu nous a montré à tous qu'avec un peu (beaucoup) d'organisation, on pouvait mener de front une paternité biologique et une paternité scientifique. Charlotte, ton mariage aura rythmé la presque dernière ligne droite de ma rédaction ! Je profite de l'évocation de ce mariage pour remercier aussi Claire et Fabrice.

Merci ensuite aux "aussi vieux que moi": Julie, Alkéos et son talent déroutant pour créer des débats à partir de tout et de rien. Courage à vous deux pour finir votre rédaction ! Maud, merci d'avoir partagé cette dernière année ma passion pour l'administration de l'éducation nationale (ainsi que les stages Maths C2+ !). Enfin, la relève semble bien partie, merci à Andrea, Fabien, Ismaël, Léo, Vivien, Warith...

Bien sûr, je ne pouvais pas finir cette partie sur Descartes sans parler du fameux bureau 725-C1. Malgré les départs et les arrivées, je n'y ai toujours trouvé que des amis. Merci encore une fois à Rémy, Ronan, Fanny, Angelina. Merci à Alexandre, Mélina (et son goût étrange pour les piscines extérieures lointaines), Antoine (malgré sa présence parcimonieuse), Cambyse (enfin quelqu'un qui aime le foot !), Jean-Marc (rattaché au bureau 725-C1 et solide acolyte des Friday beer), Noura qui nous manque à tous depuis son départ pour la Nouvelle-Orléans et Valentin (promis, après la soutenance j'aurai le temps pour une soirée foot !). Enfin une pensée pour Edoardo, dont le passage à Descartes fut bref mais intense. Bon courage pour ta nouvelle vie à Bordeaux !

Toujours dans ce bureau 725-C1 qui est décidément une véritable mine d'or, je souhaiterai remercier Alasdair, Claire et Vincent, véritables amis qui ont largement contribué à rendre mes dernières années de thèse heureuses. Merci à Sonia, coach de ma deuxième année. C'était un plaisir de t'avoir dans ce bureau ! Enfin, merci à Anne-Sophie, avec qui j'ai grandi en thèse. Merci pour ton soutien moral précieux, ton dynamisme à toute épreuve et ta bonne humeur (presque aussi légendaire que ta mauvaise humeur !). Courage, tu es la prochaine à soutenir ! Et bien sûr, un grand merci à Arthur, mentor scientifique mais avant tout humain de ces années

cartésiennes. Faire une thèse est tout de suite plus simple entouré de personne comme toi. On peut dire sans hésiter que tu nous as rendu la pareille.

Je remercie aussi les amis que j'ai connu par Anaïs, je pense à Étienne, et bien évidemment à Adrien, Agnès, Laura et Pablo. Merci aussi à Léonard et Chloé et leurs soirées jeux (même si je ne vous remercie pas d'avoir initié Anaïs aux chats). Enfin merci à Laura, pour une année d'agrégation riche en émotions et pour son accueil en Guadeloupe !

Puisque j'avais une vie avant la thèse, je remercie mes amis cachanais, membres de la coloc' ou de la coloc++ et qui ont rendu ces années d'ENS si joyeuses. Merci à Chris (l'hyperactif futur papa, courage pour la suite !), Keurcien (compagnon de galère, ou plutôt de Prius, pour le MSV), Matthieu (et les vacances à Cerbère !), Maxime (et les vacances en Alsace !), Romain et Melwenn (et les vacances à Estrablin !), Thibaud (expert en Thibauds), William (et les vacances à Trouville !). Bien sûr, ces quelques lignes ne suffisent pas pour exprimer tout ce que l'on a vécu. Un merci particulier pour William, et les soirées foot, concerts, spectacles, cinés, manifs ou simplement kebab/FIFA. L'air de rien, tout ça aide à passer les moments difficiles de thèse.

La prépa au Lycée du Parc a aussi été riche en émotions et en amitiés. Merci à Alexandre, Alexis, Anis, Aude (dont le mariage approche !), Coralie, Charles, Sulivan. Merci aussi à Thomas, et sa discrétion légendaire qui aura marqué mes années de sup, spé et ENS. Et évidemment merci à Lucas, coloc hyperactif pendant 2 ans, qui a visiblement décidé de s'éloigner un peu plus chaque année. Londres, New-York, Hong-Kong... Cela me permet au moins de voyager !

Merci aussi à mes amis du lycée, que je prends plaisir à retrouver régulièrement à Lyon : merci Daniel, Éric, Farid (et Maud). Bientôt le road trip aux Etats-Unis, hein ? Farid, ça fait maintenant 16 ans (!!) qu'on se connait !

Merci ensuite à la famille, et tout d'abord la belle-famille. Merci à Odile et Yves de m'avoir si bien accueilli, que ça soit à Rethel, Bordeaux, voire en Indonésie ! Merci d'avoir été des hôtes si attentionnés lors de la dernière ligne droite, que ce soit en mai, juin ou juillet. Cela a été d'une grande aide pour finir la rédaction.

Merci à ma famille, Denis, Sylvette, Roland (dont j'ai grandement recopié le parcours scolaire), mes cousins Yohan, Joana et Mathias avec qui les vacances au ski étaient toujours un moment à part. Merci à mes grands parents, Monique, Maurice et Raymonde pour leur gentillesse tout au long de ma vie. Merci d'être venu jusqu'ici pour assister à ma soutenance. J'espère au moins que vous comprendrez mes travaux ! Bien évidemment merci à mon frère, Benjamin et à mes parents, Éric et Laurence pour leur soutient sans faille et tous ces moments partagés, en vacances ou dans la vie de tous les jours. C'est grâce à vous si j'en suis ici aujourd'hui.

Je finis par Anaïs, évidemment. Tu sais déjà tout ce que je pense de toi, mais je tenais à te remercier d'avoir rendu ces années de thèse si facile grâce à ta bonne humeur constante et ton dynamisme enjoué. Plus qu'une semaine avant la vie de docteurs !

Contents

Notations

- E^* is the algebraic dual of the vector space E, i.e. the vector space of all the linear forms on E. If E is endowed with a topology, E' is the topological dual of E, i.e. the vector space of all the *continuous* linear forms on E.
- $\langle .,. \rangle$ is the canonical scalar product on a Euclidean space E. $|.|$ is the associated norm.
- $\langle | \rangle : E' \times E \to \mathbb{R}$ is the duality product. If $(\varphi, x) \in E' \times E$, $\langle \varphi | x \rangle := \varphi(x)$.
- $S^{d-1} = \Big\{ x \in \mathbb{R}^d \;\Big|\; |x| = 1 \Big\}$, the unit sphere of $\mathbb{R}^d$.
- $\langle .,. \rangle_V$, $\|.\|_V$: Given a Hilbert space V, $\langle .,. \rangle_V$ is its scalar product and $\|.\|_V$ its norm.
- $\mathcal{K}_V : V' \to V$ is the canonical isometry between V' and V. If $(\varphi, v) \in V' \times V$, $\langle \varphi | v \rangle = \langle \mathcal{K}_V \varphi, v \rangle_V$.
- $E \hookrightarrow F$. If E and F are two normed vector space, $E \hookrightarrow F$ means that E is continuously embedded in F, i.e. that there exists a continuous injection from E to F.
- $L^2_V = \Big\{ (v_t)_{0 \leq t \leq 1} \in V^{[0,1]} \;\Big|\; \int_0^1 \|v_t\|_V^2 \, dt < +\infty \Big\}$.
- $H^s(S^{d-1})$ is the s-Sobolev space of S^{d-1}.
- $Y_{l,m}$ is the spherical harmonic of order (l, m) (see Appendix B).
- $\|\|_\infty$ is the infinity norm. If $f \in L^\infty(\mathbb{R}^d)$, $\|f\|_\infty = \sup_{x \in \mathbb{R}^d} |f(x)|$.
- $\Lambda_m(\mathbb{R}^d)$ is the space of m-covectors or m-forms of $\mathbb{R}^d$, $\Lambda^m(\mathbb{R}^d) = \Lambda_m(\mathbb{R}^d)^*$ is the space of m-vectors of $\mathbb{R}^d$ (see section 2.1).
- $\mathcal{L}(\mathbb{R}^d)$ is the space of linear applications of $\mathbb{R}^d$.
- $\mathscr{H}^m_S$ is the m-dimensional Hausdorff measure of the space S (in this manuscript, S will be $\mathbb{R}^d$ or $\mathbb{R}^d \times S^{d-1}$ and we will denote $\mathscr{H}^m$ instead of $\mathscr{H}^m_S$ since there will be no ambiguity.)
- $\Omega^m(\mathbb{R}^d) = \mathscr{C}^\infty\big(\mathbb{R}^d, \Lambda^m(\mathbb{R}^d)\big)$ is the space of smooth, m-differential forms of $\mathbb{R}^d$.

- $\Omega^m_{k,0}(\mathbb{R}^d) = \mathscr{C}^k_0\big(\mathbb{R}^d, \Lambda^m(\mathbb{R}^d)\big)$ is the space of $\mathscr{C}^k$ m-differential forms of $\mathbb{R}^d$, vanishing at infinity, as well as the derivative up to order k.
- $\Omega^m_0(\mathbb{R}^d \times S^{d-1}) = \mathscr{C}^k_0\big(\mathbb{R}^d \times S^{d-1}, \Lambda^m(\mathbb{R}^d \times \mathbb{R}^d)\big)$ is the space of $\mathscr{C}^k$ m-differential forms of $\mathbb{R}^d \times S^{d-1}$, vanishing at infinity, as well as the derivative up to order k.
- X_ε. Given a set X in $\mathbb{R}^d$, $X_\varepsilon = \big\{x \in \mathbb{R}^d | d(x, X) \leq \varepsilon\big\}$.
- ∂X is the boundary of X. With these notations, $\partial X_\varepsilon = \big\{x \in \mathbb{R}^d | d(x, X) = \varepsilon\big\}$.
- P_X is the projection on X (when it is well defined).
- $T_x X$ is the tangent cone of X at point $x \in X$. See definition 2.33.
- $\mathrm{Nor}(X, x)$ is the normal cone of X at point x. See definition 2.33
- $\mathrm{Nor}^u(x, X)$ is the unitary normal cone, i.e. $\mathrm{Nor}^u(x, X) = \mathrm{Nor}(X, x) \cap S^{d-1}$. See definition 2.33.
- $\mathcal{N}_X$ is the unit normal bundle of X. Given a set X with positive reach, $\mathcal{N}_X := \Big\{(x, n) \mid x \in X, n \in \mathrm{Nor}^u(X, x)\Big\}$. This is a subset of $\mathbb{R}^d \times S^{d-1}$. $\mathcal{N}^{pln}_X, \mathcal{N}^{cyl}_X, \mathcal{N}^{sph}_X$ are respectively the planar, the cylindrical and the spherical part of the unit normal bundle.
- $\tau_X(x)$. If X is an oriented m-rectifiable set of $\mathbb{R}^d$, and $(e_1(x), \ldots, e_m(x))$ a positively oriented orthonormal basis of $T_x X$, then $\tau_X(x) = e_1(x) \wedge \cdots \wedge e_m(x)$ is the m-vector associated with the orthonormal basis.
- $\tau_{\mathcal{N}_X}(x, n)$ is the $(d-1)$-vector associated with a positively oriented, orthonormal basis of $T_{(x,n))}\mathcal{N}_X$.
- $k_i(x, n)$, for $1 \leq i \leq d$ is the *i-th generalized curvature* at x and in the direction n of a set X with positive reach. See subsection 2.4.2
- $[X]$ is the current associated with a rectifiable set X.
- μ_X is the varifold associated with a rectifiable set X.
- $N(X) = [\mathcal{N}_X]$ is the normal cycle associated with a set X with positive reach.

Introduction

This thesis takes place in the context of computational anatomy, an active research field which models and studies the biological variability of the human anatomy. Computational anatomy draws its inspiration from the pioneer work of the biologist D'Arcy Thompson [Thompson, 1917]. At that time, Darwin's theory of evolution was widely accepted in the scientific community. For D'Arcy Thompson, the biologists of the twentieth century were focused on genetic evolution and underestimated the role of physical constraints in the morphogenesis (the process by which patterns are formed). According to him, the observed variability in the inter-species anatomy is not only the result of a purely random process but also accounts for mechanical constraints. Those can be modelled as geometrical transformations that explain the variability across the species (see figure 1). The term "computational anatomy" was first introduced by Grenander and Miller [Grenander and Miller, 1998] and aims at providing a mathematical framework to study the variability of anatomical structures among a population of subjects.

There has been a growing interest in computational anatomy in the past decades: the recent development of acquisition techniques (among which Magnetic Resonance Imaging, coherence tomography, Diffusion-Tensor Imaging, Functional MRI) enables the imaging of new anatomical structures. Also, the ever-increasing accessibility of these devices leads to a growing number of individuals for each structure and allows for a mapping of the shapes' variability that is almost representative of the population. From there, it may be possible to indicate anatomical abnormalities and this opens the way to an early diagnosis of diseases that cause or are caused by unexpected deformations. A qualitative approach is not anymore sufficient and one necessitates an automatized procedure for an analysis that fully exploits the size of the database. This automation implies a quantitative approach, and thus a mathematical modelling of shape variability and how to measure it.

This problematic is at the heart of computational anatomy. Formally, one estimates from a "healthy" dataset a statistical model of the shapes' variability. From there, it is possible to provide statistical tests to discriminate between a pathological and a normal shape variation. Of course, this is a very large and complex problem. From a mathematical point of view, the measure of shapes variability necessitates a framework that provides theoretical and numerical guarantees. From a medical point of view, the relevance and the interpretation of such applications need to be evaluated depending on the anatomical structure at stake. Yet, numerous studies has shown promising results. Let us quote for example works on Alzeihmer's dis-

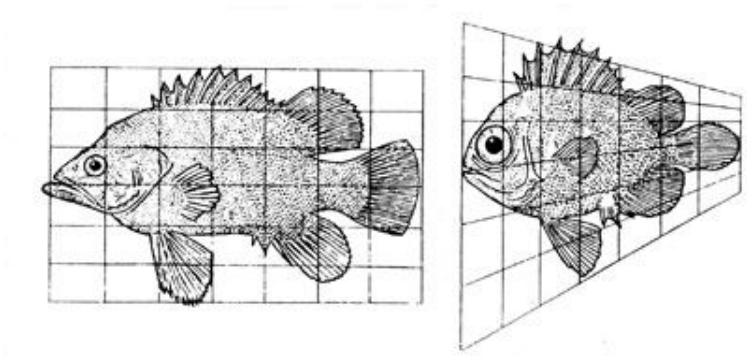

Fig. 150. *Polyprion.*

Fig. 151. *Pseudopriacanthus altus.*

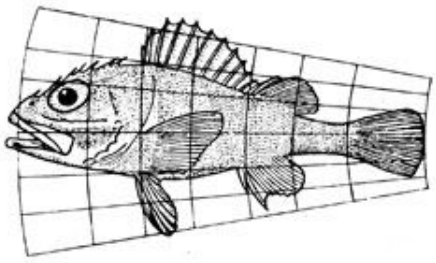

Fig. 152. *Scorpaena* sp.

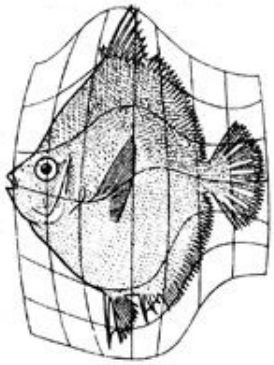

Fig. 153. *Antigonia capros.*

Figure 1: From D'Arcy Thompson's work. The variability of a fishes population is explained through geometrical transformations of the ambient space. The transformation is represented via the deformed grid.

ease [Qiu et al., 2008, Wang et al., 2007, Tang et al., 2014, Csernansky et al., 2004, Csernansky et al., 2005], on DTI images [Durrleman et al., 2011a, Pennec, 2006, Helm et al., 2006], heart malformations [Mansi et al., 2011], Down syndrom [Durrleman et al., 2014, Durrleman et al., 2013] and retina layer for glaucoma diagnosis [Charlier et al., 2015a, Lee et al., 2017a, Lee et al., 2017b].

Shape Analysis through Large deformations

In its original formulation, computational anatomy is "a generative model of shape and form from exemplars acted upon via transformations" [Grenander and Miller, 1998]. In other words, we model a generative shape that contains all the shared features of the dataset. This shape is often called the template or the mean shape of the dataset. The observed variability is then explained as the result of "random" deformations of the template. The statistical analysis of a database is performed through the estimation of the mean shape, jointly with the deformations that generate the database from the template.

The transition from this rather abstract idea to a mathematical formulation relies on the construction of geometrical transformations that account for the shapes variability. In this manuscript, we use more specifically the previous works of Large Deformations Diffeomorphic Metric Mapping that we will write LDDMM ([Trouvé, 1995, Christensen et al., 1996, Dupuis et al., 1998, Trouvé, 1998] for the seminal articles, [Younès, 2010] for a summary of the concepts). In this framework, the deformations are generated through the integration of time-varying vector fields of $\mathbb{R}^d$, $(v_t)_{0\leq 1\leq t}$. This concept is close to fluid mechanics where we follow the path of a given particle, initially at position $x \in \mathbb{R}^d$ and evolving through a velocity field $(v_t)_{0\leq t\leq 1}$. The position at time t of the particle is denoted $\varphi_t^v(x)$, and the path is given by the following equation:

$$\forall x \in \mathbb{R}^d,\ \forall t \in [0,1],\ \frac{\partial \varphi_t^v(x)}{\partial t} = v_t \circ \varphi_t^v(x) \tag{1}$$

with $\varphi_0^v = \mathrm{Id}_{\mathbb{R}^d}$. The final deformation, φ_1^v is obtained with the integration at time $t = 1$ of the previous differential equation. To ensure the regularity of the final deformation, we need to assume some spatial regularity on the vector fields v_t. In fact, we will chose the vector fields as elements of a Hilbert space V such that we have the *admissibility* property: $V \hookrightarrow \mathscr{C}_0^1(\mathbb{R}^d, \mathbb{R}^d)$. This embedding property guarantees that the final deformation is a diffeomorphism ([Trouvé, 1995, Dupuis et al., 1998]), and that the Hilbert space V is in fact a Reproducing Kernel Hilbert Space of vector fields ([Glaunès, 2005]). The theory of RKHS is recalled in the beginning of Chapter 3. The appearance of a RKHS is good news, since it will simplify the numerical implementations through the associated kernel K_V. V is endowed with a norm $\|.\|_V$ that represents the infinitesimal cost of displacement, and we consider deformation with finite energy, i.e. with velocity field in L^2: $\int_0^1 \|v_t\|_V^2\, dt < +\infty$. The space of time-varying vector fields in V with finite energy is denoted L_V^2. This means that the set of deformations that we consider is exactly $G_V := \left\{ \varphi_1^v \;\middle|\; v \in \right.$

$L^2_V\Big\}$ where φ_1^v is obtained through integration of (1). It can be shown that this is a (sub-)Riemannian manifold with geodesic distance between the identity and a deformation $\varphi \in G_V$:

$$d_{G_V}(\mathrm{Id}, \varphi)^2 := \inf_{\substack{v \in L^2_V \\ \varphi_1^v = \varphi}} \int_0^1 \|v_t\|_V^2 \, dt.$$

that we extend to a right-invariant metric on all G_V:

$$d_{G_V}(\varphi_1, \varphi_2)^2 := d(\mathrm{Id}, \varphi_2 \circ \varphi_1^{-1})^2 = \inf_{\substack{v \in L^2_V \\ \varphi_1^v \circ \varphi_1 = \varphi_2}} \int_0^1 \|v_t\|_V^2 \, dt.$$

(see [Arguillère et al., 2015] for more details). The Riemannian framework is especially well adapted for a statistical analysis ([Pennec, 2006]).

An elementary block for shape analysis is the problem of shapes registration: given two shapes C and S, find a physically relevant optimal deformation φ that matches the two shapes. This problem is also interesting for itself since many applications in medical image analysis require a coherent alignment of images as a pre-processing step, using efficient rigid or non-rigid registration algorithms. If we fit this problem in the previous Riemannian framework, this writes:

$$\arg \min_{\substack{\varphi \in G_V \\ \varphi(C) = S}} d(\mathrm{Id}, \varphi)^2 = \arg \min_{\substack{v \in L^2_V \\ \varphi_1^v(C) = S}} \int_0^1 \|v_t\|_V^2 \, dt$$

where φ_1^v is obtained through equation (1).

For applicative purpose, one does not want to perform an exact matching between shapes as this imposes too many constraints on the deformations and would make the procedure too sensitive to noise or artefacts. To relax this hypothesis, one needs a data-attachment term that measures the residual distance between the deformed shape and the target. In the following, we denote A this data attachment term. Non-rigid registration is then classically tackled down by minimizing a functional composed of two terms, one enforcing the regularity of the mapping (in our setting, the energy of the deformation $\int_0^1 \|v_t\|_V^2 \, dt$), and the data-attachment term which evaluates dissimilarity between shapes $A(\varphi(C), S)$.

The inexact registration problem between two shapes C and S then writes as the minimization of

$$\arg \min_{v \in L^2_V} \int_0^1 \|v_t\|_V^2 \, dt + A\big(\varphi(C), S\big). \tag{2}$$

that also writes:

$$\arg \min_{v \in L^2_V} d_{G_V}(\mathrm{Id}, \varphi_1^v)^2 + A\big(\varphi(C), S\big).$$

Defining good data-attachment terms is important, as it may improve the minimization process, and focus the registration on the important features of the shapes

to be matched. In the case of n landmarks (labelled points) in $\mathbb{R}^d$ (i.e. C and S are two sets of n points), a simple data attachment term is the Euclidean norm on $(\mathbb{R}^d)^n$: $A\big((x_1,\dots,x_n),(y_1,\dots,y_n)\big) = \sum_{i=1}^n \|x_i - y_i\|^2_{\mathbb{R}^d}$. In the case of images, the L^2 norm is the first idea: $A(I_1,I_2) = \int_\Omega \Big|I_1(x) - I_2(x)\Big|^2 dx$. At the beginning of computational anatomy, these were the main data-attachment terms (e.g. [Beg et al., 2005] for images, [Joshi and Miller, 2000] for landmarks). However, it restricts considerably the domain of applications since for landmarks it assumes points correspondence. This was a motivation for other data-attachment terms that we will see in the next section.

The design of an interesting dissimilarity measure between shapes is closely linked to the question of shapes representation. This is of importance since it is the starting point to the embedding of shapes in a space endowed with a metric. Let us illustrate the problematic of shapes representation with a toy example: given a surface S, one can consider it as an unstructured set of points, or as a submanifold with a tangent space at each point. These two representations do not contain the same information about S: the former encodes only an "order 0" information, whereas the latter encodes a first-order information, i.e. a tangential information.

Geometric measure theory in computational anatomy

In the past decades, computational anatomy has greatly benefited from the use of *geometric measure theory*, where shapes representation (surfaces, curves, etc.) is central. The main motivation in this field is to provide a mathematical framework to consider variational problem involving surfaces. Let just mention for example the *Plateau's problem*: given a prescribed $(m-1)$-dimensional border Γ, does a minimizing area surface with border Γ exist? To answer (positively) to this problem, new theoretical tools were developed in order to consider surfaces as elements of a normed vector space, with nice properties such as compactness. *Integral currents* ([Federer and Fleming, 1960]) and *varifolds* ([Allard, 1972]) were introduced for this purpose. The space of m-dimensional currents is the topological dual of some space of m-differential forms, and an oriented submanifold S can be considered as a current, denoted $[S]$, through integration of differential forms over S:

$$[S](\omega) := \int_S \langle \omega(x) | \tau_S(x) \rangle \, d\mathscr{H}^m(x).$$

We recall that since S is an oriented submanifold, there exists a coherent orientation of orthonormal basis of the tangent space at each point $x \in S$. If $e_1(x),\dots,e_m(x)$ is such a basis, then $\tau_S(x) = e_1(x) \wedge \cdots \wedge e_m(x)$ is the m-vector canonically associated with this basis. It can be shown that this expression is independent of the choice of the positively oriented orthonormal basis.

We will consider in this manuscript the space of m-differential forms of $\mathbb{R}^d$ that vanish at infinity, and denote it $\Omega_0^m(\mathbb{R}^d)$. For the sake of simplicity, we will define

the space of m-currents in $\mathbb{R}^d$ as the topological dual of $\Omega_0^m(\mathbb{R}^d)$ endowed with the infinity norm. It is more restrictive than Federer's classical definition of currents, but it will be sufficient for our applications.

With this construction, m-submanifolds are embedded in a topological dual (which is a vector space) and it remains to define an interesting norm on this space. This has been extensively studied in [Federer and Fleming, 1960, Federer, 1969].

In [Vaillant and Glaunès, 2005, Glaunès, 2005] a new framework for dissimilarity measures between sub-manifolds was proposed using *kernel metrics* defined on spaces of currents. In this framework, shapes are elements of a dual Hilbert space W', with an explicit scalar product thanks to a scalar kernel k_p. If C and S are two m-dimensional, oriented shapes:

$$\langle [C], [S] \rangle_{W'} = \int_C \int_S k_p(x,y) \, \langle \tau_C(x), \tau_S(y) \rangle \, d\mathscr{H}^m(x) d\mathscr{H}^m(y). \tag{3}$$

and the dissimilarity measure d between two shapes is:

$$d(C,S)^2 := \|[C] - [S]\|^2_{W'} .$$

This setting is now commonly used in computational anatomy; its advantages lie in its simple implementation, its parametrization-free representation and the fact that it provides a common framework for continuous and discrete shapes (see [Durrleman, 2010] for a computational analysis of currents and their numerical implementation). However, currents are oriented objects and thus a consistent orientation of shapes is needed for a coherent matching. Moreover, due to this orientation property, artificial cancellation can occur with shapes with high local variations.

This can even be quantified, as illustrated in [Charon, 2013] and reproduced in figure 2: consider a closed, oriented rectangle, with length 1 and width ε. If we denote R_ε this rectangle, and $\|[R_\varepsilon]\|_{W'}$ the norm of the associated current, we have:

$$\|[R_\varepsilon]\|^2_{W'} = \int_{R_\varepsilon} k_p(x,y) \, \langle \tau_{R_\varepsilon}(x), \tau_{R_\varepsilon}(y) \rangle \, d\mathscr{H}^1(x) d\mathscr{H}^1(y).$$

The scalar product between the tangent vectors of the vertical and horizontal part vanishes. Moreover, if we suppose that the kernel k_p is translation-invariant, this gives:

$$\|[R_\varepsilon]\|^2_{W'} = 2\big(\|[C_{V_1}]\|^2_{W'} - 2 \langle [C_{V_1}], [C_{V_2}] \rangle_{W'} \big) + 2\big(\|[C_{H_1}]\|^2_{W'} - 2 \langle [C_{H_1}], [C_{H_2}] \rangle_{W'} \big)$$

where C_{V_1} and C_{V_2} are the two vertical segments and C_{H_1}, C_{H_2} the two horizontal ones. When $\varepsilon \to 0$, we have $\|[C_{H_1}]\| \to 0$ and $\langle [C_{H_1}], [C_{H_2}] \rangle_{W'} \to 0$ and $2 \langle [C_{V_1}], [C_{V_2}] \rangle_{W'} \to \|[C_{V_1}]\|^1_{W'}$ which proves that

$$\|[R_\varepsilon]\|_{W'} \underset{\varepsilon \to 0}{\longrightarrow} 0.$$

Thus the norm of the rectangle for the kernel metric vanishes whereas the associated shape is non negligible.

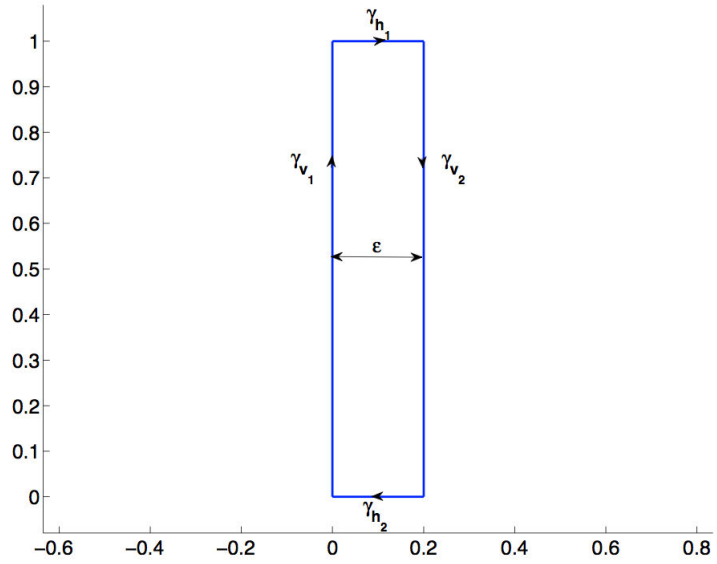

Figure 2: A closed oriented rectangle with length 1 and width ε. Due to the orientation, when $\varepsilon \to 0$, the norm for the kernel metric of the associated current goes to 0 whereas the limit geometrical object is a segment.

This cancellation effect due to orientation may induce poor behaviour for a registration purpose. If one uses the kernel metric on currents as a data attachment term, the registration may suffers from the cancellation effect, and we give two illustrations of problems that arise. In figure 3, we perform a registration between a blue circle and an orange circle with a spike (the target). We do not enter yet into the details of such procedure, but we provide the result of such registration, with the kernel metric on currents as data-attachment term. One can observe that the spike is not matched. This is due to the cancellation effect: the spatial frequency of the spike is high compared to the other part of the curve, and because of the orientation, this feature vanishes in the space of currents. Another phenomenon that may occur for the same reason is the "pinching" effect. In figure 4, we show this time a matching of a circle with a spike to a circle. The obtained registration is not satisfactory: with the metric on currents, it costs less to pinch the spike (so that it vanishes in the space of currents) rather than to stretch out the spike in order to match it well on the circle.

To deal with this problem, a more advanced model based on *varifolds* has been introduced recently [Charon, 2013]. Varifolds are measures over fields of non-oriented linear subspaces and will be reminded in Chapter 2. In this thesis, we propose to use a second-order model called *normal cycle* for defining shape dissimilarities.

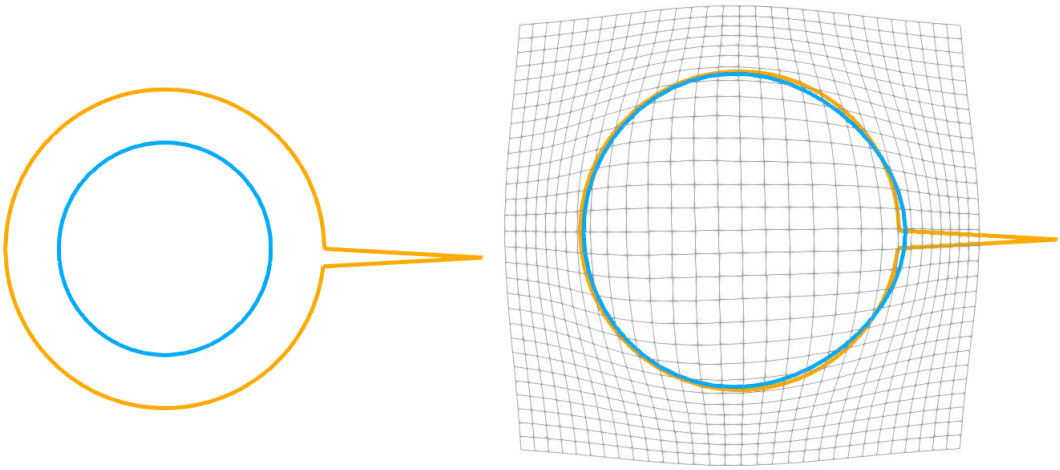

(a) Initial configuration

(b) Result of the registration with the deformation grid.

Figure 3: Registration of a blue circle to an orange circle with a spike with a kernel metric on current as dissimilarity measure. The spike is not matched since in the space of currents, this feature is negligible for the kernel metric.

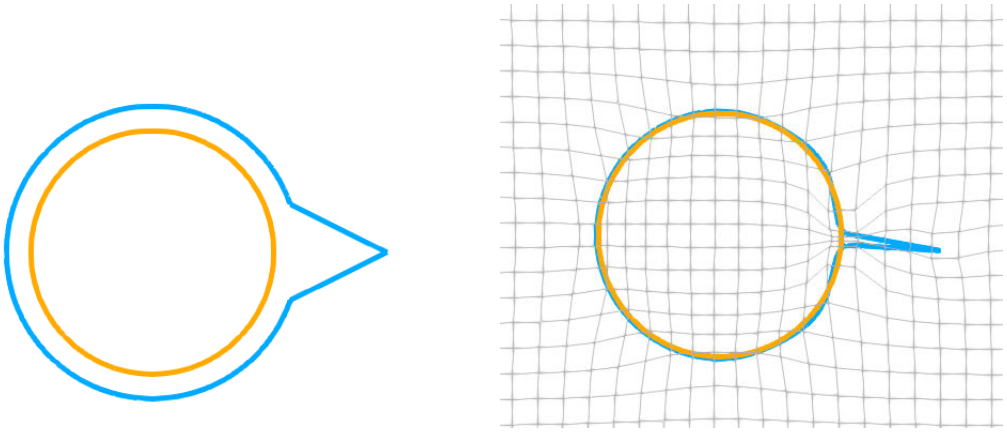

(a) Initial configuration

(b) Result of the registration with the deformation grid

Figure 4: Registration of a blue circle with a spike to an orange circle with a kernel metric on current as dissimilarity measure. The spike is not pinched during the matching since in the space of currents, it is negligible for the kernel metric.

Curvature measures and normal cycles

Normal cycles find their roots in the seminal work of Federer [Federer, 1959], where he provided a unified framework for curvature measures. Before 1959, curvature was studied through two similar yet theoreticaly different formulas. The first one was for convex bodies, where the Steiner formula expresses the volume of the ε-offset of a convex set as a polynomial in ε ([Steiner, 1840]). Steiner defined generalized curvature measures for convex sets as the coefficients of this polynomial. The same formula was proved by Weyl for compact $\mathscr{C}^2$ submanifolds using Riemannian curvature tensor ([Weyl, 1939]). If the result is analogous the theory behind is very different and each case does not contain the other one. It was an important step forward when Federer introduced curvature measures for a generalized type of sets which encompasses both the convex and the $\mathscr{C}^2$-submanifold cases: sets with positive reach, that will be introduced in definition 2.31. The reach of a set X is the smaller ε for which if a point x is such that $d(x, X) \leq \varepsilon$, then x has a unique projection on X.

In [Federer, 1959], Federer expresses the d-dimensional volume of the ε-offset for a set X with positive reach R. If we denote $X_\varepsilon = \{x \in \mathbb{R}^d | d(x, X) \leq \varepsilon\}$ for $\varepsilon \leq R$, and P_X the projection on X and if we consider Q a Borel set of $\mathbb{R}^d$, then

$$\mathrm{Vol}(X_r \cap P_X^{-1}(Q)) = \sum_{i=0}^{d} \alpha(d-i)\mathcal{C}_i(X; Q) r^{d-i}, \tag{4}$$

where $\alpha(i)$ is the i-volume of the i-dimensional unit ball. The $\mathcal{C}_k(X; .)$ can be interpreted as generalized curvature measures on the set X. It can be striking at first that the only hypothesis of positive reach for a set allows to consider its curvature, although it is a second-order information. However, the existence of a positive reach implies much more regularity than it may seem as we will see in proposition 2.37. A fundamental example of such regularity is that for a set with positive reach, one can define a generalization of *normal vectors at point* x, denoted $\mathrm{Nor}(x, X)$, and thereafter of *unit normal bundle*, denoted $\mathcal{N}_X$: $\mathcal{N}_X := \{(x, n) | x \in X, n \in$

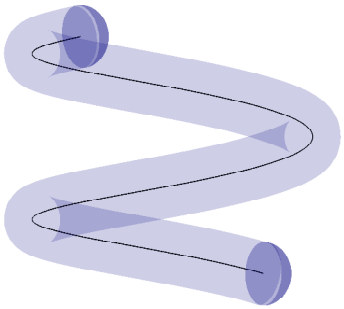

Figure 5: In blue the ε-offset (or parallel body) of dark curve.

$\mathrm{Nor}(x, X) \cap S^{d-1}\big\}$. $\mathcal{N}_X$ is an $(d-1)$-dimensional set of $\mathbb{R}^d \times S^{d-1}$, independently of the dimensionality of X. One should notice that this definition coincides with the classical definition of unit normal bundle for a $\mathscr{C}^2$ submanifold of $\mathbb{R}^d$.

In [Zähle, 1986], Zähle showed that Federer's curvature measures can be retrieved by integrating adequate differential forms over the unit normal bundle $\mathcal{N}_X$ associated with X: this is exactly the normal cycle of X, that we will denote $N(X)$. With the vocabulary of geometric measure theory, a normal cycle of a set with positive reach is rigorously the current associated with its unit normal bundle, $N(X) = [\mathcal{N}_X]$. A normal cycle is thus an element of $\Omega_0^{d-1}(\mathbb{R}^d \times S^{d-1})'$. If $\omega \in \Omega_0^{d-1}(\mathbb{R}^d \times S^{d-1})$, then

$$N(X)(\omega) := [\mathcal{N}_X](\omega) = \int_{\mathcal{N}_X} \langle \omega(x,n) | \tau_{\mathcal{N}_X}(x,n) \rangle \, d\mathscr{H}^{d-1}(x,n)$$

where $\tau_{\mathcal{N}_X}(x,n)$ is the $(d-1)$-vector associated with a positively oriented, orthonormal basis of $T_{(x,n)}\mathcal{N}_X$, the tangent space of $\mathcal{N}_X$ at (x,n). Zähle showed that there exists explicit, universal differential forms $(\boldsymbol{\omega}_k)_{1 \leq k \leq d-1}$ such that

$$\mathcal{C}_k(X; B) = N(X)(\boldsymbol{\omega}_k \llcorner \mathbb{1}_{B \times S^{d-1}}).$$

These differential forms are called *Lipschitz-Killing differential forms*.

Representation of shapes with normal cycles

In this manuscript, we develop the representation of shapes with normal cycles in the framework of computational anatomy, inspired by the previous work on dissimilarity measure [Vaillant and Glaunès, 2005, Glaunès, 2005, Charon, 2013] that we have recalled above. To a shape X, we associate its normal cycle $N(X)$. As previously said, the main advantage of the concepts of currents or varifolds is that they encompass in the same framework both the continuous and discrete cases. This is a nice feature since it provides an immediate and simple computational setting to work with discrete curves or triangulated surfaces, coupled with strong theoretical guarantees (e.g. convergence results of the discrete approximations of a continuous shape). At first, the theory of normal cycles was only valid for sets with positive reach. This is a limiting assumption since a shape as simple as a unions of two segments has not positive reach. This prevents us for a direct application of normal cycles in the case of discrete shapes. Hopefully, in [Zähle, 1987, Rataj and Zähle, 2001], the authors extended the notion of normal cycles for sets that are union of sets with positive reach, using an additive property of normal cycles.

With all these shape representations used in computational anatomy, it is natural to study the relations between them. An important step forward is made in this manuscript, where we draw a precise link between the varifold μ_X and the normal cycle $N(X)$ associated with a submanifold X. We show that in some sense, μ_X is a projection of $N(X)$ that looses all the curvature informations. The projection

operator is made explicit and this paves the way to a unification of the different representations, as well as the associated metrics.

As we have seen above, normal cycles encode all the curvatures information of a set with positive reach. This remains true for the generalization with discrete shapes. In fact, normal cycles have already been applied to computational analysis of discrete surfaces to estimate curvature of surfaces approximations [Cohen-Steiner and Morvan, 2003, Chazal et al., 2008, Morvan, 2008].

Kernel metrics on normal cycles

Once the representation of shapes with normal cycles is set for the continuous and the discrete case, we focus on the metric that we can put on normal cycles. For this, we follow the construction of kernel metrics on currents that was introduced in [Vaillant and Glaunès, 2005, Glaunès, 2005]. A normal cycle being a current (associated with a normal bundle), the construction is for the theoretical part very similar: we define a Reproducing Kernel Hilbert Space W of differential forms, $W \hookrightarrow \Omega_0^{d-1}(\mathbb{R}^d \times S^{d-1})$. Considering the dual applications, we have $\Omega_0^{d-1}(\mathbb{R}^d \times S^{d-1})' \subset W'$, so that the space of currents $\Omega_0^{d-1}(\mathbb{R}^d \times S^{d-1})'$ (containing the normal cycles) can be seen as a subset of a Hilbert space with an explicit scalar product thanks to the kernel. For current, the kernel is classically a scalar kernel $k_p : \mathbb{R}^d \times \mathbb{R}^d \to \mathbb{R}$ so that we retrieve the announced scalar product of equation (3):

$$\langle [C], [S] \rangle_{W'} = \int_C \int_S k_p(x,y) \, \langle \tau_C(x), \tau_S(y) \rangle \, d\mathscr{H}^m(x) s\mathscr{H}^m(y).$$

With the same construction for normal cycles, this leads to a scalar kernel $k : (\mathbb{R}^d \times S^{d-1})^2 \to \mathbb{R}$, generating a RKHS of differential forms $W \hookrightarrow \Omega_0^{d-1}(\mathbb{R}^d \times S^{d-1})$ such that

$$\langle N(C), N(S) \rangle_{W'} = \int_{\mathcal{N}_C} \int_{\mathcal{N}_S} k\big((x,u),(y,v)\big) \, \langle \tau_{\mathcal{N}_C}(x,u), \tau_{\mathcal{N}_S}(y,v) \rangle \, d\mathscr{H}^{d-1}(x,u) d\mathscr{H}^{d-1}(y,v).$$

The kernel k involves spatial points, x and y and normal points u and v. The "spatial space" $\mathbb{R}^d$ and the "normal space" S^{d-1} have different significations and should be considered independently. That is why we choose k as a product of two kernels: a spatial kernel $k_p : \mathbb{R}^d \times \mathbb{R}^d \to \mathbb{R}$ and a normal kernel $k_n : S^{d-1} \times S^{d-1} \to \mathbb{R}$ such that $k\big((x,u),(y,v)\big) = k_p(x,y)k_n(u,v)$ and the scalar product between two normal cycles writes:

$$\langle N(C), N(S) \rangle_{W'} = \int_{\mathcal{N}_C} \int_{\mathcal{N}_S} k_p(x,y)k_n(u,v) \, \langle \tau_{\mathcal{N}_C}(x,u), \tau_{\mathcal{N}_S}(y,v) \rangle \, d\mathscr{H}^{d-1}(x,u) d\mathscr{H}^{d-1}(y,v). \tag{5}$$

The spatial kernel k_p has a similar role as in the scalar product for currents (see equation (3)), and will mostly be a Gaussian kernel with width σ_W: $k_p(x,y) = \exp\big(-\|x-y\|^2/\sigma_W^2\big)$. The choice of the normal kernel k_n is driven by two constraints. The first one is that the kernel should provide a theoretical and interpretable formulae, as it is for the Gaussian kernel on the spatial space. For example,

given a specific kernel k_n, will the associated metric on normal cycles be able to retrieve curvatures information? This is not immediate, as we may choose coarse kernels for efficiency reasons, such as the constant kernel $k_n(u, v) = 1$. The second constraint, probably the most important, is that the obtained metric should be calculable and not too complex for discrete shapes (discrete curves and triangulation meshes). Indeed, normal cycles are a more complex shape representation that implies an increasing complexity of the metric. This was expected, as we encode more information on the shapes. However, this should lead to a reasonable increase of the calculation time of the distance. These two constraints are not necessarily jointly achievable. A kernel as simple as a constant or linear kernel will give a metric that is easier to compute, but will provide less theoretical guarantees. On the contrary, a good candidate for scalar kernel on S^{d-1} is a Sobolev kernel, associated with a Sobolev space on the sphere $H^s(S^{d-1})$. This kernel provides a metric with strong theoretical properties but we are not able to compute yet the scalar product for triangulation meshes.

In this thesis, we develop kernel metrics on normal cycles with the use of three normal kernel k_n: Sobolev, constant and linear for curves. For surfaces, we study mainly the constant and linear normal kernels.

As previously said, the Sobolev kernel is the one with the strongest theoretical guarantees, as for example the *universality* of the associated RKHS of differential forms W (see section 3.4). This property ensures that the norm on W' is a proper metric on normal cycles. This is not obvious at first since the framework of RKHS provides an embedding $W \hookrightarrow \Omega_0^{d-1}(\mathbb{R}^d \times S^{d-1})$, but the dual application $\Omega_0^{d-1}(\mathbb{R}^d \times S^{d-1})' \to W'$ needs not be injective, resulting in a pseudo-metric only.

For the computational aspect, using an expansion in spherical harmonics, we are able to provide an explicit metric on discrete curves with this kernel, but not for triangulation meshes. That is why we introduced simpler kernels such as the constant kernel ($k_n(u, v) = 1$) or the linear kernel ($k_n(u, v) = \langle u, v \rangle$). They have the advantage to be easier to compute in the discrete case, although the computation are still involved for the linear kernel on triangulated meshes. At first, those two kernels may seem too simple to have interesting properties. However, we are able to show exactly to what extend second order information are encoded by the corresponding metric. For example, in the case of surfaces, the metric on normal cycle with constant normal kernel contains information associated with the mean curvature, whereas the metric with linear normal kernel contains information associated with the Gaussian curvature of the surfaces. An interesting and interpretable metric is then a metric associated with the sum of the constant and linear kernel: $k_n(u, v) = 1 + \langle u, v \rangle$. It is noteworthy that up to a multiplicative constant, the sum of the constant and linear normal kernels can be interpreted as a truncation at order 1 of the spherical harmonics expansion of the Sobolev normal kernel.

Metrics with constant or linear kernels or the sum of the two kernels will be the main studied metric in the applications.

Computing the metric with discrete shapes

At this point, we have designed a dissimilarity measure between shapes that contains specific curvatures information and which are valid for continuous and discrete shapes. To apply this distance as a data-attachment term in the setting of computational anatomy, the next step is to explicit and implement the distance on discrete shapes as unions of segments and triangulated meshes (as well as the gradient of the distance for a minimization purpose). We provide in this manuscript the computation of the distance for discrete curves with the constant, the linear and the Sobolev normal kernel, and for discrete surfaces with constant kernel, and a truncation with the linear normal kernel. The scalar product between normal cycles involves integrations over sets associated with the triangles, the edges and the vertices of the discrete surfaces. To improve the calculation times, we compute an approximation of the integration over the sets associated with the edges and the triangles. This approximation is similar to the one of currents on discrete curves or surfaces. For the sets associated with vertices however, we cannot approximate the integration. Indeed, for triangulation meshes, this quantity is closely related to the angle of the triangles and for now we have not interesting approximation with convergence result when the size of the meshes goes to 0. This is the main reason why we compute explicitly this part of the scalar product, and this is the limiting aspect to explicit the metric on triangulated meshes.

In each case, the gradient is also computed, and we compare the complexity of the obtained distance with the metrics on currents or varifolds. We observe that the higher order representation with normal cycles leads to more intricate formulas. However, the complexity remains similar to currents or varifolds (i.e. basically a double loop on the faces of the discrete shapes), even though each step of the loop involves two or three times more computations. The main difference with currents and varifolds is that for the latter, each step of the double loop necessitates a single evaluation of the kernels at the barycenters of the triangles, whereas for the metric on normal cycles, it involves also the edges and the vertices of the triangles.

Registration and Atlas estimation with normal cycles

In concrete applications, this inexact registration problem will be discretized: the shapes C and S will be unions of segments or triangulated meshes, which means that they are encoded by a set of vertices and a connectivity matrix that specifies the link between the vertices. Using approximation on normal cycles for the dissimilarity part, we are able to express the data-attachment term $\left\|N\left(\varphi_1^v(C)\right) - N(S)\right\|_{W'}^2$ as a function of the vertices only. Also, to simplify the computation, we suppose that the deformations act on the vertices only, leaving a rigid meshes for the discrete shapes. With the Riemannian framework of G_V, and the previous approximation, one can show that the optimal deformation of (2) is generated by a time-varying vector field

v_t that takes explicit expression with the kernel $K_V : \mathbb{R}^d \times \mathbb{R}^d \to \mathbb{R}$:

$$v_t(x) = \sum_{i=1}^{n} K_V(x, x_{i,t}) p_{i,t}$$

where the $(x_{i,t})_{1\leq i\leq n} \in (\mathbb{R}^d)^n$ are the positions at time t of the discretization points, and the $(p_{i,t})_{1\leq i\leq n} \in (\mathbb{R}^d)^n$ are auxiliary variables, called *momenta*. Moreover, as it may be expected in a Riemannian setting, the energy of the optimal path $(v_t)_{0\leq t\leq 1}$ is constant: $\forall t \in [0,1],\ \|v_t\|_V^2 = \|v_0\|_V^2 = \sum_{i,j=1}^n p_{j,0}^T K_V(x_{i,0}, x_{j,0}) p_{i,0}$ and finally, the optimal deformation φ_1^v depends only on the initial positions of the discretization points $(x_i)_{1\leq i\leq n}$ that are fixed, and on the initial momenta $(p_i)_{1\leq i\leq n}$. Starting from this initialization $(x_i, p_i)_{1\leq i\leq n}$, one can retrieve all the trajectory of the path through coupled differential equations that are called *geodesic equations*:

$$\begin{cases} \dfrac{\partial x_{i,t}}{\partial t} = \displaystyle\sum_{j=1}^{n} K_V(x_{i,t}, x_{j,t}) p_{j,t} \\ \dfrac{\partial p_{i,t}}{\partial t} = -\displaystyle\sum_{j=1}^{n} \nabla_1 \big(p_{i,t}^T K_V(x_{i,t}, x_{j,t}) p_{j,t}\big) \end{cases}$$

Eventually, the inexact registration problem for discrete shapes can be written as a function of the initial momenta only, and if we denote φ_1^p the obtained deformation at time 1, starting with the initial momenta $p = (p_i)_{1\leq i\leq n}$, we obtain the next registration problem:

$$\arg \min_{(p_i)_{1\leq i\leq N} \in (\mathbb{R}^d)^N} \sum_{i,j=1}^{N} p_i K_V(x, x) p_j^T + g\big(\varphi_1^p((x_k)_{1\leq k\leq N})\big). \tag{6}$$

It can be solved with a geodesic shooting (to evaluate the functional, as well as its gradient, see [Arguillère et al., 2015] and section 1.4), and coupled with adequate minimization procedure. In this thesis we present examples of registrations for surfaces with a large number of points (around 10 000) in reasonable time (from 1 to 3 hours).

In this manuscript, a full chapter (Chapter 4) focuses on experimental results of registrations with normal cycles; and comparison with currents and varifolds are made. The chosen examples show different properties of the metric on normal cycles for an applicative purpose that may be an indication for future use. For example, on the contrary to currents or varifolds, normal cycles are sensitive to the boundaries of the shapes or to branching points. For a registration purpose, the obtained matching takes into account the boundaries in a much more natural way than varifolds or currents, and leads to a smoother deformation. One of the consequences of this sensitivity is that normal cycles see topology changes. This can be an advantage or a drawback depending on the certainty we have on the data. Another property that was expected is that the metric on normal cycles is sensitive to high curvature points, with as a result, more precise registrations, but also poor behaviour when it comes to noisy data.

The last part of Chapter 4 is a preliminary work on *atlas estimation* with normal cycles. The aim of atlas estimation is, given a dataset of shapes, to provide a "mean shape", as well as deformations from the mean shape to the target shapes of the dataset. This is the heart of the applicative side of computational anatomy, since it allows to perform statistical analysis of a dataset of shapes, and a lot of works have been done on different datasets of shapes or functional shapes (see for example [Durrleman et al., 2013, Charon, 2013, Charlier et al., 2015b, Lee et al., 2017b]). In this manuscript however, we focus only on the atlas estimation, the statistical analysis on a relevant dataset is postponed for future work. The first results provided in this thesis are promising and indicate benefits of the use of normal cycles.

Organization of the manuscript and contributions of this work

The work presented in this thesis has led to several publications: one in a journal (published, [Roussillon and Glaunès, 2016]) and two proceeding papers (one published [Roussillon and Glaunès, 2015], one accepted for publication [Roussillon and Glaunès, 2017]). The materiel of these works are included in Chapters 2 to 4. This manuscript is composed of four chapters.

Chapter 1

This chapter is a review on shape analysis as introduced by d'Arcy Thompson [Thompson, 1917], and formalized by Greenander [Grenander and Miller, 1998]. We recall the main considerations for the mathematical setting of shape analysis, and insist on the field of Large Deformations Diffeomorphic Metric Mapping in section 1.2. The construction of the group of deformations is recalled, as well as the geodesic equation governing optimal path. The inexact registration framework is tackled in section 1.3 in the general case, as well as the computational aspects in section 1.4. The reader familiar with LDDMM and shape analysis can go straight to Chapter 2.

Chapter 2

Chapter 2 is where the shape representation with normal cycles is introduced. After a brief recall of the necessary notions of differential forms and rectifiable sets in section 2.1 and section 2.2, we review the *currents* and *varifolds* representation of shapes, as well as their properties and discrete implementations in section 2.3. The theory of normal cycles is fully detailed in section 2.4, starting with the description of the unit normal bundle of a set with positive reach, and its associated normal cycles and extending the definition to union of sets with positive reach which encompasses the case of discrete shapes. The normal cycles of union of segments and triangulation meshes are detailed, as well as some approximations that will prove useful for numerical implementations. In section 2.5, we study precisely to what

extend normal cycles encode curvatures information of the shapes, as it was made explicit by Zähle in [Zähle, 1986]. Introducing specific spaces of differential forms in $\mathbb{R}^d \times S^{d-1}$, we are able to interpret unsigned curvature informations as infinity norms on these spaces. Finally, section 2.6 draws a precise link between the shape representation with varifolds and with normal cycles. We prove that the varifold of a smooth submanifold is, in a specified sense, the projection of the normal cycle associated with this submanifold. This projection operator loses all the curvature informations contained in the normal cycle.

Chapter 3

In Chapter 3, we introduce kernel metrics on normal cycles. Section 3.1 is a reminder of the theory of vector-valued reproducing Hilbert spaces, as well as possible ways to define interesting kernels that generate Reproducing Kernel Hilbert Space. Section 3.2 and section 3.3 are based on this reminder. Section 3.2 reviews the construction of kernel metrics on the spaces of currents and varifolds, and their discrete expression. In section 3.3, we define a kernel metric on normal cycles, using a scalar kernel k that is a product of two kernels: a spatial kernel k_p and a normal k_n. The properties of the metrics, depending on the choice of the kernel is studied in sections 3.4 and 3.5, notably the kind of curvature that is encoded with the constant and linear normal kernels. After proving a convergence result for discrete approximations of a continuous shape in section 3.6, the scalar product for discrete shapes is expressed in section 3.7. One can find the details of the calculus in Appendices A to C.

Chapter 4

This chapter presents experimental results of curves and surfaces registrations, as well as first results of atlas estimations for curves and surfaces. In section 4.1, we recall the theoretical and computational framework for shape registration. We prove the existence of a minimizer for the inexact matching problem with normal cycles and detail the numerical implementation for our applications. Subsection 4.1.4 and subsection 4.1.5 provide several examples of shape registrations with normal cycles. We show the different specificities of the matching with normal cycles, such as the consideration of the extremities or branching points, and the registration of regions with high curvature. We compare the results with other dissimilarity metrics, and we study the computational time. In section 4.2, we fit our data-attachment term in the framework of atlas estimation, i.e. a mean shape given a dataset of shapes, as well as the associated set of optimal deformations. We prove the existence of an atlas for the forward scheme with hypertemplate as used in [Charlier et al., 2015b] and provide examples with sets of curves or surfaces.

Chapter 1

Computational Anatomy

Sommaire

In the past decades, computational anatomy has gained a growing interest: the development of new acquisition technologies induces an ongoing increase in the number of biological structures that can be imaged, as well as in the number of subjects for each structure. The size of the database prevents from a manual analysis and requires an automatized method. These new technologies facilitate the setting of databases of a given anatomical structure that are almost representative of the population variability. A statistical analysis would make possible the detection of anatomical abnormalities and would pave the way to an early diagnosis for diseases that cause or are caused by anatomical degradation. If the problematic is clear, it raises nonetheless a lot of difficulties. First of all the data range at stake is very large and can be as different as images (MRI, X-rays, ...), 3D meshes (triangulations, volumetric meshes, ...), tensors (Diffusion Tensor Imaging), fiber sets, geometrico-functional structures (functional MRI for example) and so on. This variety has to be kept in mind for modelling issues. Another difficulty concerns the problematic itself and can be summed up in the following question: how to provide a mathematical framework that allows for relevant statistical analysis of shapes dataset? In computational anatomy, the analysis of shapes variability is not based on the shapes themselves but made through the deformations that map one shape to another. Hence, the major modelling effort is transferred to the construction of a set of deformations that will play the role of the "measure" of variability. Precisely, the group of deformations is endowed with a (sub-)Riemannian structure that induces a metric on shapes. A shape is then considered as an element of a (possibly infinite dimensional) manifold with a Riemannian structure. The Riemannian framework fits well with the problematic of shapes analysis: geodesic between shapes illustrates the deformation from one shape to another and the tangential setting provides efficient statistical tools for the dataset analysis.

In section 1.1, we briefly overview the different approach for shape analysis, and the mathematical embedding that allows to represent shapes in a structured set. An important part of this section focuses on Grenander's approach [Grenander and Miller, 1998] which is the analysis of shapes through deformations. Section 1.2 focuses on the specific field of Large Deformation Diffeomorphic Metric Mapping [Beg et al., 2005], [Miller et al., 2006]: the group of deformations is constructed from the integration of time-varying vector fields living in a Hilbert space. It provides a Riemannian framework for deformations and the metric depends on the Hilbertian norm.

For applications, the exact registration between two shapes is not appropriate: it would implies too many constraints on the deformations and would make the matching sensitive to noise. To overcome this and perform inexact registrations, one needs a residual distance between a deformed shape and its target. This problematic is briefly overviewed in section 1.3. It raises the problem of shape representation: we need to embed the shapes in a space with an explicit distance. This space should compensate for all the variability that is not taken into account with the model of deformations. The use of *currents* and *varifolds* have been introduced in computational anatomy for this purpose. This will be studied more specifically in Chapter 2

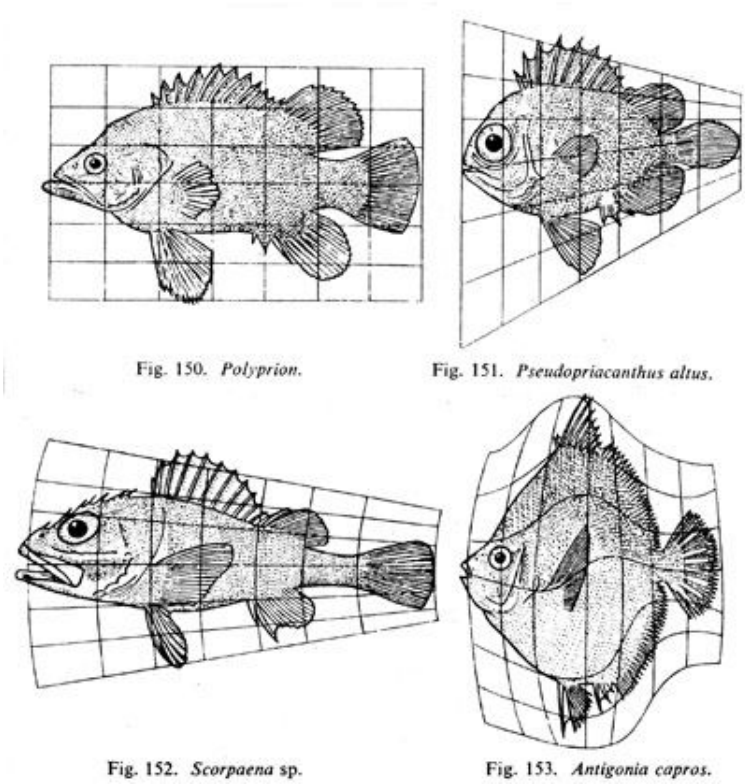

Figure 1.1: From D'Arcy Thompson's work. The variability of a fishes population is explained through geometrical transformations of the ambient space. The transformation is represented via the deformed grid.

and Chapter 3, where we introduce also a new dissimilarity measures using kernel metrics on normal cycles. Section 1.4 focuses on the computational framework: what are the available algorithms to perform inexact registration between two discretized shapes in concrete applications ?

1.1 Shape Analysis

The notion of shape may reference a set of labelled or unlabelled points, a curve, a surface, an image, a volumetric mesh, among other possible. In fact, the definition of shape varies with the applications in mind and we are not interested in the shape itself, but rather in its variability across the dataset. A first idea for shape analysis could be to extract relevant numerical indicators from each shape of the dataset (for example the volume, the diameter, the length of specific parts, etc) and apply a post process on these figures. However, it is obvious that using the whole geometrical information of shapes would improve the analysis. This remark leaves the mathematician with the hard task of designing a framework to consider shapes with all the interesting geometrical features and that allows for a statistical analysis...

1.1.1 A foundational example: Kendall's triangles

Probably the first step forward in the mathematical analysis of shapes is the pioneer work of Kendall. In [Kendall, 1984], the author focuses on the configurations of labelled k-points in $\mathbb{R}^m$, namely $(\mathbb{R}^m)^k$. His definition of shapes is the following:

"We here define 'shape' informally to be 'what is left when the differences which can be attributed to translations, rotations and dilatations have been quotiented out.'"

This means that Kendall is interested in the global shape of the configuration or in other words in the configuration of k points up to isometries of $\mathbb{R}^m$. Since we are looking only at the relative position of the k-points, one can suppose that they are centered in their centroid. This reduces the degree of freedom and we can work on $\mathbb{R}^{m(k-1)}$. The space of interest, that we will call "shape space" is then the quotient space

$$\Sigma_m^k = \left(\mathbb{R}^{m(k-1)} \setminus \{0\}\right) \diagup \mathrm{Sim}(\mathbb{R}^m).$$

where $\mathrm{Sim}(\mathbb{R}^m)$ is the set of all the rotations and dilatations. The quotient topology is a natural topology on Σ_m^k. In order to describe this quotient topology, it is easier to normalize the data first: if $z = (z_1, \dots z_{k-1}) \in \mathbb{R}^{m(k-1)}$, we consider $\frac{z}{\|z\|} \in S^{m(k-1)-1}$ where $\|.\|$ is the Euclidean norm. For convenience, we will represent an element $z/\|z\| \in S^{m(k-1)-1}$ as a matrix $W \in \mathcal{M}_{m,k-1}(\mathbb{R})$, each column being a point of the configuration in $\mathbb{R}^m$. The fact that $z/\|z\| \in S^{m(k-1)-1}$ implies that $\mathrm{tr}(WW^T) = 1$.

Normalizing the data is equivalent to quotienting $\mathbb{R}^{m(k-1)}$ by the dilatations, and the quotient topology on $S^{m(k-1)-1}$ is the classical topology on the sphere, given by the metric $d(W_1, W_2) = \arccos\left(\mathrm{tr}(W_1 W_2)\right)$ (this is the Riemannian metric on the sphere). We are then left to quotient this sphere by the rotations of $\mathbb{R}^m$, $SO(m)$. We denote p the projection from $S^{m(k-1)-1}$ to $S^{m(k-1)-1} \diagup SO(m) = \Sigma_m^k$. This is an easy verification that the metric d is invariant by left composition with a rotation of $\mathbb{R}^m$, namely if $R \in SO(m)$,

$$d(RW_1, RW_2) = d(W_1, W_2).$$

This invariance implies that

$$\rho(pW_1, pW_2) := \inf_{R \in SO(m)} d(RW_1, W_2) \tag{1.1}$$

is a metric on Σ_m^k that defines the same topology as the quotient topology.

Let sum up the process. We started with a metric set (X, d) (here $S^{m(k-1)-1}$) and a group G that acts on X (here $SO(m)$) and such that the metric is left or right invariant. Then under some conditions on the topology of the orbit, we can "descend" the metric d on a metric ρ on $X \diagup G$: $\rho([x_1], [x_2]) = \inf_{g \in G} d(gx_1, x_2)$. This is a classical construction to get rid of all the transformations that we do not want to be taken into account.

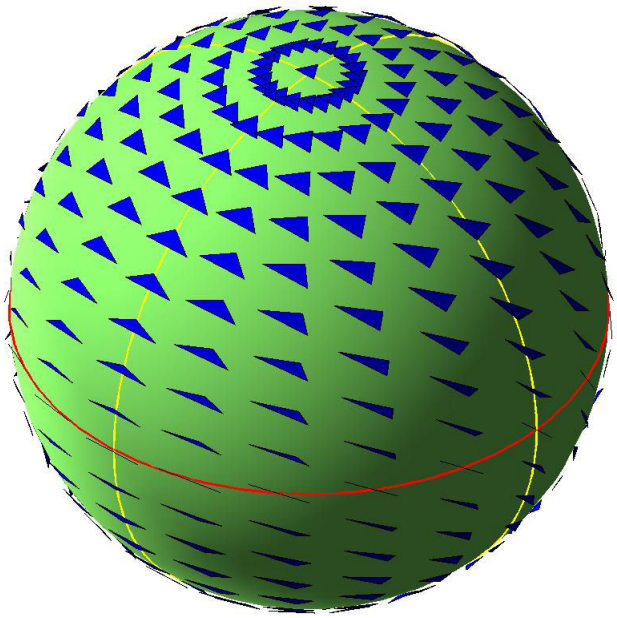

Figure 1.2: Kendall's representation of triangles: the class of triangles up to translations, rotations and dilatations is isometric to the sphere $S^2(1/2)$. The geodesics on the sphere give geodesics on Σ_2^3 and one can follow the deformation between to triangles along the geodesic.

In the case $m = 2$, Kendall notices that Σ_2^k is a Riemannian manifold and the metric ρ is explicit (see section 3 of [Kendall, 1984]). All this becomes even simpler in the specific case of triangles in $\mathbb{R}^2$, namely Σ_2^3: Kendall showed that Σ_2^3 is isometric to the 2-dimensional sphere of radius $1/2$. This framework provides a representation of triangles (up to translations, rotations and dilatations) in a space as simple as a sphere endowed with its classical Riemannian metric. To each class of a triangles corresponds a point on the sphere $S^2(1/2)$ (see figure 1.2).

This framework, besides its simplicity, suffers from several drawbacks. First of all, the shapes we are working with are labelled points. In concrete applications, this means that we have performed a pre-process to label the points, which is often a manual procedure prone to errors or imprecisions. Moreover, the Riemannian metric on Σ_2^k comes from a Euclidean metric. Hence, even though one shape is obtained through a small non linear deformation of another shape, the metric will not account for this proximity. These limitations are a motivation to go deeper in the construction of shape spaces with interesting features for shape analysis.

1.1.2 Shape spaces and group of deformations

The previous example of Kendall's shape spaces is an *intrinsic* way of defining a shape space, with a Riemannian metric that we can call an *inner metric*: the

shapes variability is measured directly on the shape manifold. This term is not a standardized mathematical notion but is to distinguish with the *outer metric* that we will see right now.

With so called *outer metric*, the difference between two shapes is "measured" through deformations of the ambient space: how complex is a deformation to match one shape to another. Thus, the quantification of the variability is made on a group of transformations acting on shapes rather than on shapes themselves. This concept is close to D'Arcy Thompson's one and it was fully formalized by Grenander [Grenander and Miller, 1998]. The following briefly summarizes the setting.

In this approach, we consider a set M, called "the shape space" constituted of "shapes" living in $\mathbb{R}^d$ and on which a group G of transformations of $\mathbb{R}^d$ acts on the left. This is a generic situation that encompasses various examples as points, images, curves, surfaces, etc. Besides, we suppose that M is a *homogeneous space* under the action of G, or in other words that the action is transitive:

$$\forall m_0, m_1 \in M,\ \exists g \in G \mid g.m_0 = m_1$$

In a modelling point of view, this means that the complexity of the deformations of G is enough to explain all the shape variability in M. This may seem as a strong assumption. However, the motivation behind is rather the following: the variation observed across a set of shapes is the result of multitude of deformations of an "ideal shape" m_0. m_0 contains all the typical features of the set of shapes, and the shape space M is the *orbit* of m_0 under the action of G, which means that $G.m_0 = M$. m_0 is often called the *template*.

Let us now give example of classical shape spaces, as well as the description of the action of G.

Example 1.1 (Landmarks)**.** *We define* $\mathcal{L}_n(\mathbb{R}^d) := \left\{(x_1, \dots, x_n) \in (\mathbb{R}^d)^n \mid \forall i \neq j,\ x_i \neq x_j\right\}$. *This is the set of* n*-labelled points in* $\mathbb{R}^d$. *The group of diffeomorphisms* $G = \mathrm{Diff}(\mathbb{R}^d)$ *acts on the left on* $\mathcal{L}_n(\mathbb{R}^d)$*: for every* $m = (x_1, \dots x_n) \in \mathcal{L}_n(\mathbb{R}^d)$, $\varphi \in G$,

$$\varphi.m := (\varphi(x_1), \dots, \varphi(x_n)).$$

For $d \geq 2$*, the action is transitive and* $\mathcal{L}_n(\mathbb{R}^d)$ *is a shape space as previously defined.*

Example 1.2 (Images)**.** *Another classical example of shape space is the set of continuous images of* $\mathbb{R}^d$. *Consider* Ω *a domain of* $\mathbb{R}^d$ *and the space* $L^2(\Omega, \mathbb{R})$. *The group* $G = \mathrm{Diff}(\Omega)$ *acts on the left on* $L^2(\Omega, \mathbb{R})$ *as follow:*

$$\forall I \in L^2(\Omega, \mathbb{R}), \varphi \in G,\ \varphi.I := I \circ \varphi^{-1}.$$

Note that the set $I(\Omega)$ *remains unchanged under this action. This obviously prevents the action from being transitive. However, the set* $M = G.I_0$ *is a shape space as previously defined.*

This formal approach becomes fruitful when one sets a structure on the group G. Suppose that G is endowed with a right invariant metric d_G and consider a shape space M that is the orbit of a template m_0, i.e. $M = G.m_0$. We denote $\mathrm{Stab}_G(m_0) := \{g \in G | g.m_0 = m_0\}$ the stabilizer (or isotropy group) of m_0. To construct a distance on M from the distance on G, we start with the classical identification between the homogeneous space M to $G/\mathrm{Stab}_G(m_0)$: an element $[g] \in G/\mathrm{Stab}_G(m_0)$ is uniquely associated with $g.m_0 \in M$. On $G/\mathrm{Stab}_G(m_0)$, we define

$$d_{G/\mathrm{Stab}_G(m_0)}([g_1],[g_2]) := \inf_{\substack{g\in[g_1]\\ g'\in[g_2]}} d_G(g,g').$$

Now if $m_1, m_2 \in M$ and $g_1, g_2 \in G$ such that $g_1.m_0 = m_1,\ g_2.m_0 = m_2$, then we define on M

$$d_M(m_1,m_0) := d_{G/\mathrm{Stab}_G(m_0)}([g_1],[g_2]) = \inf_{\substack{g.m_0=m_1\\ g'.m_0=m_2}} d_G(g,g').$$

Using the right invariance of the metric on G, we get:

$$d_M(m_1,m_0) = \inf_{\substack{g\in G\\ g.m_1=m_2}} d_G(\mathrm{Id},g).$$

d_M is thus a natural candidate to provide a metric on M. Moreover, it has a simple interpretation: given two shapes m_1 and m_2, we consider the "optimal" deformation g, that is the one closest to the identity of G. The next theorem justifies the above construction of d_M.

Theorem 1.3 ([Younès, 2010], chapter 12)**.** *Suppose that d_G is a right-invariant metric on G, i.e.*

$$\forall g, g_0, g_1 \in G,\ d_G(g_0.g, g_1.g) = d_G(g_0, g_1),$$

and M is a homogeneous space under the action of G. Then d_M defines a pseudo-distance on M. Besides, if $\mathrm{Stab}_G(m_0)$ is closed for the topology induced by d_G, then d_M is a proper distance.

Hence, the metric on G "descends" to a metric on M and allows for shapes comparison. This is the starting point for computational anatomy. The next step is thus to construct the group of deformation G and this will be seen in the next section.

Let us just remark that not all shape spaces in the active research field are based on the action of a group of geometrical transformations. For example in an overview of shape spaces, [Bauer et al., 2013], the authors study the shape spaces of geometrical closed curves in $\mathbb{R}^2$. They start considering $\mathrm{Imm}([0,2\pi],\mathbb{R}^2)$, the space of parametrized closed curves $c : [0,2\pi] \to \mathbb{R}^2$ with $\forall t \in [0,2\pi],\ |c'(t)| \neq 0$. One can show that $T_c\mathrm{Imm}([0,2\pi],\mathbb{R}^2) = \mathscr{C}^\infty([0,2\pi],\mathbb{R}^2)$. A classical (weak-)Riemannian

metric on this space is the L^2 metric: at point $c \in \mathrm{Imm}([0,2\pi],\mathbb{R}^2)$, the local metric G_c is defined as:

$$G_c(h,k) = \int_0^{2\pi} \langle h(\theta), k(\theta)\rangle \, |c'(\theta)| d\theta, \ \forall h,k \in T_c\mathrm{Imm}([0,2\pi],\mathbb{R}^2).$$

Of course the assumption of parametrized curves is not suited for shape analysis. To get a parametrization-free framework, they quotiented out this space by the group of re-parametrizations, namely $\mathrm{Diff}([0,2\pi])$, the space of diffeomorphisms of $[0,2\pi]$. The L^2 metric is right invariant under the action of $\mathrm{Diff}([0,2\pi])$ and descends to a metric on $B_i([0,2\pi],\mathbb{R}^2) := \mathrm{Imm}([0,2\pi],\mathbb{R}^2)/\mathrm{Diff}([0,2\pi])$. This metric suffers from a major drawback: the geodesic distance between two curves vanishes. This means that one can link two elements of $B_i([0,2\pi],\mathbb{R}^2)$ with a path of arbitrary small length. To overcome this issue, stronger metrics can be endowed in the initial space $\mathrm{Imm}([0,2\pi],\mathbb{R}^2)$ as Sobolev metrics and are studied in sections 5 and 6 of [Bauer et al., 2013], see also [Trouvé and Younes, 2011], 30.3.4.

1.2 Large Deformations

The previous section focused on the formalism of shape analysis through deformations. In this section we tackle the construction of the group of deformations. This is an active research field with different approaches. Let us first consider the simpler case where the deformations are obtained through *displacement fields*.

A major contribution in the domain of shapes comparison was addressed by Bookstein, [Bookstein, 1989]. In this paper, the author focuses on the interpolation between landmark displacements: given two sets of labelled points $(x_1,\dots,x_n) \in (\mathbb{R}^2)^n$, $(y_1,\dots,y_n) \in (\mathbb{R}^2)^n$, the aim is to find a vector field of displacement v such that

$$x_i + v(x_i) = y_i, \text{ for every } 1 \leq i \leq n. \tag{1.2}$$

Of course, with no more assumption the problem is ill-posed. A classical way to solve this is to constrain the problem by introducing an energy associated with vector fields. The chosen vector field will be the one that fulfils (1.2) and that minimizes the energy. In this spirit, Bookstein introduced a bending energy of a vector field v, which corresponds to the energy needed to bend a thin plate by a displacement v. This framework is in fact inspired by the Thin Plate Spline (TPS) theory developed by Duchon and Meinguet ([Duchon, 1976, Duchon, 1977, Meinguet, 1979, Meinguet, 1984]). The optimal vector field v_0 has a closed form thanks to the radial kernel $k(r) = r^2 \log r^2$ (k is the green function of the biharmonic equation $\Delta^2 u = 0$, i.e. $\Delta^2 k = \delta_{(0,0)}$). The total deformation of the ambient space is then $\varphi = \mathrm{Id} + v_0$.

The pros of this construction is that the cost of an affine transformation is zero, thus the TPS perform a "free" rigid registration. Moreover, it gives an explicit pseudo-metric on the space of landmarks that allows for a statistical

analysis. It has been successfully applied in medical imaging [Sprengel et al., 1996] or for fingerprints comparison [Bazen and Gerez, 2003]. However, some drawbacks prevent this method for an extensive application in computational anatomy. First of all, this framework is valid only when shapes are landmarks, which means labelled points. Most of the time, this labelling is made manually and is subject to errors. Moreover, the total deformation φ needs not be diffeomorphic: foldings may appear, which is a concern for applications.

The fact that the global deformation is not diffeomorphic is not specific to the TPS model. In the case of image registration, Thirion [Thirion, 1998] developed an algorithm inspired by a diffusion process. The registration is obtained with a displacement field as for TPS and it is diffeomorphic only for small deformations. In [Vercauteren et al., 2009], the authors introduced a diffeomorphic variation of this algorithm.

The advantage of diffeomorphisms is that the transformation is one-to-one, and preserve the structure of the shapes: the image of a surface is still a surface and more generally the differential structures of the shapes are maintained. In the following, we will overview the construction of a set G of deformations that is a subgroup of the group of diffeomorphisms. This framework in the one of Large Deformations Diffeomorphic Metric Mapping (LDDMM). Starting with a Hilbert space of vector fields V, we consider all the diffeomorphisms flows of time varying vector fields. The generated diffeomorphisms form a group G, with a right-invariant Riemannian metric given by the Hilbertian norm of V. V can be seen as the tangent space of G at the identity and its norm represent the cost of infinitesimal displacements. This setting is drawn from mathematical mechanics where the flow of the time varying vector fields represents the evolution of particles along a force field (see for example [Arnold, 1989]). It was introduced in computational anatomy in the nineties ([Trouvé, 1995, Christensen et al., 1996, Dupuis et al., 1998, Trouvé, 1998]).

One should notice that other construction of groups of transformations could have been chosen, as for example *conformal transformations*, [Sharon and Mumford, 2006]. However, in this manuscript we will restrict ourselves to the framework of LDDMM.

1.2.1 Group of diffeomorphisms as flows of time varying vector fields

The original idea of LDDMM is inspired by fluid mechanics: if we consider the evolution of particles along a time varying velocity field, the resulting deformation at time one of the system will be obtained by integrating this vector field. And we can defined an energy of this deformation: the integration of the infinitesimal cost of displacement.

It is possible to write it in a more formal way: let V be a continuous embedding onto $\mathscr{C}_0^1(\mathbb{R}^d, \mathbb{R}^d)$ (we write it $V \hookrightarrow \mathscr{C}_0^1(\mathbb{R}^d, \mathbb{R}^d)$) and suppose that V is a Hilbert space of vector fields (e.g. a Sobolev space), whose norm $\|.\|_V$ represents the infinitesimal

cost of displacement. We define $L^2_V = \left\{(v_t)_{0\leq t\leq 1} \in V^{[0,1]} \middle| \int_0^1 \|v_t\|^2_V \, dt < +\infty\right\}$, the set of all time-varying vector fields with finite energy (with respect to the norm on V). We define $G_V := \{\varphi_1^v, v \in L^2_V\}$ with

$$\begin{cases} \dfrac{\partial \varphi_t^v}{\partial t} = v_t \circ \varphi_t^v \\ \varphi_0 = \mathrm{Id} \end{cases} \tag{1.3}$$

which means that we consider deformations at time one, with finite energy. All this construction has been widely detailed for example in [Beg et al., 2005], [Younès, 2010], Chap. 8. and following. The spatial regularity of the elements of V implies nice structure for the set G_V:

Theorem 1.4 ([Dupuis et al., 1998, Trouvé, 1995])**.** *G_V is a group of diffeomorphisms.*

By diffeomorphism we mean an application $\varphi : \mathbb{R}^d \to \mathbb{R}^d$ with a given regularity ($\mathscr{C}^1$ or $\mathscr{C}^\infty$ for example) such that φ is invertible and φ^{-1} has the same regularity as φ.

The question is now how to endow a metric on G_V from the norm on V? Let us first remark that we are interested in the relative configuration of the shapes only, which means that we consider right-invariant metrics on G_V. If d is such a metric, and $g, g' \in G_V$, we have:

$$d(g, g') = d(gg^{-1}, g'g^{-1}) = d(\mathrm{Id}, g'g^{-1})$$

and we are left to design the distance from the identity only. As said previously, the norm on V can be seen as the cost of an infinitesimal displacement. Thus it is natural to consider that the energy of $v \in L^2_V$, namely $\int_0^1 \|v_t\|^2_V \, dt$ is the cost of the global deformation φ_1^v. We define

$$d_{G_V}(\mathrm{Id}, \varphi) := \inf_{v \in L^2_V} \left\{ \left(\int_0^1 \|v_t\|^2_V \, dt \right)^{1/2} \middle| \, \varphi_1^v := \varphi \right\} \tag{1.4}$$

where φ_1^v is obtained through integration of (1.3). We extend d_{G_V} to a right invariant distance on whole G_V via:

$$d_{G_V}(\varphi, \varphi') := d_{G_V}(\mathrm{Id}, \varphi' \circ \varphi^{-1}) = \inf_{v \in L^2_V} \left\{ \left(\int_0^1 \|v_t\|^2_V \, dt \right)^{1/2} \middle| \, \varphi' = \varphi_1^v \circ \varphi \right\}$$

Theorem 1.5 ([Trouvé, 1995])**.** *d_{G_V} is a metric on G_V. (G_V, d_{G_V}) is complete.*

One can show that the distance between two diffeomorphisms of G_V is attained for a $v \in L^2_V$ ([Younès, 2010], chapter 8). For such an optimal v, the norm $\|v_t\|_V$ is constant along the path $t \mapsto \|v_t\|_V$: $\forall t \in [0,1]$, $\|v_t\|_V = \|v_0\|_V$. d_{G_V} can be interpreted as a *geodesic distance*: given two diffeomorphisms φ, φ' of G_V, the distance $d_G(\varphi, \varphi')$ is associated with an optimal path $(\varphi_t^v)_{0\leq t\leq 1}$ that minimizes the energy $\int_0^1 \|v_t\|^2_V \, dt$.

Remark 1.6. *The structure on G_V is close to a Lie group structure, with $V = T_{\mathrm{Id}}G_V$ that would be a Lie algebra. However, the infinite dimensional framework is intricate. In [Bauer et al., 2013], section 7, the authors show that* $\mathrm{Diff}^\infty_c(\mathbb{R}^d) := \left(\mathrm{Id} + \mathscr{C}^\infty_c(\mathbb{R}^d)\right) \cap \mathrm{Diff}^\infty(\mathbb{R}^d)$*, modelled on the Fréchet space $\mathscr{C}^\infty_c(\mathbb{R}^d)$ is a Lie group, but this is not the case for G_V. In fact, the composition and the inverse operations need not to be smooth on G_V.*

In [Bruveris and Vialard, 2014], the authors study the properties of the group of diffeomophisms $\mathrm{Diff}_{H^s}(\mathbb{R}^d) = \left\{\varphi \in \mathrm{Id} + H^s(\mathbb{R}^d), \varphi \in \mathrm{Diff}_{\mathscr{C}^1}\right\}$ *where $H^s(\mathbb{R}^d)$ is the Sobolev space of degree s, for $s > d/2 + 1$. Among others, they show that $G_{H^s(\mathbb{R}^d)} = \mathrm{Diff}_{H^s}(\mathbb{R}^d)$, which means that with the construction of the group of diffeomorphisms through integration of a time varying vector field living in $H^s(\mathbb{R}^d)$, we retrieve all the Sobolev-diffeomorphisms.*

Now, we set this framework in the one of shape analysis: consider a shape m_0 living in $\mathbb{R}^d$, and G_V acting on m_0, generating an orbit $M = G_V.m_0$. With theorem 1.3, the distance on G_V induces a distance on M:

$$d_M(m, m') = \inf_{v \in L^2_V} \left\{ \int_0^1 \|v_t\|^2_V \, dt \;\middle|\; \varphi^v_1.m = m' \right\}.$$

For a computational anatomy purpose, it is necessary to find the optimal deformation φ^v_1 (which exists) that matches the two shapes m and m'. Or put another way, to find the *geodesic path* between m and m'. This problem can be seen as an optimal control problem:

$$\begin{cases} \min\limits_{v \in L^2([0,1],V)} J(v) := \displaystyle\int_0^1 \|v_t\|^2_V \, dt \\ \dfrac{\partial(\varphi^v_t.m)}{\partial t} = (v_t \circ \varphi^v_t).m \\ \varphi^v_1.m = m', \; \varphi^v_0 = \mathrm{Id} \end{cases} \tag{1.5}$$

This equation corresponds to a geodesic path projected on the shape space.

1.2.2 Geodesic equations

The problem (1.5) is to find the geodesic path between two shapes m and m'. In this section we express the geodesic equations that govern the optimal path. To simplify the presentation, we will only consider the case of landmarks, i.e. $M = (\mathbb{R}^d)^n$. This case is not so restrictive. Indeed, every numerical implementation deals with discretized shapes, represented as a finite number of points (and possibly a connectivity matrix for meshes) and the optimal trajectories of these points will follow geodesic equations for landmarks.

Suppose that we want to express the geodesic equations between $m = (x_0, \ldots, x_n)$ and $m' = (y_0, \ldots, y_n)$. Problem (1.5) reformulates:

$$\begin{cases} \min\limits_{v\in L^2([0,1],V)} J(v) := \displaystyle\int_0^1 \|v_t\|_V^2 \, dt \\ \dot{x}_{i,t} = v_t(x_{i,t}),\ 1 \leq i \leq n, \\ x_{i,1} = y_i,\ 1 \leq i \leq n \end{cases} \tag{1.6}$$

It is *a priori* an infinite dimensional optimization problem. However, it simplifies greatly when considering the properties of the Hilbert space V of vector fields. We recall that V is an admissible Hilbert space of vector fields, which means that we have a continuous embedding $V \hookrightarrow \mathscr{C}_0^1(\mathbb{R}^d, \mathbb{R}^d)$. If so, one can show that V is a Reproducing Kernel Hilbert Space (RKHS) (see [Micheli and Glaunès, 2014]). We will study with more details this notion in Chapter 3. Let us summarize the main properties of the RKHS here. There exists a kernel $K_V : \mathbb{R}^d \times \mathbb{R}^d \to \mathcal{L}(\mathbb{R}^d)$ where $\mathcal{L}(\mathbb{R}^d)$ is the space of linear applications of $\mathbb{R}^d$, and such that

- $\forall x, \alpha \in \mathbb{R}^d,\ y \mapsto K_V(y,x)\alpha \in V$,
- $\forall x, y \in \mathbb{R}^d,\ K_V(x,y) = K_V(y,x)$,
- $\forall x_1, \ldots, x_n \in \mathbb{R}^d, \alpha_1, \ldots \alpha_n \in \mathbb{R}^d,\ \displaystyle\sum_{i=1}^n \alpha_j^T K_V(x_j, x_i)\alpha_i, \geq 0$,
- $\forall x, y, \alpha, \beta \in \mathbb{R}^d,\ \langle K_V(.,x)\alpha, K_V(.,y)\beta\rangle_V = \beta^T K_V(y,x)\alpha$,
- $V = \overline{\text{Span}\left\{K_V(.,x)\alpha,\ x, \alpha \in \mathbb{R}^d\right\}}$ for the norm $\|.\|_V$.

The emergence of this RKHS simplifies the computations of the geodesic equations. In fact, one can show ([Glaunès, 2005]) that in the case of landmarks, an optimal vector field takes the form:

$$v_t = \sum_{j=1}^n K_V(., x_{j,t})p_{j,t} \tag{1.7}$$

where $x_{j,t}$ are the current positions at time t of the landmarks, and the $p_{j,t}$ are auxiliary variables and are called *momenta*. Both $x_{i,t}$ and $p_{i,t}$ follow explicit equations that are the geodesic equations [Miller et al., 2006]:

$$\begin{cases} \dot{x}_{i,t} = v_t(x_{i,t}) \\ \dot{p}_{i,t} = -\big(dv_t(x_{i,t})\big)^T p_{i,t}. \end{cases} \tag{1.8}$$

with v_t as in (1.7). In term of kernel, the previous expression writes:

$$\begin{cases} \dot{x}_{i,t} = \displaystyle\sum_{j=1}^n K_V(x_{i,t}, x_{j,t})p_{j,t} \\ \dot{p}_{i,t} = -\left(\displaystyle\sum_{j=1}^n d_1(K_V(x_{i,t}, x_{j,t})p_{j,t})\right)^T p_{i,t}. \end{cases} \tag{1.9}$$

with $d_1(K_V(x, x_{j,t})p_{j,t})$ the differential at x of the application $y \mapsto K_V(y, x_{j,t})p_{j,t}$. We see here that the geodesic equations are explicit through the kernel K_V and its derivative.

The previous equations are obtained through the *Euler-Lagrange equation* that characterize the extremal paths of (1.5) (see [Arnold, 1989] for the study of the Euler-Lagrange equation in the framework of classical mechanics). A Hamiltonian formalism is possible, that focuses on the conserved quantities of the system. In our situation one can introduce the *reduced Hamiltonian*:

$$H_r(q, p) = \sum_{i,j=1}^{n} p_i^T K_V(x_i, x_j) p_j.$$

where $q = (x_1, \dots, x_n)$ and $p = (p_1, \dots, p_n)$. On geodesic path, H_r is constant, and equals the energy of the initial velocity field v_0. In this formalism, the geodesic equations writes

$$\begin{cases} \dot{q}(t) = \dfrac{\partial H_r}{\partial p}(q(t), p(t)) \\ \dot{p}(t) = -\dfrac{\partial H_r}{\partial q}(q(t), p(t)). \end{cases}$$

This is an ordinary differential equation and as one could expect, the geodesic equations are parametrized by few parameters that are the initial positions of the particles $q(0) = (x_1, \dots, x_n) \in (\mathbb{R}^d)^n$ and their initial momenta $p(0) = (p_1, \dots, p_n) \in (\mathbb{R}^d)^n$.

In figure 1.3, one can observe the integration of the geodesic equations in the case of 3 landmarks in $\mathbb{R}^2$, i.e. $q(0), p(0) \in (\mathbb{R}^2)^3$. The kernel K_V of deformation is chosen Gaussian, with width $\sigma_V = 0.5$. The optimal vector field at time t is expressed through the current positions of the landmarks: $v_t(x) = \sum_{i=1}^{3} K_V(x, x_{i,t})p_{i,t}$ where x_i and p_i follow the geodesic equations (1.9). The integration at time 1 of the vector field v_t provides a deformation of the ambient space φ_1^v that we represent with a grid.

To summarize this section, we have seen that the optimal trajectories (i.e. trajectories with least energy) in the shape space of landmarks follow geodesic equations that are explicit with the kernel K_V of the RKHS V. The Hamiltonian formalism allows for a compact expression of these equations. They are parametrized by initial positions and momenta. If the geodesic equations are explicit, we have not tackled yet the expression of optimal path in concrete applications (exact or inexact registration). In section 1.4, we discuss the different algorithm to retrieve the optimal deformation. But first, we briefly introduce the *inexact registration problem*.

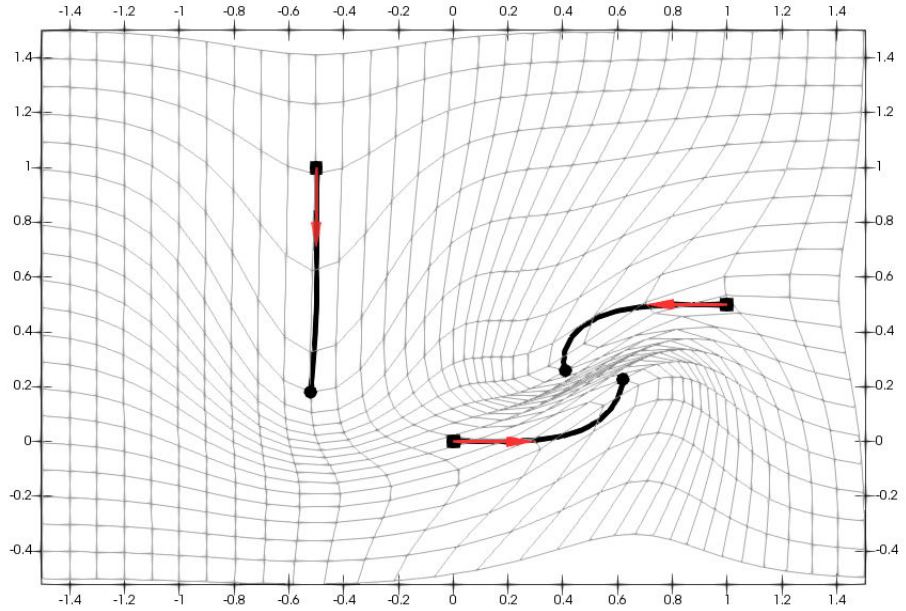

Figure 1.3: Shooting of 3 landmarks (represented with a dark square) with a Gaussian kernel of size $\sigma_V = 0.5$. The initial momenta $p(0) \in (\mathbb{R}^2)^3$ are represented with the three arrows attached to the initial points. The trajectories of the landmarks are represented with the dark curve. The integration of the geodesic equations provides a deformation of the ambient space that is visualized through the grid.

1.3 Inexact Registration

The LDDMM framework is convenient since we focus our modelling effort on the group G_V, and not on the shapes themselves. Thus, it can be applied to a wide range of matching problems (images, landmarks, curves, surfaces, etc.). For now, we have supposed that the shape space was homogeneous under the action of a group of transformations. But of course, the assumption of exact registration between any two shapes of a dataset is not realistic because it enforces too many constraints on the deformations. Moreover, in case of artefacts or noisy data, the exact matching is not interesting. That is why it seems necessary to relax this hypothesis and to allow for inexact matching. This is classically done by introducing a data attachment term A that will be a residual distance between the deformed shape $\varphi.m$ and the target shape m'. In the general case, the new functional to minimize is the following:

$$\begin{cases} \min\limits_{v \in L^2([0,1],V)} J(v) := \displaystyle\int_0^1 \|v_t\|_V^2 \, dt + A(\varphi_1^v.m, m') \\ \dfrac{\partial \varphi_t^v}{\partial t} = v_t \circ \varphi_t^v, \ \varphi_0^v = \mathrm{Id}. \end{cases} \tag{1.10}$$

This is a compromise between the closeness of the final registration (quantified by $A(\varphi_1^v.m, m')$) and the cost of the deformation (quantified by $\int_0^1 \|v_t\|_V^2 \, dt$). One can easily see that a minimizer of (1.10) still generates a geodesic path $(\varphi_t)_{0 \leq t \leq 1}$ on G_V.

The next theorem tackles the existence of a solution for (1.10):

Theorem 1.7 ([Glaunès, 2005]). *If, for every C, S, $v \mapsto A\left(\varphi_1^v.C, S\right)$ is weakly continuous from L^2_V to $\mathbb{R}$ then* (1.10) *has a solution.*

Of course, the optimal deformation will critically depend on the choice of A. In the case of landmarks registration (Example 1.1), A can be the classical l^2 norms: $A\big((x_1,\dots,x_n),(y_1,\dots,y_n)\big) = \sum_{i=1}^n \|x_i - y_i\|^2$. In the case of images (Example 1.2), the L^2 norm may be a first choice: $A(I_1, I_2) = \int_\Omega \|I_1(x) - I_2(x)\|^2 \, dx$. In the case of curves or surfaces, several dissimilarity measures have been developed using kernel metrics on currents ([Glaunès, 2005, Durrleman, 2010]) or on varifolds ([Charon, 2013]). This will be recalled in Chapter 2 and Chapter 3. The aim of this thesis is to design a new data attachment term A that takes into account the curvature information of the shapes (curves or surfaces), using kernel metric on normal cycles. The advantage of such dissimilarity measure is that it will drive the matching considering the curvature features of the shapes.

1.4 Computational Framework

In this section, we focus on the existing algorithms to obtain the optimal transformation between two configurations in the inexact matching problem (1.10). Let us first notice that in applications, the data are always discrete (e.g. pixels images, discrete curves, triangulated meshes, etc.) and for numerical implementation, the data attachment term A is in fact a dissimilarity measure between discrete structures. Thus, the inexact registration problem always depends on a finite number of points, namely the discretization points. Moreover, since the target shape is fixed, A depends only on the shape that is being deformed.

1.4.1 Discretization of the inexact matching problem

For the sake of simplicity, and since it will be our study subjects, we focus on the case where shapes are curves or surfaces. Two discrete shapes C and S are represented by a finite number of points, $x_1, \dots, x_N$ for C and $y_1, \dots, y_M$ for S (notice that there is no given correspondence between the points x_i and y_j, and even not the same number of points in C and S). The structure of C and S is given by a connectivity matrix that links the vertices x_i or y_j. For a shape C, the connectivity matrix M is a $n \times 2$ (or 3) matrix, where n is the number of faces in C and such that $x_{M_{l,2}}$ and $x_{M_{l,1}}$ (and $x_{M_{l,3}}$ in the case of discrete surface) represents the vertices of the face number l.

To reduce the complexity of the matching problem, we suppose that a diffeomorphism φ transforms a discrete shape C by moving each vertex x_i to $\varphi(x_i)$ but leaving the rigid structure of the triangulation unchanged. This means that $\varphi(C)$ is approximated by the triangulated mesh with vertices $(\varphi(x_i))_{1\leq i\leq N}$ and the same connectivity matrix. The registration problem depends thus only on a finite number of points: the current points $(\varphi(x_i))_{1\leq i\leq N}$, and it writes

$$\arg\min_{v\in L^2_V} \int_0^1 \|v_t\|^2_V \, dt + A\big((\varphi^v_1(x_i))_{1\leq i\leq N}\big). \tag{1.11}$$

where φ^v_1 is obtained through the flow of the vector field v_t:

$$\begin{cases} \dfrac{\partial \varphi^v_t}{\partial t} = v_t \circ \varphi^v_t \\ \varphi^v_0 = \mathrm{Id}. \end{cases}$$

1.4.2 Optimization on the initial momenta and geodesic shooting algorithm

Different strategies have been developed throughout the years to optimize (1.11). In [Beg et al., 2005], the authors derive the Euler-Lagrange equation of the registration problem in the case of images. The gradient of $E(v) = \int_0^1 \|v_t\|^2_V \, dt + \|I_0 \circ (\varphi^v_1)^{-1} - I_1\|^2_{L^2}$ is given, and the optimization procedure is made directly on $v \in L^2_V$. The main limitation of this approach is that at each step of the minimization, one needs to store the current trajectory $t \mapsto v_t$ on a grid associated with the image. Moreover, the trajectory $t \mapsto \varphi^v_t$ has no reason to be a geodesic path before convergence.

In [Glaunès, 2005], the author takes advantage of equation (1.7): the optimal vector field has an explicit expression thanks to the kernel K_V and the current positions of the points $x_{i,t}$:

$$v_t = \sum_{i=1}^{n} K_V(., x_{i,t}) p_{i,t}$$

where we recall that the p_i are called the momenta. This reduces the dimensionality of the problem, and the optimization can be made on the momenta $t \mapsto p_{i,t}$ rather than on the vector field v_t. However, there is still no guarantee that the path is a geodesic before convergence. The computational cost of such procedures was a motivation to develop greedy version of the LDDMM. In [Arsigny et al., 2006a], the authors focus on a one parameter subgroup of the group G_V. This is equivalent to considering the generated group of diffeomorphisms by integrating stationary vector field $u \in V$. From there, algorithms are proposed to compute the (approximated) exponential map (i.e. computing the flow of the constant vector field) and the logarithm map around the identity. This framework is valid only for small deformation, but it allows statistical analysis through the log-Euclidean metric: the statistic is done on the constant vector fields u, and the metric on diffeomorphisms is the Euclidean metric on the logarithms of the diffeomorphisms. This framework was first developed for diffusion tensor images, [Arsigny et al., 2006b].

A major step forward was made in [Miller et al., 2006]: they found out that in the LDDMM framework, the Lagrangian momentum is conserved. This conserved quantity gives an equation followed by the $p_{i,t}$, which allows for explicit geodesic equations

that we have already seen in (1.9). The geodesic path depends on few parameters: $q(0)$ and $p(0)$. This paves the way for new optimization strategy that relies on the geodesic shooting ([Miller et al., 2006, Miller et al., 2006], [Arguillère et al., 2015], [Arguillère, 2014] chapter 7) and that we explain in the following.

We can rewrite the inexact registration problem (1.11) as depending only on the initial momenta $p_0 = (p_{1,0}, \dots, p_{n,0})$:

$$\arg \min_{p_0 \in (\mathbb{R}^d)^n} J(p_0) := p_0^T K_V(q_0, q_0) p_0 + g(q(1)) \tag{1.12}$$

where $g(q(1)) = A(\varphi_v^1(q(0)), S)$, q_0 being fixed, and the geodesic path $(p(t), q(t))_{0 \leq t \leq 1}$ being obtained through the geodesic equations

$$\dot{q} = \partial_p H_r(q, p), \;\; \dot{p} = -\partial_q H_r(q, p). \tag{1.13}$$

This new formulation has several advantages. First, the minimization can be done on the initial momenta only, which reduces the problem to a finite dimensional problem. Moreover, at each step of the minimization, the trajectories are geodesics, obtained through the integration of (1.13). Finally, the representation of deformations with initial momenta is of great interest for statistical analysis. The deformations are indeed parametrized by vectors in $(\mathbb{R}^d)^n$, where all the classical statistical tools are available (e.g. [Durrleman et al., 2014]).

This new formulation requires to compute at each step the gradient of J with respect to p_0. It is immediate for the first term $p_0^T K_V(q_0, q_0) p_0$, but it is more involved for $g(q(1))$. Indeed, $g(q(1))$ depends on p_0 through the integration of geodesic equations. The quantity that is immediately accessible is $\nabla_{q(1)} g(q(1))$. Starting from $\nabla_{q(1)} g(q(1))$, we can obtain $\nabla_{p_0} g(q(1))$ with *backward integration of the linearized adjoint Hamiltonian system*:

$$\begin{cases} \begin{pmatrix} \dot{z} \\ \dot{\alpha} \end{pmatrix} = \begin{pmatrix} \partial_p(\partial_q H_r)^* z - \partial_q(\partial_q H_r)^* \alpha \\ \partial_p(\partial_p H_r)^* z - \partial_q(\partial_p H_r)^* \alpha \end{pmatrix}, \\ z(1) = -\nabla_{q(1)} g(q(1)), \\ \alpha(1) = 0 \end{cases} \tag{1.14}$$

and one can show (see for example [Arguillère et al., 2015]) that $\alpha(0) = -\nabla_{p_0} g(q(1))$. This allows to derive an explicit algorithm to solve the variational problem of inexact registration. This algorithm is often called *geodesic shooting*.

We describe the geodesic shooting in the case of a fixed step gradient descent but it can be set in any minimization procedure. We will go back to this consideration in Chapter 4.

Algorithm 1 Geodesic shooting with fixed-step gradient descent.

Input: q_0 (initial shape), δ (step size)
Output: $\arg\min_{p_0 \in (\mathbb{R}^d)^n} J(p_0)$
initialization: $p_0 = 0$
repeat
  Compute $(q(1), p(1))$ through *forward integration* of (1.13)
  Compute $\nabla_{q(1)} g(q(1))$
  Compute $\nabla_{p_0} g(q(1))$ through *backward integration* of (1.14)
  Compute $\nabla_{p_0} J(p_0) = K_v(q_0, q_0)p_0 + \nabla_{p_0} g(q(1))$
  $p_0 \leftarrow p_0 - \delta \nabla_{p_0} J(p_0)$.
until Convergence

1.5 Conclusion

In this chapter, we detailed the modelling aspect of computational anatomy and focused on the construction of the group of diffeomorphisms G_V as well as the geodesic equations that describe optimal paths in G_V when projected on the Landmarks shape space. Geodesic shooting allows to minimize the variational problem of inexact registration in a computational framework. However, the crucial point of the data attachment term has not been tackled yet in this manuscript. The next two chapters address the question of geometrical shapes representation. This representation is the first step to embed shapes in a space with an explicit metric that will play the role of the data attachment term A. As explained previously, this data attachment term is of importance since it drives the registration procedure (as it can be seen for example in the geodesic shooting algorithm with the appearance of $\nabla_{p_0} g(q(1))$). The properties of A will have a major impact on the quality of the matching. The contributions of the next two chapters is the design of a new data attachment term A, using kernel metrics on normal cycles, that takes into account the curvature information of the geometrical shapes (curves, surfaces).

Chapter 2

Theoretical Ground of the Shapes Representation with Normal Cycles

Sommaire

In this chapter, we focus on three different shapes representations: *currents*, *varifolds* and *normal cycles*. These notions are borrowed from the field of *geometric measure theory* whose reference book is from Federer [Federer, 1969]. This field was motivated in the second half of the 20th century by the calculus of variation, and more specifically by the *Plateau's problem* of finding a minimal area surface with constrained boundary: given a closed $(m-1)$-dimensional surface $\Gamma \subset \mathbb{R}^d$, find an m-dimensional surface S of least area such that $\partial S = \Gamma$. Solving this problem was a conceptual breakthrough. Indeed if the formulation is a classical minimization problem with constraint, the main difficulty was to provide a theoretical setting to embed surfaces in a topological space with nice properties. The specifications of this framework are the following: define a space where the surfaces can be represented, with a topology that allows some compactness properties for a minimizing sequence of the Plateau's Problem.

It is in this very spirit that Federer and Fleming developed the notion of *integral currents* as a generalization of oriented surfaces [Federer and Fleming, 1960] and positively answered the Plateau's problem. However, the orientation of currents is not always well suited to model surfaces. This is the case when considering soap bubbles that merge together. The frontier between two bubbles cannot be oriented in a way that is physically relevant. To overcome this limitation, one needs a generalization to *non-oriented surfaces*. This work was done by Almgren in [Almgren, 1966] where he introduced *varifolds*, later developed by Allard [Allard, 1972]. The varifold representation of surfaces allows to model film soap, and for example to prove that given n volumes in $\mathbb{R}^d$, there exists an area-minimizing cluster for those volumes. As convenient as these two settings may be, in this chapter we investigate the finer shape representations of *normal cycles*. The theory of normal cycles originated from Federer's work on *curvature measures* [Federer, 1959] and was pushed forward by Zähle [Zähle, 1986] who gave integral representation of these measures: this is the *normal cycle*. It provides another theoretical tool to represent surfaces and more generally shapes, encoding higher order informations as curvature.

Currents and varifolds have been successfully used in the field of computational anatomy to construct dissimilarity measures between shapes (see [Glaunès, 2005, Durrleman, 2010] for currents and [Charon, 2013] for varifolds). In these articles, an explicit metric is endowed in the space of currents or varifolds that gives a measure of the shapes dissimilarity. This aspect will be studied in Chapter 3. The present chapter focuses on the geometrical models.

Section 2.1 is a reminder of the vocabulary of differential forms. Section 2.2 recalls the concept of *rectifiability* as developed by Federer in [Federer, 1969]. Rectifiable sets are generalizations of submanifolds in the measure theory point of view. This is the appropriate notion of regularity, which we introduce for considering currents and varifolds in section 2.3. In section 2.4 we define the normal cycle of a set with *positive reach*. In subsection 2.4.3, we extend the notion of normal cycles for sets that are unions of sets with positive reach. This extension gives a setting that allows to represent discrete shapes (union of segments or triangulation meshes) as normal cycles. Section 2.5 focuses on the way the normal cycle encodes the curvature

on the shape. In section 2.6, we investigate the link between a shape represented as a varifold and a shape represented as a normal cycle. We will see that in some sense, the varifold representation is a projection of the normal cycle representation. This work paves the way for a unified framework for these representations as well as the endowed metrics.

2.1 Differential Forms

2.1.1 Exterior algebra and m-vectors

This section is a brief reminder for differential forms, as it underpins the theory of currents. Let us start with the *tensor algebra*. In the following, we denote $T^k(\mathbb{R}^d)$ the vector space of k-linear forms of $\mathbb{R}^d$.

Definition 2.1 (Tensor product)**.** *The tensor product* $\otimes : T^k(\mathbb{R}^d) \times T^l(\mathbb{R}^d) \to T^{k+l}(\mathbb{R}^d)$ *is a bilinear application defined as:*

$$f \otimes g(x_1, \dots x_k, y_1, \dots, y_l) = f(x_1, \dots, x_k) g(y_1, \dots, y_l).$$

If $(e_1, \dots, e_d)$ is a basis of $\mathbb{R}^d$ and $(dx_1^*, \dots dx_d^*)$ its dual basis, then $(dx_{i_1}^* \otimes \cdots \otimes dx_{i_k}^*)_{1 \leq i_1, \dots, i_k \leq d}$ is a basis of $T^k(\mathbb{R}^d)$. Moreover, if we denote $T(\mathbb{R}^d) := \bigoplus_{k=0}^{+\infty} T^k(\mathbb{R}^d)$, then $\big(T(\mathbb{R}^d), +, \otimes\big)$ is an algebra called the *tensor algebra.*

Definition 2.2 (The exterior algebra and exterior product)**.** *The exterior algebra,* $\Lambda(\mathbb{R}^d)$ *is the quotient of the tensor algebra* $T(\mathbb{R}^d)$ *by the two sided ideal* I*, generated by elements of the form* $f \otimes f$*. We endow this space with the operation called the* exterior product*,* $\wedge$*. The exterior product fulfils the following algebraic properties:*

1. $\wedge$ *is bilinear*
2. $\wedge$ *is skew-symmetric: if* $x, y \in \Lambda(\mathbb{R}^d)$*,* $x \wedge y = -y \wedge x$*.*

The quotient of $T(\mathbb{R}^d)$ by I can be decomposed as follows:

$$\Lambda(\mathbb{R}^d) = T(\mathbb{R}^d)/I = \left(\bigoplus_{i=0}^{+\infty} T^k(\mathbb{R}^d) \right) / I = \bigoplus_{i=0}^{+\infty} \big(T^k(\mathbb{R}^d)/I \big)$$

and we define the space of m-forms (or m-covectors) $\Lambda_m(\mathbb{R}^d) := T^k(\mathbb{R}^d)/I$. The exterior product provides a bilinear application $\wedge : \Lambda_k(\mathbb{R}^d) \times \Lambda_l(\mathbb{R}^d) \to \Lambda_{k+l}(\mathbb{R}^d)$. Starting from this, one can define in another way the spaces $\Lambda_m(\mathbb{R}^d)$:

$$\Lambda_1(\mathbb{R}^d) = (\mathbb{R}^d)^*, \ \Lambda_m(\mathbb{R}^d) = \mathrm{Span}\big\{ u_1 \wedge \cdots \wedge u_m \mid u_i \in (\mathbb{R}^d)^* \big\}$$

and one can see that a basis of $\Lambda_m(\mathbb{R}^d)$ is given by $(dx_{i_1}^* \wedge \cdots \wedge dx_{i_m}^*)_{1 \leq i_1 < \cdots < i_m < d}$.

It is possible to construct in an exact similar way the space of *m-vectors*:

$$\Lambda^m(\mathbb{R}^d) = \mathrm{Span}\{ x_1 \wedge \cdots \wedge x_m \mid x_i \in \mathbb{R}^d \}.$$

An element $\tau \in \Lambda^m(\mathbb{R}^d)$ is called a *simple* m-vector if it can be written $\tau = x_1 \wedge \cdots \wedge x_m$. If $\omega = u_1 \wedge \cdots \wedge u_m \in \Lambda_m(\mathbb{R}^d)$ and $\tau = x_1 \wedge \cdots \wedge x_m \in \Lambda^m(\mathbb{R}^d)$ are simple m-vector and simple m-forms, we have the dual pairing

$$\langle \omega | \tau \rangle = \det \left(u_i(x_j)_{1 \leq i,j \leq m} \right).$$

Remark 2.3. *We sum up here some consequences of the definition of* $\Lambda_m(\mathbb{R}^d)$*:*

- $u_1 \wedge \cdots \wedge u_m = 0$ *as soon as* $u_i = u_j$ *for some* i, j*. More generally, for any permutation* σ *of* $\{1, \ldots, m\}$*,*

$$u_{\sigma(1)} \wedge \cdots \wedge u_{\sigma(m)} = \varepsilon(\sigma) u_1 \wedge \cdots \wedge u_m.$$

- $\dim(\Lambda_m(\mathbb{R}^d)) = \binom{d}{m}$*. In particular,* $\dim(\Lambda_d(\mathbb{R}^d)) = 1$ *and is generated by the* d*-alternate form* det*.*
- *One can identify* $\Lambda^m(\mathbb{R}^d)$ *and* $\Lambda^{d-m}(\mathbb{R}^d)$*. To* $\tau = x_1 \wedge \cdots \wedge x_m \neq 0$*, we associate* τ' *the unique* $(d-m)$*-simple vector such that* $\tau' = x'_1 \wedge \cdots \wedge x'_{d-m}$ *with* $(x_1, \ldots, x_m, x'_1, \ldots, x'_{d-m})$ *a positively oriented basis of* $\mathbb{R}^d$ *and* $|\tau| = |\tau'|$*.*

one gets that $\Lambda_m(\mathbb{R}^d)^*$ is isomorph to $\Lambda^m(\mathbb{R}^d)$.

$\Lambda^m(\mathbb{R}^d)$ is an euclidean space (and so is $\Lambda_m(\mathbb{R}^d)$), with the canonical scalar product on m-simple vectors (denoted $\langle ., . \rangle_{\Lambda^m(\mathbb{R}^d)}$ or simply $\langle ., . \rangle$ when there is no ambiguity)

$$\langle u_1 \wedge \cdots \wedge u_m, v_1 \wedge \cdots \wedge v_m \rangle = \det \left((u_i \cdot v_j)_{1 \leq i,j \leq m} \right)$$

where $x \cdot y$ is the canonical scalar product on $\mathbb{R}^d$. The norm associated with this scalar product in $\Lambda^m(\mathbb{R}^d)$ is denoted $|.|_{\Lambda^m(\mathbb{R}^d)}$ or $|.|$. Via the Riesz representation theorem, we can associate to $w \in \Lambda_m(\mathbb{R}^d)$ a unique m-vector $\overline{w}$ such that $\forall u \in \Lambda^m(\mathbb{R}^d), \langle w | u \rangle = \langle \overline{w}, u \rangle$. A m-simple vector $x_1 \wedge \cdots \wedge x_m$ encodes all the information of the *oriented* m-parallelotope generated by the vectors $x_1, \ldots, x_m$. $|x_1 \wedge \cdots \wedge x_m|$ is the half of the m-volume of this parallelotope. In particular, if $e_1, \ldots, e_m$ is an orthonormal frame, $e_1 \wedge \cdots \wedge e_m$ is of unit norm and contains all the information of the oriented vector space $\text{span}\{e_1, \ldots, e_m\}$.

Remark 2.4. *The reader should pay attention: the notation* $\Lambda_m(\mathbb{R}^d)$ *and* $\Lambda^m(\mathbb{R}^d)$ *may be inverted depending on the references. With the Riesz representation theorem, we have an isomorphism between* $\Lambda_m(\mathbb{R}^d)$ *and* $\Lambda^m(\mathbb{R}^d)$*. It is usually not recommended to assimilate the two. However for our application, this identification is not problematic.*

The dual norm of $\omega \in \Lambda_m(\mathbb{R}^d)$ coincides with the Euclidian norm on $\Lambda_m(\mathbb{R}^d)$

$$|\omega| = \sup_{\substack{\tau \in \Lambda^m(\mathbb{R}^d) \\ |\tau| \leq 1}} \langle \omega | \tau \rangle .$$

In a geometric point of view, it may be interesting to consider the supremum over m-simple vectors rather than over $\Lambda^m(\mathbb{R}^d)$, as an m-simple vector encodes a clear geometrical information. This is the point of the *mass* of a m-form:

$$M(\omega) = \sup_{\tau \in \Lambda^m(\mathbb{R}^d)} \left\{ \langle \omega | \tau \rangle \;\middle|\; |\tau| \leq 1 \text{ and } \tau \text{ simple} \right\}$$

2.1.2 Differential forms

Now that we have an object that represents the oriented tangent space, we can define differential forms:

Definition 2.5 (smooth m-differential forms)**.** *The space of $\mathscr{C}^\infty$ m-differential forms of $\mathbb{R}^d$ is $\mathscr{D}^m(\mathbb{R}^d) := \mathscr{C}^\infty\big(\mathbb{R}^d, (\Lambda^m\mathbb{R}^d)^*\big)$.*

For our purpose, we will consider a simpler space of differential forms:

Definition 2.6 (m-differential forms)**.** *The space of continuous differential forms of degree m (or m-differential forms) vanishing at infinity is $\Omega_0^m(\mathbb{R}^d) := \mathscr{C}_0^0(\mathbb{R}^d, (\Lambda^m\mathbb{R}^d)^*)$. This is a Banach space with the supremum norm $\|\omega\|_\infty = \sup_{x\in\mathbb{R}^d} |\omega(x)|$ for $\omega \in \Omega_0^m(\mathbb{R}^d)$. We also define $\Omega_{k,0}^m(\mathbb{R}^d) := \mathscr{C}_0^k(\mathbb{R}^d, (\Lambda^m\mathbb{R}^d)^*)$ the space of m-differential forms of class $\mathscr{C}^k$, with partial derivatives up to order k vanishing at infinity.*

If $e_1, \dots, e_d$ is an orthonormal basis of $\mathbb{R}^d$, and $\omega \in \Omega_0^m(\mathbb{R}^d)$, then we can express ω in coordinates:

$$\omega(x) = \sum_{i_1<\dots<i_m} \alpha_{i_1,\dots,i_m}(x) dx_{i_1}^* \wedge \dots \wedge dx_{i_m}^*,$$

where $\alpha_{i_1,\dots,i_m} \in \mathscr{C}_0(\mathbb{R}^d, \mathbb{R})$.

Definition 2.7 (Pull-back of a differential form)**.** *Let $\omega \in \Omega_0^m(\mathbb{R}^d)$, $x \in \mathbb{R}^d$ and $\tau_1 \wedge \dots \wedge \tau_m \in \Lambda^m(\mathbb{R}^d)$, φ a diffeomorphism of $\mathbb{R}^d$. The* pull-back *action of φ on ω, $\varphi^\sharp\omega$ is:*

$$\big\langle \varphi^\sharp\omega(x) \big| \tau_1 \wedge \dots \wedge \tau_m \big\rangle = \langle \omega(\varphi(x)) | d\varphi_x.\tau_1 \wedge \dots \wedge d\varphi_x.\tau_m \rangle$$

Several operators on differential forms will be used in this manuscript We recall them in the following. We define first the *exterior derivative* of a m-differential form:

Definition 2.8 (Exterior derivative)**.** *The exterior derivative is the unique operator $d : \mathscr{D}^m(\mathbb{R}^d) \to \mathscr{D}^{m+1}(\mathbb{R}^d)$ such that:*

1. *d coincides with the differentiation on $\mathscr{C}^1(\mathbb{R}^d)$.*
2. *$d(\omega_1 \wedge \omega_2) = d\omega_1 \wedge \omega_2 + (-1)^{\deg\omega_1}\omega_1 \wedge d\omega_2$.*
3. *$d \circ d = 0$.*

If $\omega \in \mathscr{D}^m(\mathbb{R}^d)$ and its expression in the coordinates is

$$\omega(x) = \sum_{i_1<\dots<i_m} \alpha_{i_1,\dots,i_m}(x) dx_{i_1}^* \wedge \dots \wedge dx_{i_m}^*,$$

then

$$d\omega(x) = \sum_{i_1<\dots i_m} d\alpha_{i_1,\dots,i_m}(x) \wedge dx_{i_1}^* \wedge \dots \wedge dx_{i_m}^*.$$

Definition 2.9 (Interior product)**.** *Let $\omega \in \Omega_0^m(\mathbb{R}^d)$ and $X \in \mathscr{C}^0(\mathbb{R}^d, \mathbb{R}^d)$, the* interior product *of ω by X is the $(m-1)$-differential form ι_X defined as*

$$\iota_X\omega(x)(u_1 \wedge \cdots \wedge u_{m-1}) = \omega(x)(X(x) \wedge u_1 \wedge \cdots \wedge u_m)$$

Definition 2.10 (Lie derivative)**.** *Let $\omega \in \Omega_{1,0}^m(\mathbb{R}^d)$ and $X \in \mathscr{C}^0(\mathbb{R}^d, \mathbb{R}^d)$. X generates a one parameter subgroup of diffeomorphisms φ_t. The* Lie derivative $L_X\omega$ *of ω along X is*

$$L_X\omega = \frac{d}{dt}\Big|_{t=0}\left(\varphi_t^\sharp\omega\right).$$

2.2 Rectifiable Sets

In all this manuscript, m is a non-negative integer. We recall briefly the notion of m-dimensional Hausdorff measure $\mathscr{H}^m$. Let S be a set of $\mathbb{R}^d$. First, we define:

$$\mathscr{H}_\delta^m(S) = \inf\left\{\sum_{i=1}^{\infty}\alpha(m)\left(\frac{\operatorname{diam} A_i}{2}\right)^s \Big| S \subset \bigcup_{i=1}^{+\infty} A_i, \text{ and } \operatorname{diam} A_i \leq \delta\right\}$$

where $\alpha(m)$ is a normalization constant. Note that $\mathscr{H}_\delta^m(S)$ is non negative but can be infinite. The Hausdorff measure is

$$\mathscr{H}^m(S) := \sup_{\delta>0}\mathscr{H}_\delta^m(S) = \lim_{\delta\to 0}\mathscr{H}_\delta^m(S).$$

This is a Borelian measure in $\mathbb{R}^d$ and the d-dimensional Hausdorff measure coincides with the classical Lebesgue measure: $\mathscr{H} = \lambda^d$.

The Hausdorff measure is of importance since it allows to consider sub-dimensional volume in $\mathbb{R}^d$. For example, the Lebesgue measure of a curve in $\mathbb{R}^3$ is null but with the one dimensional Hausdorff measure, we retrieve the length of the curve. Moreover, with the properties of the Hausdorff measure we can define the Hausdorff dimension, $\dim_{\mathscr{H}}$ of a set X in $\mathbb{R}^d$:

$$\dim_{\mathscr{H}}(X) = \inf\{s \geq 0 \mid \mathscr{H}^s(X) = 0\} = \sup\{t \geq 0 \mid \mathscr{H}^t(X) = \infty\}.$$

For X a m-dimensional submanifold, $\mathscr{H}^m$ coincides on X with the volume form of X. For more details on the Haussdorff measure, one can see [Federer, 1969], 2.10.

We define now *m-rectifiable sets*, which are basically submanifolds defined via Lipschitzian maps ([Federer, 1969], 3.2.14)

Definition 2.11 (m-rectifiable sets)**.** *A set X of $\mathbb{R}^d$ is said* m-rectifiable *if there exists $(U_i)_{i\in\mathbb{N}}$ a sequence of bounded sets of $\mathbb{R}^m$ and $(f_i)_{i\in\mathbb{N}}$ a sequence of Lipschitz functions $f_i : U_i \to \mathbb{R}^d$ such that $\mathscr{H}^m\left(X \setminus \cup_{i\in\mathbb{N}} f(U_i)\right) = 0$*

Remark 2.12. *In the references, this definition corresponds to the notion of* countably rectifiable set*, but authors usually mean countably rectifiable when they write rectifiable.*

Remark 2.13. *There is an equivalent definition due to Federer ([Federer, 1969], 3.2.29): a set X is m-rectifiable if and only if $\mathscr{H}^m$-almost all of X is contained in a countable union of m-dimensional, $\mathscr{C}^1$-submanifolds.*

If X is a compact, m-rectifiable set, we can consider for $\mathscr{H}^m$-almost every $x \in X$ the tangent space of X at x, T_xX ([Federer, 1969], 3.2.16 and 3.2.19), and an *orientation* of X will be simply an orientation $o_x \in \{-1, 1\}$ of every tangent space T_xX such that the application $x \mapsto (T_xX, o_x)$ is $\mathscr{H}^m$ measurable on X. $o_x = 1$ if, and only if the orientation is the one induced by the canonical orientation of $\mathbb{R}^d$. Note that the orientation in the sense of a rectifiable set is far less restrictive than the classical orientation for a $\mathscr{C}^1$ submanifold and that some unorientable submanifolds can still be given an orientation in the sense of rectifiable sets.

The existence of a tangent space almost everywhere for a rectifiable set is closely linked to the existence of derivative for Lipschitzian maps:

Theorem 2.14 (Rademacher)**.** *Let $f : A \to \mathbb{R}^d$ where f is a Lipschitz function and A an open subset of $\mathbb{R}^m$. Then f is differentiable almost everywhere.*

If $f_i : U_i \to X$ is a local Lipschitz map of the rectifiable set X, then for almost all $x \in f(U_i)$, $T_xX = \mathrm{Im}\Big(df_i\big(f_i^{-1}(x)\big)\Big)$. The regularity of Lipschitz functions gives a generalization of the change of variables formula. For this, we need first to define the Jacobian of a Lipschitz function:

Definition 2.15 (m-Jacobian of a Lipschitz function)**.** *The m-dimensional Jacobian $J_mf(x)$ of a Lipschitz function $f : \mathbb{R}^m \to \mathbb{R}^d$ at point x is defined almost everywhere as:*

$$J_mf(x) := \big|df(x)(e_1) \wedge \cdots \wedge df(x)(e_m)\big|$$

where $e_1, \ldots, e_m$ is a positively oriented, orthonormal basis of $\mathbb{R}^m$.

Theorem 2.16 (Area formula, [Federer, 1969], 3.2.3)**.** *Suppose that $d \geq m$ and let A be a $\mathscr{H}^m$-measurable set . Let $u : A \subset \mathbb{R}^m \to \mathbb{R}$ be an integrable function, and $f : \mathbb{R}^m \to \mathbb{R}^d$ Lipschitz. Then*

$$\int_A u(x)J_mf(x)d\mathscr{H}^m(x) = \int_{\mathbb{R}^d} \sum_{x \in f^{-1}(y)} u(x)d\mathscr{H}^m(y).$$

Remark 2.17. *For $u \equiv 1$, the area formula generalizes the area for a Lipschitz image of a $\mathscr{H}^m$ mesurable set $f(A)$:*

$$\mathrm{Area}\big(f(A)\big) := \int_A J_mf = \int_{\mathbb{R}^d} \mathrm{Card}\Big(x \in f^{-1}(y)\Big)d\mathscr{H}^m(y)$$

The Co-Area formula handles the case where $m > d$ and will prove very useful since it allows slicing integrals.

Theorem 2.18 (Co-Area formula, [Federer, 1969], 3.2.12)**.** *Suppose that $m > d$. Let $f : \mathbb{R}^m \to \mathbb{R}^d$ be a Lipschitz map, $g : \mathbb{R}^m \to \mathbb{R}$ an integrable function and $A \subset \mathbb{R}^m$ a $\mathscr{H}^m$-measurable set. Then*

$$\int_A g(x) J_m f(x) d\mathscr{H}^m(x) = \int_{z \in \mathbb{R}^d} \left(\int_{f^{-1}(z)} g(x) d\mathscr{H}^{m-d}(x) \right) d\mathscr{H}^d(z).$$

Note that this theorem can be extended to the case where f is a Lipschitz function between two rectifiable sets X and W ([Federer, 1969], 3.2.22). We will make use of the Co-Area formula later in this manuscript.

The framework of rectifiable sets is very convenient to work with since it encompasses both the smooth case (smooth submanifold of $\mathbb{R}^d$) and the polyhedral case (e.g. triangulation meshes). Rectifiability is the right regularity for shapes to consider currents or varifolds that we introduce in the next section.

2.3 Various Shapes Representation: Currents and Varifolds

2.3.1 Currents

The concept of currents was first developed as a generalization of distributions. Similarly to Schwartz' theory of distribution, Federer and Fleming [Federer and Fleming, 1960] defined the space of m-dimensional currents, denoted $\mathscr{D}_m$ as the topological dual of the space of smooth, m-differential forms with compact support in $\mathbb{R}^d$, denoted $\mathscr{D}^m$, endowed with the topology of $\mathscr{C}^\infty$-convergence on compact subsets. A compact, oriented, m-rectifiable set X defines a current $[X]$ through the integration of differential forms on X ([Federer, 1969], Chap. 4):

$$[X](\omega) := \int_X \langle \omega(x) | \tau_X(x) \rangle \, d\mathscr{H}^m(x) \tag{2.1}$$

where $\tau_X(x) = \tau_1(x) \wedge \cdots \wedge \tau_m(x)$, with $(\tau_i(x))_{1 \leq i \leq m}$ a positively oriented, orthonormal basis of $T_x X$. Suppose that $f : U \subset \mathbb{R}^m \to X$ is a Lipschitz global parametrization of X, then

$$[X](\omega) = \int_U \left\langle \omega\Big(f(u)\Big) \middle| \frac{\partial f}{\partial u_1}(u) \wedge \cdots \wedge \frac{\partial f}{\partial u_m}(u) \right\rangle du_1 \ldots du_m.$$

If $\tilde{X}$ denotes the same rectifiable set X with opposite orientation, we have $[\tilde{X}] = -[X]$. A current T associated with the integration of differential forms over a rectifiable set X (i.e. $T = [X]$) is called a *rectifiable current*. We define also the *boundary* of a current: if $\omega \in \mathscr{D}^{m-1}$, $\partial T(\omega) := T(d\omega)$. Since $d^2 = 0$, ∂T has no boundary. If T is rectifiable and ∂T is rectifiable as well, T is said to be an *integral*

current.

The space of currents is inherently endowed with the weak topology as the dual of $\mathscr{D}^m$. However this topology is not interesting for the Plateau's problem since a limit of rectifiable currents needs not to be rectifiable. It is possible to define other topologies on this space. For example the *mass* of a current:

$$M(T) = \sup\Big\{T(\omega)|\omega \in \mathscr{D}^m, M(\omega) \leq 1\Big\}$$

where $M(\omega) = \sup_{x\in\mathbb{R}^d} M(\omega(x))$. If $T = [X]$ is rectifiable, then $M(T) = \mathscr{H}^m(X)$. At first, one could think of the mass to define a distance between shapes. However, if S and C are two m-rectifiable sets, with empty intersection, then $M([S] - [C]) = \mathscr{H}^m(S) + \mathscr{H}^m(C)$. This shows that M is not relevant for dissimilarity measure. Also, the topology defined by M is too strong to have interesting properties such as compactness. To overcome this, one defines the *flat norm*:

$$F(T) = \sup\Big\{T(\omega)|\omega \in \mathscr{D}^m, M(\omega) \leq 1,\ M(d\omega) \leq 1\Big\}.$$

The weak topology is weaker than the flat topology which is weaker than the mass topology. The next theorem justifies the introduction of the flat norm.

Theorem 2.19 (Compactness theorem. [Federer, 1969] 4.2.17)**.** *If K is a compact set in $\mathbb{R}^d$, $c > 0$, the set of integral currents with support in K such that $M(T) + M(\partial T) \leq c$ is compact for the flat topology.*

This compactness theorem is the heart of the existence of a solution for the Plateau's problem. However, for the purpose of computational anatomy, the flat semi-norm is not convenient since it has no closed form. Moreover the sophistication of the $\mathscr{C}^\infty$-topology is not necessary. That is why we will simplify the definition of currents for our use.

Remark 2.20. *There is another approach to define currents: the one of* flat chains *over a normed abelian group G, developed by Fleming in [Fleming, 1966]. Starting from formal finite sum of compact convex oriented polyhedra with coefficients in G, it allows to define currents with multiplicity in G rather than in $\mathbb{Z}$ as for the currents defined previously. If $G = \mathbb{Z}$, then this construction gives the same notion of currents. We will not investigate this point of view.*

The following definition of currents is the one that will be used in this manuscript.

Definition 2.21 (Currents)**.** *The space of m-currents in $\mathbb{R}^d$ is defined as the topological dual of $\Omega_0^m(\mathbb{R}^d) := \mathscr{C}_0^0\big(\mathbb{R}^d, (\Lambda^m(\mathbb{R}^d))^*\big)$, i.e. we consider $\Omega_0^m(\mathbb{R}^d)'$. $T \in \Omega_0^m(\mathbb{R}^d)'$ maps every differential form ω to $T(\omega) \in \mathbb{R}$ and*

$$T(\omega) \leq C_T \left\|\omega\right\|_\infty .$$

Now if X is a m-rectifiable set, let check that $[X]$ is a current in the sense of definition 2.21:

$$\begin{aligned}|[X](\omega)| &= \left| \int_X \langle \omega(x) | \tau_X(x) \rangle \, d\mathscr{H}^m(x) \right| \\ &\leq \int_X |\langle \omega(x) | \tau_X(x) \rangle| \, d\mathscr{H}^m(x) \\ &\leq \|\omega\|_\infty \, \mathscr{H}^m(X).\end{aligned}$$

Thus, $[X] \in \Omega_0^m(\mathbb{R}^d)'$.

Remark 2.22. *The space of currents contains rectifiable sets, but also much more irregular objects. For example, the so-called "punk" current (figure 2.1) is not rectifiable. In fact this remark prevents from the use of currents as it is for shape analysis. For example, given two rectifiable sets C and S one could think first of the straight line joining $[C]$ and $[S]$ in the space of currents as the interpolation between the shapes C and S. However, this straight line goes through irregular objects that have no geometrical meaning and thus have no interesting interpretation for shape analysis.*

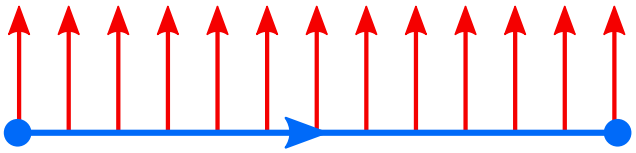

Figure 2.1: The "punk" current, P: the support of the current is the blue oriented curve C, but the tangential information in red does not correspond to the tangent space of the blue curve. Indeed, if $\omega \in \Omega_0^1(\mathbb{R})$, $P(\omega) = \int_C \langle \omega(x) | n(x) \rangle \, d\mathscr{H}^1(x)$ where $n(x)$ is the normal vector of C at x. The punk current is not associated with the integration over the blue rectifiable curve and thus is not a rectifiable current.

Approximation of the currents in a discrete setting

Definition 2.23 (Dirac current)**.** *Let $x \in \mathbb{R}^d$, $\alpha \in \Lambda^m(\mathbb{R}^d)$. For $\omega \in \Omega_0^m(\mathbb{R}^d)$, we define δ_x^α as follow:*

$$\delta_x^\alpha(\omega) := \langle \omega(x) | \alpha \rangle \, .$$

A dirac current δ_x^α contains a spatial information with x and a tangential information through α. The dirac current is usefull to approximate discrete shapes. Let illustrate this with a segment $C = [a, b]$ in $\mathbb{R}^d$, oriented from a to b. For such C, we have $\forall x \in C, \tau_C(x) = \frac{b-a}{|b-a|}$. If ω is a 1-differential form, we recall that the current associated with C, $[C]$ corresponds to the integration over C.

$$[C](\omega) = \int_C \langle \omega(x) | \tau_C(x) \rangle \, d\mathscr{H}^1(x)$$

We define an approximation of this integral, with an approximated current denoted $[C]_{approx}$:

$$\begin{aligned}[C]_{approx} &= \int_C \left\langle \omega\left(\frac{a+b}{2}\right) \middle| \frac{b-a}{|b-a|} \right\rangle d\mathscr{H}^1(x) \\ &= \left\langle \omega\left(\frac{a+b}{2}\right) \middle| b-a \right\rangle \\ &= \delta^{b-a}_{(a+b)/2}(\omega).\end{aligned}$$

Remark 2.24. *Of course, the notion of approximation depends on the metric we are considering. For now, we can suppose that $\delta^{b-a}_{(a+b)/2}$ approximate $[C]$ in the sense of the infinity norm on $\Omega^m_0(\mathbb{R}^d)$. Other metrics on the space of currents will be detailed in the next chapter.*

Now, if $\mathcal{C}$ is a union of segments $\mathcal{C} = \cup_{i=1}^n C_i$, $C_i = [a_i, b_i]$ with centre $c_i = \frac{a_i+b_i}{2}$, and $f_i = b_i - a_i$, then we immediately get the approximation of $[\mathcal{C}]$ that we will use in the numerical implementation:

$$[\mathcal{C}]_{approx} = \sum_{i=1}^n \delta^{f_i}_{c_i}. \tag{2.2}$$

The same work can be done for triangulated meshes, and with the canonical identification between $\Lambda^2(\mathbb{R}^3)$ and $\Lambda^1(\mathbb{R}^3) = \mathbb{R}^3$, we obtain for $\mathcal{T} = \cup_{i=1}^n T_i$ with barycentre c_i and orienting normal vector n_i:

$$[\mathcal{T}]_{approx} = \sum_{i=1}^n \mathrm{Area}(T_i)\delta^{n_i}_{c_i}. \tag{2.3}$$

Push-forward of a current

For a matching purpose, we will consider diffeomorphisms transforming our shapes. In order to have a shape representation with currents that is compatible with a registration problem, it is necessary to describe how a diffeomorphism acts on the current associated with a shape. For this, we define two actions: the *pull-back* action of diffeomorphisms on differential forms, and the dual *push-forward* action on currents.

Definition 2.25. *Let $\omega \in \Omega^m_0(\mathbb{R}^d)$, $x \in \mathbb{R}^d$ and $\tau_1 \wedge \cdots \wedge \tau_m \in \Lambda^m(\mathbb{R}^d)$, φ a diffeomorphism of $\mathbb{R}^d$.*

- *The* pull-back *action of φ on ω, $\varphi^\sharp\omega$ is:*

$$\left\langle \varphi^\sharp\omega(x) \middle| \tau_1 \wedge \cdots \wedge \tau_m \right\rangle = \langle \omega(\varphi(x)) | d\varphi(x)(\tau_1) \wedge \cdots \wedge d\varphi(x)(\tau_m) \rangle$$

- *The* push-forward *action of φ on $T \in \Omega^m_0(\mathbb{R}^d)'$, $\varphi_\sharp T$ is:*

$$\varphi_\sharp T(\omega) := T(\varphi^\sharp\omega)$$

The push-forward action on currents is geometric in the sense that if X is a m-rectifiable set of $\mathbb{R}^d$, then $\varphi_\sharp[X] = [\varphi(X)]$.

Cartan's formula and variation of the metric for currents

An important point to tackle is the variation of the current $[X]$ with respect to an infinitesimal displacement of the shape X. For this, we consider the continuous case and a smooth vector field $v : \mathbb{R}^d \to \mathbb{R}^d$. ϕ_t is the resulting flow of the vector field v. Let X be a m-dimensional smooth oriented compact submanifold of $\mathbb{R}^d$. We are interested here in the quantity:

$$\frac{d}{dt}\Big|_{t=0} \left\langle \phi_t^\sharp[X] \middle| \omega \right\rangle,$$

with $\omega \in \Omega^m_{1,0}(\mathbb{R}^d)$. This expression can be computed using the expression of the *Lie derivative* for differential form, namely :

$$L_v\omega := \frac{d}{dt}\Big|_{t=0} \phi_t^\sharp \omega.$$

Theorem 2.26 (Cartan's Formula)**.**

$$L_v\omega = \iota_v(d\omega) + d(\iota_v\omega).$$

Using Cartan's formula and Stokes' theorem, we get

$$\frac{d}{dt}\Big|_{t=0} \left\langle \phi_t^\sharp[X] \middle| \omega \right\rangle = \int_X \iota_v(d\omega) + \int_{\partial X} \iota_v\omega. \tag{2.4}$$

Now, in order to interpret this formula, let us anticipate the next chapter. We consider that the space of currents is embedded in a Hilbert space W' with a scalar product $\langle ., . \rangle_{W'}$, providing a metric on currents, and specifically on shapes represented as currents. Using the Riesz representation theorem, the current of a shape $[Y]$ is canonically associated with a differential form ω_Y and we have

$$\frac{d}{dt}\Big|_{t=0} \left\langle \phi_t^\sharp[X], [Y] \right\rangle_{W'} = \frac{d}{dt}\Big|_{t=0} \left\langle \phi_t^\sharp[X] \middle| \omega_Y \right\rangle.$$

A few comments can be made : first of all, the submanifold X needs to be oriented since we consider its current, and we used the Stokes formula. The second term expresses a specific behaviour on the border of X. Moreover, one can easily see that only the normal component of v is taken into account in (2.4): indeed, if v is tangent at X on every point, then the integrand vanishes. This remark shows that the gradient of the metric is orthogonal to the shape X.

2.3.2 Varifolds

As mentioned and studied in [Charon and Trouvé, 2013], the *orientation*, inherent in the concept of currents is a challenging issue in computational anatomy. Hence, any matching problem between two shapes requires first of all a coherent orientation for both shapes. Assigning coherent orientations between corresponding shapes can be difficult or even arbitrary in some practical applications. More importantly,

when using kernel metrics on the space of currents, this orientation issue can lead to artificial cancellation in the space of currents. A high spatial variation of the shape (compared to the typical size of the kernel used for the kernel metric) will not be seen by the metric, due to the orientation. To overcome this problem, Nicolas Charon proposed a model based on *varifolds* [Charon and Trouvé, 2013]. A varifold can be heuristically seen as an *unoriented* distribution of measures with support in the set of all *unoriented* tangent spaces of the shape.

To formalize this, consider the Grassmann manifold $G(d,m)$: it is the set of all *unoriented* m-dimensional subspaces in $\mathbb{R}^d$. It can be easily equipped with a metric d. Indeed, for a subspace $S \in G(d,m)$, we associate the orthogonal projection on S, denoted P_S. This is a linear application of $\mathbb{R}^d$. The distance d between $S,T \in G(d,m)$ is then the Frobenius norm of the associate orthogonal projections P_S and P_T:

$$d(S,T) := \sqrt{\sum_{i,j} |(P_S)_{i,j} - (P_T)_{i,j}|^2}.$$

where we assimilate P_S and its matrix in the canonical basis of $\mathbb{R}^d$.
We can now define varifolds, following [Allard, 1972].

Definition 2.27 (Varifolds)**.** *A m-dimensional varifold is a Borel finite measure on the product space $\mathbb{R}^d \times G(m,d)$. This is an element of $\mathscr{C}_0(\mathbb{R}^d \times G(d,m))'$.*

A m-rectifiable set X of $\mathbb{R}^d$ is canonically associated with a varifold denoted μ_X. For all Borel subsets of $\mathbb{R}^d \times G(d,m)$:

$$\mu_X(A) := \mathscr{H}^m\big(\{x | (x, T_x X) \in A\}\big). \tag{2.5}$$

With the Riesz representation theorem, μ_X can be associated with a unique linear form on $\mathscr{C}_0(\mathbb{R}^d \times G(d,m))$, still denoted μ_X:

$$\mu_X(u) = \int_X u(x, T_x X) d\mathscr{H}^m(x),\ \forall u \in \mathscr{C}_0(\mathbb{R}^d \times G(d,m)). \tag{2.6}$$

A varifold that is associated with a m-rectifiable set is called a *m-rectifiable varifold*. With a varifold V, we define a Radon measure on $\mathbb{R}^d$, $\|V\|$, called the *mass* of V. For all Borel subset B of $\mathbb{R}^d$

$$\|V\|(B) := V(\pi^{-1}(B)).$$

where $\pi : \mathbb{R}^d \times G(d,m) \to \mathbb{R}^d$, $(x,T) \mapsto x$ is the projection on $\mathbb{R}^d$. In other words, $\|V\|$ is the push-forward of V by π: $\|V\| = \pi_\sharp V$.

Approximation of the varifolds in the discrete setting

Definition 2.28 (Dirac varifold)**.** *If $(x,P) \in \mathbb{R}^d \times G(d,m)$, we define $\delta_{(x,P)}$ the varifold such that:*

$$\forall u \in \mathscr{C}^0(\mathbb{R}^d \times G(d,m)),\ \delta_{(x,P)}(u) = u(x,P).$$

As for currents, varifolds provide a representation of shapes that encompasses both the continuous and the discrete cases. We use a similar approximation as in (2.2), (2.3) for currents. If $\mathcal{C} = \cup_{i=1}^{n} C_i$ is a union of segments, with center c_i, we approximate $\mu_{\mathcal{C}}$ by $\mu_{\mathcal{C},approx}$:

$$\mu_{\mathcal{C},approx} = \sum_{i=1}^{n} \text{Length}(C_i)\delta_{(c_i,<C_i>)} \tag{2.7}$$

with $< C_i >$ the one dimensional space generated by C_i.

If $\mathcal{T} = \cup_{i=1}^{n} T_i$ is a triangulation mesh, with barycentre c_i for each T_i, then

$$\mu_{\mathcal{T},approx} = \sum_{i=1}^{n} \text{Area}(T_i)\delta_{(c_i,<T_i>)}. \tag{2.8}$$

One should notice that all these approximations are explicit given the polygonal mesh, and that they do not depend on the orientation given to each mesh.

Push-forward of a varifold

As for currents, the framework of varifolds allows to represent shapes in a dual vector space. Moreover, it is possible to define the *push-forward* action of diffeomorphisms on varifolds in a way that is compatible with the transport of shapes. If φ is a diffeomorphism of $\mathbb{R}^d$ and μ a varifold:

$$\forall u \in \mathscr{C}_0(\mathbb{R}^d \times G(d,m)),\ \varphi_\sharp\mu(u) := \mu(\varphi^\sharp u)$$

where $\varphi^\sharp u(x,T) = |J_m\varphi(x)|u\Big(\varphi(x), d\varphi(x)(T)\Big)$. If μ is a rectifiable varifold, *i.e.* $\mu = \mu_X$ where X is a m-rectifiable set, we have

$$\varphi_\sharp\mu_X = \mu_{\varphi(X)}.$$

First variation of a varifold

Varifolds are naturally endowed with a notion of convergence, coming from the weak topology on $\mathscr{C}_0(\mathbb{R}^d \times G(d,m))'$. This topology provides compactness properties that can be usefull for a calculus of variation point of view. However the limit varifold obtained after extraction needs not to be associated with a rectifiable set as explained in [Buet, 2014], 1.2.2. In order to guarantee such regularity for the limit object, we have to assume more regularity on varifolds. For this purpose, Allard introduced the *first variation of varifolds* ([Allard, 1972]). The link between the first variation of a varifold and a generalization of the mean curvature will be briefly tackled below. The interested reader can find more details in [Allard, 1972] and [Buet, 2014]. The study of the kind of curvature that is contained in the first variation of a varifold is interesting as this work will be done for normal cycles in section 2.5.

If $v \in \mathscr{C}^1(\mathbb{R}^d, \mathbb{R}^d)$ is a vector field, consider φ_t the local 1-parameter group of diffeomorphisms generated by v. The infinitesimal action of v on the mass of varifold μ is

$$\left.\frac{d}{dt}\right|_{t=0} \|\varphi_{t\sharp}\mu\| .$$

For B a Borel set of $\mathbb{R}^d$, one can see that the derivative at $t = 0$ of $\|\varphi_{t\sharp}\mu\|$ depends linearly on v and one can show that

$$\left.\frac{d}{dt}\right|_{t=0} \|\varphi_{t\sharp}\mu\| (B) = \int_{B\times G(d,m)} \operatorname{div}_P v(x) d\mu(x, P)$$

where $\operatorname{div}_P v(x) = \sum_{i=1}^m \langle dv(x)(e_i), e_i\rangle$ with $(e_1, \ldots, e_m)$ an orthonormal basis of P.

Definition 2.29 (First variation of a varifold)**.** *Let μ be a m-varifold. The* first variation *of μ is the linear form $\delta\mu : \mathscr{C}^1_c(\mathbb{R}^d, \mathbb{R}^d) \to \mathbb{R}$*

$$\delta\mu(v) = \int_{\mathbb{R}^d\times G(d,m)} \operatorname{div}_P(v)(x) d\mu(x, P). \tag{2.9}$$

The divergence of v on μ, and thereafter the first variation of a varifold is closely linked to the *mean curvature*. Indeed, if M is a smooth m-dimensional submanifold of $\mathbb{R}^d$, one defines the vector of mean curvature H as:

$$H(x) = -\sum_{j=1}^{d-m} \Big(\operatorname{div}_{T_xM} \nu_j(x)\Big)\nu_j(x).$$

where $(\nu_j(x))_{1\le j\le d-m}$ is an orthonormal frame of $N_xM = (T_xM)^\perp$ in $\mathbb{R}^d$. Now if v is a normal vector field, *i.e.* v is a section of the normal bundle, then:

$$\operatorname{div}_M v = -\langle v, H\rangle .$$

A varifold μ is said to have bounded first variation if $\delta\mu$ extend to a continuous linear functional on $\mathscr{C}_c(\mathbb{R}^d, \mathbb{R}^d)$. If so, we can associate with $\delta\mu$ a vectorial Radon measure still denoted $\delta\mu$. With the Radon-Nikodym theorem, we know that $\delta\mu$ can be decomposed as a sum of an absolutely continuous measure with respect to $\|\mu\|$ and a singular measure:

$$\delta\mu = -H\|\mu\| + \delta\mu_{sing}.$$

As explained in [Allard, 1972], H is a generalization of the mean curvature vector and $\delta\mu_{sing}$ is associated with the boundary of μ.

First variation of a curve. Let us now illustrate this fact in the case of a smooth curve in $\mathbb{R}^2$, parametrized with $\gamma : [0, L] \to \mathbb{R}^2$, with $|\gamma'(t)| = 1$, $\forall t \in [0, L]$. Then

if μ_γ is the varifold associated with $\gamma^* = \gamma([0, L])$ and $v \in \mathscr{C}^1_c(\mathbb{R}^2, \mathbb{R}^2)$, $v = v^\perp + v^\top$ with $v^\top$ the tangential part of v with respect to γ and $v^\perp$ the normal part of v.

$$\begin{aligned}
\delta\mu_\gamma(v) &= \int_\gamma \operatorname{div}_\gamma v = \int_\gamma \operatorname{div}_\gamma \left(v^\top + v^\perp\right) \\
&= \int_\gamma \operatorname{div}_\gamma v^\perp + \int_\gamma \operatorname{div}_\gamma \left(\widetilde{v^\top}\tau\right) \quad \text{where } v^\top = \widetilde{v^\top}\tau \\
&= -\int_\gamma \left\langle v^\perp, H\right\rangle + \int_\gamma d\widetilde{v^\top}(x)(\tau(x))d\mathscr{H}^1(x) + \int_\gamma \widetilde{v^\top} \underbrace{\operatorname{div}_\gamma \tau}_{=0} \\
&= -\int_\gamma \left\langle v^\perp, H\right\rangle + [\gamma^*](d\widetilde{v^\top}) = -\int_\gamma \left\langle v^\perp, H\right\rangle + \partial[\gamma^*](\widetilde{v^\top}) \\
&= -\int_\gamma \langle v, H\rangle + \widetilde{v^\top}(\gamma(L)) - \widetilde{v^\top}(\gamma(0)).
\end{aligned}$$

We have proven here that $\delta\mu_\gamma = -H\,\|\mu_\gamma\| + \delta_{\gamma(L)}\gamma'(L) - \delta_{\gamma(0)}\gamma'(0)$.

Remark 2.30. *Besides giving generalization of the mean curvature, the notion of first variation of a varifold provides a nice framework for compactness. Indeed, if μ_j is a bounded sequence of m-rectifiable varifolds, with bounded first variation, then one can extract a weak convergent subsequence from the μ_j such that the limit varifold μ is m-rectifiable. There is a guarantee that the limit object is associated with a m-rectfiable set. One can find more details in [Allard, 1972] and [Buet, 2014], theorem 1.13.*

We have seen in this section that shapes can be represented as Radon measures through the notion of varifolds. This representation does not require any orientation of the shapes contrary to the notion of currents. Moreover, we have seen that the first variation of a varifold encodes curvature information on the shape (scalar curvature for a curve, mean curvature for a surface). However, the varifold associated with a shape does not encode all the curvature information of the shape, even through the first variation. For example, the Gaussian curvature does not appear in the first variation.

The next section focuses on another shape representation: the normal cycle, also borrowed from geometric measure theory. We will see that the normal cycle of a shape encodes all the curvature information of the shape. Moreover, a theoretical link between varifolds and normal cycles will be drawn in section 2.6.

2.4 Normal Cycles

Normal cycles were introduced by the pioneer articles of [Wintgen, 1982] and [Zähle, 1986], inspired by Federer's work on curvature measure for a general type of sets (set with positive reach)[Federer, 1959]. The normal cycle of a shape is rigourosly the current associated with its normal bundle. The normal cycle encodes curvature information of X; more precisely one can compute integrals of curvatures

by evaluating the normal cycle over simple differential forms. This is explained by Zähle in [Zähle, 1986] :"Although curvature measures describe second order properties of the sets, the first order theory suffices for deriving integral geometric relations. The key is to consider the unit normal bundle of the sets as a locally $(d-1)$-rectifiable subset of $\mathbb{R}^{2d}$ and to observe that the first order infinitesimal behaviour of the unit normal bundle determines the curvature measures.". Moreover, it has a canonical orientation which is independent of the orientation of X (in fact X does not need to be oriented).

The aim of this section is to introduce properly the framework to define the normal cycle of a set with positive reach (subsection 2.4.1). Once this theoretical background is set, we will see in subsection 2.4.2 how normal cycles can be use as a shape representation. We describe the normal cycles of elementary shapes as a segment and a triangle. The setting of sets with positive reach is too restrictive to consider the normal cycles of polyhedral shapes. Hopefully, following the work of Zähle, [Zähle, 1987], it is possible to generalize normal cycles for unions of sets with positive reach that encompass the case of polyhedral shapes (subsection 2.4.3). In 2.4.4 we fit this framework in the field of computational anatomy i.e. we describe the action of diffeomorphisms on normal cycles. The precise link between normal cycles and curvature is postponed to the next section, 2.6.

2.4.1 Sets with Positive Reach and Unit Normal Bundle

The first step is to define a proper framework to consider shapes. For currents and varifolds for example, this framework is the one of m-rectifiable sets. Here, as we want to define a normal bundle associated with the shape, we will need a slightly different framework, which is sets with positive reach. The reach of a set $X \subset \mathbb{R}^d$ is closely linked to the uniqueness of projection on this set for sufficiently close points.

Definition 2.31 (Reach)**.** *For $\varepsilon > 0$, we define $X_\varepsilon = \{x \in \mathbb{R}^d | d(x, X) \leq \varepsilon\}$ and $\partial X_\varepsilon = \{x \in \mathbb{R}^d | d(x, X) = \varepsilon\}$. The reach of X, denoted reach(X), is the supremum of real numbers $\varepsilon > 0$ such that there exists a unique projection of any $x \in X_\varepsilon$ onto X. X is said to be a* positive reach set *if reach$(X) > 0$. If $0 < \varepsilon < $ reach(X), we denote $P_X : X_\varepsilon \to X$ the projection application.*

PR is the class of sets with positive reach.

Remark 2.32. *If X is convex,* Reach$(X) = +\infty$. *If X is a compact $\mathscr{C}^2$-submanifold, X has a positive reach.*

On a set with positive reach R, we can roll a ball of radius less than R. Thus, a set with positive reach can be seen heuristically as a set with bounded below curvature.

Definition 2.33 (Tangent Bundle and Unit Normal bundle)**.** *Let X be a set with positive reach.*

1. *The* tangent cone of X at point x *is*

$$T_x X := \left\{v \in \mathbb{R}^d, \forall \varepsilon > 0, \exists y \in X, \exists c > 0, |x - y| < \varepsilon \text{ and } |c(y - x) - v| < \varepsilon\right\}$$

It is a closed cone ([Federer, 1959]).
2. $TX := \{(x, v) : x \in X, v \in T_x X\}$ *is the* tangent bundle of X.
3. The normal cone of X at point x *is defined as the polar cone of* $T_x X$*:*

$$\mathrm{Nor}(X, x) := \left\{u \in \mathbb{R}^d, \forall v \in T_x X, \langle u, v\rangle \leq 0\right\}$$

$\mathrm{Nor}(X, x)$ *is a closed convex cone.*
4. The set of unit normal vectors *is defined as* $\mathrm{Nor}^u(X, x) := \mathrm{Nor}(X, x) \cap S^{d-1}$.
5. $\mathcal{N}_X = \{(x, n) \in \mathbb{R}^d \times S^{d-1}, x \in X, n \in \mathrm{Nor}^u(X, x)\}$ *is the* unit normal bundle of X.

Remark 2.34. *For a* $\mathscr{C}^2$*-submanifold, the unit normal bundle defined here coincides with the classical one, which is a* $(d-1)$*-submanifold in the* $(2d-1)$ *dimensional space* $\mathbb{R}^d \times S^{d-1}$.

Remark 2.35. *If* $x \in \mathring{X}$*, the interior of* X*, then* $T_x X = \mathbb{R}^d$ *and consequently* $\mathrm{Nor}^u(X, x) = \emptyset$.

Example 2.36 (Unit normal bundle of a curve in $\mathbb{R}^d$)**.** *We give here the description of the normal bundle associated with a regular curve in* $\mathbb{R}^d$*. Let* $\gamma : [0, L] \to \mathbb{R}^d$ *be the parametrization of a* $\mathscr{C}^2$ *regular non-intersecting and non-closed curve* C *in* $\mathbb{R}^d$*. On a regular point along the curve (i.e.* $\gamma(t)$*,* $0 < t < L$*), one has* $\mathrm{Nor}^u(C, \gamma(t)) = \gamma'(t)^\perp \cap S^{d-1}$*. For the singular part (i.e. the two endpoints), we denote* $S^+_v := \{u \in S^{d-1} \mid \langle u, v\rangle \geq 0\}$*. One can easily show that* $\mathrm{Nor}^u(C, \gamma(0)) = S^+_{-\gamma'(0)}$ *and* $\mathrm{Nor}^u(C, \gamma(1)) = S^+_{\gamma'(1)}$*. These are two half spheres with a coherent orientation with respect to the normal bundle (independent of the parametrization). See figure* 2.2 *for an illustration.*

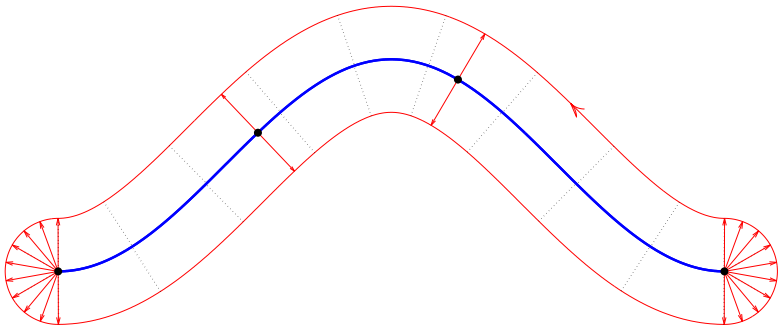

Figure 2.2: Illustration of the unit normal bundle for a regular non closed curve in the plane. The curve is in blue, the unit normal vectors associated with four points are represented as red arrows, and the resulting unit normal bundle is represented in red, with its canonical orientation. Note that this representation is only illustrative, as the true normal bundle belongs to the space $\mathbb{R}^2 \times S^1$ in this case

The generalized normal bundle $\mathcal{N}_X$ is a subset of $\mathbb{R}^d \times S^{d-1} \subset \mathbb{R}^d \times \mathbb{R}^d$, and since X is a set with positive reach, we can visualize $\mathcal{N}_X$ in $\mathbb{R}^d$: choose $0 < \varepsilon < \mathrm{Reach}(X)$ and consider the application

$$(x, n) \in \mathcal{N}_X \mapsto x + \varepsilon n \in \mathbb{R}^d \tag{2.10}$$

Thus, the normal bundle can be depicted in $\mathbb{R}^d$, using (2.10) by considering the ε-tube around the set X. This is the representation seen in figure 2.2.

Even if the definition of positive reach relies on few hypotheses, a set with positive reach has remarkable regularity properties:

Proposition 2.37. *Let X be a set with positive reach $R > 0$, and $0 < \varepsilon < R$. ∂X_ε is a $\mathscr{C}^1$-hypersurface (a $(d-1)$-dimensional, $\mathscr{C}^1$-submanifold in $\mathbb{R}^d$), with Lipschitzian normal vector field.*

Proof. We summarize here the main results of [Federer, 1959], 4.8. On X_ε, the projection P_X is well defined. Moreover, if we denote $\delta(x) = d(x, X)$ for every $x \in X_\varepsilon$, we can rewrite: $\partial X_\varepsilon = \{x \in \mathbb{R}^d | \delta(x) = \varepsilon\}$. 4.8. (5) of [Federer, 1959] guarantees that δ is continuously differentiable on the interior of $X_\varepsilon \setminus X$, with $\nabla\delta(x) = \frac{x - P_X(x)}{\delta(x)}$. Thus, ∂X_ε is defined as an implicit $\mathscr{C}^1$ real valued function, with non zero differential, and therefore is an hypersurface.

Moreover, one can show that the outward unit normal vector of ∂X_ε at point x is given by $n(x) = \frac{x - P_X(x)}{\delta(x)} = \nabla\delta(x)$. And 4.8 (9) of [Federer, 1959] states that $\nabla\delta$ is Lipschitzian on ∂X_ε. Thus, ∂X_ε has Lipschitzian normal vector field. □

The next proposition draws a more precise link between ∂X_ε and the normal bundle $\mathcal{N}_X$.

Proposition 2.38. *Let X be a set with positive reach, $0 < \varepsilon < Reach(X)$ and P_X be the projection on X, which is well defined on X_ε. Then*

$$\varphi_\varepsilon : \partial X_\varepsilon \to \mathcal{N}_X : y \mapsto \left(P_X(y), \frac{y - P_X(y)}{\varepsilon} \right)$$

is bijective and bi-Lipschitz, with inverse mapping

$$g_\varepsilon : \mathcal{N}_X \to \partial X_\varepsilon : (x, n) \mapsto x + \varepsilon n.$$

This proposition is the key argument to obtain the next theorem, which is fundamental to define normal cycles.

Theorem 2.39. *If X is a set with positive reach, $\mathcal{N}_X$ is a $(d-1)$-rectifiable set in $\mathbb{R}^d \times \mathbb{R}^d$.*

Proof. This is just an application of proposition 2.38 with proposition 2.37, and by using the definition of rectifiability seen above: $\mathcal{N}_X$ is the image of the Lipschitzian map g_ε of the $\mathscr{C}^1$ submanifold ∂X_ε. □

Thus, to a set with positive reach, one can associate the current of its $(d-1)$-rectifiable unit normal bundle. To have an explicit expression of this current, we need first to describe the tangent space.

Orthonormal basis of $T_{(x,n)}\mathcal{N}_X$

In order to consider the current associated with $\mathcal{N}_X$, it is interesting to describe the tangent space $T_{(x,n)}\mathcal{N}_X$ of the normal bundle at point (x,n). Let us start by considering ∂X_ε. It is a smooth hypersurface without border and thus it is canonically oriented. For $(x,n) \in \mathcal{N}_X$, $x+\varepsilon n \in \partial X_\varepsilon$ and we denote $\left(b_i^\varepsilon(x,n)\right)_{1\leq i\leq d-1}$ the directions of principal curvatures of ∂X_ε associated with the curvatures $(k_i^\varepsilon(x,n))_{1\leq i\leq d-1}$. As explained in [Zähle, 1986], $b_i^\varepsilon(x,n)$ is independant of ε and we write it $b_i(x,n)$. Moreover, we define $k_i(x,n) := \lim_{\varepsilon\to 0} k_i^\varepsilon(x,n)$. $k_i(x,n)$ expresses the curvature of X at point x, seen with n as the reference direction. For example, if X is a closed smooth surface of $\mathbb{R}^3$, oriented with a normal vector field $x \mapsto n(x)$, then we have $k_i(x,n(x)) = \kappa_i(x)$ where $\kappa_i(x)$ is the i-th principal curvature (signed). And one can show that

$$k_i(x,-n(x)) = -k_i(x,n(x)) = -\kappa_i(x).$$

This means that the curvature considered with $-n(x)$ as reference direction is opposite of the one considered with $n(x)$ as reference direction.

[Zähle, 1986] showed that an orthonormal basis of $T_{(x,n)}\mathcal{N}_X$ is then

$$a_i(x,n) := \left(\frac{b_i(x,n)}{\sqrt{1+k_i^2(x,n)}}, \frac{k_i(x,n)b_i(x,n)}{\sqrt{1+k_i^2(x,n)}}\right), \quad \text{for } i=1,\dots,d-1. \tag{2.11}$$

In case $k_i(x,n)=\infty$, we use the convention $\frac{1}{\sqrt{1+\infty^2}} = 0$ and $\frac{\infty}{\sqrt{1+\infty^2}} = 1$.

Remark 2.40. *A few comments can be made on this orthonormal basis. This expression formalizes the fact that the first order information of the normal bundle gives curvature information of the initial shape X through the $k_i(x,n)$. We separate two cases.*

Let start with the degenerate case $k_i(x,n) = \infty$. It occurs if, and only if $k_i^\varepsilon(x,n) = \frac{1}{\varepsilon}$. This corresponds to direction $b_i^\varepsilon(x,n)$ such that $\partial X_\varepsilon \cap \left(x + \operatorname{span}\left\{b_i^\varepsilon(x,n), n\right\}\right)$ is a circle with center x and radius ε. For example suppose that C is a curve in $\mathbb{R}^3$, $(x,n) \in \mathcal{N}_C$ and $\tau(x)$ is a unit tangent vector of C at x. Then $b_2^\varepsilon(x,n) = \tau(x) \times n$ is a direction of principal curvature for ∂C_ε and $k_2^\varepsilon(x,n) = \frac{1}{\varepsilon}$. Heuristically, $k_i(x,n) = \infty$ implies that the considered set with positive reach X is of dimension less than $d-1$ and the direction $b_i(x,n)$ is orthogonal to the tangent space of X at x.

The case $k_i(x,n) \neq \infty$ corresponds to $b_i(x,n)$ in the tangent space of X at x. We see in the expression of the orthonormal basis of $\mathcal{N}_X$ that the curvature of the set X mixes spatial and spherical components. If $k_i(x,n) = 0$, i.e. if the direction $b_i(x,n)$ corresponds to a flat direction on X, then the spherical component of the vector $a_i(x,n)$ vanishes.

We see with this remark that the information on the curvatures of the set X can be read on the expression of the orthonormal basis of $T_{(x,n)}\mathcal{N}_X$.

Orientation of $\mathcal{N}_X$

A last aspect to precise is the orientation. We recall that a current is an oriented object, hence to define the current associated with the normal bundle, the normal bundle needs to be oriented. Again, a nice property of a set with positive reach is that its normal bundle has a canonical orientation which does not require the set itself to be oriented. From now on, we denote by π_0 the projection on the spatial space, and π_1 the projection on the normal space: $\pi_0 : (x,n) \in \mathbb{R}^d \times S^{d-1} \mapsto x$, $\pi_1 : (x,n) \in \mathbb{R}^d \times S^{d-1} \mapsto n$. *The unit normal bundle has a canonical orientation* arising from the orientation of ∂X_ε as follows: let $(e_1, \dots, e_d)$ be the standard basis of $\mathbb{R}^d$, and $(a_1(x,n), \dots, a_{d-1}(x,n))$ an orthonormal basis of $T_{(x,n)}\mathcal{N}_X$ (which is well defined $\mathscr{H}^{d-1}$-almost everywhere on $\mathcal{N}_X$). We say that $(a_1(x,n), \dots, a_{d-1}(x,n))$ is positively oriented if

$$\langle ((\pi_0 + \varepsilon\pi_1)(a_1(x,n)) \wedge \cdots \wedge (\pi_0 + \varepsilon\pi_1)(a_{d-1}(x,n)) \wedge n, e_1 \wedge \cdots \wedge e_d \rangle > 0. \quad (2.12)$$

This quantity is independent of $0 < \varepsilon < \mathrm{Reach} X$ [Zähle, 1986]. Then $a(x,n) = a_1(x,n) \wedge \cdots \wedge a_{d-1}(x,n)$ fulfilling (2.12) (independent of the choice of the orthonormal basis verifying the last hypothesis) may be considered as a $(d-1)$-vectorfield orienting $\mathcal{N}_X$.

2.4.2 Normal Cycle of a Set with Positive Reach

Before defining normal cycles, let us define decompositions of the spaces $\Lambda^1(\mathbb{R}^2 \times \mathbb{R}^2)$ and $\Lambda^2(\mathbb{R}^3 \times \mathbb{R}^3)$ and then of the spaces $\Omega_0^1(\mathbb{R}^2 \times S^1)$ and $\Omega_0^2(\mathbb{R}^3 \times S^2)$ into orthogonal sums. These decompositions will prove useful to formalize the curvature information contained in the normal cycles.

Proposition 2.41.

1. $\Lambda^1(\mathbb{R}^2 \times \mathbb{R}^2) = F_1^1 \oplus F_0^1$ *where*

$$F_1^1 = \mathrm{Span}\left\{ \begin{pmatrix} \alpha \\ 0 \end{pmatrix} \middle| \alpha \in \mathbb{R}^2 \right\}, \quad F_0^1 = \mathrm{Span}\left\{ \begin{pmatrix} 0 \\ \alpha \end{pmatrix} \middle| \alpha \in \mathbb{R}^2 \right\}.$$

   F_1^1 is called the planar space and F_0^1 is called the spherical space.

2. $\Lambda^2(\mathbb{R}^3 \times \mathbb{R}^3) = F_2^2 \oplus F_1^2 \oplus F_0^2$ *where*

$$F_2^2 = \mathrm{Span}\left\{ \begin{pmatrix} \alpha \\ 0 \end{pmatrix} \wedge \begin{pmatrix} \beta \\ 0 \end{pmatrix} \middle| \alpha, \beta \in \mathbb{R}^3 \right\}, \; F_1^2 = \mathrm{Span}\left\{ \begin{pmatrix} \alpha \\ 0 \end{pmatrix} \wedge \begin{pmatrix} 0 \\ \beta \end{pmatrix} \middle| \alpha, \beta \in \mathbb{R}^3 \right\},$$

$$F_0^2 = \mathrm{Span}\left\{ \begin{pmatrix} 0 \\ \alpha \end{pmatrix} \wedge \begin{pmatrix} 0 \\ \beta \end{pmatrix} \middle| \alpha, \beta \in \mathbb{R}^3 \right\}.$$

   F_2^2 is the planar space, F_1^2 the cylindrical space and F_0^2 the spherical space.

These sums are orthogonal with respect to the canonical scalar product (see section 2.1).

Definition 2.42.

1. $\Omega_0^1(\mathbb{R}^2 \times S^1) = W_1^1 \oplus W_0^1$ *with*

$$W_i^1 = \text{Span}\left\{\omega \in \Omega_0^1(\mathbb{R}^2 \times S^1) \middle| \forall (x,n) \in \mathbb{R}^2 \times S^1,\ \omega(x,n) \in (F_i^1)^*\right\}.$$

W_1^1 is still called the planar space of $\Omega_0^1(\mathbb{R}^2 \times S^1)$ and W_0^1 the spherical space.

2. $\Omega_0^2(\mathbb{R}^3 \times S^2) = W_2^2 \oplus W_1^2 \oplus W_0^2$ *with*

$$W_i^2 = \text{Span}\left\{\omega \in \Omega_0^2(\mathbb{R}^3 \times S^2) \middle| \forall (x,n) \in \mathbb{R}^2 \times S^1,\ \omega(x,n) \in (F_i^2)^*\right\}.$$

W_2^2 is the planar space, W_1^2 the cylindrical space and W_0^2 the spherical space.

Remark 2.43. *It is possible to generalize this construction for $\Omega_0^{d-1}(\mathbb{R}^d \times S^{d-1})$:*

$$\Omega_0^{d-1}(\mathbb{R}^d \times S^{d-1}) = W_{d-1}^{d-1} \oplus \cdots \oplus W_0^{d-1}.$$

W_{d-1}^{d-1} is called the planar space of $\Omega_0^{d-1}(\mathbb{R}^d \times S^{d-1})$ and W_0^{d-1} the spherical space.

We will see in section 2.5 that each space (planar, cylindrical and spherical) will allow to retrieve a specific kind of curvature when applied on a normal cycle.

Since $\mathcal{N}_X$ is an orientable rectifiable set of $\mathbb{R}^d \times \mathbb{R}^d$ (independently of any orientation of X), we can consider its current, an element of $\Omega_0^{d-1}(\mathbb{R}^d \times \mathbb{R}^d)'$, which is called the normal cycle. For later considerations, we introduce also the space $\Omega_0^{d-1}(\mathbb{R}^d \times S^{d-1}) = \mathscr{C}_0^0(\mathbb{R}^d \times S^{d-1}, \Lambda^{d-1}(\mathbb{R}^d \times \mathbb{R}^d)^*)$ and its topological dual $\Omega_0^{d-1}(\mathbb{R}^d \times S^{d-1})'$. Since integration of a differential form ω over $\mathcal{N}_X$ only depends on the values of ω in $\mathbb{R}^d \times S^{d-1}$, it is equivalent to consider the normal cycle as an element of $\Omega_0^{d-1}(\mathbb{R}^d \times \mathbb{R}^d)'$ or $\Omega_0^{d-1}(\mathbb{R}^d \times S^{d-1})'$.

Definition 2.44 (Normal cycle)**.** *The normal cycle of a set X with positive reach is the $(d-1)$-current associated with $\mathcal{N}_X$. If $\omega \in \Omega_0^{d-1}(\mathbb{R}^d \times S^{d-1})$ is a $(d-1)$-differential form on $\mathbb{R}^d \times S^{d-1}$, one has*

$$N(X)(\omega) := [\mathcal{N}_X](\omega) = \int_{\mathcal{N}_X} \langle \omega(x,n) | \tau_{\mathcal{N}_X}(x,n) \rangle \, d\mathscr{H}^{d-1}(x,n) \tag{2.13}$$

where $\tau_{\mathcal{N}_X}(x,n)$ is the $(d-1)$-vector associated with an orthonormal positively oriented basis of $T_{(x,n)}\mathcal{N}_X$. For any Borel subset $B \subset \mathbb{R}^d \times S^{d-1}$, we also define the restricted current $N(X) \llcorner \mathbb{1}_B$:

$$N(X) \llcorner \mathbb{1}_B(\omega) := N(X)(\omega \mathbb{1}_B) \tag{2.14}$$

Remark 2.45. *In the previous definition of the restriction of $N(X)$, $\omega \mathbb{1}_B$ is not necessarily continuous, which might seem as a problem given the definition of a normal cycle. However, as explained in [Federer, 1969], 4.1.7, since $N(X)$ is representable by integration (here it is canonically associated with the rectifiable set $\mathcal{N}_X$), it is sufficient for the differential form to be integrable over $\mathcal{N}_X$.*

Thus, with normal cycles we have a tool to canonically represent sets with positive reach. One should notice that the unit normal bundle of a shape is a $d-1$ dimensional object of $\mathbb{R}^d \times S^{d-1}$ and every single part of the initial shape has a component in the normal bundle that is not $\mathscr{H}^{d-1}$ negligible. This is a major difference compared to the currents or varifolds approach. Indeed, let consider any shape X that is m-rectifiable, with border ∂X that is $m-1$-rectifiable. Since the current or the varifold of X is a m-dimensional object, it will not take into account the border of X that is strictly less dimensional. This is not the case with the normal cycle since the unit normal bundle above the border is also $d-1$ dimensional.

This property makes the transition from the representation of a single convex cell (segment, triangle) to a polyhedral mesh not straightforward. Considering a polyhedral mesh, the intersection of two cells is strictly less dimensional than the initial cell. Thus, for a currents or varifolds representation, the intersection of two cells is not taken into account. This makes the additive property immediate: the current or the varifold of a polyhedral mesh is the sum of the current or varifold of the cells. However, for the normal cycles representation, intersection also has a component in the normal bundle and has to be considered. We need an additive property (see subsection 2.4.3). Another way of seeing this is that an object as simple as a union of two segments may not have positive reach. More generally, a polygonal mesh has not necessary a positive reach, and we will need a generalization of the definition of normal cycles to consider its normal cycle.

But first let us give the description of a normal cycle for elementary convex cells: a segment and a triangle. This description is of importance since it is the basic for the construction of normal cycles of discrete shapes (i.e. polyhedral approximations of curves or surfaces).

Normal cycle of a segment

Let $a, b \in \mathbb{R}^d$ and $C = [a, b]$ be the segment with extremities a and b. We denote $\tilde{C} = C \setminus \{a, b\}$. Following the reasoning in Example 2.36 one can make explicit the normal bundle of C. The notations are the same as in definition 2.33: for $x \in \tilde{C}$, $\mathrm{Nor}(C, x)$ is a $(d-2)$-sphere, orthogonal to C: $\mathrm{Nor}(C, x) = (b-a)^\perp \cap S^{d-2}$. For $x = a$ or b, $\mathrm{Nor}(C, x)$ is a half $(d-1)$-sphere, oriented in the outward direction to the segment: $\mathrm{Nor}(C, a) = S^+_{a-b}$ and $\mathrm{Nor}(C, b) = S^+_{b-a}$, where we recall that $S^+_u = \{v \in S^{d-1} | u.v \geq 0\}$.

Thus, the unit normal bundle is composed of two parts, a cylindrical part and a spherical part. By cylindrical part, we mean a subset of the normal bundle whose tangent spaces have one dimension in the spatial space and all the other dimensions in the normal space. By a spherical part, we mean a subset for which the tangent spaces all belong to the normal space. More precisely, $\mathcal{N}_C = \mathcal{N}_C^{cyl} \cup \mathcal{N}_C^{sph}$ with $\mathcal{N}_C^{cyl} := \tilde{C} \times ((b-a)^\perp \cap S^{d-1})$ (represented in red in figure 2.3 and figure 2.4) and $\mathcal{N}_C^{sph} := (\{a\} \times S^+_{a-b}) \cup (\{b\} \times S^+_{b-a})$ (represented in green in figure 2.3 and figure 2.4). These two parts are disjoint and the normal cycle $N(C)$ satisfies $N(C) = N(C)^{cyl} + N(C)^{sph}$ with $N(C)^{cyl} := [\mathcal{N}_C^{cyl}]$ and $N(C)^{sph} := [\mathcal{N}_C^{sph}]$.

Moreover, we have $N(C)^{cyl} \in \left(W_1^{d-1}\right)' \subset \Omega_0^{d-1}(\mathbb{R}^d \times S^{d-1})'$ and $N(C)^{sph} \in \left(W_0^{d-1}\right)' \subset \Omega_0^{d-1}(\mathbb{R}^d \times S^{d-1})'$ (with the notations of definition 2.42)

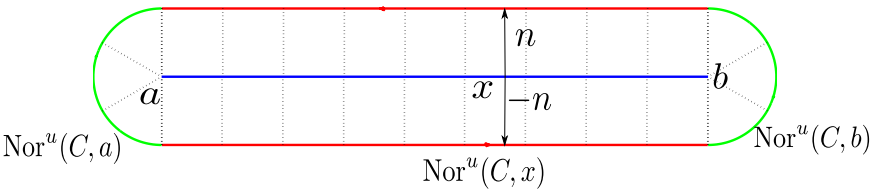

Figure 2.3: Illustration of the decomposition of the normal bundle of a segment in $\mathbb{R}^2$ with a cylindrical part (in red) and a spherical part (in green). Note that the actual normal bundle lives in $\mathbb{R}^2 \times S^1$

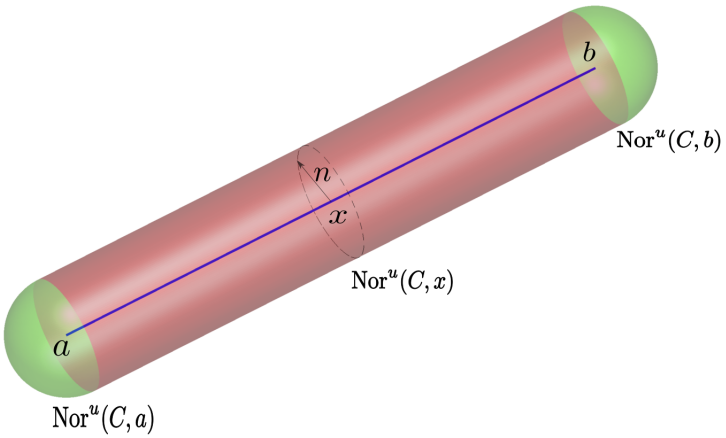

Figure 2.4: Illustration of the decomposition of the normal bundle of a segment in $\mathbb{R}^3$ with a cylindrical part (in red) and a spherical part (in green). Note that the actual normal bundle lives in $\mathbb{R}^3 \times S^2$

Normal Cycle of a Triangle

Let T be a triangle of $\mathbb{R}^3$ with vertices x_1, x_2, x_3 and edges : $f_1 = x_2 - x_1$, $f_2 = x_3 - x_2$, $f_3 = x_1 - x_3$. The normal vectors of the face are : $n_T = \frac{f_1 \times f_2}{|f_1 \times f_2|}$ and $-n_T$.

Note that the description of the normal cycle of a 2-dimensional polyhedral has been studied in [Cohen-Steiner and Morvan, 2003]. The description of the normal bundle of a triangle is quite straightforward. As illustrated in figure 2.5, it can be decomposed into a planar part, composed of two triangles (in cyan), a cylindrical part, composed of three "half" cylinders located at the edges (in red), and a spherical part, composed of three portions of sphere located at the vertices (in green).

$$\begin{aligned} \mathcal{N}_T^{pln} &:= \cup_{x \in T \setminus \partial T} \text{Nor}^u(T,x) = T \times \{-n_T, n_T\}, \\ \mathcal{N}_T^{cyl} &:= \cup_{i=1}^3 [x_i, x_{i+1}] \times S^{\perp +}_{f_i, f_i \times n_T}, \\ \mathcal{N}_T^{sph} &:= \cup_{i=1}^3 \{x_i\} \times S^{+}_{f_{i-1}, -f_{i+1}}, \end{aligned}$$

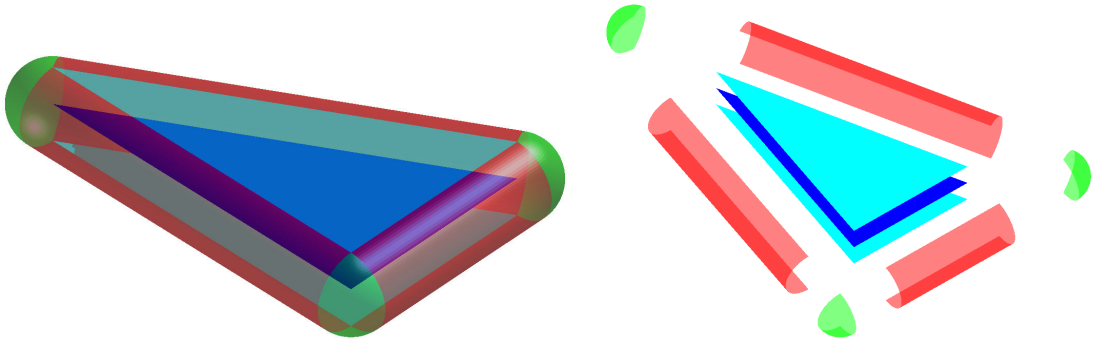

(a) Representation of the normal bundle in $\mathbb{R}^3$.

(b) Separation of the normal bundle for better visualisation.

Figure 2.5: Illustration of the decomposition of the normal bundle of a dark blue triangle into a planar (in cyan), a cylindrical (in red) and a spherical (in green) parts. Note that the actual normal bundle lives in $\mathbb{R}^3 \times S^2$.

where for any non zero vectors $\alpha, \beta \in \mathbb{R}^3$, we denote the semicircle $S^{\perp+}_{\alpha,\beta} = \left(S^2 \cap \alpha^\perp\right) \cap \{u | \langle u, \beta \rangle \geq 0\}$, and the portion of sphere $S^{+}_{\alpha,\beta} := \{u \in S^2, \langle u, \alpha \rangle \geq 0, \langle u, \beta \rangle \geq 0\}$. Note that f_i and n_T are oriented but this is not the case for $f_i \times n_T$ that represent a vector located in an edge and oriented outward from the triangle (independently of any orientation of the triangle). The sets $\mathcal{N}_T^{pln}$, $\mathcal{N}_T^{cyl}$ and $\mathcal{N}_T^{sph}$ have empty intersection and we define the associate currents:

$$
\begin{aligned}
N(T)^{pln} &= [\mathcal{N}_T^{pln}] \in \left(W_2^2\right)' \\
N(T)^{cyl} &= [\mathcal{N}_T^{cyl}] \in \left(W_1^2\right)' \\
N(T)^{sph} &= [\mathcal{N}_T^{sph}] \in \left(W_0^2\right)'.
\end{aligned}
$$

We have straightforwardly $N(T) = N(T)^{pln} + N(T)^{cyl} + N(T)^{sph}$.

We have seen the description of the normal bundle for segment and triangle. Notice that as previously said, every part of the segment or the triangle appears in the unit normal bundle: for a segment, the extremities are associated with half spheres, and for a triangle the edges are associated with half cylinders, and the vertices with portions of spheres. Starting from this description, we will see how to consider the normal cycle of a polyhedral mesh.

2.4.3 Unions of Sets with Positive Reach and Normal Cycles of Discrete Shapes

The theory of normal cycles can be extended to a class of sets containing unions of sets with positive reach, as developed in [Zähle, 1987, Rataj and Zähle, 2001, Thäle, 2008]. We briefly introduce this extension here, referring to these works for all details. The $\mathcal{U}_{PR}$ class is defined as the class of sets X which can be written as a locally finite union of sets X_i, $i \in \mathbb{N}$, such that for any finite subset of indices $I \subset \mathbb{N}$, $\cap_{i \in I} X_i$ is of positive reach. In particular sets of positive reach belong of course to

this class, and it contains also all finite unions of non-empty closed convex sets. The normal cycle $N(X)$ associated with a set $X \in \mathcal{U}_{PR}$ can be defined in a recursive way so that the following fundamental additive property is satisfied:

Definition 2.46 (Additive property)**.** *Assume that sets X, Y, $X \cap Y$ are with positive reach. Then we define*

$$N(X \cup Y) := N(X) + N(Y) - N(X \cap Y) \tag{2.15}$$

In the case where $X \cup Y$ is with positive reach, this definition is coherent : the left hand side and the right hand side in the definition are equal. In the case of a finite union of sets with positive reach: $X = \cup_{i=1}^{n} X_i$, belonging to $\mathcal{U}_{PR}$, it is easy to see that any combination of unions and intersections of the X_i also belongs to $\mathcal{U}_{PR}$. Hence the additive formula allows to write a recursive expression for the normal cycle of X, which can serve as a definition for normal cycle in this case: for $1 \leq k \leq n$, one has

$$N(X_1 \cup \cdots \cup X_k) = N(X_1 \cup \cdots \cup X_{k-1}) + N(X_k) - N((X_1 \cup \cdots \cup X_{k-1}) \cap X_k)$$

It is possible to define normal cycles in a more intrinsic way (see [Rataj and Zähle, 2001]), using the index function: for a closed subset $X \subset \mathbb{R}^d$, $x \in \mathbb{R}^d$ and $n \in S^{d-1}$, we define:

$$i_X(x,n) = \mathbb{1}_X(x)\left(1 - \lim_{\varepsilon \to 0} \lim_{\delta \to 0} \chi\big(X \cap B(x + (\varepsilon + \delta)n, \varepsilon)\big)\right)$$

where χ is the Euler-Poincaré characteristic. One can find an illustration of the index function in [Thäle, 2008], Section 3.3.

The normal bundle of $X \in \mathcal{U}_{PR}$ is then

$$\mathcal{N}_X = \left\{(x,n) \in \mathbb{R}^d \times S^{d-1} : i_X(x,n) \neq 0\right\}. \tag{2.16}$$

It can be shown ([Rataj and Zähle, 2001]) that $\mathcal{N}_X$ is a $(d-1)$-rectifiable set and the index function can be seen as a multiplicity function for the tangent space of the normal bundle at point x, with direction n. For $X \in \mathcal{U}_{PR}$, ι_X is locally integrable on $\mathcal{N}_X$ (proposition 4.3.1 [Zähle, 1987]). We define the normal cycle for a set $X \in \mathcal{U}_{PR}$ as

$$N(X)(\omega) := \int_{\mathcal{N}_X} \langle i_X(x,n)\omega(x,n) | \tau_{\mathcal{N}_X}(x,n)\rangle \, d\mathscr{H}^{d-1}(x,n) = \big([\mathcal{N}_X] \llcorner \iota_X\big)(\omega) \tag{2.17}$$

where we recall that when f is an integrable function, $\big([\mathcal{N}_X] \llcorner f\big)(\omega) := [\mathcal{N}_X](f\omega)$. Notice that when X is compact, $[\mathcal{N}_X] \llcorner f$ is a current as well (an element of $\Omega_0^{d-1}(\mathbb{R}^d \times S^{d-1})'$).

$i_X(x,n)$ can be seen as the multiplicity of the tangent space of the normal bundle at point (x,n), and is so that this definition of normal cycle is coherent with the additive property (2.15).

Decomposition of the Normal Cycle for Unions of Segments

The intersection of two non parallel segments is either empty or a single point. This means that we can always consider the normal cycle associated with an intersection of two segments. Thus, the formula (2.15) makes always sense when dealing with a union of segments. However, this formula is not ready to use. In order to overcome this difficulty, we introduce here a new decomposition of the normal bundle of a union of segments. As we will see, this decomposition will make the additive property straightforward and the normal cycle of each part of this cutting will be explicit.

In order to get a nice decomposition in the case of unions of segments, it is convenient to define the normal cycle associated with the "open" segment $\tilde{C}$ as: $N(\tilde{C}) := N(C) - N(\{a\}) - N(\{b\})$. Since the normal bundles of $\{a\}$ and $\{b\}$ are entire spheres, we see that $N(\tilde{C})$ expresses also as a sum of a cylindrical part and a spherical part: $N(\tilde{C}) = N(C)^{cyl} + N(\tilde{C})^{sph}$ with $N(\tilde{C})^{sph} := -[\{a\} \times S^+_{b-a}] - [\{b\} \times S^+_{a-b}]$. The sign $-$ indicates that the spheres have an orientation that is opposite to the canonical orientation of the sphere with outward normal vectors.

Now let $C_1 \cup \cdots \cup C_n$ be a union of n segments in $\mathbb{R}^d$. We can consider without loss of generality that the intersection of two segments $C_i \cap C_j$ is either empty or composed of a single point. Using the additive property (2.15) and the previous definition of the normal cycles of an "open" segment, it can be easily seen that the normal cycle of a union of segments can be obtained by summing the normal cycles associated with open segments and vertices. More precisely, if we denote $\{v_1, \ldots, v_N\}$ the vertices of $\cup_{i=1}^n C_i$, our decomposition of the normal bundle satisfies:

$$N(C_1 \cup \cdots \cup C_n) = \sum_{i=1}^{n} N(\tilde{C}_i) + \sum_{j=1}^{N} N(\{v_i\}) \tag{2.18}$$

Even though the additive property is now straightforward, we will go a bit further in this decomposition, as it will prove to be more efficient with the kernel metric. We can decompose (2.18) into cylindrical and spherical parts as follows:

$$N(C_1 \cup \cdots \cup C_n) = \left(\sum_{i=1}^{n} N(C_i)^{cyl} \right) + \left(\sum_{i=1}^{n} N(\tilde{C}_i)^{sph} + \sum_{j=1}^{N} N(\{v_i\}) \right) \tag{2.19}$$

This decomposition is sketched in figure 2.6.

Decomposition of the normal cycle for triangulation meshes

A slightly more complex decomposition is necessary for a union of triangles in $\mathbb{R}^3$. We apply the same process as for the union of segments. Let T be a triangle of $\mathbb{R}^3$ with vertices x_1, x_2, x_3 and edges : $f_1 = x_2 - x_1$, $f_2 = x_3 - x_2$, $f_3 = x_1 - x_3$. We denote by e_i the geometrical edges (i.e. unoriented) of the triangle. The normal vectors of the face are : $n_T = \frac{f_1 \times f_2}{|f_1 \times f_2|}$ and $-n_T$. First, we define the normal cycle of an "open" triangle $\tilde{T}$:

$$N(\tilde{T}) := N(T) - N(\partial T).$$

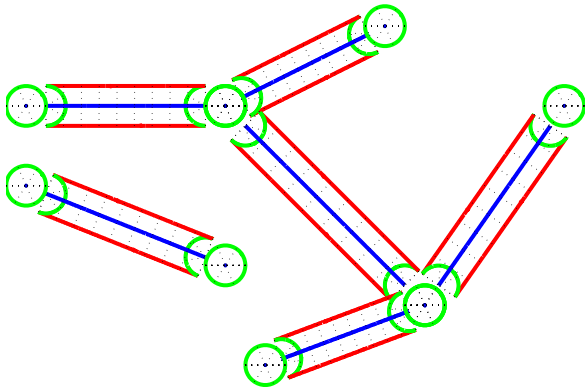

Figure 2.6: Decomposition of the normal bundle of a union of segments. In green, the spherical part (of a single point and of an extremity) and in red the cylindrical part. Note that this representation is only illustrative, as the true normal bundle belongs to the space $\mathbb{R}^2 \times S^1$ in this case.

∂T is a union of the edges $(e_i)_{1\leq i\leq 3}$, and the description of its normal bundle has been done right above: $N(\partial T) = \sum_{i=1}^{3} N(\tilde{e_i}) + \sum_{i=1}^{3} N(\{x_i\})$.

$$N(\tilde{T}) = N(T) - \sum_{i=1}^{3} N(\tilde{e_i}) - \sum_{i=1}^{3} N(\{x_i\})$$

Since we know an explicit description of $N(T)$, $N(\tilde{e_i})$ and $N(\{x_i\})$, we can express $N(\tilde{T})$ as a sum of a spherical part, cylindrical part and planar part:

$$N(\tilde{T}) = N(\tilde{T})^{pln} + N(\tilde{T})^{cyl} + N(\tilde{T})^{sph},$$

with

$$\begin{aligned}
\mathcal{N}_{\tilde{T}}^{pln} &:= \mathcal{N}_{T}^{pln} = T \times \{\pm n_T\},\\
\mathcal{N}_{\tilde{T}}^{cyl} &:= \cup_{i=1}^{3} e_i \times S^{\perp +}_{f_i, -f_i \times n_T},\\
\mathcal{N}_{\tilde{T}}^{sph} &:= \cup_{i=1}^{3} \{x_i\} \times S^{-}_{f_{i-1}, -f_{i+1}},
\end{aligned}$$

where $S^{-}_{\alpha,\beta} = \{u \in S^2 \mid \langle u, \alpha\rangle \leq 0\,,\ \langle u, \beta\rangle \leq 0\}$, and

$$\begin{aligned}
N(\tilde{T})^{pln} &:= [\mathcal{N}_{\tilde{T}}^{pl}] = \big[T \times \{\pm n_T\}\big],\\
N(\tilde{T})^{cyl} &:= -\sum_{i=1}^{3} \big[e_i \times S^{\perp +}_{f_i, -f_i \times n_T}\big],\\
N(\tilde{T})^{sph} &:= -\sum_{i=1}^{3} \big[\{x_i\} \times S^{-}_{-f_{i+1}, f_i}\big] + \sum_{i=1}^{3} N(\tilde{e_i})^{sph},
\end{aligned}$$

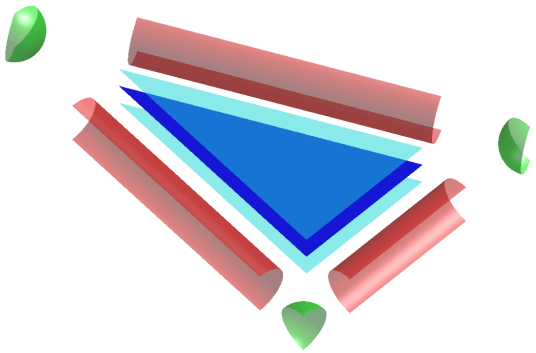

Figure 2.7: "Normal bundle" of an open triangle $\tilde{T}$ in blue. The normal bundle above the interior of the triangle, $\mathcal{N}^{pln}_{\tilde{T}}$, are two triangles in cyan. The normal bundle above the edges, $\mathcal{N}^{cyl}_{\tilde{T}}$ are three half cylinder, in red. The normal bundle over the vertices, $\mathcal{N}^{sph}_{\tilde{T}}$ are portions of sphere, in green.

In figure 2.7 one can find an illustration of the normal bundle of an open triangle.

After the introduction of $N(\tilde{T})$ we can proceed as for a union of segments. Suppose that $\mathcal{T} = \cup_{i=1}^{n_T} T_i$ is a triangulation where we require that the intersection of two triangles is either empty, or a single edge or a single vertex. We denote $(e_j)_{1\leq j\leq n_e}$ the edges and $(v_k)_{1\leq k\leq n_v}$ the vertices of the triangulation. Then one has:

$$N(\mathcal{T}) = \sum_{i=1}^{n_T} N(\tilde{T}_i) + \sum_{j=1}^{n_e} N(\tilde{e_j}) + \sum_{k=1}^{n_v} N(\{v_k\})$$

With this decomposition, the additive property is straightforward.

Approximation of normal cycles in the discrete setting

In order to get a simple formula for the kernel metric for polygonal meshes, we now approximate the planar and the cylindrical part of the normal cycle using Dirac evaluation functionals in the space of currents. For this, let us define such approximations:

Definition 2.47. *For any $x, \alpha \in \mathbb{R}^d$, $\alpha \neq 0$ and $P \in G(d,m)$, we define $\delta_{x,P^\perp}$ the current such that for any $(d-1)$-form ω in $\mathbb{R}^d \times S^{d-1}$,*

$$\delta_{x,P^\perp}(\omega) = \int_{S_P^\perp} \langle \omega(x,n) | (v_1,0) \wedge \cdots \wedge (v_m,0) \wedge \nu(n) \rangle \, d\mathcal{H}^{d-1-m}(n),$$

and

$$\delta_{x,P^\perp,\alpha}(\omega) = \int_{S_{P,\alpha}^{\perp+}} \langle \omega(x,n) | (v_1,0) \wedge \cdots \wedge (v_m,0) \wedge \nu(n) \rangle \, d\mathcal{H}^{d-1-m}(n),$$

with $S_P^\perp := S^{d-1} \cap P^\perp$, $S_{P,\alpha}^{\perp+} := S_P^\perp \cap \{u | \langle u, \alpha \rangle \geq 0\}$ and $(v_1, \ldots v_m)$ an orthonormal basis of P, $\nu(n) = (0, u_{m+1}) \wedge \ldots \wedge (0, u_{d-1-m})$ such that $(v_1, \ldots v_m, u_{m+1}, \ldots, u_{d-1-m}, n)$ is a positively oriented orthonormal basis of $\mathbb{R}^d$.

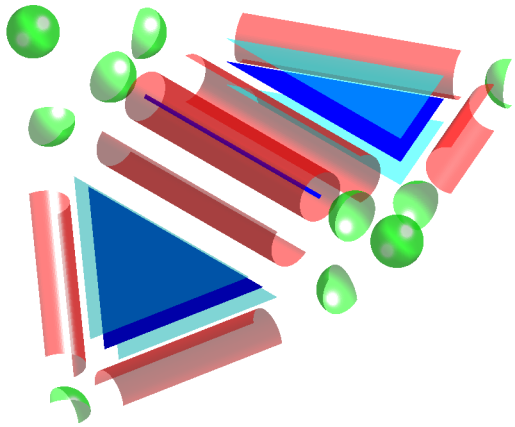

Figure 2.8: Decomposition of the normal bundle for two triangles with a common edge. In this figure, the two normal bundle of the open triangles appear. Then, we add (only once) the normal bundle of the open edge (the red cylinder and the two green half spheres). Then we add (only once) the normal bundle of the vertices of the edge (the two green spheres). Note that if the triangulation is reduced to this two triangles, we should add the normal bundle of the other edges of the triangles.

Now if we consider a union of segments C, we denote $x_1, \ldots, x_{N_C}$ the vertices of C and $f_i = x_{f_i^2} - x_{f_i^1}, 1 \leq i \leq n_C$ the edges of C (resp. S). For an edge f_i, $x_{f_i^1}$ and $x_{f_i^2}$ are its two vertices. Moreover, we define $c_i = \frac{1}{2}(x_{f_i^1} + x_{f_i^2})$ the center of the edge f_i.

We will now define the following approximation of the normal cycles $N(C)$:

$$N(C)_{approx} := N(C)^{sph} + N(C)^{cyl}_{approx}, \tag{2.20}$$

with

$$N(C)^{cyl}_{approx} := \sum_{i=1}^{n_C} \text{Length}(C_i)\delta_{c_i, <f_i>^\perp}.$$

For a triangulation $\mathcal{T}$, $\mathcal{T} = \cup_{i=1}^N T_i$, we denote $(e_j)_{1\leq j\leq n_e}$ the set of edges of $\mathcal{T}$ and $(x_k)_{1\leq k\leq n_v}$ the set of vertices . Given a triangle T_i, we consider its three edges f_i^1, f_i^2 and f_i^3. The barycentre of each triangle T_i is denoted b_i.

The normal cycles of $\mathcal{T}$ is approximated as follow:

$$N(\mathcal{T}) = N(\mathcal{T})^{sph} + N(\mathcal{T})^{cyl}_{approx} + N(\mathcal{T})^{pln}_{approx} \tag{2.21}$$

with

$$N(\mathcal{T})^{pln}_{approx} = \sum_{i=1}^{N} \text{Area}(T_i)\delta_{b_i, <T_i>} = \sum_{i=1}^{N} \delta^{\binom{f_i^1}{0}\wedge\binom{f_i^2}{0}}_{(b_i, n_{T_i})} + \delta^{-\binom{f_i^1}{0}\wedge\binom{f_i^2}{0}}_{(b_i, -n_{T_i})}$$

with $n_{T_i} = f_i^1 \wedge f_i^2$ and the notations of definition 2.23 and

$$N(\mathcal{T})^{cyl}_{approx} = \sum_{j=1}^{n_e} \text{Length}(e_j)\delta_{c_j, <e_j>^\perp} + \sum_{i=1}^{N}\sum_{l=1}^{3} -\text{Length}(f_i^l)\delta_{c_i, <f_i^l>^\perp, -f_i^l \times n_{T_i}}$$

This is an approximation for both the full cylinders (above the edges of the triangulation) and the half cylinders (above the edges seen as border of the triangles).

In short, this means we approximate integration of the differential form in the spatial domain by a single evaluation, and keep integration in the normal domain. This choice can be intuitively justified by the following reasoning: when considering a sequence of polygonal approximations of possibly non regular curves, the length of segments will always tend towards zero but some angles between segments will remain large. All this construction will simplify a lot the computation when we derive a kernel metric on the normal cycles (Chapter 3).

2.4.4 Transport of Normal Cycles with Diffeomorphisms

We focus on the action of diffeomorphism on normal cycles. We have seen in the section dedicated to currents the *push-forward* action of diffeomorphisms on currents. Since a normal cycle is a current whose support lives in $\mathbb{R}^d \times S^{d-1}$, we will use straightforwardly this action.

The question is: given a diffeomorphism φ and a shape X in $\mathbb{R}^d$, what is the action of φ on the normal bundle? Notice first that $\varphi : \mathbb{R}^d \to \mathbb{R}^d$ induces a diffeomorphism $\psi : \mathbb{R}^d \times S^{d-1} \to \mathbb{R}^d \times S^{d-1}$: for $(x, n) \in \mathbb{R}^d \times S^{d-1}$,

$$\psi(x, n) = \left(\varphi(x), \frac{d\varphi_x^{-T} n}{\|d\varphi_x^{-T} n\|}\right).$$

where $d\varphi_x^{-T} = (d\varphi_x^{-1})^T$.

In the following, we consider $\mathscr{C}^2$-diffeomorphisms.

Transport of the normal cycles associated with a set with positive reach

We suppose first that X is a set with positive reach. Since φ is a $\mathscr{C}^2$-diffeomorphism, $\varphi(X)$ is also a set with positive reach. Let $x \in X$. One can show that if $n \in \mathrm{Nor}(X, x)$, then $\frac{d\varphi_x^{-T} n}{\|d\varphi_x^{-T} n\|} \in \mathrm{Nor}(\varphi(X), \varphi(x))$ so that we have $\psi : \mathcal{N}_X \to \mathcal{N}_{\varphi(X)}$.

ψ is defined such that the action of a diffeomorphism φ on normal cycles satisfies:

$$\varphi.N(X) := \psi_\sharp N(X) = \psi_\sharp[\mathcal{N}_X] = [\psi(\mathcal{N}_X)] = [\mathcal{N}_{\varphi(X)}] = N(\varphi(X))$$

which is a geometric action as well.

It is possible to explicit this action: one needs to compute $d\psi_{(x,n)}$. As we will see, the second differential of φ is involved, which again is not surprising in view of the link between normal cycles and curvatures. We will compute the differential with respect to x: $d_x\psi_{(x,n)}$ and the differential with respect to n: $d_n\psi_{(x,n)}$. For this, recall that

$$d\left(u \mapsto \frac{u}{\|u\|}\right)_u h = \frac{1}{\|u\|}\left(h - \left\langle h, \frac{u}{\|u\|}\right\rangle \frac{u}{\|u\|}\right)$$

Then, using the chain rule for differentials, and denoting $n' = \frac{d\varphi_x^{-T} n}{\|d\varphi_x^{-T} n\|}$ we get:

$$d_n\psi_{(x,n)} = \left(0,\ \frac{1}{\|d\varphi_x^{-T}n\|}\left(d\varphi_x^{-T} - \left\langle n', d\varphi_x^{-T}\right\rangle n'\right)\right)$$

and

$$d_x\psi_{(x,n)} = \left(d\varphi_x,\ -d\varphi_x^{-T}d^2\varphi_x(.,.)^T n' + \left\langle n', d\varphi_x^{-T}d^2\varphi_x(.,.)^T n'\right\rangle n'\right)$$

where $d^2\varphi_x$ is the second differential of φ. If we let $p_{(n')^\perp}$ be the orthogonal projection on $(n')^\perp$, we can write these differentials:

$$\begin{aligned} d_x\psi_{(x,n)} &= \left(d\varphi_x,\ -p_{(n')^\perp}d\varphi_x^{-T}d^2\varphi_x(.,.)^T n'\right) \\ d_n\psi_{(x,n)} &= \left(0,\ p_{(n')^\perp}\frac{d\varphi_x^{-T}}{\|d\varphi_x^{-T}n\|}\right) \end{aligned} \tag{2.22}$$

To clarify the notation, let $(x,n) \in \mathbb{R}^d \times S^{d-1}$ and $(\tau,\nu) \in \mathbb{R}^d \times \mathbb{R}^d$. We have

$$d\psi_{(x,n)}.\begin{pmatrix}\tau\\ \nu\end{pmatrix} = \begin{pmatrix} d\varphi_x.\tau \\ \\ -p_{(n')^\perp}d\varphi_x^{-T}d^2\varphi(\tau,.)^T.n' + p_{(n')^\perp}\frac{d\varphi_x^{-T}.\nu}{\|d\varphi_x^{-T}n\|}\end{pmatrix}$$

Transport of the normal cycles associated with a set $\mathcal{U}_{PR}$

It is possible to generalize the transport of normal cycles for sets that are unions of sets with positive reach (subsection 2.4.3). Notice first that $\mathcal{U}_{PR}$ is stable under the transformation by diffeomorphisms: if φ is a $\mathscr{C}^2$-diffeomorphism of $\mathbb{R}^d$ and $X \in \mathcal{U}_{PR}$, then $\varphi(X) \in \mathcal{U}_{PR}$ (since the positive reach property is preserved by diffeomorphisms).

To extend the transport of normal cycles to sets in $\mathcal{U}_{PR}$, we will consider the definition of normal cycles seen in equation (2.23), using the index function. We recall that for a closed subset $X \subset \mathbb{R}^d$, $x \in \mathbb{R}^d$ and $n \in S^{d-1}$:

$$i_X(x,n) = \mathbb{1}_X(x)\left(1 - \lim_{\varepsilon\to 0}\lim_{\delta\to 0}\chi\big(X \cap B(x + (\varepsilon+\delta)n, \varepsilon)\big)\right)$$

where χ is the Euler-Poincaré characteristic and the normal bundle of $X \in \mathcal{U}_{PR}$ is then

$$\mathcal{N}_X = \left\{(x,n) \in \mathbb{R}^d \times S^{d-1} : i_X(x,n) \neq 0\right\}. \tag{2.23}$$

and is a $(d-1)$-rectifiable set. We recall also that the associated normal cycle $N(X)$ is defined as:

$$N(X)(\omega) := \int_{\mathcal{N}_X} \langle i_X(x,n)\omega(x,n)|\tau_{\mathcal{N}_X}(x,n)\rangle\, d\mathscr{H}^{d-1}(x,n), \tag{2.24}$$

which means that $N(X) = \big([\mathcal{N}_X]\llcorner\iota_X\big)$.

From there, we can define the action of diffeomorphism using the pull-back on differential forms: given a diffeomorphism of $\mathbb{R}^d$ φ and a set $X \in \mathcal{U}_{PR}$, we define the action of φ on $N(X)$:

$$\forall \omega \in \Omega_0^{d-1}(\mathbb{R}^d \times S^{d-1}),\ \varphi.N(X)(\omega) = \psi_\# N(X)(\omega) = N(X)(\psi^\# \omega)$$
$$= \int_{\mathcal{N}_X} \left\langle \iota_X(x,n)\omega(\psi(x,n)) \middle| d\psi_{(x,n)} \tau_{\mathcal{N}_X}(x,n) \right\rangle d\mathscr{H}^{d-1}(x,n)$$

where $\psi(x,n) = \left(\varphi(x), \frac{d\varphi_x^{-T} n}{\left\| d\varphi_x^{-T} n \right\|}\right)$ has been defined in the previous paragraph.

Notice that since the Euler-Poincaré characteristic is a topological invariant and ψ is a diffeomorphism, we can deduce that

$$\iota_X(x,n) = \iota_{\varphi(X)}(\psi(x,n)),$$

so that we have:

$$\begin{aligned} N(X)(\psi^\# \omega) &= \int_{\mathcal{N}_X} \left\langle \iota_X(x,n)\omega(\psi(x,n)) \middle| d\psi_{(x,n)} \tau_{\mathcal{N}_X}(x,n) \right\rangle d\mathscr{H}^{d-1}(x,n) \\ &= \int_{\mathcal{N}_X} \left\langle \iota_{\varphi(X)}(\psi(x,n))\omega(\psi(x,n)) \middle| d\psi_{(x,n)} \tau_{\mathcal{N}_X}(x,n) \right\rangle d\mathscr{H}^{d-1}(x,n) \\ &= \int_{\psi(\mathcal{N}_X)} \left\langle \iota_{\varphi(X)}(x',n')\omega(x',n') \middle| \tau_{\mathcal{N}_{\varphi(X)}}(x',n') \right\rangle d\mathscr{H}^{d-1}(x',n') \\ &= N(\varphi(X)). \end{aligned}$$

The action is thus geometric and we have:

$$\varphi.N(X) := \psi_\# N(X) = N(\varphi(X)).$$

This means that we can straightforwardly extend the action of diffeomorphisms of $\mathbb{R}^d$ on normal cycles to $\mathcal{U}_{PR}$ by taking into account the index function ι_X.

Variation of the metric for normal cycles

We are interested here in the infinitesimal variation of the normal cycle under the action of a vector field v. v generates a one parameter subgroup of diffeomorphisms, $(\phi_t)_{0 \leq t \leq \varepsilon}$. As explained for the variation of the metric for currents, the quantity of interest is

$$\left.\frac{d}{dt}\right|_{t=0} \langle \phi_t.N(X), N(S) \rangle_{W'}$$

where we anticipate again and suppose that our normal cycles are embedded in a dual Hilbert space W'. With the canonical isometry $\mathcal{K}_W : W' \to W$ we can write $\langle \phi_t.N(X), N(S) \rangle_{W'} = \langle \phi_t.N(X) | \mathcal{K}_W N(S) \rangle$. Thus it is sufficient to express the quantity

$$\left.\frac{d}{dt}\right|_{t=0} \langle \phi_t.N(X) | \omega \rangle$$

for $\omega \in \Omega_0^m(\mathbb{R}^d \times S^{d-1})$.

Since in our framework shapes are represented as current over the normal bundle, we can use equation (2.4) to compute the variation of the metric. Given a vector field v of displacement of X, we only have to express the resulting displacement $\tilde{v}$ of the unit normal bundle $\mathcal{N}_X$.

We will show that

$$\tilde{v}(x,n) = \begin{pmatrix} v(x) \\ -p_{n^\perp} \circ dv_x^T(n) \end{pmatrix} \tag{2.25}$$

which means that a point x of the spatial space is transported with v, and a corresponding unit normal vector is transported with the transpose of the differential of v at point x and projected on the orthogonal space of n.

To prove this, we start with the flow of diffeomorphisms ϕ_t generated by v. It induces a diffeomorphism ψ_t on the normal bundle:

$$\psi_t(x,n) = \left(\phi_t(x), \frac{d(\phi_t)_x^{-T} n}{\|d(\phi_t)_x^{-T} n\|}\right)$$

If we derive with respect to the time at $t = 0$ this expression, we get the vector field displacement $\tilde{v}$ of the normal bundle:

$$\tilde{v}(x,n) = \frac{d}{dt}\Big|_{t=0} \psi_t(x,n) = \left(v(x), \frac{d}{dt}\Big|_{t=0} \frac{d(\phi_t)_x^{-T} n}{\|d(\phi_t)_x^{-T} n\|}\right)$$

Using the same chain rule as for the derivative of ψ with respect to x, and the fact that $\frac{d}{dt}\Big|_{t=0} d(\phi_t)_x = dv_x$, we obtain the result.

Thus, with (2.4) we get immediately :

$$\frac{d}{dt}\Big|_{t=0} \langle \phi_t.N(X) | \omega \rangle = \int_{\mathcal{N}_X} \iota_{\tilde{v}}(d\omega) + \int_{\partial \mathcal{N}_X} \iota_{\tilde{v}}(\omega)$$

Since $\partial \mathcal{N}_X = \emptyset$, we get

Theorem 2.48 (variation of the metric for normal cycles)**.** *Let X be a m-dimensional compact submanifold of $\mathbb{R}^d$. v a smooth vector field of $\mathbb{R}^d$ and ϕ_t its associated flow. Then*

$$\frac{d}{dt}\Big|_{t=0} \langle \phi_t.N(X) | \omega \rangle = \int_{\mathcal{N}_X} \iota_{\tilde{v}}(d\omega) \tag{2.26}$$

where $\omega \in \Omega_{1,0}^m(\mathbb{R}^d \times S^{d-1})$

Now, if we explicit the last expression :

$$\begin{aligned} \frac{d}{dt}\Big|_{t=0} \langle \phi_t.N(X) | \omega \rangle &= \int_{\mathcal{N}_X} \iota_{\tilde{v}}(d\omega) \\ &= \int_{\mathcal{N}_X} \langle d\omega(x,n) | \tilde{v}(x,n) \wedge a_1(x,n) \wedge \cdots \wedge a_{d-1}(x,n) \rangle \, d\mathscr{H}^{d-1}(x,n) \end{aligned}$$

where $(a_1(x,n),\dots,a_{d-1}(x,n))$ is an orthonormal frame of $T_{(x,n)}\mathcal{N}_X$. If v is a tangential vector field, one can show that $\frac{d}{dt}\big|_{t=0}\langle\phi_t.N(X)|\omega\rangle = 0$.
To conclude this section, we have seen that the theory of normal cycles allows to represent shapes as currents with support in $\mathbb{R}^d\times S^{d-1}$. The additive property allows in particular to include polygonal meshes in the setting, and thus to consider both continuous shapes and their discrete representations in the same framework. This representation is independent of the initial orientation of the shapes, and encodes curvature information. Moreover, it can fit well in a matching problem with an explicit action of diffeomorphisms on normal cycles.

2.5 Curvatures and Normal Cycle

2.5.1 Lipschitz-Killing curvature

Here we formalize more specifically the link between the normal cycle of a set X with positive reach, and its curvatures. For this purpose, we define some *invariant, universal differential forms* on $\mathbb{R}^d\times S^{d-1}$, the Lipschitz-Killing forms.

Let $(x,n)\in\mathbb{R}^d\times S^{d-1}$. We set $e_1(x,n),\dots,e_{d-1}(x,n)\in\mathbb{R}^d$ such that $(e_1(x,n),\dots,e_{d-1}(x,n),n)$ is an orthonormal basis of $\mathbb{R}^d$, and we denote

$$\begin{aligned}\varepsilon_1 &= \begin{pmatrix} e_1 \\ 0\end{pmatrix},\dots,\varepsilon_d = \begin{pmatrix} n \\ 0\end{pmatrix}\\ \tilde{\varepsilon}_1 &= \begin{pmatrix} 0 \\ e_1\end{pmatrix},\dots,\tilde{\varepsilon}_{d-1} = \begin{pmatrix} 0 \\ e_{d-1}\end{pmatrix}\end{aligned} \tag{2.27}$$

where we omit the dependency on (x,n). This enables us to define a polynomial in the real variable t:

$$\nu(t) = (\varepsilon_1 + t\tilde{\varepsilon}_1)\wedge\cdots\wedge(\varepsilon_{d-1}+t\tilde{\varepsilon}_{d-1})$$

which is a $(d-1)$-vector field in $\mathbb{R}^d\times S^{d-1}$. Even though the $(e_i)_{1\le i\le d-1}$ are not uniquely defined (an orthonormal change of basis is still a valid candidate), the expression of ν is independent of the choice of this orthonormal basis, and thus is well defined.

For $0\le k\le d-1$, we denote ν_k the coefficient of the monomial t^{d-k-1} of ν, and define the $(d-1)$-form $\boldsymbol{\omega}_k$ which is canonically identified to the $(d-1)$-vector field

$$\overline{\boldsymbol{\omega}}_k := \frac{\nu_k}{(d-k)\alpha_{d-k}}$$

where α_k is the volume of the k-dimensional unit ball.

Definition 2.49 (Lipschitz-Killing forms)**.** *$\boldsymbol{\omega}_k$, $0\le k\le d-1$ is called the k^{th} Lipschitz-Killing form. The Lipschitz-Killing forms are euclidean motion invariants (see [Morvan, 2008], Chap. 19).*

Remark 2.50. *Notice that with this decomposition, and notations of definition* 2.42*, we have*

1. *for* $d = 2$, $\boldsymbol{\omega}_0$ *has values in* F_0^1 *and* $\boldsymbol{\omega}_1$ *has values in* F_1^1.
2. *for* $d = 3$, $\boldsymbol{\omega}_0$ *has values in* F_0^2, $\boldsymbol{\omega}_1$ *in* F_1^2 *and* $\boldsymbol{\omega}_2$ *in* F_2^2.

We can sum up the results of Federer and Zähle on these curvature measures in a theorem (see [Federer, 1959, Zähle, 1986, Zähle, 1987])

Theorem 2.51. *If* X *is a set with positive reach* $R > 0$ *and* $\varepsilon < R$, B *a Borel set of* $\mathbb{R}^d$, *we have*

$$\mathrm{Vol}\left((X \cap B)_\varepsilon\right) = \sum_{k=0}^{d} \alpha_k \mathcal{C}_{d-k}(X; B)\varepsilon^k \tag{2.28}$$

where $\mathcal{C}_k(X; B) = N(X) \llcorner \mathbb{1}_{B \times S^{d-1}}(\boldsymbol{\omega}_k)$, *for* $0 \leq k \leq d-1$ *and* $\mathcal{C}_d(X; B) := \mathscr{H}^d(X \cap B)$.

It can be shown, as detailed in [Bernig, 2003], that these $\mathcal{C}_k(X; .)$ coincide with the classical definition of curvatures for $\mathscr{C}^2$ hypersurfaces. In the case of an oriented m-dimensional submanifold X of $\mathbb{R}^d$ without boundary, one has (see [Morvan, 2008], chap. 21)

$$\mathcal{C}_i(X; \cdot) = 0, \quad m < i \leq d$$

which means that the first coefficients of the polynomial (2.28) vanish. Moreover, $\mathcal{C}_m(X; B) = \mathscr{H}^m(X \cap B)$ and $\mathcal{C}_{m-2}(X; B) = \int_{X \cap B} s(x) d\mathscr{H}^m(x)$ up to a constant, where $s(x)$ is the scalar curvature of X at x. The next proposition justifies the designation of curvature measures.

Proposition 2.52. *The* $\mathcal{C}_k(X; .)$ *are euclidean motion invariant, signed Radon measures. Moreover, they are additive: if* X, Y, $X \cup Y$ *and* $X \cap Y$ *have positive reach, then*

$$\mathcal{C}_k(X \cup Y; \cdot) = \mathcal{C}_k(X; \cdot) + \mathcal{C}_k(Y; \cdot) - \mathcal{C}_k(X \cap Y; \cdot)$$

To compute the evaluation of the normal cycle on the Lipschitz-Killing differential forms in the general case (C is a smooth m-dimensional submanifold of $\mathbb{R}^d$), we are interested in the quantity

$$N(C)(\omega) = \int_{\mathcal{N}_C} \langle \omega(x, n) | \tau_{\mathcal{N}_C}(x, n) \rangle \, d\mathscr{H}^{d-1}(x, n),$$

for ω a Lipschitz-Killing curvature. We use the Co-Area formula to slice the previous integral, integrating first on C, and then on the unit normal cone at point $x \in C$. We still denote $\pi_0 : \mathcal{N}_C \to C$, $(x, n) \mapsto x$. Moreover, for $x \in C$, $\pi_0^{-1}(x) = \mathrm{Nor}^u(x, C)$. An application of the Co-Area formula, theorem 2.18 gives:

$$\int_{\mathcal{N}_C} J_m \pi_0(x, n) \, \langle \omega(x, n) | \tau_{\mathcal{N}_C}(x, n) \rangle d\mathscr{H}^{d-1}(x, n) =$$

$$\int_C \left[\int_{\mathrm{Nor}^u(x,C)} \langle \omega(x, n) | \tau_{\mathcal{N}_C}(x, n) \rangle \, d\mathscr{H}^{d-1-m}(n) \right] d\mathscr{H}^m(x)$$

We need to compute $J_m\pi_0(x,n)$:

$$J_m\pi_0(x,n) = \sup_{i_1,\dots,i_m} \left(\left| d\pi_0(x,n)(a_{i_1}) \wedge \cdots \wedge d\pi_0(x,n)(a_{i_m}) \right| \right)$$

with $(a_1,\dots,a_{d-1})$ an orthonormal basis of $T_{(x,n)}\mathcal{N}_C$. We can choose the expression (2.11) for the a_i. One should notice that if X is m-dimensional, there are exactly m $k_i(x,n)$ that are not infinite, for almost every $x \in X$, and since $d\pi_0(x,n) = \pi_0$, we have:

$$J_m\pi_0(x,n) = \prod_{i=1|k_i(x,n)\neq\infty}^{d-1} \frac{1}{\sqrt{1+k_i^2(x,n)}}.$$

Note that if $x \in \partial C$, the m-dimensional Jacobian vanishes. Finally, we get

$$\int_C \left[\int_{\mathrm{Nor}^u(x,C)} \prod_{\substack{i=1 \\ k_i\neq\infty}}^{d-1} \sqrt{1+k_i^2(x,n)}\, \langle \omega(x,n) | \tau_{\mathcal{N}_C}(x,n) \rangle \, d\mathscr{H}^{d-1-m}(n) \right] d\mathscr{H}^m(x)$$
$$= \int_{\mathcal{N}_C \cap \pi_0^{-1}(C\setminus\partial C)} \langle \omega(x,n) | \tau_{\mathcal{N}_C}(x,n) \rangle \, d\mathscr{H}^{d-1}(x,n) \tag{2.29}$$

2.5.2 Examples of curvature measures for smooth curves and surface

To make the connection with the usual notion of curvature in differential geometry, we will derive the expression of the normal cycle in the simple cases of a smooth curve in $\mathbb{R}^2$ and a smooth surface in $\mathbb{R}^3$. Using two different methods, we will detail the evaluation of the Lipschitz-Killing differential forms on the normal cycle. First, we follow a "geometric measure point of view", with the Co-Area formula (theorem 2.18) and more specifically, Eq. (2.29). We cannot expect the Lipschitz Killing differential forms to retrieve information about signed curvature since these differential forms and the normal cycle do not depend of the orientation of the object. Hence, we will neither be able to have the *oriented* curvature of the curve, nor the mean curvature of the surface. However the length of the curve, the area of the surface and the Gaussian curvature of the surface, are unoriented quantities that will be retrieved.

The second method uses a parametrization of the normal bundle. This explicit parametrization gives more insight on how the normal cycle encodes the curvature information of the shape. We will see that choosing more specific differential forms than the Lipschitz-Killing's, we are able to have all the curvature information on the shape.

Smooth curve in $\mathbb{R}^2$

We now specify theorem 2.51 in the case of a regular curve C in $\mathbb{R}^2$. The Lipschitz-Killing 1-differential forms on $\mathbb{R}^2$ are

$$\boldsymbol{\omega}_0 = \frac{\tilde{\varepsilon}_1}{2},\ \boldsymbol{\omega}_1 = \frac{\varepsilon_1}{2},$$

where we keep the same notations as in definition 2.49.

Let $\gamma : [0, L] \to \mathbb{R}^2$ be an arc-length parametrization of C, with L its length. We denote $\tau(s) = \gamma'(s)$ the unit tangent vector and $n(s) = \tau(s)^\perp$ the unit normal vector such that $(\tau(s), n(s))$ is positively oriented. The scalar curvature $\kappa(s)$ is defined via the formula $n'(s) = \kappa(s)\tau(s)$. At each point $x = \gamma(s)$ of the curve, there are two unitary normal vectors $n(s)$ and $-n(s)$. Note that as explained when describing the generalized curvature $k_i(x, n)$, in the case of the curve in $\mathbb{R}^2$, $k_1(\gamma(s), n(s)) = \kappa(s)$ and $k_1(\gamma(s), -n(s)) = -\kappa(s)$. With a slight abuse of notation, we still write $\kappa(x)$ for $x \in C$ instead of $\kappa(s)$, with $x = \gamma(s)$. We do the same identification for n and τ. With (2.29), and since $\mathrm{Nor}^u(x, C) = \{n(x), -n(x)\}$, we obtain for the evaluation of $N(C)$:

$$\begin{aligned}\int_{\mathcal{N}_C} \langle \omega(x,n) | \tau_{\mathcal{N}_C}(x,n)\rangle \, d\mathscr{H}^1(x,n) = &\int_C \sqrt{1+\kappa^2(x)}\, \langle \omega(x,n(x)) | \tau_{\mathcal{N}_C}(x,n(x))\rangle \, d\mathscr{H}^1(x) \\ &+ \int_C \sqrt{1+\kappa^2(x)}\, \langle \omega(x,-n(x)) | \tau_{\mathcal{N}_C}(x,-n(x))\rangle \, d\mathscr{H}^1(x) \\ &+ \int_{S_a^+} \langle \omega(a,n) | \tau_{\mathcal{N}_C}(a,n)\rangle \, d\mathscr{H}^1(n) \\ &+ \int_{S_b^+} \langle \omega(b,n) | \tau_{\mathcal{N}_C}(b,n)\rangle \, d\mathscr{H}^1(n)\end{aligned} \tag{2.30}$$

where for $x \in C \setminus \partial C$,

$$\tau_{\mathcal{N}_C}(x, n(x)) = \frac{1}{\sqrt{1 + k_1^2(x, n(x))}} \begin{pmatrix} \tau(x) \\ k_1(x, n(x))\tau(x) \end{pmatrix} = \frac{1}{\sqrt{1+\kappa^2(x)}} \begin{pmatrix} \tau(x) \\ \kappa(x)\tau(x) \end{pmatrix}$$

and

$$\tau_{\mathcal{N}_C}(x, -n(x)) = \frac{1}{\sqrt{1 + k_1^2(x, -n(x))}} \begin{pmatrix} -\tau(x) \\ -k_1(x, -n(x))\tau(x) \end{pmatrix} = \frac{1}{\sqrt{1+\kappa^2(x)}} \begin{pmatrix} -\tau(x) \\ \kappa(x)\tau(x) \end{pmatrix}$$

and for $x = a$,

$$\tau_{\mathcal{N}_C}(a, n) = \begin{pmatrix} 0 \\ n(x)^\perp \end{pmatrix}$$

Finally, we have

$$\begin{aligned}N(C)(\omega) = &\int_C \left\langle \omega(x, n(x)) \middle| \begin{pmatrix} \tau(x) \\ \kappa(x)\tau(x) \end{pmatrix} \right\rangle d\mathscr{H}^1(x) + \int_C \left\langle \omega(x, -n(x)) \middle| \begin{pmatrix} -\tau(x) \\ \kappa(x)\tau(x) \end{pmatrix} \right\rangle d\mathscr{H}^1(x) \\ &+ \int_{S_a^+} \left\langle \omega(a,n) \middle| \begin{pmatrix} 0 \\ n(x)^\perp \end{pmatrix} \right\rangle d\mathscr{H}^1(n) + \int_{S_b^+} \left\langle \omega(b,n) \middle| \begin{pmatrix} 0 \\ (-n(x))^\perp \end{pmatrix} \right\rangle d\mathscr{H}^1(n).\end{aligned}$$

Now, all we have to do is to evaluate this expression on the Lipschitz-Killing differential forms. For $\boldsymbol{\omega}_1(x,n) = \varepsilon_1(x,n)/2$, we get $N(C)(\omega_1) = \text{Length}(C)$ and for $\boldsymbol{\omega}_0 = \tilde{\varepsilon}_1$, we get $N(C)(\omega_0) = 0$. It was expected since the scalar curvature κ is an oriented curvature. Note that it is possible to localize these expression. If B is a Borel set of $\mathbb{R}^2$, $\mathcal{C}_1(C;B) = N(C) \llcorner \mathbb{1}_{B\times S^1}(\boldsymbol{\omega}_1) = \text{Length}(\gamma([0,L]) \cap B)$ and $\mathcal{C}_0(C;B) = N(C) \llcorner \mathbb{1}_{B\times S^1}(\boldsymbol{\omega}_0) = 0$.

In fact the sign of the scalar curvature depends on the choice of orientation of the curve, whereas the normal cycle does not encode orientation. Thus it is normal that one cannot hope to retrieve the integral of the signed curvature from the full expression of the normal cycle. The non trivial application of theorem 2.51 in this case appears when considering the normal cycle of the compact domain $V \subset \mathbb{R}^2$ such that $\partial V = C$ (which exists via Jordan's theorem). It can be easily seen that $\mathcal{N}_V$ has two connected component and if $N(C)_1$ is the current associated with the first connected component of $\mathcal{N}_V$, we have $N(V) = N(C)_1$, so that the curvature measure $C_1(V,\cdot)$ corresponds to the integral of κ:

$$\mathcal{C}_0(V;B) = \int_{\gamma^{-1}(C\cap B)} \kappa(s) ds.$$

In general however, when considering non closed curves in $\mathbb{R}^2$ or curves in $\mathbb{R}^3$, C does not correspond to the boundary of any domain, and there is no way to get rid of the cancelling effect. In fact, it can be shown that $\mathcal{C}_{m-i}$ vanishes for i odd, in the case of a m submanifold of $\mathbb{R}^d$. But one should not misinterpret this point: it only means that the Lipschitz-Killing forms and the curvature measures are not the right tool in this context; the normal cycle itself still encodes all curvature information.

If we focus now on a parametrization of the normal bundle, we will see how to retrieve some (absolute) scalar curvature information on the curve. At each point $x = \gamma(s)$ of the curve, there are two unitary normal vectors $n(s)$ and $-n(s)$, so that the unit normal bundle $\mathcal{N}_C$ is composed of two disconnected curves with parametrizations $\Gamma_1(s) = (\gamma(s), n(s))$ and $\Gamma_2(s) = (\gamma(L-s), -n(L-s))$ (taking into account the canonical orientation of $\mathcal{N}_C$). The expression of the normal cycle over a 1-form ω thus writes

$$N(C)(\omega) = N(C)_1(\omega) + N(C)_2(\omega)$$

with

$$N(C)_1(\omega) := \int_0^L \langle \omega(\Gamma_1(s)) | \Gamma_1'(s) \rangle \, ds, \quad N(C)_2(\omega) := \int_0^L \langle \omega(\Gamma_2(s)) | \Gamma_2'(s) \rangle \, ds.$$

The 1-form ω can be identified to a vector-field $\bar{\omega}$ on $T(\mathbb{R}^2 \times S^1)$ written in the form

$$\bar{\omega}(x,n) = (\bar{\omega}_p(x,n), \bar{\omega}_n(x,n) e_1),$$

where $\bar{\omega}_p(x,n) \in \mathbb{R}^2$, $\bar{\omega}_n(x,n) \in \mathbb{R}$ and, as defined previously, e_1 the unitary vector such that (e_1, n) is a positively oriented basis of $\mathbb{R}^2$. With these notations one gets

after computations

$$N(C)_1(\omega) = \int_0^L \langle \bar{\omega}_p(\gamma(s), n(s)), \tau(s)\rangle \, ds + \int_0^L \bar{\omega}_n(\gamma(s), n(s))\kappa(s)ds,$$

and

$$N(C)_2(\omega) = -\int_0^L \langle \bar{\omega}_p(\gamma(s), -n(s)), \tau(s)\rangle \, ds - \int_0^L \bar{\omega}_n(\gamma(s), -n(s))\kappa(s)ds.$$

This shows clearly the link between the normal cycle and curvature in this case. For example it is clear from these expressions that one has

$$\sup\left\{N(C)(\omega), \omega \in \Omega_0^1(\mathbb{R}^2 \times S^1), \|\omega\|_\infty \leq 1\right\} = 2L + 2\int_0^L |\kappa(s)|ds,$$

and further one gets the length and the integral of the absolute value of the curvature as

$$L = \frac{1}{2}\sup\left\{N(C)(\omega), \omega \in W_1^1, \|\omega\|_\infty \leq 1\right\} = N(C)(\boldsymbol{\omega}_1),$$

$$\int_0^L |\kappa(s)|ds = \frac{1}{2}\sup\left\{N(C)(\omega), \omega \in \Omega_0^1(\mathbb{R}^2 \times S^1), \|\omega\|_\infty \leq 1, \bar{\omega}_p = 0\right\}.$$

And using the notations of definition 2.42,

$$L = \frac{1}{2}\sup\left\{N(C)(\omega), \omega \in W_1^1, \|\omega\|_\infty \leq 1\right\} = N(C)(\boldsymbol{\omega}_1) = \|N(C)\|_{\infty, W_1^1},$$

$$\int_0^L |\kappa(s)|ds = \frac{1}{2}\sup\left\{N(C)(\omega), \omega \in W_0^1, \|\omega\|_\infty \leq 1\right\} =: \|N(C)\|_{\infty, W_0^1}.$$

which can be also localized: for any Borel subset $B \in \mathbb{R}^2$,

$$\begin{aligned} \mathcal{H}^1(C \cap B) &= N(C) \llcorner \mathbb{1}_{B \times S^{d-1}}(\boldsymbol{\omega}_1) \\ \int_{\gamma^{-1}(C \cap B)} |\kappa(s)|ds &= \frac{1}{2}\sup\left\{N(C)(\omega), \omega \in W_0^1, \right. \\ &\qquad \left. \|\omega\|_\infty \leq 1, \operatorname{supp}\omega \subset B \times S^1\right\}. \end{aligned}$$

This clearly shows that curvature is encoded in the normal cycle representation of the curve. However, applying $N(C)$ to the Lipschitz-Killing form $\boldsymbol{\omega}_0$ gives the following (since $\boldsymbol{\omega}_0 = \tilde{\varepsilon}_1 = (0, e_1)$):

$$N(C)_1(\boldsymbol{\omega}_0) = \int_0^L \kappa(s)ds, \quad N(C)_2(\boldsymbol{\omega}_0) = -\int_0^L \kappa(s)ds,$$

so that $N(C)(\boldsymbol{\omega}_0) = 0$.

Surface in $\mathbb{R}^3$

We now specify theorem 2.51 in the case of a regular surface in $\mathbb{R}^3$. The Lipschitz-Killing 2-differential forms on $\mathbb{R}^3$ are

$$\boldsymbol{\omega}_0 = \frac{\tilde{\varepsilon}_1 \wedge \tilde{\varepsilon}_2}{4\pi}, \ \boldsymbol{\omega}_1 = \frac{\tilde{\varepsilon}_1 \wedge \varepsilon_2 + \varepsilon_1 \wedge \tilde{\varepsilon}_2}{4\pi}, \ \boldsymbol{\omega}_2 = \frac{\varepsilon_1 \wedge \varepsilon_2}{2}$$

where we keep the same notations as in definition 2.49.

For the sake of simplicity, we will consider a closed smooth surface S in $\mathbb{R}^3$, oriented with a normal vector field $x \mapsto n(x)$. With the same calculations as the one to obtain (2.30), we get:

$$\begin{aligned} N(S)(\omega) = &\int_S \left\langle \omega(x, n(x)) \middle| \begin{pmatrix} e_1(x) \\ \kappa_1(x) e_1(x) \end{pmatrix} \wedge \begin{pmatrix} e_2(x) \\ \kappa_2(x) e_2(x) \end{pmatrix} \right\rangle d\mathscr{H}^2(x) \\ &+ \int_S \left\langle \omega(x, -n(x)) \middle| - \begin{pmatrix} e_1(x) \\ -\kappa_1(x) e_1(x) \end{pmatrix} \wedge \begin{pmatrix} e_2(x) \\ -\kappa_2(x) e_2(x) \end{pmatrix} \right\rangle d\mathscr{H}^2(x) \end{aligned} \tag{2.31}$$

With this expression, we see that

$$\begin{cases} N(S)(\boldsymbol{\omega}_2) = \text{Area}(S), \\ N(S)(\boldsymbol{\omega}_1) = 0, \\ N(S)(\boldsymbol{\omega}_0) = \dfrac{1}{2\pi} \displaystyle\int_S \kappa_1(x)\kappa_2(x) d\mathscr{H}^2(x). \end{cases}$$

Once again, we see that with the Lipschitz-Killing differential forms, we are not able to retrieve the mean curvature of the surface S since it depends on the orientation of S. However, we retrieve the area and the Gaussian curvature of the surface. These expression can also be localized: for any Borel set $B \subset \mathbb{R}^3$,

$$\begin{cases} N(S) \llcorner \mathbb{1}_{B \times S^2}(\boldsymbol{\omega}_2) = \text{Area}(S \cap B), \\ N(S) \llcorner \mathbb{1}_{B \times S^2}(\boldsymbol{\omega}_1) = 0, \\ N(S) \llcorner \mathbb{1}_{B \times S^2}(\boldsymbol{\omega}_0) = \dfrac{1}{2\pi} \displaystyle\int_{S \cap B} \kappa_1(x)\kappa_2(x) d\mathscr{H}^2(x). \end{cases}$$

Consider now a global parametrization of the surface S, with

$$\gamma : U \subset \mathbb{R}^2 \to S, \ (u, v) \mapsto \gamma(u, v).$$

S is oriented with a normal vector field defined as

$$n(u, v) = \frac{\partial_u \gamma(u, v) \wedge \partial_v \gamma(u, v)}{\| \partial_u \gamma(u, v) \wedge \partial_v \gamma(u, v) \|},$$

where $\partial_u \gamma(u,v) = \frac{\partial \gamma}{\partial u}(u,v)$. The normal bundle of S has two connected component, $\mathcal{N}_S^1$ and $\mathcal{N}_S^2$ with parametrization

$$\Gamma(u,v) = \begin{pmatrix} \gamma(u,v) \\ n(u,v) \end{pmatrix} \text{ for } \mathcal{N}_S^1,$$
$$\tilde{\Gamma}(u,v) = \begin{pmatrix} \gamma(u,v) \\ -n(u,v) \end{pmatrix} \text{ for } \mathcal{N}_S^2.$$

Using these parametrizations, we compute $N(S)(\omega)$

$$\begin{aligned} N(S)(\omega) = &\int_U \big\langle \omega\big(\gamma(u,v), n(u,v)\big) \big| \partial_u \Gamma(u,v) \wedge \partial_v \Gamma(u,v) \big\rangle \, dudv \\ &+ \int_U \Big\langle \omega\big(\gamma(u,v), -n(u,v)\big) \Big| \partial_u \tilde{\Gamma}(u,v) \wedge \partial_v \tilde{\Gamma}(u,v) \Big\rangle \, dudv \end{aligned} \tag{2.32}$$

We can suppose that γ is a parametrization such that $(\partial_u \gamma, \partial_v \gamma)$ is an orthogonal frame of the tangent space, and such that $\partial_u \gamma$ is the direction of first principal curvature κ_1, and $\partial_v \gamma$ is the direction of second principal curvature κ_2, so that:

$$\begin{aligned} \partial_u \Gamma \wedge \partial_v \Gamma &= \begin{pmatrix} \partial_u \gamma \\ \kappa_1 \partial_u \gamma \end{pmatrix} \wedge \begin{pmatrix} \partial_v \gamma \\ \kappa_2 \partial_v \gamma \end{pmatrix} \\ &= \det\Big(\partial_u \gamma, \partial_v \gamma\Big) \left[\begin{pmatrix} b_1 \\ 0 \end{pmatrix} + \begin{pmatrix} 0 \\ \kappa_1 b_1 \end{pmatrix} \right] \wedge \left[\begin{pmatrix} b_2 \\ 0 \end{pmatrix} + \begin{pmatrix} 0 \\ \kappa_2 b_2 \end{pmatrix} \right] \end{aligned}$$

with $(b_1 = \frac{\partial_u \gamma}{\|\partial_u \gamma\|}, b_2 = \frac{\partial_v \gamma}{\|\partial_v \gamma\|})$ an orthonormal frame of principal directions. With the previous expression, we see that:

$$\partial_u \Gamma \wedge \partial_v \Gamma = \det\Big(\partial_u \gamma, \partial_v \gamma\Big) \Big(\varepsilon_1 \wedge \varepsilon_2 + \kappa_1 \tilde{\varepsilon}_1 \wedge \varepsilon_2 + \kappa_2 \varepsilon_1 \wedge \tilde{\varepsilon}_2 + \kappa_1 \kappa_2 \tilde{\varepsilon}_1 \wedge \tilde{\varepsilon}_2 \Big)$$

where the ε_i and $\tilde{\varepsilon}_j$ are defined via (2.27). This last expression is interesting because it specifies how the tangent space of the normal bundle (represented via $\partial_u \Gamma \wedge \partial_v \Gamma$ and $\partial_u \tilde{\Gamma} \wedge \partial_v \tilde{\Gamma}$) contains the different curvature information. With this expression and with (2.32), one can show that

$$\begin{aligned} \text{Area}(S) &= \frac{1}{2} \sup\big\{ N(S)(\omega) \mid \omega \in W_2^2, \ \|\omega\|_\infty \leq 1 \big\} =: \frac{1}{2} \|N(S)\|_{\infty, W_2^2}, \\ \int_U \frac{|\kappa_1| + |\kappa_2|}{2} &= \frac{1}{2} \sup\big\{ N(S)(\omega) \mid \omega \in W_1^2, \ \|\omega\|_\infty \leq 1 \big\} =: \frac{1}{2} \|N(S)\|_{\infty, W_1^2}, \\ \int_U |\kappa_1 \kappa_2| &= \frac{1}{2} \sup\big\{ N(S)(\omega) \mid \omega \in W_0^2, \ \|\omega\|_\infty \leq 1 \big\} =: \frac{1}{2} \|N(S)\|_{\infty, W_0^2}. \end{aligned}$$

And once again, it is possible to localize these measures. For any Borel set $B \subset \mathbb{R}^3$,

$$\begin{aligned}
\mathrm{Area}(S \cap B) &= \frac{1}{2} \sup \left\{ N(S)(\omega) \mid \omega \in W_2^2,\ \|\omega\|_\infty \leq 1,\ \mathrm{supp}\, \omega \subset B \times S^2 \right\}, \\
\int_{U \cap \gamma^{-1}(B)} \frac{|\kappa_1| + |\kappa_2|}{2} &= \frac{1}{2} \sup \left\{ N(S)(\omega) \mid \omega \in W_1^2,\ \|\omega\|_\infty \leq 1,\ \mathrm{supp}\, \omega \subset B \times S^2 \right\}, \\
\int_{U \cap \gamma^{-1}(B)} |\kappa_1 \kappa_2| &= \frac{1}{2} \sup \left\{ N(S)(\omega) \mid \omega \in W_0^2,\ \|\omega\|_\infty \leq 1,\ \mathrm{supp}\, \omega \subset B \times S^2 \right\}.
\end{aligned} \tag{2.33}$$

This makes clear that even though the Liscphitz-Killing forms are not sufficient to retrieve the mean curvature of a surface, the normal cycle contains all the (unsigned) curvature information. These curvatures can be obtained with via a supremum rather than a direct formula.

2.5.3 Discrete curvatures and normal cycles

Curvature measures, and more specifically Lipschitz-Killing forms applied on normal cycles are a way to generalize the notion of curvature for sets with positive reach. Moreover, we have seen in subsection 2.4.3 how to define normal cycles for a broader range of sets, namely union of sets with positive reach. This extension of the definition allows to consider normal cycles for polygonal meshes as union of segments or triangulated meshes. It is of interest to apply what we have done right above in the case of polyhedral shapes. We will see that we are able to retrieve classical definition of discrete curvatures.

As we are working with curvature measure, we can localize the configuration. This implies that the study that has been done previously for a smooth curve or a smooth surface is still valid in the neighbourhood of a regular point in the discrete case. The only point to tackle here is in the neighbourhood of an extremity for segments and in the neighbourhood of an edge or a vertex for triangulation.

Consider first a union of two segments $C_1 = [x_1, x_2]$ and $C_2 = [x_2, x_3]$ with a common vertex x_2 in $\mathbb{R}^3$. With the same notations as previously, we get:

$$\begin{aligned}
N(C_1 \cup C_2)(\boldsymbol{\omega}_1) &= 2\pi \mathrm{Length}(C_1 \cup C_2), \\
N(C_1 \cup C_2)(\boldsymbol{\omega}_0) &= 4\pi^2.
\end{aligned}$$

Once again, this is not surprising that we do net retrieve the signed curvature information. However, if we consider the supremum norm, we obtained finer information:

Consider again a borel set B of $\mathbb{R}^3$, containing x_2 but not the extremities x_1 and x_3, then one get:

$$\begin{cases}
\sup\limits_{\omega \in W_2^1 \cap \Omega_0^{d-1}} N(C_1 \cup C_2) \llcorner \mathbb{1}_B(\omega) = 0, \\
\sup\limits_{\omega \in W_1^1 \cap \Omega_0^{d-1}} N(C_1 \cup C_2)(\omega) \llcorner \mathbb{1}_B = 2\pi \mathrm{Length}\big((C_1 \cup C_2) \cap B\big), \\
\sup\limits_{\omega \in W_0^1 \cap \Omega_0^{d-1}} N(C_1 \cup C_2)(\omega) \llcorner \mathbb{1}_B = 2\pi(\pi - \theta)
\end{cases}$$

where θ is the unoriented angle between C_1 and C_2 (i.e. $\theta = \arccos(\left\langle \frac{x_2-x_1}{|x_2-x_1|}, \frac{x_3-x_2}{|x_3-x_2|} \right\rangle)$ and we retrieve a classical definition of curvature for union of segments that is the angle deflection at a vertex.

For a triangulation $\mathcal{T}$ in $\mathbb{R}^3$, we use also a decomposition of the normal bundle into planar, cylindrical and spherical part. If B is any borel set of $\mathbb{R}^3$, we have:

$$N(\mathcal{T})\llcorner \mathbb{1}_B(\boldsymbol{\omega}_2) = \|N(\mathcal{T})\llcorner \mathbb{1}_B\|_{\infty, W_2^2 \cap \Omega_0^{d-1}} = 2\text{Area}\big(\mathcal{T} \cap B\big)$$

Let B be a Borel set of $\mathbb{R}^3$ intersecting only one edge e of $\mathcal{T}$. We have:

$$N(\mathcal{T})\llcorner \mathbb{1}_B(\boldsymbol{\omega}_1) = 0$$

due to the orientation. Considering the supremum, we get:

$$\|N(\mathcal{T})\llcorner \mathbb{1}_B\|_{\infty, W_1^2 \cap \Omega_0^{d-1}} = 2\text{Length}(e \cap B)(\pi - \theta)$$

where θ is the angle between the two triangles adjacent to the considered edge. This is again a classical definition for the (unsigned) mean curvature of a triangulation.

The case in the neighbourhood of a vertex is more intricate, but one can show that if B is a Borel set of $\mathbb{R}^3$ containing only one vertex, one get:

$$N(\mathcal{T})\llcorner \mathbb{1}_B(\boldsymbol{\omega}_0) = \|N(\mathcal{T})\llcorner \mathbb{1}_B\|_{\infty, W_0^2} = 2\pi - \sum_{i=1}^{m} \theta_i$$

where θ_i is the angle at the vertex x of the triangle i that has x as in vertex. This is again the classical definition of the Gaussian curvature for triangulation.

This consideration is closed to the curvature estimation: is it possible to retrieve curvature information of a smooth surface given a polyhedral approximation of it ? A classical approach is to fit a quadratic surface on the triangulated mesh and estimate the curvature of this smooth surface. Numerous methods have been developed and one can find a survey of some of them in [Petitjean, 2002]. In [Meyer et al., 2003], authors introduced discrete operators as the discrete Laplace-Beltrami operator, or the Gaussian curvature operators to estimate curvature of triangulated surfaces.

The framework provided by the geometric measure theory has several advantages. First of all, the setting of normal cycles (or varifolds) encompasses in a common space the continuous and the discrete cases. This means that smooth shapes and their polyhedral approximations live in a common normed vector space. Thus, one can obtain convergence results of the curvature estimation in a very natural way. For example, in [Buet et al., 2015], the authors use the first variation of a varifold to define generalized mean curvature of a shape. This generalized curvature is valid for continuous shapes as well as their polyhedral approximations and a convergence results of the curvature of the discrete approximation toward the curvature of the continuous shape is provided under some conditions on the mesh.

Normal cycles have also been applied to curvature estimation from triangulations: in [Cohen-Steiner and Morvan, 2003], the authors use the Lipschitz-Killing

forms to generalized the mean and Gaussian curvatures that encompasses the polyhedral case. They also use vector valued differential forms to extend the notion of second fundamental form operator and get finer results: the principal curvatures as well as the principal directions may be estimated from this. Moreover, an upper bound of the error of the estimated curvature from a triangulated approximation of a smooth shape is proven. The estimation of the second fundamental form is refined in [Cohen-Steiner and Morvan, 2006] in a Riemannian framework. [Chazal et al., 2009] extend the stability result of [Cohen-Steiner and Morvan, 2003] that was valid only for approximation of smooth hypersurfaces. Introducing the μ-reach of a set, that is a weaker regularity hypothesis than positive reach, they provide curvature stability with respect to the Hausdorff distance of compact subset that has positive μ-reach, still using the theory of normal cycles. For example a finite set of points in $\mathbb{R}^3$ has a positive μ-reach and the authors derived an algorithm to explicit the curvature measure in this case from a description of its normal bundle. Some of the previous curvature estimation with normal cycles are sum up in [Morvan, 2008].

In this section, we have formalized the link between the normal cycle of a shape and its curvature. The Lipschitz-Killing differential forms introduced by Zähle are independent of the shape and gives all the Federer's curvature measures. However they do not capture the oriented curvatures. This fact was expected since the normal cycle is independent of any orientation of the initial shape. Nonetheless, we have seen that all the unsigned curvature information is contained in the normal cycle through a supremum norm on the dual of some restricted space of differential forms $(W_0^1, W_0^2, W_1^2, \dots)$.

2.6 Link Between the Varifold and the Normal Cycle Associated with a Shape

This section focuses on the link between varifolds and normal cycles. As it will be seen in the next chapters, when a kernel metric is given on the spaces of varifolds and normal cycles, the expression of the metric for triangulated meshes on varifolds is a projection of the metric on normal cycles. Our aim here is to formalize this projection in the continuous case. For this, let consider a smooth m dimensional submanifold X in $\mathbb{R}^d$. $N(X)$ is its associated normal cycle and μ_X its associated varifold.

We recall that varifolds are elements of $\mathscr{C}_0(\mathbb{R}^d \times G(d,m))'$ and normal cycles elements of $\Omega_0^{d-1}(\mathbb{R}^d \times S^{d-1})'$. In this section, we construct a projection p that, given a normal cycle $N(X)$, provides the varifold μ_X: $p(N(X)) = \mu_X$, and an injection i that given a varifold μ_X provides an element $i(\mu_X) \in \Omega_0^{d-1}(\mathbb{R}^d \times S^{d-1})'$, and such that $p \circ i = \mathrm{Id}$. Of course, we cannot have $i(\mu_X) = N(X)$ since a normal cycle contains more information about the shape X than a varifold. In fact we will see that $i(\mu_X)$ is a "coarse" version of the normal cycle $N(X)$, with no curvature

information.

To construct i and p, we decompose the space $\Omega_0^{d-1}(\mathbb{R}^d \times S^{d-1})$ as in remark 2.43:

$$\Omega_0^{d-1}(\mathbb{R}^d \times S^{d-1}) = \big(W_{d-1} \oplus \cdots \oplus W_m \oplus \cdots \oplus W_0\big)$$

The space that we will be interested in is W_m. Indeed it corresponds to differential forms with values in

$$F_m = \text{Span}\left\{ \begin{pmatrix} \alpha_1 \\ 0 \end{pmatrix} \wedge \cdots \wedge \begin{pmatrix} \alpha_m \\ 0 \end{pmatrix} \wedge \begin{pmatrix} 0 \\ n_1 \end{pmatrix} \wedge \cdots \wedge \begin{pmatrix} 0 \\ n_{d-1-m} \end{pmatrix} \Big| \alpha_i, n_i \in \mathbb{R}^d \right\}.$$

Our interest in W_m comes from remark 2.40 where we have seen that the curvature information contained in the orthonormal basis of $T_{(x,n)}\mathcal{N}_X$ mixes the spatial and the spherical component. Moreover, we have seen that the spatial component of $a_i(x,n)$ is vanishes if, and only if the associated direction $b_i(x,n)$ is orthogonal to the tangent space of X. Since varifolds do not contain curvature information, and are m-dimensional objects, the only way to link varifolds and normal cycles is to project in some sense the information on the orthonormal basis onto F_m. Doing so, we lose the curvature information, since there is no mixing between the spatial and the spherical part, and we keep the m-dimensional tangential information of X since there are m non zero vectors on the spatial component.

For this, let first define the projection and the injection on the spaces $\mathscr{C}^0(\mathbb{R}^d \times G(d,m))$ and $\Omega_0^{d-1}(\mathbb{R}^d \times S^{d-1})$. If $\omega \in \Omega_0^{d-1}(\mathbb{R}^d \times S^{d-1})$, the idea is to construct an element of $\mathscr{C}^0(\mathbb{R}^d \times G(d,m))$ using projection of ω on some well chosen subspaces of W_m. For this, we define for $P \in G(d,m)$ and $n \in S^{d-1}$

$$F(P,n) = \text{Span}\left\{ \begin{pmatrix} \alpha_1 \\ 0 \end{pmatrix} \wedge \cdots \wedge \begin{pmatrix} \alpha_m \\ 0 \end{pmatrix} \wedge \begin{pmatrix} 0 \\ n_1 \end{pmatrix} \wedge \cdots \wedge \begin{pmatrix} 0 \\ n_{d-1-m} \end{pmatrix} \Big| \alpha_i \in P,\ n_i \in P^\perp \cap n^\perp \right\}.$$

One can check that $\dim F_m(P,n) = 1$, and we consider the basis

$$f_{P,n} = \begin{pmatrix} e_1 \\ 0 \end{pmatrix} \wedge \cdots \wedge \begin{pmatrix} e_m \\ 0 \end{pmatrix} \wedge \begin{pmatrix} 0 \\ n_1 \end{pmatrix} \wedge \cdots \wedge \begin{pmatrix} 0 \\ n_{d-1-m} \end{pmatrix}$$

with $(e_1, \ldots, e_m)$ an orthonormal basis of P and $(e_1, \ldots, e_m, n_1, \ldots, n_{d-1-m}, n)$ a positively oriented orthonormal basis of $\mathbb{R}^d$. $F(P,n)$ represents the information of the plane P on the spatial component and of the orthogonal of $n \cup P$ on the spherical component. We denote also $f^*_{P,n}(\tau)$ the coordinate of $\tau \in \Lambda^{d-1}(\mathbb{R}^d \times \mathbb{R}^d)$ on the one dimensional subspace $F(P,n)$ with basis $f_{P,n}$. Now, given $\omega \in \Omega_0^{d-1}(\mathbb{R}^d \times S^{d-1})$, we construct $\pi(\omega) \in \mathscr{C}_0(\mathbb{R}^d \times G(d,m))$ as follow:

$$\pi(\omega)(x,P) = \frac{1}{\text{Vol}\big(S^{d-1-m}\big)} \int_{S^{d-1} \cap P^\perp} f^*_{P,n}\Big(\omega(x,n)\Big) d\mathscr{H}^{d-1-m}(n)$$

The idea is given a direction n, to get the coordinate of the differential form at (x,n) on the space $F(P,n)$ and integrate this scalar over all the $n \in S^{d-1} \cap P^\perp$. π is a

continuous application from $\Omega_0^{d-1}(\mathbb{R}^d \times S^{d-1})$ to $\mathscr{C}_0(\mathbb{R}^d \times G(d,m))$ and can be seen as a projection.

Now, given an element $u \in \mathscr{C}_0(\mathbb{R}^d \times G(d,m))$, we want to construct an element $\iota(u) \in \Omega_0^{d-1}(\mathbb{R}^d \times S^{d-1})$. We define:

$$\iota(u)(x,n)(\tau) = \int_{G(d,m)\cap n^\perp} u(x,P)\,\langle f_{P,n}|\tau\rangle\,dP$$

We have constructed two operators:

$$\begin{aligned}\pi :\ &\Omega_0^{d-1}(\mathbb{R}^d \times S^{d-1}) \to \mathscr{C}_0(\mathbb{R}^d \times G(d,m))\\ \iota :\ &\mathscr{C}_0(\mathbb{R}^d \times G(d,m)) \to \Omega_0^{d-1}(\mathbb{R}^d \times S^{d-1}).\end{aligned}$$

Moreover if $u \in \mathscr{C}_0(\mathbb{R}^d \times G(d,m))$, we have

$$\begin{aligned}\pi\circ\iota(u)(x,T) &= \pi\left((y,n)\mapsto \int_{G(d,m)\cap n^\perp} u(y,P)\,\langle f_{P,n}|.\rangle\,dP\right)(x,T)\\ &= \frac{1}{\mathrm{Vol}\big(S^{d-1-m}\big)}\int_{S^{d-1}\cap T^\perp} f_{T,n}^*\Big(\int_{G(d,m)\cap n^\perp} u(x,P)\,\langle f_{P,n}|.\rangle\,dP\Big)d\mathscr{H}^{d-1-m}(n)\\ &= \frac{1}{\mathrm{Vol}\big(S^{d-1-m}\big)}u(x,T)\int_{S^{d-1}\cap T^\perp} d\mathscr{H}^{d-1-m}(n)\\ &= u(x,T)\end{aligned}$$

Thus $\pi\circ\iota = \mathrm{Id}$. Now we can define our operator of interest, which are the dual operators of ι and π:

$$\begin{aligned}\iota^* :\ &\Omega_0^{d-1}(\mathbb{R}^d \times S^{d-1})' \to \mathscr{C}_0(\mathbb{R}^d \times G(d,m))'\\ \pi^* :\ &\mathscr{C}_0(\mathbb{R}^d \times G(d,m))' \to \Omega_0^{d-1}(\mathbb{R}^d \times S^{d-1})'.\end{aligned}$$

We will see that $\iota^* =: p$ is the projection of the normal cycles on the space of varifolds and $\pi^* =: i$ is an injection from the space of varifolds to the space of normal cycles. For this, consider a m-dimensional smooth submanifold of $\mathbb{R}^d$, $N(X)$ its normal cycle and μ_X its varifold.

$$\begin{aligned}p(N(X))(u) = N(X)(\iota(u)) &= \int_{\mathcal{N}_X} \langle \iota(u)|\tau_{\mathcal{N}_X}(x,n)\rangle\,d\mathscr{H}^{d-1}(x,n)\\ &= \int_{\mathcal{N}_X}\int_{G(d,m)\cap n^\perp} u(x,P)\,\langle f_{P,n}|\tau_{\mathcal{N}_X}(x,n)\rangle\,dP d\mathscr{H}^{d-1}(x,n)\end{aligned}$$

Noticing that $\langle f_{P,n}|\tau_{\mathcal{N}_X}(x,n)\rangle = 0$ if $P \neq T_xX$, we get:

$$p(N(X))(u) = \int_{\mathcal{N}_X} u(x,T_xX)\,\langle f_{T_xX,n}|\tau_{\mathcal{N}_X}(x,n)\rangle\,d\mathscr{H}^{d-1}(x,n)$$

We recall that $\tau_{\mathcal{N}_X}(x,n) = a_1(x,n) \wedge \cdots \wedge a_{d-1}(x,n)$ where the a_i are defined in (2.11) and one can show that

$$\langle f_{T_xX,n} | \tau_{\mathcal{N}_X}(x,n) \rangle = \prod_{i=1 | k_i(x,n) \neq \infty}^{d-1} \frac{1}{\sqrt{1+k_i^2(x,n)}} = J_m \pi_0(x,n),$$

where we recall that π_0 is the projection from $\mathcal{N}_X$ onto X. Using a Co-Area formula, we obtain:

$$\begin{aligned} p(N(X))(u) &= \int_{\mathcal{N}_X} u(x, T_xX) J_m \pi_0(x,n) d\mathscr{H}^{d-1}(x,n) \\ &= \int_X u(x, T_xX) \left(\int_{\mathrm{Nor}^u(x,X)} d\mathscr{H}^{d-1-m}(n) \right) d\mathscr{H}^m(x) = \mathrm{Vol}\big(S^{d-1-m}\big) \mu_X(u). \end{aligned}$$

We have proven here that $p(N(X)) = \mathrm{Vol}\big(S^{d-1-m}\big)\mu_X$.

Now, we compute

$$\begin{aligned} i(\mu_X)(\omega) = \mu_X(\pi(\omega)) &= \int_X \pi(\omega)(x, T_xX) d\mathscr{H}^m(x) \\ &= \int_X \frac{1}{\mathrm{Vol}\big(S^{d-1-m}\big))} \int_{S^{d-1} \cap T_xX^\perp} f^*_{T_xX,n}\Big(\omega(x,n)\Big) d\mathscr{H}^{d-1-m}(n) d\mathscr{H}^m(x) \\ &= \frac{1}{\mathrm{Vol}\big(S^{d-1-m}\big)} \int_X \int_{\mathrm{Nor}^u(x,X)} \langle \omega(x,n) | f_{T_xX,n} \rangle \, \mathscr{H}^{d-1-m}(n) d\mathscr{H}^m(x) \end{aligned}$$

and using again a Co-Area formula, we obtain:

$$\begin{aligned} i(\mu_X)(\omega) &= \frac{1}{\mathrm{Vol}\big(S^{d-1-m}\big)} \int_{\mathcal{N}_X} \big\langle \omega(x,n) \big| P_{F_m}\big(\tau_{\mathcal{N}_X}(x,n)\big) \big\rangle \, \mathscr{H}^{d-1}(x,n) \\ &= \frac{1}{\mathrm{Vol}\big(S^{d-1-m}\big)} \int_{\mathcal{N}_X} \big\langle P_{F_m}\big(\omega(x,n)\big) \big| \tau_{\mathcal{N}_X}(x,n) \big\rangle \, \mathscr{H}^{d-1}(x,n) \\ &= \frac{1}{\mathrm{Vol}\big(S^{d-1-m}\big)} \int_{\mathcal{N}_X} \big\langle P_{W_m}\big(\omega\big)(x,n) \big| \tau_{\mathcal{N}_X}(x,n) \big\rangle \, \mathscr{H}^{d-1}(x,n) \end{aligned}$$

Here, we have proven that $i(\mu_X) = P^*_{W_m}(N(X))$. We sum up the main results in the next theorem:

Theorem 2.53. *If X is a m-dimensional submanifold of $\mathbb{R}^d$, we have:*

1. $p(N(X)) = \mathrm{Vol}\big(S^{d-1-m}\big)\mu_X$.
2. $i(\mu_X) = \dfrac{1}{\mathrm{Vol}\big(S^{d-1-m}\big)} P^*_{W_m}(N(X))$.
3. $p \circ i(\mu_X) = \mu_X$.

Let's make some remarks here: first of all, given a normal cycle associated with a submanifold X, we are able to retrieve the varifold μ_X associated with X. On the contrary, given μ_X, we cannot retrieve $N(X)$, but only a "rough" version of it. Indeed, the object $P^*_{W_m} N(X)$ is a projection of $N(X)$ on a subspace where there is no curvature information. Heuristically the current $P^*_{W_m} N(X)$ is associated with the "locally flattened" submanifold X. To make it more precise, consider a Dirac $\delta^\tau_{(x,n)}$. Suppose that $\tau \in \Lambda^{d-1}(\mathbb{R}^d \times \mathbb{R}^d)$ writes

$$\tau = \left(\bigwedge_{i=1}^{m} \begin{pmatrix} e_i \\ k_i e_i \end{pmatrix} \right) \wedge \left(\bigwedge_{i=m+1}^{d-1} \begin{pmatrix} 0 \\ e_i \end{pmatrix} \right)$$

with $(e_1, \ldots, e_{d-1}, n)$ a positively oriented orthonormal basis. As explained previously, all the curvature information is contained in the k_i. Now one can show that $i \circ p(\delta^\tau_{(x,n)}) = \delta^{P_{F_m}\tau}_{(x,n)}$ with

$$P_{F_m}\tau = \left(\bigwedge_{i=1}^{m} \begin{pmatrix} e_i \\ 0 \end{pmatrix} \right) \wedge \left(\bigwedge_{i=m+1}^{d-1} \begin{pmatrix} 0 \\ e_i \end{pmatrix} \right).$$

Thus, projecting the Dirac on the space of varifolds, and injecting it back on the normal cycles, we have lost all the curvature information.

Secondly, one should notice that the expression of the projection and injection are much simpler in the case of a $(d-1)$-submanifold in $\mathbb{R}^d$, as we have a canonical identification between a normal vector and the hyperplane defined as the orthogonal of this normal vector. Moreover, the integrals over $G(d, d-1) \cap n^\perp$ and $S^{d-1} \cap P^\perp$ reduces to a sum of two elements.

2.7 Discussion

Using the theory of currents, and following the pioneer works of Federer and Zähle, we have presented in this chapter the representation of shapes with normal cycles. The normal cycle of a set is the current associated with its normal bundle. This model has a higher complexity than classical currents or varifolds. Indeed, the normal cycles of a shape encodes precise curvature information that have been detailed in section 2.5. In this section, following Zähle, we used the Lipschitz-Killing differential forms to retrieve different kind of curvature with normal cycles. We introduced spaces of differential forms (planar, cylindrical, spherical) that are closely linked to these curvatures (area form, mean curvature and Gaussian curvature).

For a computational purpose, we have described the normal bundle of a segment and a triangle. The additive property (2.15) allows to consider the normal cycles for a union of convex cells but the transition from the normal cycle of a convex cell to the normal cycles of a union of convex cells is complex. That is why we introduced a new decomposition of the normal bundle of discrete shapes, into spherical, cylindrical and planar part that allow for an immediate additive property. Moreover, as we

have seen in subsection 2.5.3, each component of this normal bundle has a specific interpretation in term of curvature information. It is interesting to see that with this decomposition, along with the spaces of differential forms (planar, cylindrical, spherical), we are able to retrieve in the discrete setting all the classical discrete curvatures. Normal cycles have already been applied to estimate the curvature of discrete surfaces approximating a continuous one, as it has been recalled in 2.5.3. With this work, we have provided a ready-to-use computational framework, with an explicit and easily implementable representation of discrete shapes with normal cycles.

Section 2.6 draws a precise link between the normal cycle and the varifold associated with a shape. We have seen that in some sense, the varifold of a shape can be seen as a projection of its normal cycle. Moreover, the injection of a varifold to the space of normal cycles provides a representation with no curvature information, as if the shape was "locally flattened". This section paves the way to a unification of the different representations of shapes (currents, varifolds, normal cycles), as well as the precise kind of information encoded in each representation.

Chapter 3

Reproducing Kernel Hilbert Spaces on Normal Cycles

Sommaire

The idea of normal cycles (resp. currents) is convenient because it embeds shapes in a vectorial space: the space of $(d-1)$-currents in $\mathbb{R}^d \times S^{d-1}$ (resp. the space of m-current in $\mathbb{R}^d$). These spaces, defined as dual to spaces of differential forms, come with a dual norm: if $T \in \Omega_0^m(\mathbb{R}^d)'$, we define $M(T) := \sup\left\{T(\omega), \omega \in \Omega_0^m(\mathbb{R}^d), \|\omega\|_\infty \leq 1\right\}$, called the mass norm in geometric measure theory. It would be tempting to use this norm as a distance between shapes. However this norm is not interesting for a matching purpose. Indeed, if C and S are two m-rectifiable sets, non intersecting, then one can show that $M([S]-[C]) = \mathscr{H}^m(C) + \mathscr{H}^m(S)$, and this independently of any closeness between the two sets. This happens because the set of test functions ω is too large, and thus discriminates completely the two shapes. Another norm which turns out to be useful in geometric measure theory is the flat norm: $F(T) := \sup\left\{T(\omega), \omega \in \Omega_{1,0}^m(\mathbb{R}^d)\, \|\omega\|_\infty \leq 1,\ \|d\omega\|_\infty \leq 1\right\}$ where $d\omega$ is the exterior derivative of ω. Though, this distance has several drawbacks, the main one being its non closed form. For our numerical purpose, we need a computable expression for the dissimilarity between shapes. In the very same spirit of [Glaunès, 2005], we will use the theory of reproducing kernels to provide kernel metrics on normal cycles as dissimilarity measures.

The theory of reproducing kernels arose first with Mercer in the study of integral operators ([Mercer, 1909]), but the seminal work is mostly due to Aronzajn [Aronszajn, 1950], in 1950. It has now a wide range of applications: complex analysis, harmonic analysis, machine learning, among others. In machine learning theory, reproducing kernels are a way to represent any kind of data as functions in a functional Hilbert space, with an explicit scalar product. Thus, it is possible to use the classical statistical machinery in this Hilbert space to analyse the data.

This theory is widely used in computational anatomy either to have a space of deformations whose equations are easy to implement numerically (see section 1.4) or to have an explicit distance between shapes (see [Glaunès, 2005, Durrleman, 2010, Charon, 2013]). Suppose that we have two curves C and S in $\mathbb{R}^2$. Representing these two curves as currents $[C]$ and $[S]$ (figure 3.1), a kernel metric allows to consider a scalar product between those curves that takes explicit expression as integral over the curves:

$$\langle [C], [S] \rangle_{W'} = \int_C \int_S k(x,y)\, \langle \tau_x, \tau_y \rangle\, d\mathscr{H}^1(x) d\mathscr{H}^1(y).$$

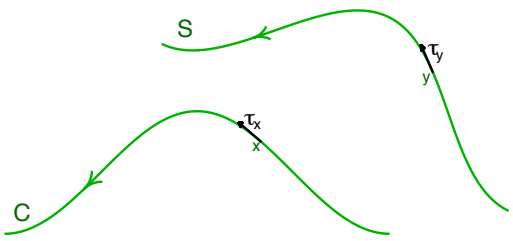

Figure 3.1: Representation of the curves C and S with currents

Now, if we represent the two curves as normal cycles (figure 3.2), the kernel metric will consider integrals over the normal bundle rather than integrals over the

curves themselves. Precisely, we will construct two scalar kernels k_p and k_n where k_p takes into account the relative spatial position of the curves and k_n the relative position of the normal vectors u and v at point $x \in C$ and $y \in S$.

$$\langle N(C), N(S) \rangle_{W'} = \int_{\mathcal{N}_C} \int_{\mathcal{N}_S} k_p(x,y) k_n(u,v) \left\langle \tau_{(x,u)}, \tau_{(y,v)} \right\rangle d\mathscr{H}^1(x,u) d\mathscr{H}^1(y,v).$$

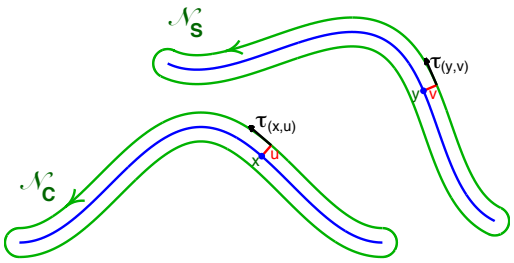

Figure 3.2: Representation of the curves C and S with normal cycle

In section 3.1 we recall the basics of Reproducing Kernel theory in the vectorial case and the construction of positive definite kernels. For a complete study of Reproducing Kernel Hilbert Spaces in the vectorial case, one can refer to [Micheli and Glaunès, 2014]. In section 3.2, we derive kernel metrics on the space of currents and varifolds, following the previous works of [Glaunès, 2005] for currents and [Charon and Trouvé, 2013] for varifolds. Sections 3.3, 3.5 and section 3.7 are the heart of this chapter. We construct kernel metrics on the space of normal cycles using a product of two kernels: a spatial kernel k_p and a normal kernel k_n. We explicit different kernels that we can use as well as embedding properties of the generated RKHS (3.3). Section 3.5 focuses on two simple kernels for k_n: the constant kernel $k_n = 1$ and the linear kernel $k_n(u,v) = \langle u, v \rangle$. We detail the kind of curvatures that each kernel captures. These simple kernels will ease the complexity of the calculus when dealing with numerical implementation as we will see in section 3.7.

3.1 Vector-Valued Reproducing Kernel Hilbert Spaces

3.1.1 General setting

Let H be a Hilbert space of functions from $\mathbb{R}^d$ to a euclidean space E : $H \subset \mathscr{F}(\mathbb{R}^d, E)$. We denote $\langle ., . \rangle_H$ the scalar product on H and $\langle ., . \rangle_E$ the one on E.

Definition 3.1 (Reproducing Kernel Hilbert Space)**.** *H is a Reproducing Kernel Hilbert Space if there exists $K : \mathbb{R}^d \times \mathbb{R}^d \to \mathcal{L}(E)$ such that*

- *for all $x \in \mathbb{R}^d$, $\alpha \in E$, $y \mapsto K(x,y)\alpha \in H$*

- *For every* $x \in \mathbb{R}^d, f \in H, \alpha \in E$*:*

$$\langle K(.,x)\alpha, f\rangle_H = \langle f(x), \alpha\rangle_E$$

A kernel fulfilling these properties is a reproducing kernel*. H is then a Reproducing Kernel Hilbert Space (RKHS) with kernel K.*

The next proposition is a more concise, yet more abstract, characterization of RKHS:

Proposition 3.2. *A Hilbert space H of $\mathscr{F}(\mathbb{R}^d, E)$ is a RKHS if, and only if for every $x \in \mathbb{R}^d$, $\alpha \in E$, the applications*

$$\delta_x^\alpha : h \in H \mapsto \langle h(x), \alpha\rangle_E \in \mathbb{R}.$$

are continuous, i.e. in the topological dual of H, denoted H'.

Proof. First, if H is a RKHS with reproducing kernel K, let $\alpha \in E$ and $x \in \mathbb{R}^d$. For every $f \in H$ we have

$$\begin{aligned}
|\delta_x^\alpha(f)| &= |\langle f(x), \alpha\rangle_E| \\
&= |\langle K(.,x)\alpha, f\rangle_H| \\
&\leq \|K(.,x)\alpha\|_H \|f\|_H \text{ (Cauchy-Schwarz)} \\
&\leq \langle K(x,x)\alpha, \alpha\rangle_E \|f\|_H
\end{aligned}$$

and thus δ_x^α is continuous.

Conversely, we suppose that all the δ_x^α are in H'. Thanks to the Riesz representation theorem, a canonical isometry exists between H' and $H : \mathcal{K}_H : H' \to H$. We note also $\langle .|. \rangle$ the duality product between an element of H' and one of H. The application $(\alpha, \beta) \in E^2 \mapsto \left\langle \mathcal{K}_H\delta_x^\alpha, \mathcal{K}_H\delta_y^\beta \right\rangle_H$ is obviously bilinear. This bilinearity enables us to define a kernel K_H:

$$\begin{aligned}
\langle \beta, \mathcal{K}_H(\delta_x^\alpha)(y)\rangle_E &= \left\langle \delta_y^\beta \middle| \mathcal{K}_H\delta_x^\alpha \right\rangle \\
&= \left\langle \mathcal{K}_H\delta_x^\alpha, \mathcal{K}_H\delta_y^\beta \right\rangle_H \\
&= \left\langle \delta_x^\alpha, \delta_y^\beta \right\rangle_{H'} \\
&=: \langle K_H(x,y)\alpha, \beta\rangle_E
\end{aligned}$$

where the last row can be taken as a definition of the application $K_H(x,y)$. From the properties of bilinearity and positivity of the scalar products, one can deduce (see [Micheli and Glaunès, 2014]) :

1. $K_H(x,.)\alpha = \mathcal{K}_H\delta_x^\alpha \in H$.
2. $\langle K_H(x,.)\alpha, f\rangle_H = \langle f(x), \alpha\rangle_E$.

And these are the properties of a reproducing kernel. Thus, H is a RKHS with reproducing kernel K_H. □

Moreover, one can deduce the following properties for K_H:

1. $\forall x, y \in \mathbb{R}^d$, $K_H(x,y)$ is a linear application on E
2. $K_H(x,y)^* = K_H(y,x)$ (symmetry)
3. $\forall N \in \mathbb{N}$, $\forall (x_i)_{1\leq i\leq N}, (\alpha_i)_{1\leq i\leq N}$: $\sum_{i,j} K_H(x_i,x_j)(\alpha_i,\alpha_j) \geq 0$.

A kernel fulfilling these three completely algebraic properties is called a positive definite kernel. We see here that a reproducing kernel is a positive definite kernel. The next theorem draws a link between both kernels :

Theorem 3.3 ([Aronszajn, 1950], [Micheli and Glaunès, 2014])**.**

1. *For every RKHS H, one can associate a unique positive definite kernel K which is the reproducing kernel of H.*
2. *Conversely, if K is a positive definite kernel, there exists a unique RKHS H whose reproducing kernel is K.*

For our need, we will rather consider the second aspect: the space H is constructed with starting with a kernel K. The kernel K generates a pre-Hilbert space: $H_0 = \text{Vect}\left\{K(x,.)\alpha | x \in \mathbb{R}^d, \alpha \in E\right\} \subset \mathscr{F}(\mathbb{R}^d, E)$, with scalar product:

$$\left\langle \sum_{i=1}^{n} K(x_i,.)\alpha_i, \sum_{j=1}^{m} K(y_j,.)\beta_j \right\rangle := \sum_{i=1}^{n}\sum_{j=1}^{m} \langle \alpha_i, K(x_i,y_j)\beta_j \rangle_E$$

so that the scalar product, and the norm is explicit. The space H is obtained by completion of H_0 with respect to the scalar product (see [Micheli and Glaunès, 2014] for technical details).

Regularity of the RKHS

Given a RKHS H constructed via a positive definite kernel K_H, it is of interest to know which regularity have the functions $f \in H$. And even more, do we have embedding results of H onto some regular spaces?

Since the functions of the form $\sum_{i=1}^{n} K_H(x_i,.)\alpha_i$ are in H, it seems obvious that the regularity of the generated RKHS H is linked to the regularity of the kernel K_H. More precisely, we have

Theorem 3.4 ([Micheli and Glaunès, 2014], thm. 2.11)**.** *Let H be a RKHS of kernel $K_H : \mathbb{R}^d \times \mathbb{R}^d \to E$, $s \geq 0$ an integer. The following two statements are equivalent:*

1. *$H \hookrightarrow \mathscr{C}^s(\mathbb{R}^d, E)$ where $\mathscr{C}^s(\mathbb{R}^d, E)$ is endowed with the topology of uniform convergence for the derivatives up to order s on every compact set.*
2. *For every multi index p, $0 \leq |p| \leq s$, $\partial_1^p \partial_2^p K_H$ exists, is continuous in each of the two variables and is locally bounded.*

Moreover, if $K(x,.)\alpha \in \mathscr{C}_0^s(\mathbb{R}^d, E)$ for all $x \in \mathbb{R}^d$, $\alpha \in E$, then $H \hookrightarrow \mathscr{C}_0^s(\mathbb{R}^d, E)$.

Vector field interpolation

Let us illustrate how convenient the setting of a RKHS can be with the following example. Suppose that we have n corresponding points $(x_i, y_i) \in (\mathbb{R}^d)^2$ and we want to find a vector field $v_0 \in \mathscr{C}^0_0(\mathbb{R}^d, \mathbb{R}^d)$ such that $v_0(x_i) = y_i$. This problem with no more constraint is ill-posed: there is no uniqueness for a solution.

If we suppose now that we have a RKHS $H \hookrightarrow \mathscr{C}^0(\mathbb{R}^d, \mathbb{R}^d)$, with kernel K_H. Then we can consider the regularized problem:

$$\begin{cases} \arg\min_{v \in H} \|v\|_H^2 \\ v(x_i) = y_i, \ \forall i \in \{1, \dots, n\}. \end{cases} \tag{3.1}$$

This problem is apparently infinite dimensional. However, it simplifies a lot with the Representer theorem:

Theorem 3.5 (Representer theorem)**.** *Let H be a RKHS of $\mathscr{F}(\mathbb{R}^d, E)$, with kernel K_H and $x_i \in \mathbb{R}^d$,$\psi : E^n \times \mathbb{R}$ an increasing function with respect to the last variable. Then any solution of the problem*

$$\min_{f \in H} \psi\big(f(x_1), \dots, f(x_n), \|f\|_H^2\big)$$

admits a representation of the form

$$\forall x \in \mathbb{R}^d, \ f(x) = \sum_{i=1}^n K_H(x_i, x)\alpha_i$$

The Representer Theorem guarantees that a solution v_0 of (3.1) writes

$$v_0(y) = \sum_{i=1}^n K_H(x_i, y)\alpha_i$$

where the α_i are in $\mathbb{R}^d$ and satisfy linear equations:

$$\forall j \in \{1, \dots, n\}, \ \sum_{i=1}^n K_H(x_i, x_j)\alpha_i = y_j.$$

If we denote $K_H(x, x) = \big(K_H(x_i, x_j)\big)_{1 \le i,j \le n}$, and $\alpha = (\alpha_i)_{1 \le i \le n}$, $y = (y_i)_{1 \le i \le n}$, the previous equation writes:

$$K_H(x, x)\alpha = y.$$

Thus, the infinite dimensional problem of minimizing a norm of vector field under the constraint $v(x_i) = y_i$ reduces to solve a finite dimensional linear problem, namely solving a linear system with matrix $K_H(x, x)$. Moreover, the norm of the optimal vector field has simple expression in term of the kernel:

$$\begin{aligned} \|v_0\|_H^2 &= \left\langle \sum_{i=1}^n K_H(x_i, .)\alpha_i, \sum_{j=1}^n K_H(x_j, .)\alpha_j \right\rangle_H \\ &= \sum_{i,j=1}^n \alpha_j^T K_H(x_i, x_j)\alpha_i. \end{aligned}$$

So, once we have defined a positive definite kernel, the framework of RKHS is very convenient to work with, with explicit formulation for optimal solutions.

3.1.2 Construction of vectorial kernels

We are left now to design the kernel K_H. The set of positive definite kernels has nice algebraic properties ([Aronszajn, 1950], [Micheli and Glaunès, 2014] for the vectorial case): the sum of two positive definite kernels, the multiplication by a positive constant, the tensor product of two positive definite kernels are still positive definite kernels. This properties are useful to construct kernels starting from elementary ones as we will see below. We need also some specifications on the kernel: K_H has to be regular enough to have embedding properties. Moreover, for the purpose of providing a shape dissimilarity, we are interested in RKHS whose kernel induces an inner product that is invariant under isometries. Doing so, we ensure that the distance between shapes does not change if we apply the same translation or rotation to both shapes. If K_H is invariant under isometries, one can show that K_H writes:

$$K_H(x, y) = K(\|x - y\|),$$

where $K : \mathbb{R} \to \mathcal{L}(E)$. Of course, not all such kernels fulfill the condition of positivity. For a characterization of translation-rotation invariant kernels that are definite positive, one can see [Micheli and Glaunès, 2014], section 3.

With scalar kernels

The simplest kernel K that one can think of is the scalar kernel, namely $K(r) = k(r)\mathrm{Id}$ where $k : \mathbb{R} \to \mathbb{R}$ is a positive definite kernel on $\mathbb{R}$. Several scalar kernels are used on a regular basis. The two kernels that we will use in the following are:

- The Gaussian kernel with width σ: $k(x, y) = \exp(-\|x - y\|^2 / \sigma^2)$.
- The Cauchy kernel with width σ : $k(x, y) = \frac{1}{1+\frac{\|x-y\|^2}{\sigma^2}}$. The Cauchy kernel is a good alternative to the Gaussian kernel.

One can check that these two kernels are positive definite. The parameter σ is a scale parameter and will depend on the data.

Friedrichs Extension and Reproducing Kernel

Once a positive definite kernel K_H is set, it defines a RKHS H and a continuous operator $\mathcal{K}_H : H' \to H$. We will see here another way to construct explicit scalar reproducing kernel starting with the continuous operator, rather than the positive definite kernel. We recall here some points of [Glaunès, 2005], chapter 3. For our future purpose, we will consider vector fields on a compact submanifold of $\mathbb{R}^d$, M, with volume form m. We denote $\mathscr{C}^\infty(M)$ the set of all $\mathscr{C}^\infty$ functions on M, with its canonical topology, which is the topology of uniform convergence of f and all its derivatives. We have $\mathscr{C}^\infty(M) \hookrightarrow L^2(M)$ and $\mathscr{C}^\infty(M)$ is dense in $L^2(M)$ for the

L^2 norm. Let $L_V : \mathscr{C}^\infty(M) \to L^2(M)$ be a continuous, symmetric and strongly monotone operator, i.e. :

$$\forall u, v \in \mathscr{C}^\infty(M),\ \langle L_V u, v\rangle_{L^2} = \langle u, L_V v\rangle_{L^2}\,,$$
$$L_V : \mathscr{C}^\infty(M) \to (L^2(M), \|.\|_2) \text{ is continuous,}$$

and there exists $C > 0$ such that

$$\forall u \in \mathscr{C}^\infty(M),\ \langle L_V u, u\rangle_{L^2} \geq C\,\|u\|_{L^2}$$

Then, $\langle u, v\rangle_V := \langle L_V u, v\rangle_{L^2}$ defines scalar product on $\mathscr{C}^\infty(M)$. $(\mathscr{C}^\infty(M), \|.\|_V)$ is a normed vector space, but not complete. We complete it for the norm $\|.\|_V$, and denote V the Hilbert obtained. We cannot hope for an extension of L_V on all V. However, for every $u, v \in \mathscr{C}^\infty(M)$, $\langle u, v\rangle_V = \langle L_V u, v\rangle_{L^2}$. Thus we can extend L_V (using the scalar product in V) by considering all the $u \in V$ such that there exists a $h \in L^2(M)$ with the following property:

$$\forall v \in V : \langle u, v\rangle_V = \langle h, v\rangle_{L^2}$$

If such a h exists, it is unique, and we denote it $L_V u := h$. Let $D(L_V)$ be the set of all $u \in V$ such that $L_V u$ exists. Obviously, $\mathscr{C}^\infty(M) \subset D(L_V)$, and $D(L_V)$ is dense in $L^2(M)$ for the L^2-norm. This is the Friedriechs extension of L_V, which extends L_V on a dense subspace of L^2 and the following theorem justifies the necessity of such a construction:

Theorem 3.6. *$L_V : D(L_V) \to L^2(M)$ is bijective, and $L_V^{-1} : L^2(M) \to L^2(M)$ is a continuous, symmetric definite positive operator. Moreover, if $V \hookrightarrow L^2(M)$ is compact, then L_V^{-1} is compact.*

Since under the right assumptions L_V^{-1} is compact autoadjoint, we can diagonalise it on an Hilbert basis of $L^2(M)$, $(w_i)_{i\in\mathbb{N}}$, with eigenvalues $(\mu_i)_{i\in\mathbb{N}}$, with $\mu_i > 0$ and $\mu_i \to_{i\to\infty} 0$ (see [Brézis, 2011]). We have then $L_V(w_i) = \frac{1}{\mu_i} w_i$. We denote $\lambda_i = \frac{1}{\mu_i}$. With this construction, we can redefine the sets $L^2(M), D(L_V), V$:

Proposition 3.7.

$$L^2(M) = \left\{ \sum_{i\in\mathbb{N}} \alpha_i w_i \mid \sum_i \alpha_i^2 < +\infty \right\},$$
$$V = \left\{ \sum_i \alpha_i w_i \mid \sum_i \lambda_i \alpha_i^2 < +\infty \right\},$$
$$D(L_V) = \left\{ \sum_i \alpha_i w_i \mid \sum_i \lambda_i^2 \alpha_i^2 \right\}.$$

and if we define $\tilde{w}_i = \frac{w_i}{\sqrt{\lambda_i}}$, then $(\tilde{w}_i)_{i\in\mathbb{N}}$ is a Hilbert frame of V. The scalar product on V is explicit : if $u = \sum_i \alpha_i w_i$ and $v = \sum_i \beta_i w_i$, then

$$\langle u, v\rangle_V = \sum_i \lambda_i \alpha_i \beta_i$$

It is possible to make a link between L_V and a reproducing kernel K_V if we suppose that V is continuously embedded in $\mathscr{C}(M)$, with the uniform norm. Let $x \in M$. Then, with the previous notations, we have for every $f \in V$

$$\begin{aligned} |\delta_x(f)| &= |f(x)| \\ &\leq \|f\|_\infty \\ &\leq c\,\|f\|_V \end{aligned}$$

which means that the evaluation applications are in V'. Thus (proposition 3.2), V is a RKHS with reproducing kernel K_V, and K_V has an explicit expression with the proposition 3.7: let $x \in M$. $K_V(x,.) \in V$ and therefore can be written in the Hilbert frame $(w_i)_{i\in\mathbb{N}}$:

$$K_V(x,.) = \sum_{i\in\mathbb{N}} \alpha_i(x) w_i$$

and if we take the scalar product with w_j, we get

$$\begin{aligned} \langle K_V(x,.), w_j\rangle_V &= \lambda_j \alpha_j(x) \\ &= w_j(x) \end{aligned}$$

And so

$$K_V(x,y) = \sum_{i\in\mathbb{N}} \frac{1}{\lambda_i} w_i(x) w_i(y).$$

Then, in order to have an explicit expression of a reproducing kernel using an operator L, it is sufficient to diagonalise L^{-1} with explicit eigenvalues. Given an Hilbert frame $(w_i)_{i\in\mathbb{N}}$ of $L^2(M)$, and $(\lambda_i)_{i\in\mathbb{N}} \in \mathbb{R}_+^{\mathbb{N}}$, with $\lambda_i \to_{i\to\infty} +\infty$, we can also define a set V and $D(L_V)$ as in proposition 3.7, and the operator L_V defined on the Hilbert frame: $L_V(w_i) = \lambda_i w_i$. It can be shown that given this L_V, L_V^{-1} is compact, symmetric definite positive operator, and $V \hookrightarrow L^2(M)$ is compact.

This construction allows us, given an operator L_V and a Hilbert frame $(w_i)_i$, to define L_V^s with $s \in \mathbb{R}_+$ as the following expression :

$$L_V^s(w_i) = \lambda_i^s w_i.$$

3.1.3 Reproducing Kernel of Sobolev Spaces

We illustrate here the previous construction to define RKHS on S^2, with a power of an operator $L = (\mathrm{Id} - \Delta)$ on the sphere. It will be useful to have explicit, rotational invariant kernel on the normal space of the normal bundle. Let us consider the reproducing kernel k_n associated with Sobolev spaces $H^s(S^2)$. Let us first consider the space

$$H^1(S^2) = \left\{ u \in L^2(S^2) \mid \text{the weak derivative } \nabla u \text{ exists and is in } L^2(S^2) \right\}.$$

This space is naturally endowed with a scalar product:

$$\langle u, v\rangle_{H^1(S^2)} := \int_{S^2} uv + \int_{S^2} \langle \nabla u, \nabla v\rangle,$$

and it is a classical result that $\big(H^1(S^2), \|.\|_{H^1(S^2)}\big)$ is a Hilbert space with compact injection in $L^2(S^2)$ ([Brézis, 2011], Sobolev injections). Using integration by parts, we have:

$$\begin{aligned}\langle u, v\rangle_{H^1(S^2)} &= \int_{S^2} uv + \int_{S^2} \langle \nabla u, \nabla v\rangle \\ &= \int_{S^2} uv - \int_{S^2} (\Delta u)v = \int_{S^2} v\big(\mathrm{Id} - \Delta\big)(u) \\ &= \big\langle \big(\mathrm{Id} - \Delta\big)u, v\big\rangle_{L^2(S^2)}.\end{aligned}$$

$(\mathrm{Id}-\Delta)^{-1} : \mathscr{C}^\infty(S^2) \to L^2(S^2)$ is a continuous, symmetric, strongly monotonous operator. Moreover, since $H^1(S^2) \hookrightarrow L^2(S^2)$ is compact, with theorem 3.6, $(\mathrm{Id} - \Delta)^{-1}$ is compact and one can show that the Friedrichs extension $D\big(\mathrm{Id}-\Delta\big)$ coincides with $H^1(S^2)$. We will use expansion on spherical harmonics (see Appendix B) to define $H^1(S^2)$. We recall that the spherical harmonics $(Y_{l,m})$, for $l \in \mathbb{N}, -l \leq m \leq l$ form an Hilbert frame of $L^2(S^2)$ and are the eigenvectors of $-\Delta$:

$$\big(\mathrm{Id} - \Delta\big)Y_{l,m} = \big(1 + l(l+1)\big)Y_{l,m}.$$

We can now define the operator $\big(\mathrm{Id} - \Delta\big)^s$, $s \in \mathbb{R}_+$

$$\big(\mathrm{Id} - \Delta\big)^s Y_{l,m} = \big(1 + l(l+1)\big)^s Y_{l,m}.$$

For $s > 2$, we define $H^s(S^2) := D\big((\mathrm{Id} - \Delta)^{-s}\big)$. $H^s(S^2)$ coincides with the usual defintion of the s-Sobolev space on the sphere and we have we have $H^s(S^2) \hookrightarrow \mathscr{C}^1(S^2)$ (Sobolev injections, see [Brézis, 2011], Chap. IX. The results can be applied straightforwardly to the case of compact submanifolds without boundaries using partition of unity on a finite atlas of the manifold). Thus, if $s > 2$, $H^s(S^2)$ is a RKHS with reproducing kernel k_n. The operator associated with k_n is $L = (\mathrm{Id}-\Delta)^s$. And we have by definition of k_n: $Lk_n(x,.) = \delta_x$. Using an expansion on spherical harmonics of $k_n(x,.)$ for $x \in S^2$, we get $k_n(x,.) = \sum_{l\in\mathbb{N}} \sum_{m=-l}^{l} \alpha_{l,m}(x) Y_{lm}$. By the definition of k_n, we have

$$\langle k_n(x,.), Y_{l',m'}\rangle_{H^s(S^2)} = Y_{l'm'}(x)$$

And also, by definition of the scalar product and the operator L:

$$\begin{aligned}\langle k_n(x,.), Y_{l',m'}\rangle_{H^s(S^2)} &= \langle k_n(x,.), LY_{l'm'}\rangle_{L^2(S^2)} \\ &= \left\langle \sum_{l\in\mathbb{N}} \sum_{m=-l}^{l} \alpha_{l,m}(x) Y_{lm}, (1 + l(l+1))^s Y_{l'm'} \right\rangle_{L^2(S^2)} \\ &= \alpha_{l'm'}(x)(1 + l(l+1))^s = Y_{l'm'}(x)\end{aligned}$$

which gives:

$$k_n(x,y) = \sum_{l\in\mathbb{N}} \sum_{m=-l}^{l} \frac{1}{(1 + l(l+1))^s} Y_{lm}(x) Y_{lm}(y) \tag{3.2}$$

The Sobolev kernel will be one of the used kernels to provide a metric on normal cycles.

Remark 3.8. *Conversely, we could have fixed the eigenvalues λ_l at first instead of $1 + l(l+1)$, and defined the kernel k_n as in (3.2). All rotation invariant reproducing kernels on the sphere can be obtained with this procedure. Although we only consider kernels associated with Sobolev spaces in this work, one may definitely consider general metrics here by specifying appropriate assumptions on the sequence of eigenvalues.*

3.2 Kernel Metrics on Currents and Varifolds

The theory of reproducing kernel provides a powerful tool to construct a Hilbert space with explicit scalar product. We will see how to use it in the context of currents. All this has been developed in [Glaunès, 2005], [Vaillant and Glaunès, 2005].

Kernel metrics on currents

In [Glaunès, 2005], the author defines a RKHS W in the space of m-differential forms $\Omega_0^m(\mathbb{R}^d) \subset \mathscr{F}\left(\mathbb{R}^d, \Lambda^m(\mathbb{R}^d)^*\right)$ using a positive definite kernel K_W. With the previous notation, $E = \Lambda^m(\mathbb{R}^d)^* = \Lambda_m(\mathbb{R}^d)$ that we identify with $\Lambda^m(\mathbb{R}^d)$ with the Riesz representation theorem. We suppose that $W \hookrightarrow \Omega_0^m(\mathbb{R}^d)$, i.e. for every $\omega \in W$, $\|\omega\|_\infty \leq c \|\omega\|_W$. Then if S is a compact, m-rectifiable set of $\mathbb{R}^d$, we have

$$|S(\omega)| \leq \int_S |\omega| \leq \mathscr{H}^m(S) c \|\omega\|_W , \tag{3.3}$$

so that the restriction of $[S]$ to W belongs to W'. Hence a m-rectifiable set can be considered as an element of the Hilbert W', whose norm is explicit by the reproducing kernel. This raises the question of choosing a positive definite kernel on the space of differential forms. Here we will use scalar kernels: we define for every $\alpha, \beta \in \Lambda^m(\mathbb{R}^d)$, for every $x, y \in \mathbb{R}^d$

$$\langle K_W(x,y)\alpha, \beta \rangle_{\Lambda^m(\mathbb{R}^d)} = k_W(x,y) \langle \alpha, \beta \rangle_{\Lambda^m(\mathbb{R}^d)}$$

where k_W is a scalar kernel, for example $k_W(x,y) = \exp\left(\frac{-|x-y|^2}{\sigma_W^2}\right)$, with σ_W a parameter. This is a positive definite kernel and defines a RKHS W of m-differential forms. We have to be sure that this kernel defines a RKHS W embedded in the space $\Omega_0^m(\mathbb{R}^d)$:

Proposition 3.9 ([Glaunès, 2005], chapter 2, theorem 9)**.** *Let $p \in \mathbb{N}$, and a positive definite kernel $K : \mathbb{R}^d \times \mathbb{R}^d \to \mathcal{L}(E)$, with derivatives at order $\leq 2p$ which are continuous and bounded. Suppose that for every $x \in \mathbb{R}^d$, $K(x,.)$ vanishes at infinity, and so do its derivatives at order $\leq p$. Then the RKHS W associated with K is embedded into $\mathscr{C}_0^p(\mathbb{R}^d, E)$.*

All the kernels in this paper will fulfill the previous proposition. For example a scalar Gaussian kernel guarantees that its RKHS is embedded in a space as regular as we want ($\forall p \in \mathbb{N}, W \hookrightarrow \mathscr{C}_0^p(\mathbb{R}^d, E)$).

Now let S be a m-rectifiable set in $\mathbb{R}^d$, $\alpha \in \Lambda^m(\mathbb{R}^d)$, and $x \in \mathbb{R}^d$. From the reproducing property, we have

$$\begin{aligned}\langle \alpha, \mathcal{K}_W[S](x)\rangle_{\Lambda^m(\mathbb{R}^d)} &= \langle \delta_x^\alpha | \mathcal{K}_W[S]\rangle \\ &= \langle [S] | K_W(x,.)(\alpha,.)\rangle \\ &= \int_S k_W(x,y)\,\langle \alpha, \tau_S(y)\rangle\, d\mathscr{H}^m(y).\end{aligned}$$

Thus the scalar product between two m-rectifiable orientable sets S and C can be expressed as

$$\langle [S],[C]\rangle_{W'} = \int_S \int_C k_W(x,y)\,\langle \tau_S(x), \tau_S(y)\rangle_{\Lambda^m(R^d)}\, d\mathscr{H}^m(x) d\mathscr{H}^m(y) \tag{3.4}$$

where $\tau_S(x)$ is the m-vector associated with a positively oriented orthonormal basis of T_xS.

The distance between two shapes S and C is then

$$d(C,S)^2 = \|[S]-[C]\|^2_{W'} = \langle [S],[S]\rangle_{W'} - 2\,\langle [S],[C]\rangle_{W'} + \langle [C],[C]\rangle_{W'}\,.$$

In the discrete setting, the expression of the scalar product is simple using dirac approximations in the space of currents (2.2) and (2.3) seen in Chapter 2. For two discrete curves $C = \cup_{i=1}^N C_i$ and $S = \cup_{i=1}^M S_j$,

$$\langle [C],[S]\rangle_{W'} = \sum_{i=1}^N \sum_{j=1}^M k_p(c_i,s_j)\,\langle f_i, g_j\rangle\,. \tag{3.5}$$

where c_i (resp. s_j) is the middle of the segment C_i (resp. S_j) and f_i is the *oriented* edge (a vector) associated with C_i (resp. g_j with S_j).

For two triangulation meshes $\mathcal{T} = \sum_{i=1}^N T_i$ and $\mathcal{T}' = \sum_{j=1}^M T'_j$, with n_{T_i} the oriented normal vector of the triangle T_i, we have:

$$\langle [\mathcal{T}],[\mathcal{T}']\rangle_{W'} = \sum_{i=1}^N \sum_{j=1}^M \mathcal{A}(T_i)\mathcal{A}(T'_j) k_p(b_i,b'_j)\left\langle n_{T_i}, n_{T'_j}\right\rangle, \tag{3.6}$$

where b_i is the barycentre of the triangle T_i.

Kernel metrics on varifolds

The same work can be done to provide a metric on the space of varifolds, $\mathscr{C}_0(\mathbb{R}^d \times G(d,m))'$. For this, we construct first a RKHS $W \hookrightarrow \mathscr{C}_0(\mathbb{R}^d \times G(d,m))$ (i.e. $\|u\|_\infty \leq C\,\|u\|_W$). Once the Hilbert space is set, we have for X a m-rectifiable set,

$$\begin{aligned}|\mu_X(u)| = \Big|\int_X u(x,T_xX) d\mathscr{H}^m(x)\Big| &\leq \int_X |u(x,T_xX)| d\mathscr{H}^m(x) \\ &\leq C\mathscr{H}^m(X)\,\|u\|_W\,,\end{aligned}$$

which means that $\mu_X \in W'$. The varifold representations of m-rectifiable sets are in W' and the dual scalar product on W' provides scalar product on shapes. We are left to design a scalar positive definite kernel K_W on the space $\mathbb{R}^d \times G(d,m)$ that will generate a Hilbert space $W \hookrightarrow \mathscr{C}_0(\mathbb{R}^d \times G(d,m))$. This has been done in [Charon and Trouvé, 2013, Charon, 2013] and we sum up briefly the construction of the kernel, referring to these works for more details.

The kernel $K_W : (\mathbb{R}^d \times G(d,m))^2 \to \mathbb{R}$ involves two independent aspects: the spatial information contained in $\mathbb{R}^d$ and the tangential information contained in $G(d,m)$. For this, we build the kernel as a product of two kernels: a spatial kernel $k_p : (\mathbb{R}^d)^2 \to \mathbb{R}$ and a tangential kernel $k_t : G(d,m)^2 \to \mathbb{R}$. k_p is often a Gaussian or Cauchy kernel, as for currents. The tangential kernel is more involved since it necessitates to define a coherent kernel on $G(d,m)$. The simplest way to do so is probably to identify a m dimensional subspace $Q \in G(d,m)$ with the orthogonal projection on Q, denoted P_Q. By doing so, we can consider $G(d,m)$ as a subspace of $\mathcal{L}(\mathbb{R}^d)$. This space is a vector space of dimension d^2 and is endowed with a canonical scalar product, associated with the Frobenius norm:

$$\langle A, B \rangle_{\mathcal{L}(\mathbb{R}^d)} = \mathrm{tr}(A^T B).$$

Once this observation is done, we have access to classical kernels as:

- The *linear kernel* $k_t(V,W) = \langle P_V, P_W \rangle$,
- More generally, the *polynomial kernel*, $k_t(V,W) = \langle P_V, P_W \rangle^k$, $k \in \mathbb{N}^*$.
- The *Gaussian kernel*: $k_t(V,W) = \exp\left(- \frac{|P_V - P_W|^2}{\sigma^2} \right)$.

One should notice that all these kernels have a simple expression through the *principal angles* ([Charon, 2013], chapter 3), that becomes explicit when dealing with polygonal meshes as triangulation or union of segments.

Remark 3.10. *We could also have used the identification between $G(d,m)$ and the projective space of $\Lambda^m(\mathbb{R}^d)$, denoted $P(\Lambda^m(\mathbb{R}^d))$. To a m dimensional vector space V of $\mathbb{R}^d$, we associate the one dimensional subspace generated by $\Lambda_{i=1}^m e_i$ where the frame $(e_1, \dots, e_m)$ spans V, see again [Charon, 2013], chapter 3.*

Now that we have the two kernels k_p and k_t, we define K_W as

$$K_W\big((x,V),(y,W)\big) = k_p(x,y) k_t(V,W).$$

It defines a positive definite kernel on $\mathscr{C}_0(\mathbb{R}^d \times G(d,m))$. The scalar product between "dirac" varifolds defined in definition 2.28 is explicit:

$$\big\langle \delta_{(x,P)}, \delta_{(y,Q)} \big\rangle_{W'} = k_p(x,y) k_t(P,Q),$$

and the scalar product between two varifolds associated with m-rectifiable sets S and C is:

$$\langle \mu_S, \mu_C \rangle_{W'} = \int_S \int_C k_p(x,y) k_t(T_x S, T_y C) d\mathscr{H}^m(x) d\mathscr{H}^m(y). \tag{3.7}$$

Note that for two polygonal mesh $\mathcal{P} = \cup_{i=1}^{N} P_i$ with b_i the barycentre of each convex cell P_i (resp. $\mathcal{P}' = \cup_{i=1}^{M} P'_i$, with barycentre b'_i), we get using approximations as in (2.7) and (2.8)

$$\langle \mu_{\mathcal{P}}, \mu'_{\mathcal{P}} \rangle_{W'} = \sum_{i=1}^{N} \sum_{j=1}^{M} |P_i||P'_j| k_p(b_i, b'_j) k_t\big(< P_i >, < P'_j > \big). \tag{3.8}$$

where $|P_i|$ is the area of the cell P_i and $< P_i >$ is the vector space spans by P_i.

With the same notation as for (3.5), the previous equation writes in the case of discrete curves with linear kernel for k_t

$$\langle \mu_{\mathcal{T}}, \mu_{\mathcal{T}'} \rangle_{W'} = \sum_{i=1}^{N} \sum_{j=1}^{M} k_p(c_i, s_j) |C_i||S_j| \left\langle f_i/|f_i|, g_j/|g_j| \right\rangle^2. \tag{3.9}$$

Notice that we retrieve here the fact that varifolds are non oriented objects: the scalar product does not depend on the choice of the orientation for each edge $\pm f_i$. One can check that in the case of two triangulations in $\mathbb{R}^3$, with the linear kernel for k_t, we get:

$$\langle \mu_{\mathcal{T}}, \mu_{\mathcal{T}'} \rangle_{W'} = \sum_{i=1}^{N} \sum_{j=1}^{M} k_p(t_i, t'_j) |T_i||T'_j| \left\langle n_{T_i}, n_{T'_j} \right\rangle^2 \tag{3.10}$$

where n_{T_i} is one of the two normal vectors of T_i. Once again the scalar product does not depend on the choice of the normal vector $\pm n_T$.

Remark 3.11. *An important question to tackle is the question of* universality. *With the kernels that we choose, we have an embedding $j : W \hookrightarrow \mathscr{C}_0(\mathbb{R}^d \times G(d,m))$, i.e. a continuous injection. The dual application is $j^* : \mathscr{C}_0(\mathbb{R}^d \times G(d,m))' \to W'$. However, j^* needs not be injective. This means that two distinct varifolds μ and μ' may have the same image by j^*. And so, the distance between μ and μ' in W' is null: the metric on W' is only a pseudo distance on $\mathscr{C}_0(\mathbb{R}^d \times G(d,m))'$. The property of* universality *for a kernel, introduced in [Carmeli et al., 2008], is equivalent to the fact that j^* is an embedding.*

This question has been answered in the case of varifolds in [Charon, 2013]. For example, in the case of Gaussian kernels for k_p and k_t, the kernel K_W fulfils the condition of universality and the distance on W' is a real distance on the space of varifolds. We refer to [Charon, 2013], 3.3.2 for more details. This question will be tackled more specifically in the case of kernel metrics on normal cycles in section 3.4.

A weaker result can be shown: even in the case of the linear kernel for k_t, the norm on W' defines a distance on the varifolds associated with submanifolds. *See [Charon, 2013], chapter 3 for more details.*

3.3 Kernel Metrics on Normal Cycles

3.3.1 Spatial kernel, normal kernel

Normal cycles are $(d-1)$-currents on the space $\mathbb{R}^d \times S^{d-1}$, i.e. elements of $\Omega_0^{d-1}(\mathbb{R}^d \times S^{d-1})'$. Thus, the previous construction on currents can be used to define a distance between shapes as the norm of the difference of their normal cycles for a given kernel metric. This requires only to choose a scalar positive definite kernel k on $\mathbb{R}^d \times S^{d-1}$. We define k as a product of two positive definite kernel, a point kernel k_p and a normal kernel k_n:

$$k((x,u),(y,v)) = k_p(x,y)k_n(u,v).$$

which is a positive definite kernel ([Aronszajn, 1950]). Defining k as a product of two kernels is justified by the fact that the point-space $\mathbb{R}^d$ and the normal-space S^{d-1} have different geometric meanings and therefore should be considered separately. The choice of the spatial kernel is classical in computational anatomy, and k_p is often a Gaussian kernel $k_p(x,y) = \exp\left(\frac{-|x-y|^2}{\sigma_W^2}\right)$ or a Cauchy kernel $k_p(x,y) = \frac{1}{1+\frac{|x-y|^2}{\sigma_W^2}}$.

3.3.2 Choice of the normal kernel

We focus now on the choice of k_n. The features that we want for this kernel are the following: it has to fulfil the hypothesis of proposition 3.16, namely $k_n(u,.)$ has to be $\mathscr{C}^1$. Moreover we would like to have an explicit expression of k_n, which fits well in a computational framework. For this we will intensively use expansions in spherical harmonics. For a complete summary on spherical harmonics, see [Atkinson and Han, 2012].

Following [Atkinson and Han, 2012], Sect. 3.9, we will consider kernels of the form

$$k_n(u,v) = \sum_{l\geq 0}\sum_{m=-l}^{l} \alpha_{l,m} Y_{l,m}(u) Y_{l,m}(v) \tag{3.11}$$

that is kernels with an explicit expansion in spherical harmonics. We will see that this expression encompasses some well known kernels as for example the linear kernel restricted to the sphere or some reproducing kernels of Sobolev spaces. Moreover, it is possible to link the regularity of the kernel k_n and the coefficients $\alpha_{l,m}$. Finally, we have a control of the approximation by truncation of (3.11).

First of all, for both numerical purposes and applications, the kernel k_n should be rotational invariant, i.e.

$$k_n(Ru,Rv) = k_n(u,v),\ \forall R \in O_d(\mathbb{R}^d)$$

this is the case if, and only if in the expression (3.11), $\alpha_{l,m}$ does not depend on m (Th. 3.25 of [Atkinson and Han, 2012]). Thus we are looking now at kernels with

expression

$$k_n(u,v) = \sum_{l\geq 0} a_l \sum_{m=-l}^{l} Y_{l,m}(u)Y_{l,m}(v).$$

Using real valued spherical harmonics (see Appendix B), we get

$$k_n(u,v) = \sum_{l\geq 0} a_l \left\{ Y_{l0}(u)Y_{l0}(v) + \sum_{m=1}^{l} (Y^c_{l,m}(u)Y^c_{l,m}(v) + Y^s_{l,m}(u)Y^s_{l,m}(v)) \right\}. \quad (3.12)$$

Theorem 3.12. *If $\sum_{l\geq 0} |a_l|(2l+1) < +\infty$, the kernel defined in (3.12) is continuous.*

Proof. Using the Addition Theorem (Th. 2.9 of [Atkinson and Han, 2012], recall in Appendix B), we have

$$k_n(u,v) = \sum_{l\geq 0} a_l \frac{(2l+1)}{4\pi} P_l(\langle u,v\rangle).$$

where P_l are the Legendre polynomials. We can show that $\forall x \in [-1,1]$, $|P_l(x)| \leq 1$. Thus, if $\sum_{l\geq 0} |a_l|(2l+1) < +\infty$, the sum in (3.12) uniformly converges, and thus the kernel is continuous. □

The Sobolev kernel seen in subsection 3.1.3 has nice embedding property:

Proposition 3.13. *If k_p is a scalar kernel, $k_p(x,.) \in \mathscr{C}^1_0(\mathbb{R}^d,\mathbb{R})$, k_n is the reproducing kernel of $H^s(S^{d-1})$, $s > \frac{d+1}{2}$, then $W \hookrightarrow \Omega^{d-1}_{1,0}(\mathbb{R}^d \times S^{d-1})$.*

Proof. If we choose $s > \frac{d+1}{2}$ for the Sobolev kernel k_n, then we have Sobolev injections (see [Brézis, 2011], Chap. IX. The results can be applied straightforwardly to the case of compact submanifolds without boundaries using partition of unity on a finite atlas of the manifold): $H^s(S^{d-1}) \hookrightarrow \mathscr{C}^j(S^{d-1})$, $\forall 0 \leq j < s - \frac{d-1}{2}$. Thus if $s > \frac{d+1}{2}$, $H^s(S^{d-1}) \hookrightarrow \mathscr{C}^1(S^{d-1})$. K_W, which is a tensor product of k_p and k_n is such that $\partial_1\partial_2 K$ (with the same notations as [Micheli and Glaunès, 2014]) exists, and is continuous, and locally bounded. Moreover, $K_W(.,(x,u))\tau \in \mathscr{C}^1_0\left(\mathbb{R}^d \times S^{d-1}, \Lambda^{d-1}\left(\mathbb{R}^d \times \mathbb{R}^d\right)\right)$ because $k_p(x,.) \in \mathscr{C}^1_0(\mathbb{R}^d,\mathbb{R})$. By Theorem 2.11 of [Micheli and Glaunès, 2014], we conclude that $W \hookrightarrow \Omega^{d-1}_{1,0}(\mathbb{R}^d \times S^{d-1})$. □

In one hand, the Sobolev kernel has nice regularity properties that provides a sound mathematical framework (see section 3.4). But on the other hand its complexity is prohibitive for now in the case of surfaces. This is why we will use simpler kernels: the constant kernel $k_n(u,v) = 1$ and the linear kernel $k_n(u,v) = \langle u,v\rangle$. Notice that the constant kernel is only a semi-definite kernel. However it will prove useful to simplify the computation of the discrete scalar product. The Sobolev kernel will be implemented for discrete curves only.

3.3.3 Orthogonality in the RKHS

Now the reproducing kernel for normal cycles will be $\langle K_W((x,u),(y,v))\eta,\nu\rangle_{\Lambda^{d-1}(\mathbb{R}^d\times\mathbb{R}^d)} = k_p(x,y)k_n(u,v)\langle\eta,\nu\rangle_{\Lambda^{d-1}(\mathbb{R}^d\times\mathbb{R}^d)}$ with $x,y\in\mathbb{R}^d,\ u,v\in S,\ \eta,\nu\in\Lambda^{d-1}(\mathbb{R}^d\times\mathbb{R}^d)$.

Remark 3.14. *Instead of the canonical scalar product on $\mathbb{R}^d\times\mathbb{R}^d$, we can choose a weighted scalar product, as for example: $\langle(\tau_1,\nu_1),(\tau_2,\nu_2)\rangle_\lambda := \tau_1\cdot\tau_2+\lambda\nu_1\cdot\nu_2$, where $\tau_i,\nu_i\in\mathbb{R}^d$ and $\lambda>0$. The scalar product on $\Lambda^{d-1}(\mathbb{R}^d\times\mathbb{R}^d)$ is then:*

$$\langle u_1\wedge\cdots\wedge u_{d-1}, v_1\wedge\cdots\wedge v_{d-1}\rangle_\lambda := \det\left(\langle u_i,v_i\rangle_\lambda\right)$$

where $u_i,v_i\in\mathbb{R}^d\times\mathbb{R}^d$. This introduces a new weight parameter in the model, but is justified again by the fact that the two $\mathbb{R}^d$ spaces in the cartesian product have different geometric meanings. Also, as we will see in Chapter 4, when analyzing homogeneity properties of the functional with respect to scaling, it seems clear that λ should depend on the scale σ_W of the space kernel k_p.

We recall that we can decompose the space $\Omega_0^{d-1}(\mathbb{R}^d\times S^{d-1})$ as a direct sum of W_i^{d-1} defined in definition 2.42 and following remark:

$$\Omega_0^{d-1}(\mathbb{R}^d\times S^{d-1}) = \bigoplus_{i=0}^{d-1} W_{i,0}^{d-1}.$$

where $W_{i,0}^{d-1} = W_i^{d-1}\cap\Omega_0^{d-1}(\mathbb{R}^d\times S^{d-1})$ With the choice of scalar kernels, we have an interesting feature for the scalar product on normal cycles associated wit the kernel metrics: the planar, cylindrical and spherical part are orthogonal with each other. This is sum u in the next proposition.

Proposition 3.15. *Suppose that k_p and k_n are scalar kernels. Then the sum $\bigoplus_{i=0}^{d-1} W_i^{d-1}$ is orthogonal for the kernel metric:*

$$W_{j,0}^{d-1}\cap W \perp_W W_{i,0}^{d-1}\cap W \text{ for } i\neq j$$

Proof. Since the scalar product on W comes from a scalar kernel:

$$K_W\big((x,u),(y,v)\big) = k_p(x,y)k_n(u,v)\mathrm{Id}_{\Lambda^{d-1}(\mathbb{R}^d\times\mathbb{R}^d)}.$$

Thus, we see that the spaces W_i^{d-1} are orthogonal because the spaces F_i^{d-1} are orthogonal for the canonical scalar product on $\Lambda^{d-1}(\mathbb{R}^d\times\mathbb{R}^d)$. Let us prove this property for the cylindrical and spherical part (i.e. in our case F_0^{d-1} and F_1^{d-1}. The proof of the other orthogonal properties are similar. The respective typical $d-1$-vector associated are of the form $\tau = (\tau_1,0)\wedge(0,\tau_2)\wedge\ldots\wedge(0,\tau_{d-1})$ and $\nu = (0,\nu_1)\wedge\ldots\wedge(0,\nu_{d-1})$, and the scalar product between those two vectors is:

$$\langle \tau, \nu \rangle = \begin{vmatrix} (\tau_1,0).(0,\nu_1) & (\tau_1,0).(0,\nu_2) & \cdots & (\tau_1,0).(0,\nu_{d-1}) \\ (0,\tau_2).(0,\nu_1) & (0,\tau_2).(0,\nu_2) & \cdots & (0,\tau_2).(0,\nu_{d-1}) \\ \vdots & \vdots & & \vdots \\ (0,\tau_{d-1}).(0,\nu_1) & (0,\tau_{d-1}).(0,\nu_2) & \cdots & (0,\tau_{d-1}).(0,\nu_{d-1}) \end{vmatrix} = 0$$

since all coefficients in the first line of the above matrix equal to zero. Thus the scalar product of a cylindrical part and a spherical part of normal cycles vanishes. □

This means that the spaces $(W_{i,0}^{d-1} \cap W)'$ are orthogonal for the scalar product on W'. Considering $\Omega_0^2(\mathbb{R}^3 \times S^2)$, i.e. curves or surfaces in $\mathbb{R}^3$, the planar part, cylindrical part and spherical part of the normal bundle are orthogonal for the kernel metric. This will simplify a lot the calculus of the scalar product between discrete shapes. And it inspires the decomposition of the normal cycle that has been done in subsection 2.4.3.

3.3.4 Scalar product on normal cycles

Proposition 3.16. *If k_p is a scalar kernel, $k_p(x,.) \in \mathscr{C}_0^1(\mathbb{R}^d, \mathbb{R})$, k_n is the normal kernel, $k_n(u,.) \in \mathscr{C}^1(S^{d-1})$, then $W \hookrightarrow \Omega_{1,0}^{d-1}(\mathbb{R}^d \times S^{d-1})$.*

Proof. This is simply an application of proposition 3.9. □

And for the same reason as for classical currents (see (3.3)), for every S set with positive reach, $N(S) \in W'$. Thus the Hilbert norm on W' is a dissimilarity measure for normal cycles. The fact that this norm is a proper metric on the space $\Omega_0^{d-1}(\mathbb{R}^d \times S^{d-1})'$ is not obvious and will be seen in section 3.4.

The scalar product between two shapes S and C (which are both sets with positive reach) is

$$\langle N(C), N(S) \rangle_{W'} = \int_{\mathcal{N}_C} \int_{\mathcal{N}_S} k_p(x,y) k_n(u,v) \, \langle \tau_{\mathcal{N}_S}(x,u), \tau_{\mathcal{N}_C}(y,v) \rangle_{\Lambda^{d-1}(\mathbb{R}^d \times \mathbb{R}^d)} \\ d\mathscr{H}^{d-1}(x,u) d\mathscr{H}^{d-1}(y,v) \quad (3.13)$$

The kernel in this formula takes into account both the spatial localization and the normal position through the kernel and the tangent plane of the normal bundle ($\langle \tau_{\mathcal{N}_S}(x,u), \tau_{\mathcal{N}_C}(y,v) \rangle$). The square of the distance between shapes is then:

$$d(S,C)^2 = \|N(S) - N(C)\|_{W'}^2 = \langle N(S), N(S) \rangle_{W'} \\ + \langle N(C), N(C) \rangle_{W'} - 2 \langle N(S), N(C) \rangle_{W'} \quad (3.14)$$

This equation remains valid for sets that are unions of sets with positive reach.

3.4 Universality

As explained previously, the kernel setting provides a dissimilarity measure between shapes through the expression (3.14). In this subsection we tackle briefly whether or not this dissimilarity measure is a real distance.

With proposition 3.13 we have a continuous injection $j : W \hookrightarrow \Omega_0^{d-1}(\mathbb{R}^d \times S^{d-1})$. However the dual metric that we use on normal cycles comes from the continuous dual application :

$$j^* : \Omega_0^{d-1}(\mathbb{R}^d \times S^{d-1})' \to W'$$

which may not be injective. This results in a pseudo distance only : it may be possible to have $N, M \in \Omega_0^{d-1}(\mathbb{R}^d \times S^{d-1})'$, $N \neq M$ with $\|j^*(N) - j^*(M)\|_{W'} = 0$. Thus, we have no guarantee that the distance (3.14) is a proper distance. We will prove here that with some specific kernels k_p and k_n, this does not happen, and thus the dissimilarity measure is a proper distance.

Using a corollary of the Hahn-Banach theorem ([Brézis, 2011], Corollary 1.8), it can be shown that j^* is injective if, and only if W is dense in $\Omega_0^{d-1}(\mathbb{R}^d \times S^{d-1})$. This density property of a RKHS in a space of continuous functions is called the $\mathscr{C}^0$**-universality** of the kernel. It has first interest in machine learning with kernels as it guarantees that any continuous target function can be approximated using the kernel. It has been studied for scalar kernels in [Micchelli et al., 2006], and in the case of vector valued kernels in [Carmeli et al., 2008]. Note that the universality is also useful for optimal interpolation in Hilbert subspaces [Werther, 2003], chapter 4. As far as we know, this point of universality has been first addressed in the setting of dissimilarity measure for shapes in [Charon and Trouvé, 2013], with kernel metrics on varifolds.

Theorem 3.17. *d defined in* (3.14) *with kernels of proposition* 3.13 *is a distance on* $\Omega_0^{d-1}(\mathbb{R}^d \times S^{d-1})'$.

Proof. In our framework, we have a RKHS W, with kernel $K_W : (\mathbb{R}^d \times S^{d-1})^2 \to \mathcal{L}\left(\Lambda^{d-1}(\mathbb{R}^d \times \mathbb{R}^d)\right)$, with $K_W((x,u),(y,v)) = k_p(x,y)k_n(u,v)\mathrm{Id}_{\Lambda^{d-1}(\mathbb{R}^d \times \mathbb{R}^d)}$. Using Example 14 in [Carmeli et al., 2008], K_W is a universal kernel if, and only if $k_p \otimes k_n$ is a universal scalar kernel. Moreover, using Example 15 of the same reference, for $k_p \otimes k_n$ to be universal, it is sufficient that k_p and k_n are universal. We are left to show that both k_p and k_n are universal. In our applications, k_p will be a Gaussian kernel, which is universal (see [Carmeli et al., 2008] or [Micchelli et al., 2006]). For the normal kernel k_n, we will make use of the expansion in spherical harmonics : indeed, we recall that we choose $k_n(x,y) = \sum_{l \in \mathbb{N}} \sum_{m=-l}^{l} \frac{1}{(1+l(l+1))^s} Y_{lm}(x) Y_{lm}(y)$. Using theorem 7 of [Micchelli et al., 2006], and the fact that the spherical harmonics are dense in $\mathscr{C}(S^2)$ for the norm of uniform convergence ([Gallier, 2013], Prop. 1.6), we get that k_n is a universal kernel as well. Thus the reproducing kernel K_W is a $\mathscr{C}^0$-universal kernel and the dual application j^* is one-to-one, which proves that d defined in (3.14) is a proper distance on normal cycles. □

3.5 Insight of the Properties of the Metric with Constant or Linear Normal Kernels

In this section, we study two specific normal kernels k_n: the constant kernel and the linear kernel. Both kernels give simple expression for the metric on normal cycles. In this setting, we are able to provide information in term of the curvature that is encoded for the associated metric.

3.5.1 Constant Kernel

Let us start with the constant kernel $k_n(u, v) = 1$, for all $u, v \in S^{d-1}$. The kernel K_W on $\Omega_0^{d-1}(\mathbb{R}^d \times S^{d-1})$ is then:

$$K_W\big((x,u),(y,v)\big) = k_p(x,y)\mathrm{Id}_{\Lambda^{d-1}(\mathbb{R}^d\times\mathbb{R}^d)}.$$

and the expression of scalar product between two normal cycles $N(C)$ and $N(S)$, associated with shapes S and C is

$$\langle N(C), N(S)\rangle_{W'} = \int_{\mathcal{N}_C}\int_{\mathcal{N}_S} k_p(x,y)\,\langle \tau_{\mathcal{N}_C}(x,u), \tau_{\mathcal{N}_S}(y,v)\rangle\, d\mathcal{H}^{d-1}(x,u) d\mathcal{H}^{d-1}(y,v), \tag{3.15}$$

Even though we use a constant kernel for the normal kernel k_n, this does not mean that we get rid of any information on the normal part. Indeed, as we can see in (3.15), the normal part is involved through the scalar product of the tangent vectors of the normal bundle.

Sensitivity of the kernel metric to the curvature of the shape

Let us now investigate which kind of curvature we can hope to retrieve with this coarse kernel. For this purpose, we consider C a smooth closed surface in $\mathbb{R}^3$. We recall that with the construction of the RKHS W, we have $N(C) \in \Omega_0^2(\mathbb{R}^3 \times S^2)' \subset W'$. Now we want to specify which kind of curvature about C the metric on W' is sensitive to. For this, we focus on the representation of $N(C)$ on W, i.e. $\mathcal{K}_W N(C) \in W \hookrightarrow \Omega_0^2(\mathbb{R}^2 \times S^2)$. Once this representation is clear, we can draw a link between the differential form $\mathcal{K}_W N(C)$ and the work that we have presented on curvature, section 2.5. Using the same notation as definition 2.42, we want to express $\mathcal{K}_W N(C)$ in the spaces resp. W_0^2, W_1^2 and W_2^2 as these spaces are closely linked to the curvature (respectively Gaussian, mean and area form).

For this, consider $(y, v) \in \mathbb{R}^3 \times S^2$, $\tau \in \Lambda^2(\mathbb{R}^3 \times S^2)$ and $\omega \in W$, $\omega = k_p(y, .)\,\langle \tau, .\rangle$.

$$\begin{aligned} N(C)(\omega) &= \big\langle N(C), \mathcal{K}_W^{-1}\omega\big\rangle_{W'} = \langle \mathcal{K}_W N(C), \omega\rangle_W = \mathcal{K}_W^{-1}\omega\big(\mathcal{K}_W N(C)\big) \\ &= \int_{\mathcal{N}_C} k_p(x,y)\,\langle \tau_{\mathcal{N}_C}(x,u), \tau\rangle\, d\mathscr{H}^2(x,u). \end{aligned}$$

With the same notation as in section 2.5 and with the Co-Area formula, we get:

$$\left\langle N(C), \mathcal{K}_W^{-1}\omega \right\rangle_{W'} = \int_C k_p(x,y) \left\langle \int_{\mathrm{Nor}^u(x,C)} \prod_{i=1}^{2} \sqrt{1+k_i^2(x,n)}\tau_{\mathcal{N}_C}(x,u) d\mathscr{H}^0(u), \tau \right\rangle d\mathscr{H}^2(x).$$

(we recall that $k_i(x,n)$ are generalized curvature introduced in Chapter 2, (2.11)). Let $x \in C \mapsto n(x) \in S^2$ be a normal vector field orienting the surface C. Then we recall that at each point $x \in C$, C has two directions of principal curvatures $b_1(x), b_2(x)$ associated with curvatures $\kappa_1(x)$ and $\kappa_2(x)$ and that

$$\tau_{\mathcal{N}_C}(x,n) = \frac{1}{\sqrt{1+k_1^2(x,n)}} \frac{1}{\sqrt{1+k_2^2(x,n)}} \begin{pmatrix} b_1(x,n) \\ k_1(x,n)b_1(x,n) \end{pmatrix} \wedge \begin{pmatrix} b_2(x,n) \\ k_2(x,n)b_2(x,n) \end{pmatrix}$$

and we have

$$\begin{pmatrix} b_1(x,n(x)) \\ k_1(x,n(x))b_1(x,n(x)) \end{pmatrix} \wedge \begin{pmatrix} b_2(x,n(x)) \\ k_2(x,n(x))b_2(x,n(x)) \end{pmatrix} = \begin{pmatrix} b_1(x) \\ \kappa_1(x)b_1(x) \end{pmatrix} \wedge \begin{pmatrix} b_2(x) \\ \kappa_2(x)b_2(x) \end{pmatrix}$$

and

$$\begin{pmatrix} b_1(x,-n(x)) \\ k_1(x,-n(x))b_1(x,-n(x)) \end{pmatrix} \wedge \begin{pmatrix} b_2(x,-n(x)) \\ k_2(x,-n(x))b_2(x,-n(x)) \end{pmatrix} = - \begin{pmatrix} b_1(x) \\ -\kappa_1(x)b_1(x) \end{pmatrix} \wedge \begin{pmatrix} b_2(x) \\ -\kappa_2(x)b_2(x) \end{pmatrix}$$

Thus, one gets immediately

$$\int_{\mathrm{Nor}^u(x,C)} \prod_{i=1}^{2} \sqrt{1+k_i^2(x,n)}\tau_{\mathcal{N}_C}(x,u) d\mathscr{H}^0(u) = 2\left[\begin{pmatrix} b_1 \\ 0 \end{pmatrix} \wedge \begin{pmatrix} 0 \\ \kappa_2 b_2 \end{pmatrix} + \begin{pmatrix} 0 \\ \kappa_1 b_1 \end{pmatrix} \wedge \begin{pmatrix} b_2 \\ 0 \end{pmatrix} \right](x)$$

Re-injecting this expression in $\left\langle N(C), \mathcal{K}_W^{-1}\omega \right\rangle_{W'}$, we obtain:

$$\left\langle N(C), \mathcal{K}_W^{-1}\omega \right\rangle_{W'} = 2\int_C k_p(x,y) \left\langle \left[\begin{pmatrix} b_1 \\ 0 \end{pmatrix} \wedge \begin{pmatrix} 0 \\ \kappa_2 b_2 \end{pmatrix} + \begin{pmatrix} 0 \\ \kappa_1 b_1 \end{pmatrix} \wedge \begin{pmatrix} b_2 \\ 0 \end{pmatrix} \right](x), \tau \right\rangle d\mathscr{H}^2(x).$$

and finally,

$$\mathcal{K}_W N(C) = 2\int_C k_p(x,.) \left\langle \left[\begin{pmatrix} b_1 \\ 0 \end{pmatrix} \wedge \begin{pmatrix} 0 \\ \kappa_2 b_2 \end{pmatrix} + \begin{pmatrix} 0 \\ \kappa_1 b_1 \end{pmatrix} \wedge \begin{pmatrix} b_2 \\ 0 \end{pmatrix} \right](x), . \right\rangle d\mathscr{H}^2(x) \tag{3.16}$$

We have proven that $\mathcal{K}_W N(C) \in W_1^2$. As a reminder, it was shown in section 2.5, (2.33) that the space of differential forms W_0^2 is linked to the Gaussian curvature, W_1^2 to the mean curvature and W_2^2 to the area of the surface. The expression of $\mathcal{K}_W N(C)$ implies that the constant kernel is neither sensitive to the Gaussian curvature nor to the area form of C. On the contrary, it is sensitive to the mean curvature of C. As said previously, it shows that we do not get rid of all the curvature information of the shape, even though the normal kernel is "rough". We will come

across this property of the constant kernel when dealing with triangulated meshes: the kernel metric associated with triangluation will be sensitive to the mean discrete curvature, represented by the edges of the triangles and not to the area (represented by the triangles themselves) or the Gaussian discrete curvature (represented by the vertices).

Remark 3.18. *The same work can be done for discrete curves in $\mathbb{R}^2$: doing so, one can show that*

$$\mathcal{K}_W N(C) = 2 \int_C k_p(x,.) \left\langle \begin{pmatrix} 0 \\ \kappa_1 b_1 \end{pmatrix}(x), . \right\rangle d\mathscr{H}^1(x) \tag{3.17}$$

The metric with constant kernel is sensitive to the curvature in $\mathbb{R}^2$. The calculations are more intricate for curves in $\mathbb{R}^3$, but one gets:

$$\mathcal{K}_W N(C) = \pi \int_C k_p(x,.) \left\langle \begin{pmatrix} 0 \\ \kappa_1 b_1 \end{pmatrix}(x) \wedge \begin{pmatrix} 0 \\ n_0(x) \end{pmatrix}, d \right\rangle \mathscr{H}^1(x)$$

where $n_0(x)$ is the direction of curvature for the curve C (i.e. n_0 points toward the center of the osculating circle of C at point x).

3.5.2 Linear Kernel

The second simplest example of a kernel that we can chose on S^2 is the linear kernel restricted to the sphere:

$$k_n(u,v) = \langle u, v \rangle$$

which generates the space of linear forms on $\mathbb{R}^3$ restricted to S^2. There is another way of seeing this kernel. We recall that the geodesic distance on the sphere, d_S is as follow:

$$d_S(u,v) = \arccos\big(\langle u, v \rangle\big),\ \forall u, v \in S^2$$

Then, $k_n(u,v) = \langle u, v \rangle = \cos\big(d_S(u,v)\big)$. This defines a positive definite kernel associated with the distance on the sphere. If we choose a Gaussian kernel for k_p, the vectorial kernel of the generated RKHS, K_W is then:

$$k_W\big((x,u),(y,v)\big) = \exp(-\|x-y\|^2/\sigma^2)\cos\big(d_S(u,v)\big)\mathrm{Id}_{\Lambda^2(\mathbb{R}^3\times S^2)}.$$

It is thus obvious that we have the embedding of the associated RKHS on $\mathscr{C}^1(S^2)$. However the generated RKHS is not dense in $\mathscr{C}^0(S^2)$ which implies that the universality property is not fulfilled (section 3.4).

Using spherical coordinates, one can easily express k_n using spherical harmonics :

$$k_n(u,v) = \frac{8\pi}{3}\left(Y_{10}(u)Y_{10}(v) + Y^c_{1,1}(u)Y^c_{1,1}(v) + Y^s_{1,1}(u)Y^s_{1,1}(v)\right).$$

The expression of scalar product between two normal cycles $N(C)$ and $N(S)$, associated with shapes S and C is then :

$$\langle N(C), N(S)\rangle_{W'} = \int_{\mathcal{N}_C}\int_{\mathcal{N}_S} k_p(x,y)\,\langle u,v\rangle\,\langle \tau_{\mathcal{N}_C}(x,u), \tau_{\mathcal{N}_S}(y,v)\rangle\, d\mathcal{H}^{d-1}(x,u) d\mathcal{H}^{d-1}(y,v). \tag{3.18}$$

Sensitivity of the kernel metric to the curvature of the shape

We detail here the same work as the one done for the constant kernel: the aim is to express the normal cycle $N(C)$ of a shape C in the space W, namely $\mathcal{K}_W N(C)$. Hence we can express $\mathcal{K}_W N(C)$ in the spaces W_0^2, W_1^2, W_2^2 and formalize the kind of curvature that is encoded by the kernel metric K_W.

Let $(y,v) \in R^3 \times S^2$, $\tau \in \Lambda^2(\mathbb{R}^3 \times S^2)$ and $\omega \in W$, $\omega(x,n) = k_p(y,x)\,\langle v,n\rangle\,\langle \tau, .\rangle$. Consider a closed smooth surface C. The calculations are similar to the one of constant kernel and we have:

$$\left\langle N(C), \mathcal{K}_W^{-1}\omega\right\rangle_{W'} = \int_C k_p(x,y) \left\langle \int_{\mathrm{Nor}^u(x,C)} \langle u,v\rangle \prod_{i=1}^{2} \sqrt{1+k_i^2(x,n)}\,\tau_{\mathcal{N}_C}(x,u) d\mathscr{H}^0(u), \tau \right\rangle d\mathscr{H}^2(x).$$

We suppose that the surface C is oriented by a normal vector field $x \mapsto n(x)$. We need to compute:

$$\begin{aligned}
&\int_{\mathrm{Nor}^u(x,C)} \langle u,v\rangle \prod_{i=1}^{2} \sqrt{1+k_i^2(x,n)}\,\tau_{\mathcal{N}_C}(x,u) d\mathscr{H}^0(u) \\
&= \sum_{\varepsilon=\pm 1} \langle \varepsilon n(x), v\rangle\, \varepsilon \begin{pmatrix} b_1(x,n(x)) \\ \varepsilon\kappa_1(x) b_1(x,n(x)) \end{pmatrix} \wedge \begin{pmatrix} b_2(x,n(x)) \\ \varepsilon\kappa_2(x) b_2(x,n(x)) \end{pmatrix} \\
&= 2\,\langle n(x), v\rangle \left[\begin{pmatrix} 0 \\ \kappa_1 b_1 \end{pmatrix} \wedge \begin{pmatrix} 0 \\ \kappa_2 b_2 \end{pmatrix} + \begin{pmatrix} b_1 \\ 0 \end{pmatrix} \wedge \begin{pmatrix} b_2 \\ 0 \end{pmatrix} \right](x)
\end{aligned}$$

And thus,

$$\left\langle N(C), \mathcal{K}_W^{-1}\omega\right\rangle_{W'} = 2\int_C k_p(x,y) \left\langle \langle n(x), v\rangle \left[\begin{pmatrix} 0 \\ \kappa_1 b_1 \end{pmatrix} \wedge \begin{pmatrix} 0 \\ \kappa_2 b_2 \end{pmatrix} + \begin{pmatrix} b_1 \\ 0 \end{pmatrix} \wedge \begin{pmatrix} b_2 \\ 0 \end{pmatrix} \right](x), \tau \right\rangle d\mathscr{H}^2(x). \tag{3.19}$$

This means that $\mathcal{K}_W N(C)$ has a component on the space W_0^2 and a component on the space W_2^2: the metric on normal cycles with linear normal kernel is sensitive to the Gaussian curvature and to the area form of the surface C. However, it is not sensitive to the mean curvature. We will come across this property with triangulation meshes, since the metric with linear normal kernel will have a term associated with the triangles (discrete volume form), the vertices (Gaussian discrete curvature) but not the edges (mean curvature).

Remark 3.19. *The same work can be done for discrete curves in $\mathbb{R}^2$: doing so, one can show that*

$$\mathcal{K}_W N(C) = 2 \int_C k_p(x,.) \left\langle \begin{pmatrix} b_1 \\ 0 \end{pmatrix}(x), . \right\rangle d\mathscr{H}^1(x)$$

The metric with linear kernel is sensitive to the volume form on the curve but not sensitive to the curvature in $\mathbb{R}^2$. The result is still true for curves in $\mathbb{R}^3$ but the calculations are more intricate.

Remark 3.20. *In fact, the same calculations can be done for normal kernels that write $k_n(u,v) = \langle u, v \rangle^k$, k positive integer. The kind of curvature that is retrieved with the metric on normal cycles depends on the parity of k: if k is even, only the mean curvature will be encoded, and if k is odd, the area form and the Gaussian curvature is encoded.*

A good choice of kernel would be a kernel that captures all the curvatures measures. For example this is the case for the normal kernel which is the sum of the constant kernel and the linear kernel:

$$k_n(u,v) = 1 + \langle u, v \rangle .$$

3.6 Convergence Towards the Continuous Shape

In the former sections we have seen the reproducing kernel theory, applied to obtain an explicit metric on the space of $(d-1)$-currents on $\mathbb{R}^d \times S^{d-1}$ (and in particular on the normal cycles associated with union of sets with positive reach). Now in computational anatomy, a continuous shape is approximated with a polyhedral shape. In order to have a consistent framework, we would like that the normal cycle of the approximation we are dealing with is not too far from the theoretical one. Or at least having a convergence result for the kernel metric when the diameter of meshes is close to 0. The theorem we will use here is from J. Fu [Fu, 1991]. In order to have a convergence result for normal cycle, we have to keep in mind some pathological examples as the Schwarz polyhedron (see the discussion in [Rado, 1943]): it is possible to have a polyhedral approximation of a cylinder, with diameter of meshes going to zero, and yet the area of the approximations blowing up. This is to link with of theorem 2.51 and discussion below, where we have seen that the convergence of normal cycles implies the convergence of areas. This is why it seems necessary to have a control of the way diameters tend towards 0. More precisely for the next result, we will need the notion of *fatness* of a triangulation.

Definition 3.21. *Let T be a k-simplex, with vertices $v_0, \ldots, v_k$. The* size *of T is*

$$\eta(T) := \max |v_i - v_j|$$

The fatness *of T is*

$$\Theta(T) := \min\left\{\frac{\mathcal{H}^j(\mu)}{\eta(T)^j}, \mu \text{ is a } j \text{ dimensional face of } T, j = 0, \ldots, k\right\}$$

Let Δ be a triangulation. The fatness *of Δ is*

$$\Theta(\Delta) := \min\{\Theta(T), T \text{ is a } k\text{-simplex of } \Delta\}$$

This definition of fatness is less restrictive than the usual definition because it takes into account all the j-dimensional faces. Bounding below the fatness of a triangulation guarantees that the angles of the triangles are not too close to 0. Hence we avoid pathological cases as the Schwarz polyhedron.

Now let X be a smooth submanifold in $\mathbb{R}^d$. To have a convergence result for the approximations, we will demand that the approximations are *closely inscribed* in X:

Definition 3.22. *A triangulation Δ is* inscribed *in X if:*

1. *All vertices of Δ lie in X*
2. *All vertices of $\partial\Delta$ lie in ∂X.*

Δ is closely inscribed *in X if, additionally:*

1. *$\Delta \subset X_r$ and the projection on X restricted to Δ is one-to-one.*
2. *$\partial\Delta \subset (\partial X)_r$ and the projection on ∂X restricted to $\partial\Delta$ is one-to-one.*

We can now state J. Fu's theorem:

Theorem 3.23. *Let $(P^n)_{n\in\mathbb{N}}$ be a sequence of triangulations of a smooth submanifold X in $\mathbb{R}^d$, closely inscribed in X. Suppose that $P^n \to X$ and $\partial P^n \to \partial X$ in the Hausdorff metric on subsets of $\mathbb{R}^d$, and that for every $n \in \mathbb{N}$, $\Theta(P^n) \geq c$, for some constant $c > 0$. Then $N(P^n) \xrightarrow[n\to\infty]{} N(X)$ for the flat metric.*

The proof of this theorem is far beyond the scope of this manuscript, thus we will only make a few remarks on it. The proof relies on the theory of compactness for integral currents (see [Federer, 1969], 4.2) coupled with a uniqueness result for normal cycles ([Fu, 1994], 3.). A direct corollary is the convergence of the curvatures of the approximations, in the sense of weak convergence for measures. It can be obtained using the Lipschitz-Killing differential forms (definition 2.49, [Zähle, 1987], [Morvan, 2008] chap. 21). Since this theorem uses compactness, it prevents us from a quantification of the rate of convergence. Note that in [Cohen-Steiner and Morvan, 2003], [Morvan, 2008], the authors use a different argument in order to have a bound for the convergence of curvature measures and tensors, using normal cycles.

This theorem guarantees that under some conditions on the triangulations, we have convergence of the normal cycles of the approximations towards the normal cycle of the smooth manifold, for the flat norm. Then it is sufficient that W is continuously embedded in $\Omega^{d-1}_{1,0}(\mathbb{R}^d \times S^{d-1})$ equipped with the flat norm to have the same result with the kernel metric. The next proposition shows that it depends only on the regularity of the kernel.

Proposition 3.24. *Let k be a positive kernel on the product space $\mathbb{R}^d \times S^{d-1}$, such that k is twice continuously differentiable, with bounded first derivatives. Suppose in addition that for any $(x,u) \in \mathbb{R}^d \times S^{d-1}$, $k((x,u),.)$ and its first order derivative vanish at infinity. Then, the RKHS associated with k is continuously embedded in $\Omega_{1,0}^{d-1}(\mathbb{R}^d \times S^{d-1})$ with the flat norm on differential forms.*

Proof. Following the proof of [Glaunès, 2005], theorem 9, chapter 2, we can show that for any $\omega \in W$,

$$\|\omega\|_{1,\infty} \leq \sqrt{\|k\|_{2,\infty}}\, \|\omega\|_W .$$

Here $\|\omega\|_{1,\infty} = \|\omega\|_\infty + \|D\omega\|_\infty$, where $D\omega$ refers to the differential of ω, *i.e.* ω is seen as an application from $\mathbb{R}^d \times S^{d-1}$ to the vector space $\Lambda^{d-1}(\mathbb{R}^d \times \mathbb{R}^d)^*$. This is not exactly the flat norm, which is $\|\omega\|_F := \|\omega\|_\infty + \|d\omega\|_\infty$, where $d\omega$ designates the exterior derivative of ω. However $\|\omega\|_F \leq cste\, \|\omega\|_{1,\infty}$. $d\omega(x,u)$ is indeed obtained by making $D\omega(x,u)$ into an alternating map in all of its d arguments (and not only in the last $d-1$ ones):

$$d\omega(x,u)(v_1 \wedge \cdots \wedge v_d) = \sum_{i=1}^{d} (-1)^i D\omega(x,u)(v_i)(v_1 \wedge \cdots \wedge v_{i-1} \wedge v_{i+1} \wedge \cdots \wedge v_d)$$

where $v_i \in \mathbb{R}^d$. Thus a control of the uniform norm of $D\omega$ ensures a control on the uniform norm of $d\omega$. So, there exists $C > 0$ such that for every $\omega \in \Omega_0^{d-1}(\mathbb{R}^d \times S^{d-1})$

$$\|\omega\|_F \leq C \sqrt{\|k\|_{2,\infty}}\, \|\omega\|_W$$

which proves the embedding.

□

Thereby, the dual application $j^* : \Omega_{1,0}^{d-1}(\mathbb{R}^d \times S^{d-1})' \hookrightarrow W'$ is continuous and injective with theorem 3.17, and provides a distance on $\Omega_{1,0}^{d-1}(\mathbb{R}^d \times S^{d-1})'$, resulting for the Hilbert structure of the RKHS W. This, combined with theorem 3.23 guarantees the convergence of the approximations for the kernel metric on normal cycles, under the same conditions.

Theorem 3.25. *Let $(P^n)_{n\in\mathbb{N}}$ be a sequence of triangulations of a smooth submanifold X in $\mathbb{R}^d$, closely inscribed in X. Suppose that $P^n \to X$ and $\partial P^n \to \partial X$ in the Hausdorff metric on subsets of $\mathbb{R}^d$, and that for every $n \in N$, $\Theta(P^n) \geq c$, for some constant $c > 0$. Then $N(P^n) \underset{n\infty}{\longrightarrow} N(X)$ for the kernel metric.*

Remark 3.26. *The assumption of closely inscribed triangulations is quite restrictive compared to some assumptions that one can find in the Γ-convergence for functional shapes with varifold norm ([Charlier et al., 2015b]), or in curvature approximation of smooth surfaces ([Cohen-Steiner and Morvan, 2003], [Buet et al., 2015]). We did not investigate much yet to relax it, however it does not seem immediate since we use theorem 3.23, whose proof relies on this hypothesis.*

3.7 Expression of the Kernel Metric for Discrete Shapes

In this section, we derive the expression of the kernel metric for discrete shapes (curves in $\mathbb{R}^3$ and surfaces in $\mathbb{R}^3$) for various normal kernel k_n: constant, linear and Sobolev.

3.7.1 General considerations

Let us first introduce the notations that we will use in the following.

Notations for discrete curves

$C = C_1 \cup \cdots \cup C_{n_C}$, $S = S_1 \cup \cdots \cup S_{n_S}$ will be two unions of segments in $\mathbb{R}^d$. We denote $x_1, \ldots, x_{N_C}$ (resp. $y_1, \ldots, y_{N_S}$) the vertices of C (resp. of S) and $f_i = x_{f_i^2} - x_{f_i^1}, 1 \leq i \leq n_C$ (resp. $g_j = y_{g_j^2} - y_{g_j^1}, 1 \leq j \leq n_S$) the edges of C (resp. S). For an edge f_i, $x_{f_i^1}$ and $x_{f_i^2}$ are its two vertices. Moreover, we define $c_i = \frac{1}{2}(x_{f_i^1} + x_{f_i^2})$, $d_j = \frac{1}{2}(y_{g_j^1} + y_{g_j^2})$ the middles of the edges f_i and g_j, and, $\theta_{ij} = \arccos\left(\left\langle \frac{f_i}{|f_i|}, \frac{g_j}{|g_j|} \right\rangle\right)$ the unoriented angle between f_i and g_j ($\theta_{ij} \in [0, \pi]$).

Notations for triangulated surfaces

Let $\mathcal{T} = \cup_{i=1}^{N} T_i$ and $\mathcal{T}' = \cup_{i=1}^{M} T_i'$ be two triangulated meshes. We denote $x_1, \ldots, x_{n_v}$ (resp. $y_1, \ldots, y_{m_v}$) the vertices of $\mathcal{T}$ (resp. of $\mathcal{T}'$). Given a triangle T_i (resp. T_j'), v_i^1, v_i^2, v_i^3 are its three vertices and b_i its barycentre: $b_i = \frac{1}{3}(v_i^1 + v_i^2 + v_i^3)$ (resp. b_j'). $(f_l)_{1 \leq l \leq n_e}$ (resp $(g_l)_{1 \leq l \leq m_e}$) are the edges of $\mathcal{T}$ (resp. $\mathcal{T}'$). $\pm n_{T_i}$ are the normal vectors of the triangle T_i. Moreover:

- $x_{f_i^1}$ and $x_{f_i^2}$ are the two vertices of f_i: $f_i = x_{f_i^2} - x_{f_i^1}$.
- c_i (resp. d_j) is the middle of the edge f_i (resp. g_j).
- n_{T,f_i} is the normal vector of the triangle T such that $n_{T,f_i} \times f_i$ is oriented inward for the triangle T.

We recall that with the kernel metric, the planar, cylindrical and spherical parts are orthogonal one with another. The calculation of the expression of 3.13 in this case is simplified:

Proposition 3.27. *For any two unions of segments C and S, the cylindrical part $N(C)^{cyl}$ and the approximated cylindrical part $N(C)^{cyl}_{approx}$ are orthogonal to the spherical part $N(S)^{sph}$ with respect to the kernel metric presented in section* 3.3*:*

$$\left\langle N(C)^{cyl}, N(S)^{sph} \right\rangle_{W'} = \left\langle N(C)^{cyl}_{approx}, N(S)^{sph} \right\rangle_{W'} = 0.$$

For any two triangulated surfaces $\mathcal{T}$ and $\mathcal{T}'$, the planar part (exact and approximated), the cylindrical part (exact and approximated), and the spherical part are orthogonal one with another with respect to the kernel metric presented in section 3.3:

$$\left\langle N(\mathcal{T})^{pln}, N(\mathcal{T}')^{cyl} \right\rangle_{W'} = \left\langle N(\mathcal{T})^{cyl}, N(\mathcal{T}')^{sph} \right\rangle_{W'} = \left\langle N(\mathcal{T})^{sph}, N(\mathcal{T}')^{pln} \right\rangle_{W'} = 0$$

Proof. This is an immediate application of proposition 3.15 using the fact that the planar part (resp. cylindrical part, spherical part) are elements of $(W_2^2)'$ (resp. $(W_1^2)'$, $(W_0^2)'$) □

Remark 3.28. *If we consider the weighted scalar product on $\mathbb{R}^d \times \mathbb{R}^d$ (see remark 3.14), then it can be easily shown that we have:*

$$\langle N(C), N(S) \rangle_{W'_\lambda} = \left\langle N(C)^{pln}, N(S)^{pln} \right\rangle_{W'} + \lambda \left\langle N(C)^{cyl}, N(S)^{cyl} \right\rangle_{W'} + \lambda^2 \left\langle N(C)^{sph}, N(S)^{sph} \right\rangle_{W'}$$

where $\langle \cdot, \cdot \rangle_{W'_\lambda}$ denotes the Hilbert metric induced by the weighted metric on $\mathbb{R}^d \times \mathbb{R}^d$.

We see here how convenient the decomposition introduced in subsection 2.4.3 is: we only need to compute scalar products between spherical parts, and scalar products between cylindrical parts. That is what we will do right below.

Error of the approximation

We focus here on the error of approximation between $N(C)_{approx}$ previously defined, and $N(C)$, where C is a discretized curve or surface in $\mathbb{R}^d$. More precisely, if we consider a segment C with extremities a and b, and $\omega \in \Omega^{d-1}(\mathbb{R}^d \times S^{d-1})$, we have for the cylindrical part of the original normal cycle:

$$N(C)^{cyl}(\omega) = \int_{(b-a)\times S^{\perp}_{b-a}} \langle \omega(x,n) | (\tau, 0) \wedge \nu(n) \rangle \, d\mathcal{H}^{d-1}(x,n)$$

where $\tau = \frac{b-a}{\|b-a\|}$, and $\nu(n)$ is defined as in definition 2.47 (for $v = b - a$).

Proposition 3.29. *Assume that W is continuously embedded in $\Omega^{d-1}_{1,0}(\mathbb{R}^d \times S^{d-1})$. Then if C is a discretized curve, we have*

$$\|N(C) - N(C)_{approx}\|_{W'} \leq K l(C) \delta(C)$$

where $l(C) = \mathcal{H}^1(C)$ is the length of C, and $\delta(C)$ is the maximal length of the segments of C. K is a constant.

Moreover is $\mathcal{T}$ is a triangulation mesh, we have:

$$\|N(\mathcal{T}) - N(\mathcal{T})_{approx}\|_{W'} \leq K \mathrm{Area}(\mathcal{T}) \delta(\mathcal{T})$$

with $\delta(\mathcal{T})$ is the maximal area of the triangles of $\mathcal{T}$

Proof. We prove the result for union of segments. The reasoning is similar for triangulated meshes. We recall that we do not use any approximation on the spherical part and that the cylindrical part and the spherical part are orthogonal with respect to the kernel metric. Thus, to estimate the error, it is sufficient to look at the cylindrical part of the normal cycles involved.

Let $\omega \in \Omega^{d-1}_{1,0}(\mathbb{R}^d \times S^{d-1})$ and $S = [a, b]$ be a single segment. We have:

$$\begin{aligned}\left|\left(N(S)^{cyl} - N(S)^{cyl}_{approx}\right)(\omega)\right| &= \left| \int_{(b-a)\times S^{\perp}_{b-a}} \langle \omega(x,n) | (\tau, 0) \wedge \nu(n) \rangle \, d\mathcal{H}^{d-1}(x,n) \right. \\ &\quad \left. - \int_{S^{\perp}_{b-a}} \langle \omega(c,n) | (b-a, 0) \wedge \nu(n) \rangle \, d\mathcal{H}^{d-2}(n) \right| \\ &= \int_{(b-a)\times S^{\perp}_{b-a}} |\langle \omega(x,n) - \omega(c,n) | (\tau, 0) \wedge \nu(n) \rangle| \, d\mathcal{H}^{d-1}(x,n) \quad (3.20)\end{aligned}$$

Since W is assumed to be continuously embedded in the space of $\mathcal{C}^1$ differential forms, then we have $|\omega(x,n) - \omega(c,n)| \leq \|\omega\|_{1,\infty} |x - c| \leq K \|\omega\|_W |c - x|$.

Thus

$$\left|\left(N(S)^{cyl} - N(S)^{cyl}_{approx}\right)(\omega)\right| \leq K' \|\omega\|_W |b - a|^2$$

where K' is a constant taking into account K and the Hausdorff measure of $S^{\perp}_{b-a}$.For the total discretized curve C, we get:

$$\left|\left(N(C)^{cyl} - N(C)^{cyl}_{approx}\right)(\omega)\right| \leq C \|\omega\|_W \, l(C)\delta(C)$$

which proves the result. □

3.7.2 Discrete scalar product with constant normal kernel

In this subsection, we express the discrete version of the scalar product (3.13) for union of segments and surfaces, with the constant normal kernel, $k_n(u, v) = 1$.

Scalar product of discrete curves

Proposition 3.30. *Let C and S be two unions of segments. The scalar product between the associated normal cycles with spatial kernel k_p and normal kernel $k_n(u, v) = 1$ is*

$$\langle N(C), N(S) \rangle_{W'} = \frac{\pi^2}{4} \sum_{i=1}^{N} \sum_{j=1}^{M} k_p(x_i, y_j) \langle A_i, B_j \rangle \quad (3.21)$$

where $A_i = \sum_k f^i_k / |f^i_k|$ is the sum of the normalized edges with x_i as vertex, and oriented outward from x_i.

Proof. See Appendix A.1.1 □

It encompasses the case of branching points with three or more edges with the same vertex x_i. Let us make a few remarks on this expression. Interestingly, this scalar product can be obtained with a metric on current. Indeed, if we denote $W_{curr} \hookrightarrow \Omega^1_0(\mathbb{R}^3)$ the RKHS of differential forms generated with the scalar kernel k_p, then we have

$$\langle N(C), N(S)\rangle_{W'} = \frac{\pi^2}{4}\left\langle \sum_{i=1}^{N} \delta_{x_i}^{A_i}, \sum_{j=1}^{M} \delta_{y_j}^{B_j} \right\rangle_{W'_{curr}}$$

With this metric, a union of segment is seen as a sum of dirac currents, localized at the vertices of the curve, and oriented by the vector A_i. We retrieve the fact that this metric is sensitive to curvature since $\left\|\delta_{x_i}^{A_i}\right\|_{W'_{curr}}$ grows when the discrete curvature at point x_i grows.

The computational complexity is not high compared to current or varifolds. The scalar product is basically a double loop on the vertices. However, we must pre-compute the edges that are linked to each vertex.

We refer to Appendix A.1.1 for the procedure to compute the gradient of this scalar product with respect to the vertices.

Scalar product of triangulation meshes

Proposition 3.31. *Suppose that $\mathcal{T}$ and $\mathcal{T}'$ are two triangulated meshes. The approximated scalar product between the associated normal cycles with spatial kernel k_p and constant normal kernel $k_n(u,v) = 1$ is*

$$\begin{aligned}\langle N(\mathcal{T})_{approx}, N(\mathcal{T}')_{approx}\rangle_{W'} = \frac{\pi^2}{4}\sum_{i=1}^{n_e}\sum_{j=1}^{m_e} k_p(c_i,d_j)\,\langle f_i, g_j\rangle \left\langle \sum_{\{T|f_i \text{ edge of } T\}} n_{T,f_i}, \sum_{\{T'|g_j \text{ edge of } T'\}} n_{T',g_j} \right\rangle \\ + \frac{\pi^2}{4}\sum_{\substack{x_i \text{ vertex}\\ \text{of } \partial\mathcal{T}}}\sum_{\substack{y_j \text{ vertex}\\ \text{of } \partial\mathcal{T}'}} k_p(x_i,y_j)\,\langle A_i, B_j\rangle\end{aligned} \tag{3.22}$$

where $A_i = \sum_k f_k^i/|f_k^i|$ is the sum of the normalized edges of the border, with x_i as vertex, and oriented outward from x_i, and n_{T_i,f_i} is the normal vector of the triangle T_i such that $n_{T_i,f_i} \times f_i$ is oriented inward for the triangle T.

Proof. See Appendix A.1.2 □

This can be re-written:

$$\begin{aligned}\langle N(\mathcal{T})_{approx}, N(\mathcal{T}')_{approx}\rangle_{W'} = \frac{\pi^2}{4}\sum_{i=1}^{n_e}\sum_{j=1}^{m_e} k_p(c_i,d_j)\,\langle f_i, g_j\rangle \left\langle \sum_{\{T|f_i \text{ edge of } T\}} n_{T,f_i}, \sum_{\{T'|g_j \text{ edge of } T'\}} n_{T',g_j} \right\rangle \\ + \langle N(\partial\mathcal{T}), N(\partial\mathcal{T}')\rangle_{W'}\end{aligned} \tag{3.23}$$

The expression $\langle N(\partial\mathcal{T}), N(\partial\mathcal{T}')\rangle_{W'}$ is exactly the scalar product of the curves $\partial\mathcal{T}$ and $\partial\mathcal{T}'$ that has been computed right above. Notice that the planar part and the spherical part are not involved in this scalar product (except for the spherical part of the border).

Some remarks: first, we recall that the previous expression does not necessitate a coherent orientation for the mesh. Secondly, even with a constant kernel k_n for the normal part, the metric is sensitive to curvature. Indeed, for an edge f, the cylindrical part of the scalar product involves scalar products between normal vectors of the adjacent triangles which are required quantities to compute the discrete mean curvature. Another interesting feature to notice is that the scalar product involves a specific term for the boundary which will enforce the matching of the boundaries of the shapes. The fact that the boundary has a special behaviour for the normal cycle metric is not surprising. Indeed a normal cycle encodes generalized curvature information of the shape. Hence, the boundary corresponds to a singularity of the curvature and has a specific behaviour in the kernel metric. We will see in Chapter 4 that this feature is of interest for a matching purpose.

In term of computational complexity, we see in (3.22) that the model of normal cycles on surfaces is more sophisticated, even with a constant normal kernel. The scalar product involves a double loop on the edges of the triangulations, as well as for each edge, the computation of the sum of the normal vector of the adjacent triangles. However, it is the same order of complexity as varifolds for the computation of the scalar product, i.e. $O(n_e^2)$ where n_e is the number of edges which is often the same order as the number of triangles. For the computation of the gradient (see Appendix A), the complexity remains $O(n_e^2)$ but the number of operations for each iteration increases, much more than for varifolds. Thus the evaluation of the gradient is the time-consuming part of the implementation. We refer to Chapter 4 for a further discussion of the time per iteration in the registration framework.

3.7.3 Discrete scalar product with linear normal kernel

Now, we focus on the linear normal kernel, $k_n(u, v) = \langle u, v\rangle$.

Scalar product for discrete curves

Proposition 3.32. *Let C and S be two unions of segments. The approximated scalar product between the associated normal cycles with spatial kernel k_p and linear normal kernel $k_n(u, v) = \langle u, v\rangle$ is*

$$\begin{aligned}\langle N(C)_{approx}, N(S)_{approx}\rangle_{W'} = &\frac{\pi^2}{2}\sum_{i=1}^{n_e}\sum_{j=1}^{m_e} k_p(c_i, s_j)|f_i||g_j|\cos^2\varphi_{ij}\\ &+\frac{16\pi^2}{3}\sum_{k=1}^{N}\sum_{l=1}^{M} k_p(x_k, y_l)\left(1-\frac{n_{x_k}}{2}\right)\left(1-\frac{m_{y_l}}{2}\right)\end{aligned}$$

where n_{x_k} (resp. m_{y_l}) is the number of segments with x_k as vertex (resp. y_l) and $\cos\varphi_{ij} = \langle f_i/|f_i|, g_j/|g_j|\rangle$.

Proof. See Appendix A.2.1. □

We obtain a metric that is the sum of two terms. The first term, associated with the cylindrical part is exactly a varifold term with the linear kernel on $G(d,m)$ (3.8). The second term, associated with the spherical part vanishes, except for branching points or extremities.

For a regular closed discrete curve, this metric is thus exactly the one of varifolds with the linear kernel on the Grassmanian. We retrieve the fact that with the linear normal kernel we do not get curvature information for curves. The spherical term can be seen as a measure term. In fact, if we consider the RKHS of scalar functions generated by the scalar kernel k_p, and we denote it W_{meas}, and if we denote W_{var} the RKHS of $\mathscr{C}^0(\mathbb{R}^3 \times G(3,1))$ generated by the scalar kernel $k_p \otimes k_t$ with k_t the linear kernel on the Grassmanian, then:

$$\langle N(C)_{approx}, N(S)_{approx} \rangle_{W'} = \frac{\pi^2}{2} \langle \mu_C, \mu_S \rangle_{W'_{var}} + \frac{16\pi^2}{3} \left\langle \sum_{k=1}^{N} \left(1 - \frac{n_{x_k}}{2}\right) \delta_{x_k}, \sum_{l=1}^{M} \left(1 - \frac{m_{y_l}}{2}\right) \delta_{y_l} \right\rangle_{W'_{meas}}$$

The complexity is the same as for varifolds, since for most curves, the number of extremities or branching points is very low.

Scalar product for triangulation meshes

For the linear kernel, the scalar product between spherical part is complex and thus we provide for now only a truncated version of the exact scalar product. This truncation is an important limitation: the approximated scalar product has no theoretical guarantee. However, it is still interesting to discuss it.

Proposition 3.33. *Suppose that $\mathcal{T}$ and $\mathcal{T}'$ are two triangulated meshes. The* truncated *scalar product between the associated normal cycles with spatial kernel k_p and linear normal kernel $k_n(u,v) = \langle u, v \rangle$ is*

$$\langle N(\mathcal{T})_{approx}, N(\mathcal{T}')_{approx} \rangle_{W',trunc} = 4 \sum_{i=1}^{N} \sum_{j=1}^{M} k_p(b_i, b'_j) |T_i| |T'_j| \left\langle n_{T_i}, n_{T'_j} \right\rangle^2$$
$$+ \frac{1}{3} \sum_{k=1}^{N_v} \sum_{l=1}^{M_v} k_p(x_k, y_l) \Big[\pi(4 - 2n_{x_k} + 2N_{x_k}) - 2 \sum_{i=1}^{N_{x_k}} \varphi_{i,x_k} \Big] \Big[\pi(4 - 2m_{y_l} + 2N_{y_l}) - 2 \sum_{j=1}^{M_{y_k}} \varphi_{j,y_l} \Big]$$

where N_{x_k} is the number of triangles with vertex x_k and m_{x_k} is the number of edges with vertex x_k, and φ_{i,x_k} is the angle at vertex x_k of the triangle T_i.

Proof. See Appendix A.2.2 □

The scalar product of the planar part is the same as for varifolds. The cylindrical part vanishes, as it was expected with the previous work on the curvature: with the

linear kernel, the metric is not sensitive to mean curvature, that is contained in the cylindrical part.

We investigate now the link with Gaussian curvature. Suppose for sake of simplicity that the two triangulated meshes have no border and no branching edge or vertex. Then, it is easy to see that for every vertex x of the triangulations $N_x = m_x$ and the truncated scalar product simplifies greatly:

$$\langle N(\mathcal{T})_{approx}, N(\mathcal{T}')_{approx} \rangle_{W'} = 4 \sum_{i=1}^{N} \sum_{j=1}^{M} k_p(b_i, b'_j) |T_i| |T'_j| \left\langle n_{T_i}, n_{T'_j} \right\rangle^2 + \frac{1}{3} \sum_{k=1}^{N_v} \sum_{l=1}^{M_v} k_p(x_k, y_l) G_{\mathcal{T}}(x_k) G_{\mathcal{T}'}(y_l)$$

where $G_{\mathcal{T}}(x)$ is the discrete Gaussian curvature of the triangulation $\mathcal{T}$ at vertex x. With the previous notations, this re-writes:

$$\langle N(\mathcal{T})_{approx}, N(\mathcal{T}')_{approx} \rangle_{W',trunc} = 4 \langle \mu_{\mathcal{T}}, \mu_{\mathcal{T}'} \rangle_{W'_{var}} + \frac{1}{3} \left\langle \sum_{k=1}^{N_v} G_{\mathcal{T}}(x_k) \delta_{x_k}, \sum_{l=1}^{M_v} G_{\mathcal{T}'}(y_l) \delta_{y_l} \right\rangle_{W'_{meas}}.$$

This is a classical varifold scalar product, with an additional measure term, located at the vertices, and with intensity equal to the discrete Gaussian curvature.

In term of complexity, we add to the complexity of the varifold metric (that is a double loop on the triangles $O(N^2)$) a double loop on the vertices where we need to compute for each vertex the Gaussian discrete curvature, i.e. the sum of the angles of the triangles at this vertex. This complexity is basically a $O(N_v^2)$. Very often N_v, the number of vertices and N, the number of triangles have the same order, but more operations are needed to compute the Gaussian curvature.

3.7.4 Discrete scalar product with Sobolev normal kernel

We choose the kernel metric on normal cycles to be as in (3.13), with the Sobolev normal kernel k_n as in subsection 3.1.3. Suppose that C and S are two unions of segments. The computation of the scalar product between $N(C)_{approx}$ and $N(S)_{approx}$ for the kernel metric uses expansions in spherical harmonics for the normal part. This leads to :

Proposition 3.34. *Suppose that C and S are two unions of segments. One has*

$$\langle N(C)_{approx}, N(S)_{approx} \rangle_{W'} = \left\langle N(C)^{cyl}_{approx}, N(S)^{cyl}_{approx} \right\rangle_{W'} + \left\langle N(C)^{sph}, N(S)^{sph} \right\rangle_{W'}$$

with

$$\left\langle N(C)^{cyl}_{approx}, N(S)^{cyl}_{approx} \right\rangle_{W'} = \sum_{i=1}^{n_C} \sum_{j=1}^{n_S} k_p(c_i, d_j) \langle f_i, g_j \rangle \sum_{m \geq 0} a_m \cos(m\theta_{ij}) \qquad (3.24)$$

and

$$\left\langle N(C)^{sph}, N(S)^{sph} \right\rangle_{W'} = \sum_{k=1}^{N_C} \sum_{l=1}^{N_S} k_p(x_k, y_l) \left(1 - \frac{n_{x_k} + n_{y_l}}{2}\right) \beta + \sum_{i=1}^{n_C} \sum_{j=1}^{n_S} \sum_{a,b=1}^{2} \left(b_0 + (-1)^{a+b} \sum_{m \geq 0} b_m \cos(m\theta_{ij})\right) k_p(x_{f_i^a}, y_{g_j^b}) \tag{3.25}$$

where n_{x_k} (resp. n_{y_l}) is the number of edges adjacent to the vertex x_k (resp. y_l).

Proof. The first equality comes directly from the orthogonality condition of 3.27. The two formulas are derived in Appendix C.2 and Appendix C.3. □

The constant β and the a_m and b_m coefficients have explicit expansions in spherical harmonics, and are pre-computable. See Appendix C.2 and Appendix C.3, for their expressions. Here, we just precise that the $(a_m)_{m\geq 0}$ and $(b_m)_{m\geq 0}$ vanish for m even. This is compatible with the fact that normal cycles are unoriented objects: by inverting the orientation of the edges (i.e. if we invert $x_{f_i^1}$ and $x_{f_i^2}$), the scalar product remains unchanged. With these two scalar products, we have all we need to implement an algorithm which computes dissimilarity between two discrete curves. This is the first step to have a matching algorithm.

The computational complexity of the normal cycle metric, assuming we truncate the spherical harmonics expansions at a fixed order, is of order $O(n_C^2 + N_C^2)$, with n_C the number of edges and N_C the number of vertices. In fact usually n_C and N_C are nearly equal, thus the complexity is in $O(n_C^2)$, as in the case of the currents and varifolds metrics. However, as can be seen from the formulas, more operations are needed in the case of normal cycles; in our experiments the cost of computation of the normal cycle metric and its gradient was approximately six times higher than in the case of currents.

3.8 Discussion and perspectives

In this chapter, we have endowed normal cycles with kernel metrics, that provide a scalar product between shapes as integrals over the associated normal bundles. With our construction, the metric is explicit through two scalar kernels: a spatial kernel k_p that considers the spatial configuration of the shapes, and a normal kernel k_n that takes into account the relative position of the generalized normal vectors of the shapes. In this framework, we have provided a convergence result that draws the link between the continuous and the discrete cases. We precise also an explicit quantification of the error made for computational purpose. Interestingly, the curvature properties of normal cycles are transferred to the metric, depending on the choice of the normal kernel k_n. We have seen that even with coarse normal kernels, we are able to retrieve specific curvature information of the shapes. For surfaces, we

retrieve mean curvature information for the constant normal kernel and Gaussian curvature information for the linear normal kernel. For curves, only the constant kernel allows to get curvature information, and the linear kernel provides a metric that is similar to varifolds. In any case, we see that the metric on normal cycles is sensitive to the border of the shapes, as well as branching points. This is a major difference with usual metrics on varifolds or currents and this makes the framework sensitive to topological change. We will see in the next chapter that this feature enforces the matching of the borders. Apart from computational anatomy, this setting could fit in the one of discrete differential geometry. Normal cycles have already been successfully applied for the estimation of discrete curvatures, as it was recalled in subsection 2.5.3, but the addition of explicit kernel metrics enables both explicit and interpretable considerations. For example, it would be interesting to focus on the gradient flow of shapes with the different metrics that have been introduced in 3.7.

Let come back to the work that have been presented in section 2.6, where we have drawn a precise link between the normal cycle and the varifold associated with a shape. This link remains in the expressions of the discrete scalar products in section 3.7. For example in the case of surfaces, the orthogonal projection on the planar part for the linear normal kernel gives exactly the metric on varifolds for the linear kernel on Grassmannian. It is a future work to fully integrate the link between varifolds and normal cycles in the framework of RKHS, and for example to explicit how the metric on normal cycles is projected on the metric on varifolds.

Chapter 4

Registration and Atlas Estimation with Normal Cycles

Sommaire

Chapter 2 and Chapter 3 provide a theoretical framework as well as a numerical implementation to compute distance between shapes with kernel metrics on normal cycles. In this chapter, we use this distance on normal cycles as a residual distance between a deformed shape and a target shape, in the framework of shape analysis summed up in Chapter 1.

Section 4.1 is a study as precise as possible of the inexact matching problem (4.1). After stating an existence result for this problem, we detail in subsection 4.1.3 a practical algorithm to minimize (4.1) with discrete shapes. Several examples of registration with normal cycles are proposed on synthetic and real data. For curve registration (subsection 4.1.4), three types of normal kernels are studied for the metric on normal cycles: constant, linear and Sobolev. For surface registration (subsection 4.1.5), only the constant and linear normal kernel are studied, due to the complexity of the metric in the case of surfaces. For each type of data, the different synthetic examples aim to illustrate the curvatures properties seen in section 3.5 and comparison with varifolds and currents are shown when it is relevant. The examples on real data are a first step to show the advantage of this new dissimilarity metric for applicative purpose. Finally, in 4.2, we focus on the atlas estimation for a dataset of shapes (curves or surfaces). For this, we follow the theoretical framework introduced in [Ma et al., 2008, Ma et al., 2010] and already used in [Charlier et al., 2015a]. The mean shape is obtain through the *hypertemplate algorithm* that relies on the formulation of the inexact matching problem. This is recalled in subsection 4.2.1 and subsection 4.2.2. Some examples on synthetic and real data are provided in subsection 4.2.3 and subsection 4.2.4.

4.1 Large Deformation Registration with Normal Cycles

As explained in Chapter 1, in the LDDMM framework, the study of shape variability is carried by the study of geometrical transformations from one shape to another. The group of deformations at stake, G_V, is generated through integration of time-varying vector fields living in a a Hilbert space V, with $V \hookrightarrow \mathscr{C}^1_0(\mathbb{R}^d)$. With this hypothesis, V is a Reproducing Kernel Hilbert Space with kernel K_V and G_V is endowed with a nice Riemannian structure. For example, the Riemannian distance between the identity and a deformation $\varphi \in G_V$ writes:

$$\begin{cases} d_{G_V}(\mathrm{Id}, \varphi)^2 = E(\varphi) := \inf \left\{ \displaystyle\int_0^1 \|v_t\|_V^2 \, dt \middle| (v_t)_{0\leq t\leq 1} \in L^2([0,1], V) \right\} \\ \dfrac{\partial \varphi_t}{\partial t} = v_t \circ \varphi_t \text{ and } \varphi_1 = \varphi. \end{cases}$$

This distance between can be interpreted as the energy of the deformation φ. Thus, the optimal deformation between two shapes C and S will be the deformation φ with least energy and such that $\varphi(C) = S$. For practical purpose, we can not assume that any two shapes can be registered with a deformation $\varphi \in G_V$. That is why we

relax this hypothesis, and say that the optimal deformation is the one that minimize the sum of the energy and a discrepancy measure between the deformed shape and the target, $A(\varphi(C), S)$. This new registration problem, called inexact matching problem, is a trade-off between the regularity of the deformation, quantified by the energy $E(\varphi)$ and the closeness of the registration, quantified by a term $A(\varphi(C), S)$. The aim of this chapter is to use kernel metrics on normal cycles for the dissimilarity measure A. Given two shapes C and S

$$A(C, S) := \|N(C) - N(S)\|^2_{W'}.$$

where W is a RKHS such that $W \hookrightarrow \Omega_0^{d-1}(\mathbb{R}^d \times S^{d-1})$. The minimization problem with dual Hilbert norm on normal cycles as data attachment term is then:

$$\min_{v \in L^2_V} \gamma \int_0^1 \|v_t\|^2_V \, dt + \|\varphi^v.N(C) - N(S)\|^2_{W'} \tag{4.1}$$

where γ is a trade-off parameter.

One should notice that we have defined the action $\varphi.N(C)$ of diffeomorphism on normal cycles for sets $C \in \mathcal{U}_{PR}$ in subsection 2.4.4. This includes smooth submanifolds of $\mathbb{R}^d$, but also polyhedral meshes. This general framework will be the one we work with in the following.

4.1.1 Existence of a minimizer

We remind that the notation $\varphi.N(C)$ corresponds to the transport of the normal cycle by the diffeomorphism φ: if X is a set in $\mathcal{U}_{PR}$, $\varphi : X \to \varphi(X)$ induces a diffeomorphism $\psi : \mathcal{N}_X \to \mathcal{N}_{\varphi(X)}$:

$$\psi(x, n) = \left(\varphi(x), \frac{d\varphi_x^{-T} n}{\|d\varphi_x^{-T} n\|}\right)$$

where $d\varphi_x^{-T} = (d\varphi_x^{-1})^T$. This diffeomorphism ψ is defined such that the action of a diffeomorphism φ on normal cycles satisfies:

$$\varphi.N(X) := \psi_\sharp N(X) = N(\varphi(X)).$$

and the expression of the derivative $d\psi$ is:

$$d\psi_{(x,n)}.\begin{pmatrix}\tau \\ \nu\end{pmatrix} = \begin{pmatrix} d\varphi_x.\tau \\ \\ -p_{(n')^\perp} d\varphi_x^{-T} d^2\varphi(\tau, .)^T.n' + p_{(n')^\perp} \frac{d\varphi_x^{-T}.\nu}{\|d\varphi_x^{-T} n\|} \end{pmatrix}$$

Remark 4.1. *Notice that even though for $X \in \mathcal{U}_{PR}$, we have $N(X) = [\mathcal{N}_X] \llcorner \iota_X$ which may be different from $[\mathcal{N}_X]$, the action $\varphi_\sharp N(X)$ remains valid (see subsection* 2.4.3 *and subsection* 2.4.4*).*

We now state the theorem of existence of a minimizer for (4.1) that encompasses both the case of smooth shapes and the one of polyhedral shapes:

Theorem 4.2 (Existence of a minimizer for (4.1))**.** *Suppose that C, S are two compact sets in $\mathcal{U}_{PR}$ and assume that one has the embeddings $V \hookrightarrow \mathcal{C}_0^3(\mathbb{R}^d, \mathbb{R}^d)$, and $W \hookrightarrow \Omega_{1,0}^{d-1}(\mathbb{R}^d \times S^{d-1})$. Then there exists a minimizer for the problem* (4.1)*.*

We will prove theorem 4.2 using theorem 1.7. For this, we denote $v^n \rightharpoonup v$ for the weak convergence of $(v^n)_{n\in\mathbb{N}} \in (L_V^2)^{\mathbb{N}}$ to $v \in L_V^2$. We have to show that $v \mapsto A(\varphi^v.C, S) = \|\varphi^v.N(C) - N(S)\|_{W'}^2$ is weakly continuous. The first step is to verify that if $v^n \rightharpoonup v$, then $\psi^{v^n} \to \psi^v$ and $d\psi^{v^n} \to d\psi^v$, uniformly on every compact. We will need the theorem:

Theorem 4.3 ([Glaunès, 2005])**.** *Suppose that $V \hookrightarrow \mathcal{C}_0^p(\mathbb{R}^d, \mathbb{R}^d)$ (for the topology of uniform convergence for a function and its derivatives). If v^n weakly converges towards v in L_V^2, then $d^k\varphi^{v^n}$ converges uniformly on every compact set towards $d^k\varphi^v$, $\forall 0 \leq k \leq p-1$.*

From this, we can state the next proposition:

Proposition 4.4. *Suppose that $V \hookrightarrow \mathcal{C}_0^3(\mathbb{R}^d, \mathbb{R}^d)$. If $v^m \rightharpoonup v$ in L_V^2, then on every compact set of $\mathbb{R}^d \times S^{d-1}$, $\psi^{v^m} \to \psi^v$, $d\psi^{v^m} \to d\psi^v$*

Proof. If we suppose that $v^m \rightharpoonup v$ in L_V^2, then on every compact set of $\mathbb{R}^d$, we have: $\varphi^{v^m} \to \varphi^v$, $d\varphi^{v^m} \to d\varphi^v$ and $d^2\varphi^{v^m} \to d^2\varphi^v$ uniformly, with theorem 4.3. Now, let K be a compact set of $\mathbb{R}^d$. On K, φ^{v^n} converges uniformly toward φ^v, which proves the uniform convergence for the first component of ψ. For the second component, we consider the application θ:

$$\theta : (A, n) \in GL_d(\mathbb{R}) \times S^{d-1} \mapsto \frac{A^{-T}n}{\|A^{-T}n\|} \in S^{d-1}$$

where the notation A^{-T} stands for $(A^{-1})^T$, the transpose of the inverse. θ is continuous and then is uniformly continuous on every compact sets of $GL_d(\mathbb{R}) \times S^{d-1}$. Moreover,

$$\psi(x, n) = \big(\varphi(x), \quad \theta(d\varphi_x, n)\big)$$

Denoting $d\varphi(K) = \{d\varphi_x | x \in K\}$, $d\varphi(K)$ is a compact of $GL_d(\mathbb{R})$ (the image of a compact by a continuous application is compact) θ is then uniformly continuous on $d\varphi(K) \times S^{d-1}$. Since the uniform convergence is preserved by the composition with a uniformly continuous function, and since $d\varphi^{v^m}$ uniformly converges toward $d\varphi^v$, it proves that the second component of ψ^{v^m} converges uniformly on every compact set of $\mathbb{R}^d \times S^{d-1}$. This proves that ψ^{v^m} converges uniformly towards ψ^v on every compact set.

The proof of the uniform convergence of $d\psi^{v^m}$ is similar, using the uniform convergence of $d^2\varphi^{v^m}$. □

We recall here a proposition from [Glaunès, 2005], proposition 34.

Proposition 4.5. *Let W be a RKHS of m-differential forms continuously embedded in $\Omega_{1,0}^m(\mathbb{R}^d)$. Let S be a m-current. If ϕ^n and $d\phi^n$ converge uniformly towards ϕ and $d\phi$ on the support of S, then $\phi_\sharp^n S$ converges towards $\phi_\sharp S$ in W'.*

We can now prove theorem 4.2:

Proof. Suppose that $v^n \rightharpoonup v$ in L^2_V. By proposition 4.4, $\psi^{v^n} \to \psi^v$ and $d\psi^{v^n} \to d\psi^v$. Then, with proposition 4.5, and the fact that W is embedded in $\mathcal{C}^1_0\left(\mathbb{R}^d \times S^{d-1}, \Lambda^{d-1}(\mathbb{R}^d \times \mathbb{R}^d)\right)$ we have $\psi^{v^n}_\sharp N(C) \to \psi^v_\sharp N(C)$ in W', which implies that $\left\|\psi^{v^n}_\sharp N(C) - N(S)\right\|^2_{W'} \to \left\|\psi^v_\sharp N(C) - N(S)\right\|^2_{W'}$ and this is exactly the weak continuity of our data attachment term. We conclude using theorem 1.7. □

In the following, K_V will be, depending on the application, a Cauchy kernel with width σ_V: $K_V(x,y) = \frac{1}{1+\frac{|x-y|^2}{\sigma_V^2}}$, a Gaussian kernel with width σ_W: $K_V(x,y) = \exp(-\|x-y\|^2/\sigma_V^2)$, or a sum of Gaussian kernel with decreasing width. W is as in proposition 3.13. So that we have existence of a minimizer for (4.1).

4.1.2 Discrete framework

Knowing that a minimizer exists is a first step, and we will focus now on the problem of finding such a minimizer.

In the following, we focus on the discrete problem: we consider discrete shapes C_d and S_d. The geodesic equation followed by φ^v_t are simpler and we will explicit the approximations made for the data attachment term in order to have a tractable algorithm for the minimization procedure.

A discrete shape C_d is defined by a set of N points $(x_i)_{1\leq i\leq N}$ in $\mathbb{R}^d$ (the vertices), with a connectivity matrix describing the connexion between the vertices. This applies for curves in $\mathbb{R}^3$ but also for any polyhedral shape in $\mathbb{R}^d$. However, we will restrain our problem to curves and surfaces in $\mathbb{R}^d$, and we will use the approximation of normal cycles for segments seen in definition 2.47. The functional to minimize is then:

$$J_1(v) = \int_0^1 \|v_t\|^2_V \, dt + \|\varphi^v_1.N(C_d)_{approx} - N(S_d)_{approx}\|^2_{W'} \tag{4.2}$$

However, $\varphi^v_1.N(C_d)_{approx} = \psi^v_{1\sharp}N(C_d)_{approx}$ is too complex to be implemented numerically. To overcome this difficulty, we approximate the action of φ^v on C_d. For this purpose, we define C_{d,φ^v} as the discrete curve or surface with vertices $(\varphi^v_1(x_i))_{1\leq i\leq N}$ with the same connectivity matrix as C_d. This means that we consider that φ^v induces a displacement of the vertices only, and the displaced vertices are linked with straight lines. From this, we introduce the approximate matching problem, with the functional $\tilde{J}$:

$$\tilde{J}(v) = \int_0^1 \|v_t\|^2_V \, dt + \|N(C_{d,\varphi^v})_{approx} - N(S_d)\|^2_{W'} \tag{4.3}$$

As shown in [Glaunès, 2005], and recalled in section 1.4, if we denote by $q_i(t) = \varphi^v_t(x_i)$ the points trajectories, the energy term in (4.3) enforces the optimal vector field to be a geodesic path and to write

$$v_t = \sum_{i=1}^{N} K_V(\cdot, q_i(t))p_i(t) \tag{4.4}$$

where the $p_i(t) \in \mathbb{R}^d$ are auxiliary variables and are called momentum vectors. Further, it was shown in [Miller et al., 2006] (and detailed in an optimal control point of view in [Arguillère et al., 2015]) that the problem can be written in Hamiltonian form: if we denote H_r the reduced Hamiltonian:

$$H_r(p(t), q(t)) = \frac{1}{2}\sum_{i=1}^{N}\sum_{j=1}^{N} p_j(t)^T K_V(q_i(t), q_j(t))p_i(t) = \frac{1}{2}\left\|v_t\right\|_V^2,$$

q_i and p_i must satisfy coupled geodesic equations which write

$$\begin{cases} \dot{q}_{i,t} = \dfrac{\partial H_r}{\partial p_i} = \displaystyle\sum_{j=1}^{n} K_V(q_{i,t}, q_{j,t})p_{j,t} \\ \dot{p}_{i,t} = -\dfrac{\partial H_r}{\partial q_i} = -\left(\displaystyle\sum_{j=1}^{n} d_1(K_V(q_{i,t}, q_{j,t})p_{j,t})\right)^T p_{i,t}. \end{cases} \tag{4.5}$$

This Hamiltonian is constant along geodesic path and thus is a function of the initial momenta p_0 and the initial positions q_0. As could be expected, this implies that the optimal velocity vector field v_t in (4.4) is of constant norm: $\|v_t\|_V^2 = cste = H_r(q_0, p_0)$. Initial positions being fixed, we can consider H_r and further φ^v as function of the p_0 only, and denote it φ^{p_0}. The Hamiltonian formalism reduces the initial problem of minimization on an infinite dimensional Hilbert space V (4.3) to a minimization on $(\mathbb{R}^d)^N$:

$$\min_{p_0 \in (\mathbb{R}^d)^N} 2H_r(p_0, q_0) + \left\|N(C_{d,\varphi^{p_0}})_{approx} - N(S_d)\right\|_{W'}^2 \tag{4.6}$$

and where q and p follow the coupled geodesic (4.5). The second term depends only on the position of the final vertices: $(q_i(1))_{1\leq i\leq N} = (\varphi_1^{p_0}(q_i(0)))_{1\leq i\leq N}$ that we will denote $q(1)$. The data attachment term is then a function of $q(1)$: $g(q(1))$.

$$\min_{p_0 \in (\mathbb{R}^d)^N} J(p_0) := 2\gamma H_r(p_0, q_0) + g(q(1)) \tag{4.7}$$

with q and p following (4.5). As said before, g is a measure of the residual dissimilarity between the deformed shape at time 1 with vertices $q(1)$ and the target shape S_d.

4.1.3 Registration Algorithm

This functional is explicit using the expressions for the scalar products of normal cycles appearing in $g(q(1))$ and that have been computed in Chapter 3 with respect to the kernel. We minimize it depending on the initial momenta with a geodesic

Algorithm 2 Geodesic shooting with fixed-step gradient descent.

Input: q_0 (initial source shape), δ (step size)
Output: $\arg\min_{p_0 \in (\mathbb{R}^d)^n} J(p_0)$
initialization: $p_0 = 0$
while Convergence **do**
  Compute $(q(1), p(1))$ through *forward integration* of (1.13)
  Compute $\nabla_{q(1)} g(q(1))$
  Compute $\nabla_{p_0} g(q(1))$ through *backward integration* of (1.14)
  Compute $\nabla_{p_0} J(p_0) = K_V(q_0, q_0)p_0 + \nabla_{p_0} g(q(1))$
  $p_0 \leftarrow p_0 - \delta \nabla_{p_0} J(p_0)$.
end while

shooting algorithm [Miller et al., 2006, Arguillère et al., 2015] that has been recalled in section 1.4, and that we set here again.

A numerical implementation of the minimization requires the computation of $\nabla g((x_k)_{1 \leq k \leq N}))$, which takes an explicit form. See Appendix C.4.

In our numerical implementation, we use the shooting algorithm and optimize the functional with respect to p_0. To accelerate the convergence, we use a quasi Newton Broyden Fletcher Goldfarb Shanno algorithm with limited memory (L-BFGS) [Liu and Nocedal, 1989] rather than the gradient-descent with fixed step presented in Algorithm 2. The BFGS algorithm relies on the Newton's method to find the zero of the gradient of the functional to minimize. With no simplification, this would require the computation of the Hessian of the functional at each iteration. In the BFGS agorithm, we compute an approximation of the Hessian, that is updated and improved at each step. With the limited memory implementation, there is no storage of a $N \times N$ (where N is the number of variables) matrix and the memory storage is linear with respect to N. See [Liu and Nocedal, 1989] for more details. This method provides a direction of descent and the step in this direction is fixed by a Wolfe line search. For the numerical integrations, a Runge-Kutta (4,5) scheme is used (function ode45 in Matlab).

4.1.4 Curve Registration

We present here the experimentations of curve registration with kernel metric on normal cycles as data attachment term. Most of the time, we set K_V to be a scalar Cauchy kernel $K_V(x, y) = 1/(1 + |x - y|^2/\sigma_V^2)\mathrm{Id}$, with σ_V a scale parameter.

For the normal cycles, the point kernel k_p is a Gaussian kernel, with width σ_W, and the normal kernel k_n will be either a constant kernel, or a linear kernel, or a Sobolev kernel (associated with the operator $L = (I - \Delta)^3$). All these kernels have been introduced in Chapter 3. The examples aim to show the properties of the different kernels. The constant and linear kernels are simple, and encode precise curvature information, as it has been seen in section 3.5. For the Sobolev kernel, we used a spherical harmonics expansion of this kernel truncated at order 10 for the numerical purpose.

We chose to use a weighted scalar product for normal cycles (see remark 3.14 and remark 3.28) with weight λ of the form $\lambda = \alpha\sigma_W^2$, where $\alpha > 0$ is a fixed parameter. Setting λ to be proportional to σ_W^2 comes from a simple homogeneity analysis of the functional (4.7): when scaling the data coordinates by a factor η, scaling accordingly the width parameters σ_V and σ_W by the same factor, and evaluating at $p_0' = \eta p_0$, the energy term H_r and the cylindrical parts of the scalar products in the normal cycles term are multiplied by η^2, while the spherical part is kept unchanged. Hence multiplying the spherical part by a factor proportional to σ_W^2 ensures homogeneity of the functional with respect to scaling. In all our experiments, we set $\alpha = 10$.

In this section, we show some of our results on synthetic data and compare them with the varifolds method and currents method. The point kernel chosen for the varifolds is a Gaussian kernel, with the same width σ_W as for normal cycles. The kernel associated with the Grassmannian is chosen linear (see [Charon, 2013]), so that no parameter is involved as for the normal kernel with normal cycles. Lastly, a Gaussian kernel is used as well for currents, again with width σ_W. The trade-off parameter γ is set to $\gamma = 0.1$ in all experiments. All the numerical computations have been done on a laptop using Matlab (this will not be the case for surfaces since the model is then more complex and will require a parallelization of the calculus on GPU).

The examples are classified depending on the properties that we want to spotlight (curvature properties, consideration of the branching points and the extremities, examples on real data, ...).

Remark 4.6. *In the experiments, the color code will be the following: the target will be in orange, and the source in blue. The trajectories of the vertices during the deformation will be in blue as well.*

Synthetic data: illustration of the curvature properties

As announced and studied in section 2.5 and section 3.5, the normal cycles encode curvature information of the shapes and this is expected that a registration with kernel metric on normal cycles will show this property. The next two examples are registration between shapes with high curvature spot.

Registration of fishes contours (figure 4.1, figure 4.3): Here a registration between two fishes contours is performed (see [US Dept of the Interior Fish and Wildlife Service, 1953] for the original data). Even if they are 2D objects, we consider them as 3D objects with no z variation. In this example, fishes have around 100 vertices. A first optimization of the momenta was performed with parameters $\sigma_W = 0.75$ and $\sigma_V = 0.2$. This can be seen as an initialization step to avoid local minima. Then minimization was done with $\sigma_W = 0.2$ and $\sigma_V = 0.2$. The computation time as well as the number of iterations is specified for each registration in the figures. The main difficulty of the matching is the trade off to find between the matching of the long tail of the stingray (in orange) and the high local curvature in the upper part of the fish in blue. To ease

the reader's comprehension, we show in figure 4.2 the evolution of the deformation with Sobolev normal kernel. The results are presented in figure 4.3 and show that a perfect matching with normal cycles and a constant normal kernel can be achieved, even with $\sigma_W = 0.2$ which is quite large compared to the local feature in the upper part of the fish. Notice that with the constant kernel, that encodes the curvature information of the curves, the registration takes into account the region of high curvature. With varifolds (that is in the case of closed curves exactly similar to the metric on normal cycles with linear normal kernel), one can see that this local feature still remains in the blue matched curve. To avoid this behaviour, one can decrease the size of σ_W, but it would lead to a bad matching of the tail. One should also notice that the behaviour of the constant + linear normal kernel and the Sobolev normal kernel are quite similar, which could indicate that the information encoded in the constant and linear kernel are enough for the matching of curves.

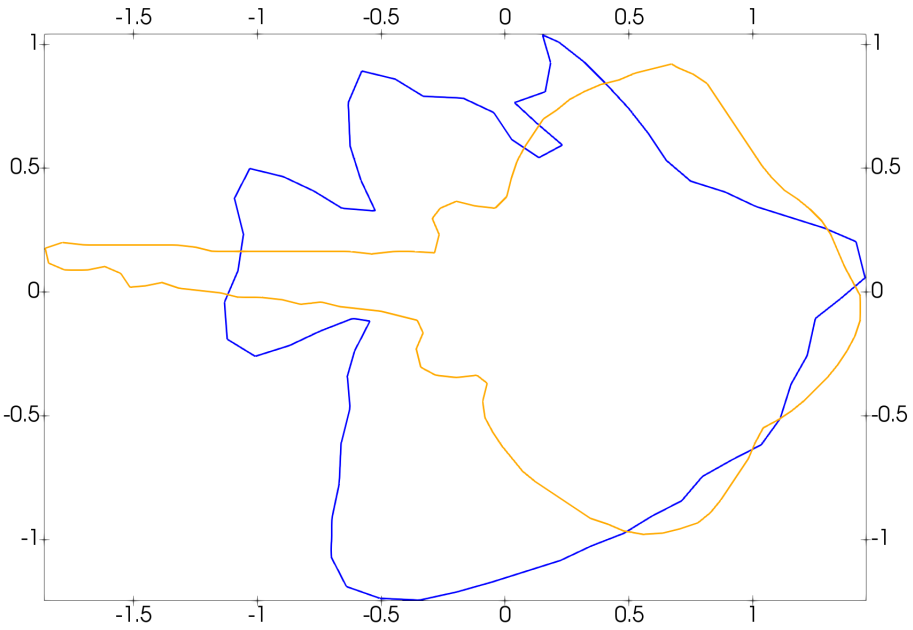

Figure 4.1: Source fish (blue) and target fish (orange)

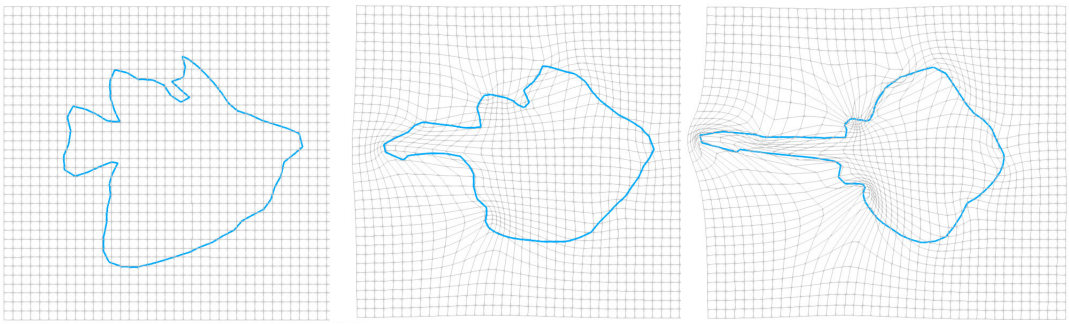

Figure 4.2: Registration of the blue fish to the orange fish with normal cycles and Sobolev normal kernel with parameters $\sigma_V = 0.2$ and $\sigma_W = 0.75$ and then 0.2. This figure aims at visualizing the evolution of the deformation at time $t = 0$, $t = 1/2$ and $t = 1$ through the grid of deformations. In figure 4.3 the reader can find a precise comparison of the registrations with different metrics.

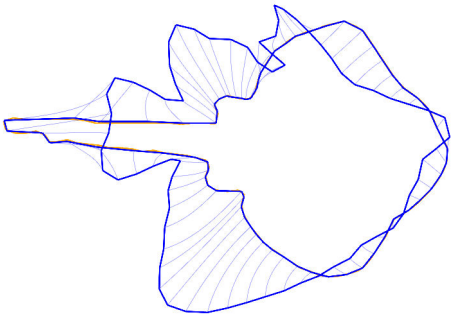

(a) Normal cycles constant, 1015 iterations (633 for run 1, 382 for run 2), in 173 seconds (0.17 s/it)

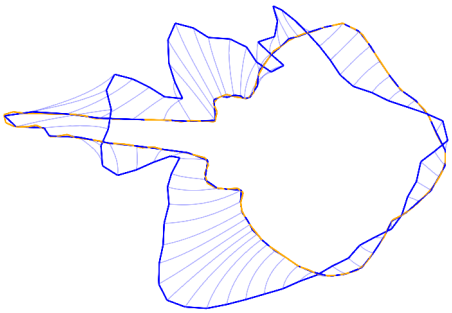

(b) Normal cycles linear (= varifolds), 914 iterations (533 for run 1, 381 for run 2) in 143 seconds (0.15 s/it)

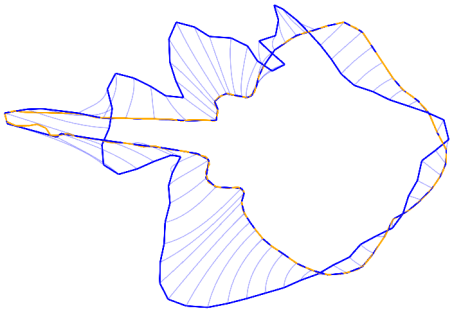

(c) Normal cycles constant + linear, 1400 iterations (644 for run 1, 756 for run 2) in 250 seconds (0.18s/it)

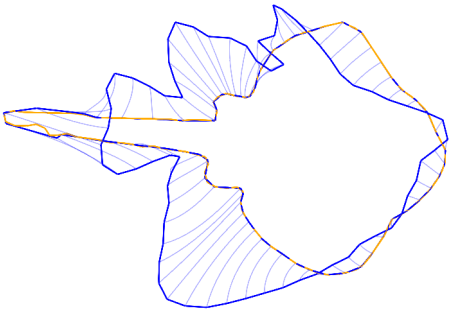

(d) Normal cycles sobolev, 1329 iterations (696 for run 1, 633 for run 2) in 244 seconds (0.18s/it)

Figure 4.3: Registration of a blue fish to an orange fish. In light blue, the trajectories of the vertices along the deformation. We used normal cycles and varifolds with the same parameters $\sigma_V = 0.2$ and $\sigma_W = 0.75$ and then 0.2. Each shape has around 100 points. The registration with currents is worse than with varifolds.

Registration of a three feet object (figure 4.4, figure 4.5 and figure 4.6): The registration presented here is harder. These are two contours of *amoeba*, presenting three protrusions and that are kindly available on Jean Feydy's website: `http://www.math.ens.fr/~feydy/research.html`. Looking at figure 4.4, the natural matching between these two shapes seems rather obvious. However, this is a hard problem for the LDDMM registration since the data attachment term tends to match points that are close. The minimization for the results presented in figure 4.6 is done with one run until convergence, with $\sigma_V = 0.1$ and $\sigma_W = 0.1$. Each shape has around 200 points. Since the deformation may be hard to understand at first, we show in figure 4.5 the evolution of two optimal deformations: one obtained with Sobolev normal kernel and one obtained with varifolds. However, once the deformation is understood, figure 4.6 shows more details of the matching. As we can see, the registration with normal cycles are very similar for constant, linear + constant and Sobolev, and the matching takes into account the corresponding "feet". For the varifold data attachment term however, we see that one of the foot is crushed to the target, and another foot is created, which does not correspond to the matching in mind. We believe that this is due to a nice property of the normal cycles, that tend to make a correspondence between points of high curvatures.

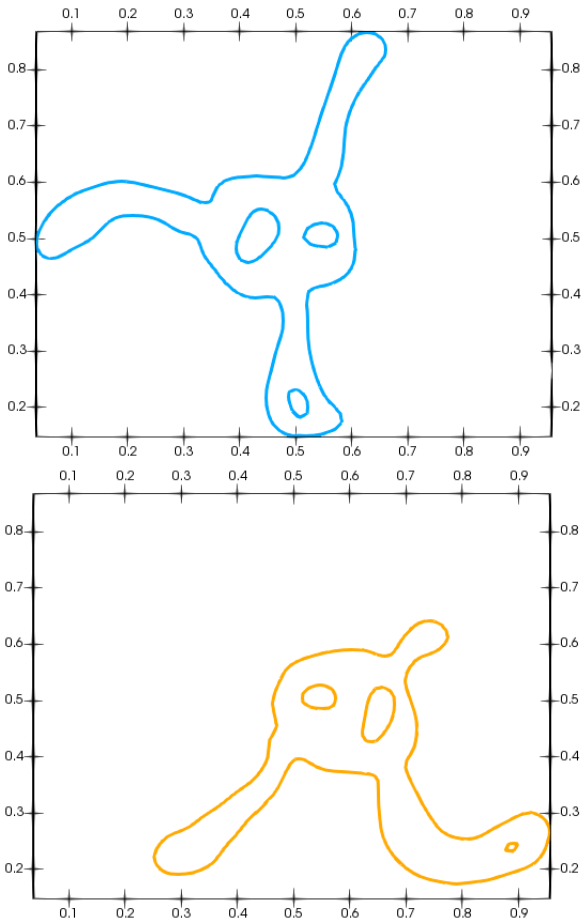

Figure 4.4: Source amoeba (blue) and target amoeba (orange)

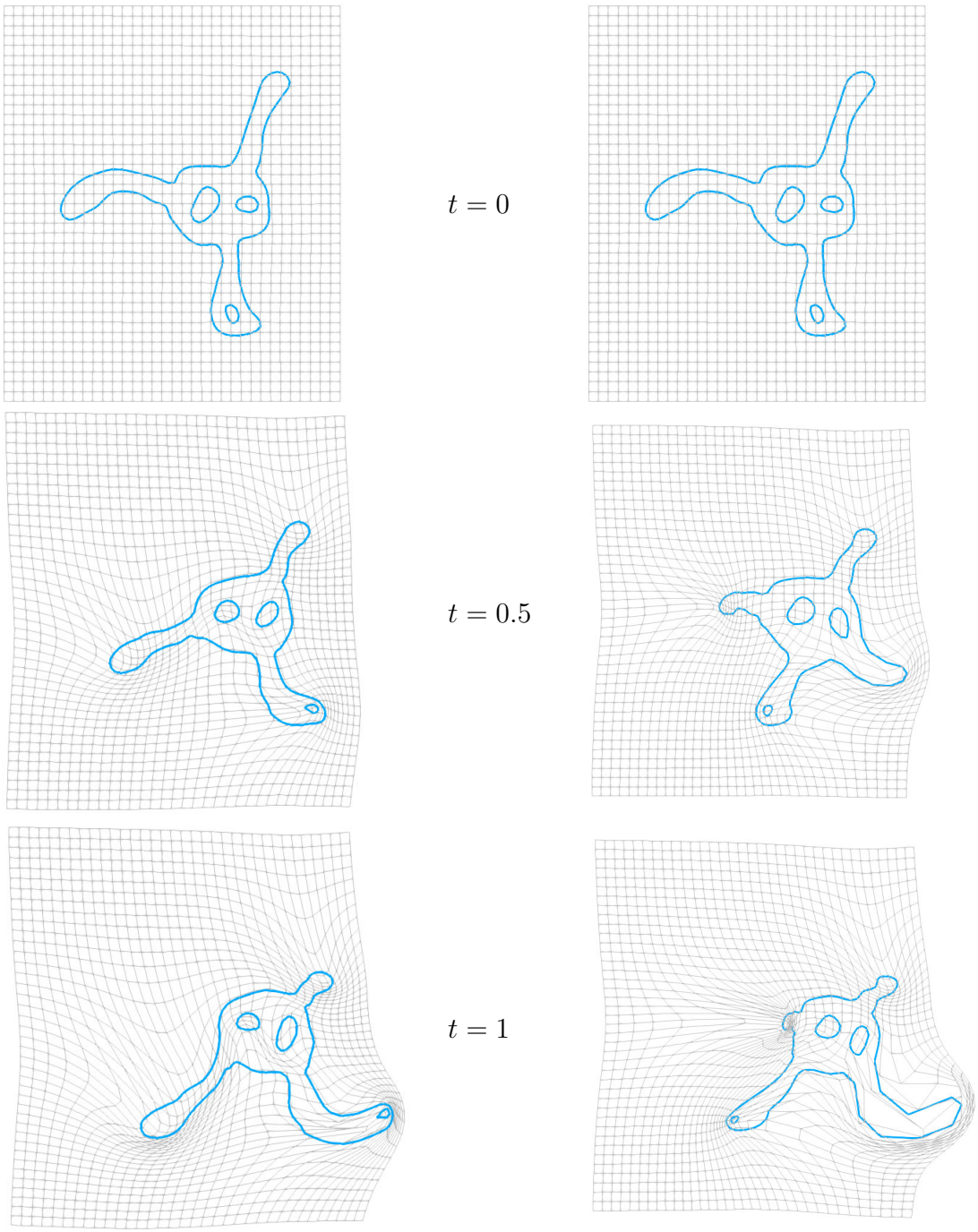

Figure 4.5: Registration of the blue amoeba to the orange amoeba, with $\sigma_V = 0.1$, $\sigma_W = 0.1$. Each column represents the evolution of the deformation, at time $t = 0$, $t = 0.5$ and $t = 1$. The first column is the registration obtained with the metric on normal cycles and the Sobolev normal kernel. he second column is the registration obtained with the metric on varifolds. We add also the grid of deformation to a better visualization. We refer also to figure 4.6 for another presentation of the registrations.

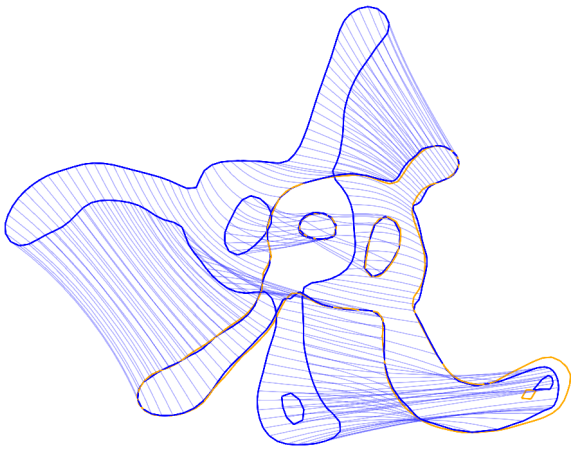

(a) Normal cycles constant, 1034 iterations in 711 sec (0.68 s/it)

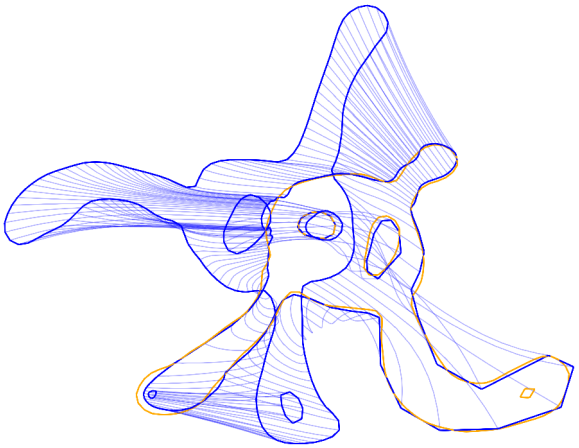

(b) Normal cycles linear (similar to varifolds), 1363 in 962 sec (0.7 s/it, 0.66s/it for varifolds)

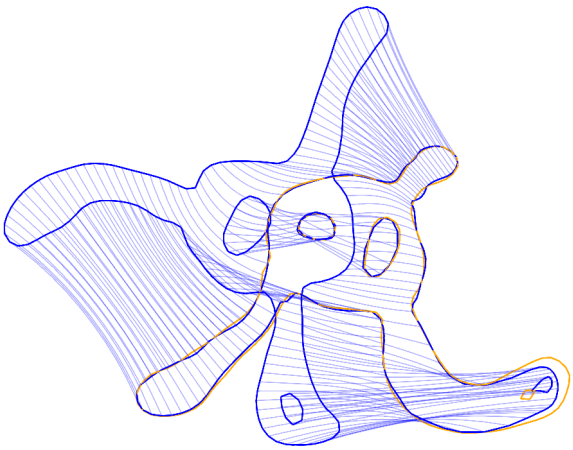

(c) Normal cycles constant + linear, 814 in 582 sec (0.71 s/it)

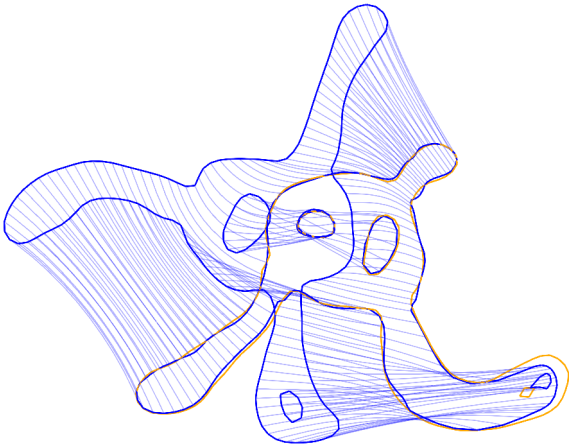

(d) Normal cycles sobolev, 673 in 545 sec (0.81 s/it)

Figure 4.6: Registration of a blue amoeba to an orange amoeba, with $\sigma_V = 0.1$, $\sigma_W = 0.1$. Each shape has around 200 points. In blue light, the trajectories of the blue amoeba's vertices along the deformation. The matching with constant, constant + linear and Sobolev normal kernel makes a correspondence between the feet on the contrary to the linear normal kernel (that generates a metric similar to the one of varifolds for closed curves).

Synthetic data: illustration of the extremities properties

Another specificity of the metric on normal cycles is that every part of the shape is taken into account and in particular, the extremities have a specific behaviour that is explicit on discrete shapes (see the scalar product between discrete shapes in section 3.7. This property will be retrieved during the registration with a good matching of corresponding extremities. This is also the case for branching points, where the metric on normal cycles creates a "connection cost". Indeed the norm of the normal cycle of two segments at distance ε with $\varepsilon \to 0$ is different from the norm of the normal cycle of the joint segments, and the difference is exactly the norm of a sphere. This observation is clear when looking at the decomposition of the normal bundle used (Subsection 2.4.3). This cost of connection does not appear for currents or varifolds. More generally, currents and varifolds are m-dimensional measures associated with a m-dimensional objects, and thus are insensitive to the boundaries (which is $m-1$ dimensional). Notice that in the case of curves with extremities, the metric given by the linear normal kernel on normal cycles has an additional term on the extremities in comparison to varifolds. That is why we will precise registrations for both varifolds and linear normal kernel in the following.

Registrations of open circle (figure 4.7, figure 4.8, figure 4.9): We start here with a rather striking toy example to illustrate the specific behaviour of the extremities for the metric on normal cycles. We want to perform a matching between a source blue circle and a target orange circle. Each circle has a a small opening. At angle $\theta = 0$ for the blue circle and $\theta \simeq \pi - \pi/10$ for the orange circle. The opening is small compared to the size of the circle. The first registration presented in figure 4.8 is with $\sigma_W = 5$ for the spatial kernel k_p on normal cycles and varifolds, and $\sigma_V = 5$. Notice that the size of the spatial kernel is big compared to the size of the opening. This implies that the metric on varifolds does not see this opening and it is impossible to achieve the matching. We observe a similar behaviour for the metric on normal cycles with constant normal kernel. However, with the linear kernel (or constant + linear or Sobolev), even though the spatial kernel does not see the opening, the normal kernel is sensitive to the extremities and this implies a good matching of the disconnections.

More striking is the second registration (figure 4.9), this time with $\sigma_W = 1000$. With such size, the spatial kernel is insensitive to any spatial localization. Thus, nothing happens for the registration with the constant normal kernel on normal cycles or with varifolds. However, with the metric on normal cycles with the linear (or constant + linear or Sobolev) normal kernel, it remains some information on the extremities that will drive the matching, as one can observe in figure 4.9. Of course the matching is far from being perfect, but it is interesting to see that the corresponding extremities are well registered. The question whether this is an advantage or a drawback depends critically on the data at stake. If there is uncertainty on the topology of the data, resulting from a bad segmentation for example, this behaviour prevents from a correct matching. Indeed, the registration will try to make a correspondence between extremities that are artefacts. However, for specific cases where

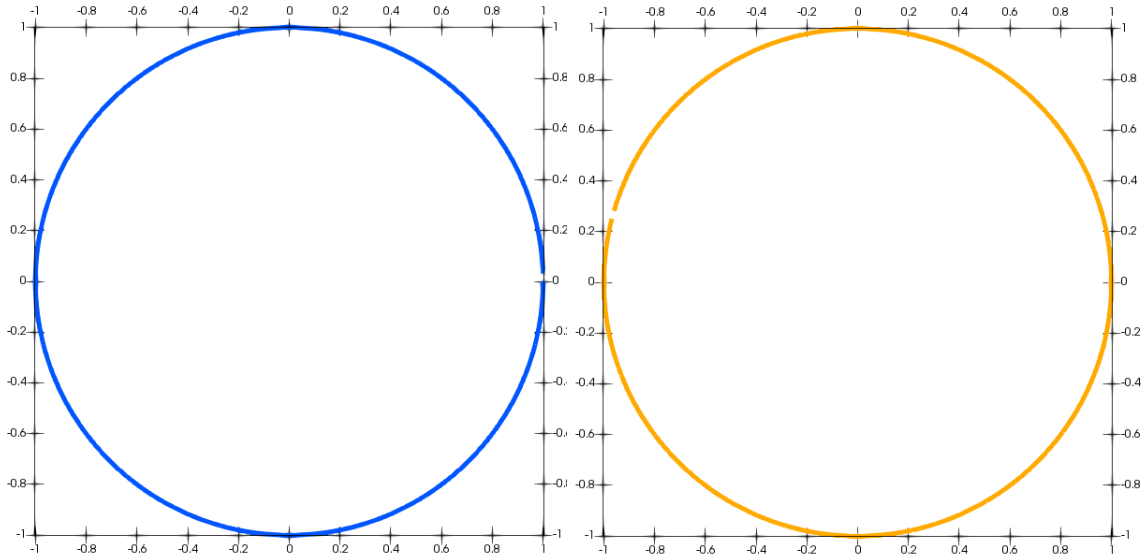

Figure 4.7: Source circle (blue) and target circle (orange)

the extremities play an important role, the metric on normal cycles (with linear or Sobolev normal kernel) can be used with benefits.

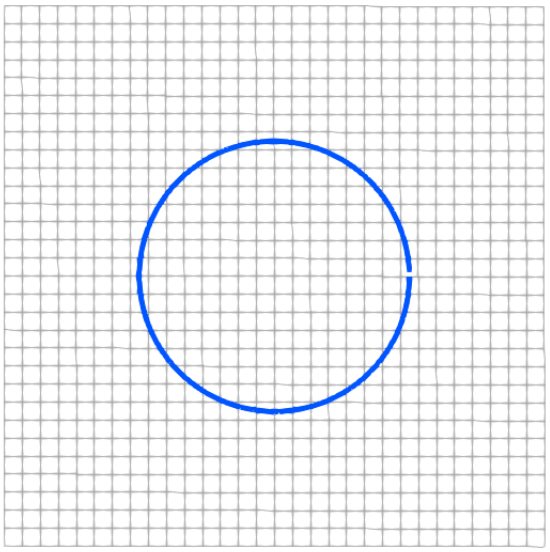

(a) Registration obtained with normal cycles with the constant normal kernel. The metric on normal cycles is not sensitive to extremities with this choice of kernel.

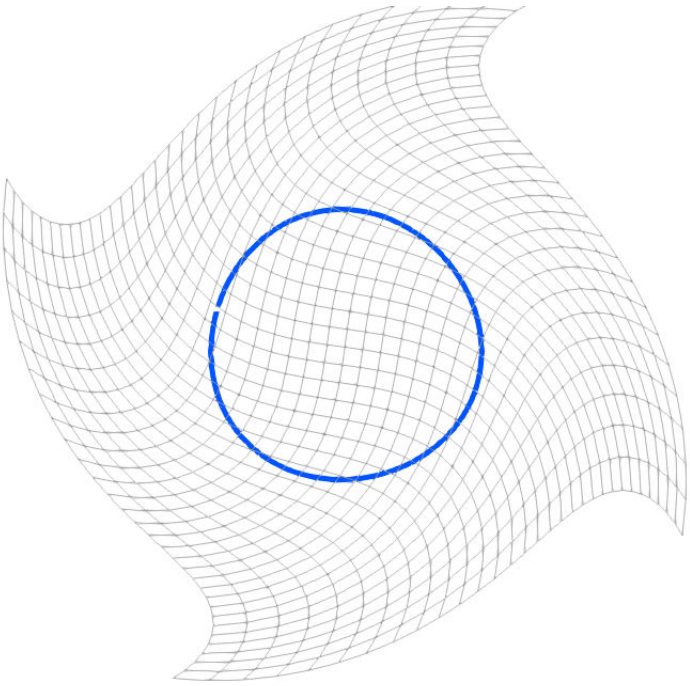

(b) Registration obtained with normal cycles and Sobolev normal kernel. The results are similar with the linear and the constant + linear normal kernel.

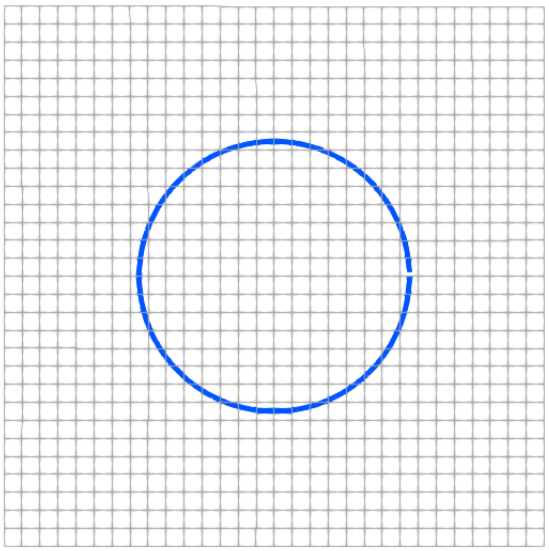

(c) Registration obtained with varifolds. The associated metric is not sensitive to extremities.

Figure 4.8: Registration of the blue circle to the orange one with $\sigma_V = 5$, $\sigma_W = 5$. One can observe the grid of deformation in grey. The metrics on normal cycles are sensitive to the deconnection of the circles and match the extremities (appart for the constant normal kernel). Since varifolds are not sensitive to this topological feature, the resulting registration is simply the identity.

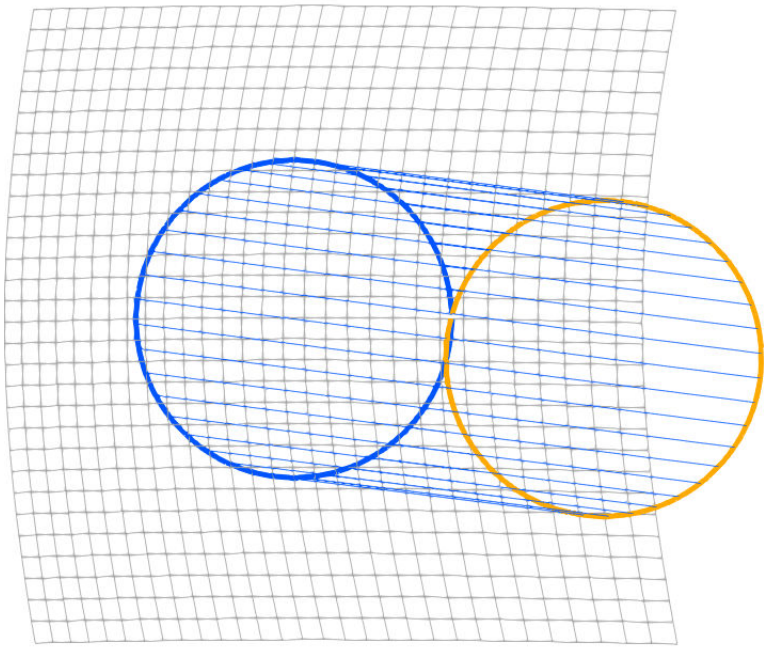

(a) Normal cycles linear, constant + linear, Sobolev

Figure 4.9: Registration of the blue circle obtained with $\sigma_V = 5$, $\sigma_W = 1000$. One can observe the grid of deformation in grey. In blue light, the trajectories of the blue vertices along the deformation. The extremities of the circles are well matched, even though the size of the spatial kernel makes the metric almost insensitive to any spatial localization.

Registrations of branching curves (figure 4.10, figure 4.11, figure 4.12): We show here registration of two 3D curves with branching. These curves were chosen because the distance between them is large compared to their typical sizes, the curves have some high local curvature and the size of the corresponding branches implies high local deformations. Besides, we would like to see the behaviour of normal cycles with respect to connecting points.

The two curves are enclosed in a cubic box of size one. Both curves have 150 vertices. In figure 4.11, figure 4.12, we show two views of a matching using normal cycles (constant, linear, constant + linear and sobolev normal kernel) and varifolds. The kernel K_V associated with the deformation space is chosen to be a Cauchy kernel, with width $\sigma_V = 0.2$.

One can see that the branching point, as well as the extremities are well matched for the registration with normal cycles, compared to the one with varifolds. This correspondence made on the extremities enforces a much more convincing registration, notably in the neighborhood of the branching point.

Remark 4.7. *As we can notice the computation time per iteration is not increasing much when using normal cycles instead of currents or varifolds. This comes from the fact that the largest part of the computation is spent in solving the ODE equations of the LDDMM shooting procedure. The cost of the data attachment evaluations (functional and gradient) themselves for this experiment reflect the increasing complexity of the methods, as expected: 0.017, 0.036 and 0.10 seconds per iteration for currents, varifolds and normal cycles respectively, but this has relatively small influence on the total time per iteration. In the end, the large total time differences in this experiment come from the number of iterations of the minimization process needed to reach the stopping criterion, which seem to increase with the complexity of the method.*

Synthetic data: fibres bundle

We present now some first result on fibres bundles. These are synthetic data, generated thanks to the fshape-toolkit that is kindly provided on line by Benjamin Charlier (http://www.math.univ-montp2.fr/~charlier/). The registration of fibres bundle is in practice pretty hard to achieve since the matching of the extremities is often difficult and not enforced by the RKHS metrics on currents or varifolds. However, we have seen that with normal cycles, the extremities have a specific behaviour that should improve the registration. The source and target are two fibres bundles with 3 branches each, each branch containing around 20 fibres, with 10 vertices each. In figure 4.13, one can see the initial configuration: we want to register the blue fibers bundle to the orange one.

This matching is hard to achieve since we have no correspondence between the set of fibers, and not necessarily the same number of fibers in each bundle. We present in figure 4.14 registrations obtained with the different metrics: on normal cycles, with the constant, linear and Sobolev normal kernel, and with varifolds, with the linear kernel on the Grassmanian. For both metric, we chose a Gaussian spatial

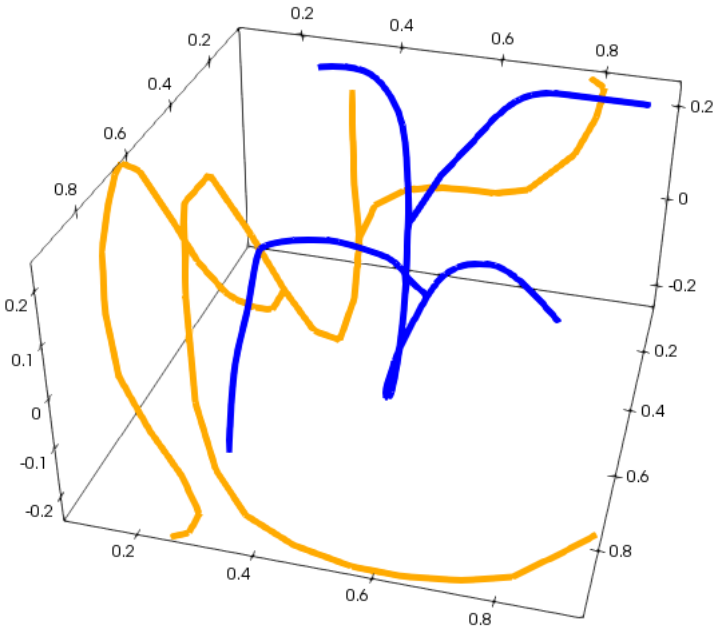

(a) View 1

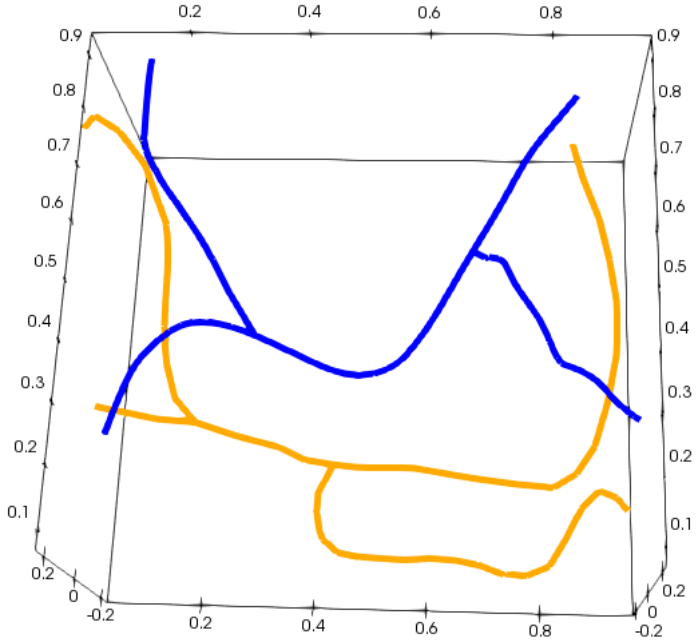

(b) View 2

Figure 4.10: Two curves with one branching points and four extremities. The source is in blue and the target in orange.

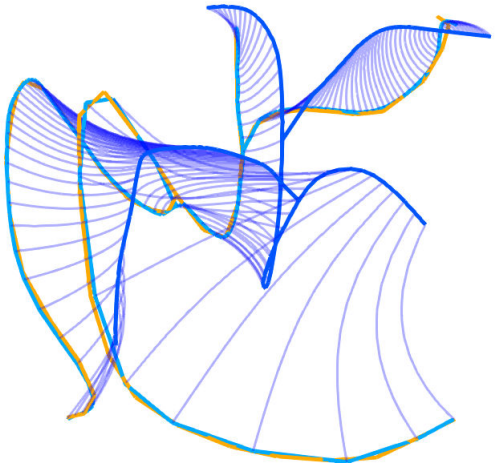

(a) Normal cycles constant, view 1, 2120 iterations in 1011 seconds (0.48 s/it)

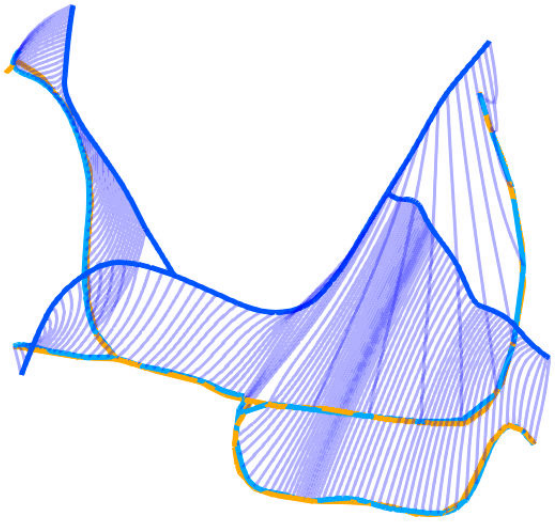

(b) Normal cycles constant, view 2

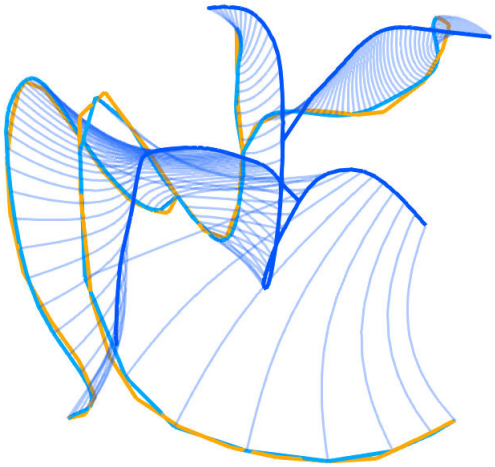

(c) Normal cycles linear, view 1, 870 iterations in 387 seconds (0.44 s/it)

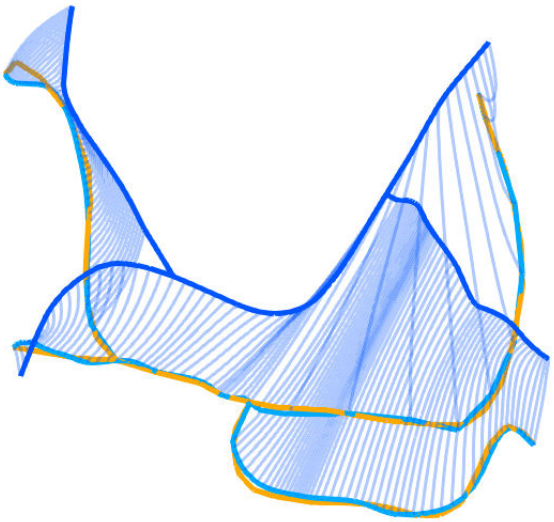

(d) Normal cycles linear, view 2

Figure 4.11: Two views of the registration of two 3D curves with different data attachment terms. Initial curve is in blue, target curve in orange, and deformed curve in light blue. Trajectories of vertices along the flow are displayed in blue. Parameters are $\sigma_V = 0.2$ and $\sigma_W = 0.3$. Each curve has around 150 points.

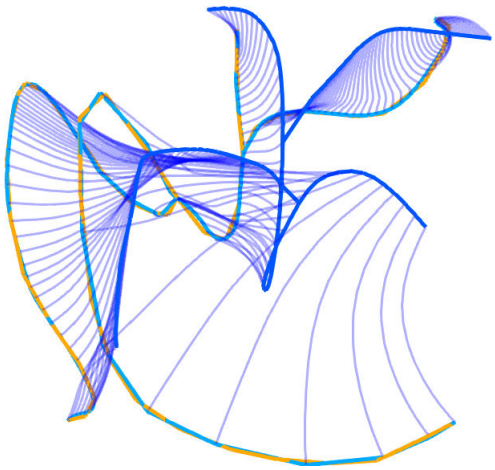

(a) Normal cycles constant linear, view 1, 1370 iterations in 869 seconds (0.63 s/it)

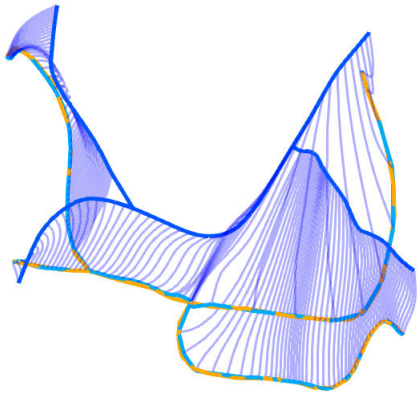

(b) Normal cycles constant linear, view 2

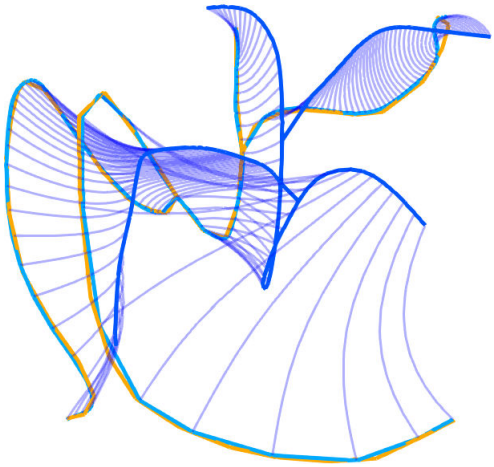

(c) Normal cycles sobolev, view 1, 1557 iterations in 920 seconds (0.6 s/it)

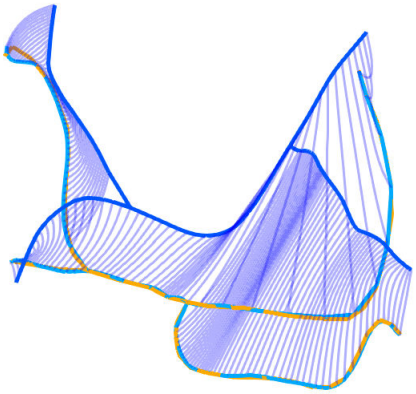

(d) Normal cycles sobolev, view 2

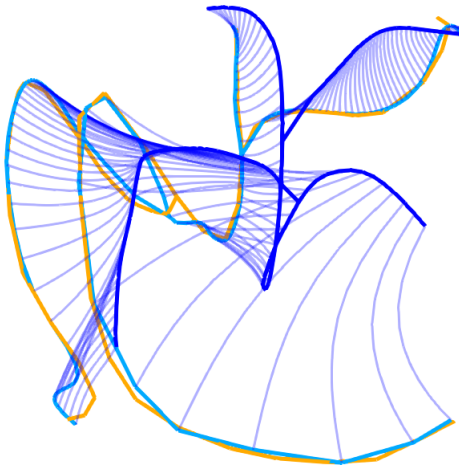

(e) Varifolds, view 1, 1058 iterations in 520 seconds (0.5s/it)

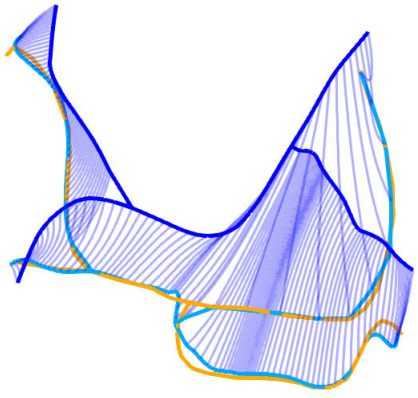

(f) Varifolds, view 2

Figure 4.12: Two views of the registration of two 3D curves with different data attachment terms. Initial curve is in blue, target curve in orange, and deformed curve in light blue. Trajectories of vertices along the flow are displayed in blue. Parameters are $\sigma_V = 0.2$ and $\sigma_W = 0.3$. Each curve has around 150 points.

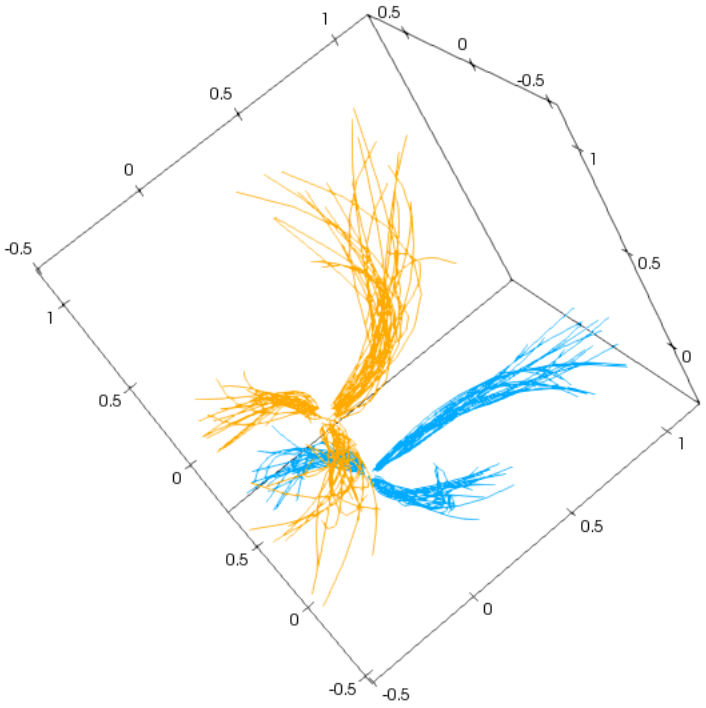

Figure 4.13: The registration problem between the blue fibers bundle and the orange one (the target)

kernel. The registration is done with one run with $\sigma_W = 0.5$. We also whose a Cauchy kernel for the deformations, of size $\sigma_V = 0.8$. The typical time for normal cycles is two and a half hour for 1000 iterations (where we stopped the algorithm). For varifolds it is 2 hours.

In this experience, the improvement provided by normal cycles is not obvious. The fact that the extremities are taken into account does not seem to improve the registration. This may be because the problem is hard. If the metric tends to match extremities, it becomes difficult when there is not the same number of extremities in the source and in the target.

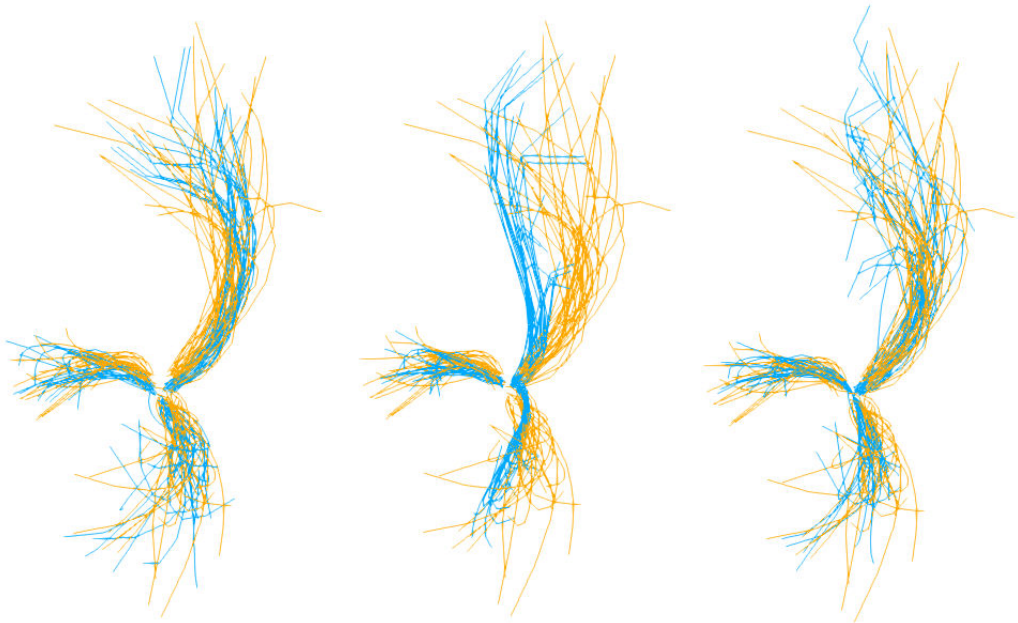

(a) constant normal kernel (b) linear normal kernel (c) constant + linear normal kernel

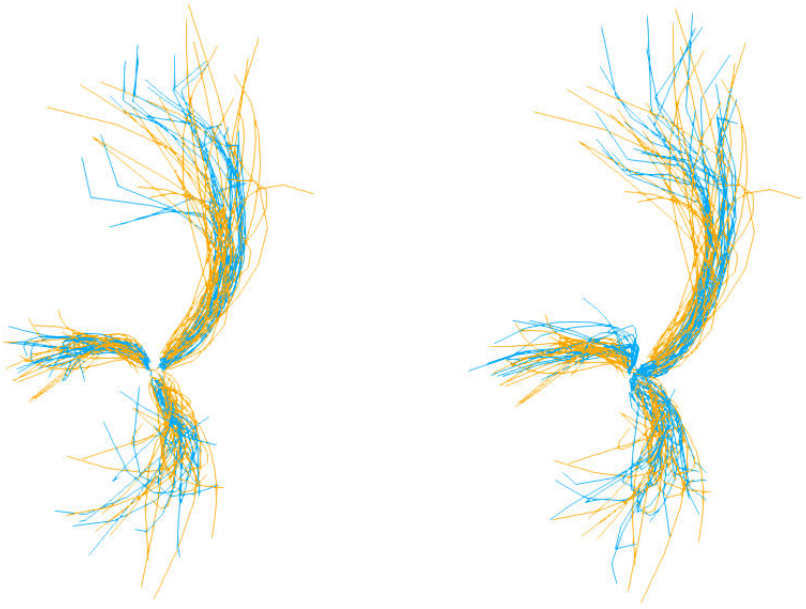

(d) Sobolev normal kernel (e) kernel metric on varifolds

Figure 4.14: Registration of two set of fibers with different data attachment terms. For the deformation : Cauchy kernel, $\sigma_V = 0.6$, for the data attachment term, Gaussian spatial kernel with $\sigma_W = 0.6$ and 0.3.

Real data: brain sulci

Registration of brain sulci (Figures 4.15, 4.16 and 4.18) We show here an example on real data. The data consist of brain sulcal curves that were automatically segmented and labelled from anatomical Magnetic Resonance Imaging (MRI) brain images, following the method described in [Auzias et al., 2011]. We chose two individuals and six labelled corresponding sulcal curves for each individual. See figure 4.15.

The matching is performed with a single deformation, but 6 data attachment terms with normal cycles or varifolds: one for each pair of corresponding sulci. Two runs are performed, with decreasing size of the spatial kernel. The first run can be considered as an initialization step at coarse scale. The parameters are the following: for the deformations, we chose a Cauchy kernel of width $\sigma_V = 20$. For the metric on normal cycles, we took a Cauchy spatial kernel with width $\sigma_W = 20$ for the fisrt run and $\sigma_W = 5$ for the second run. The normal kernel is a Sobolev kernel of order 3. For varifolds, we consider the same Cauchy spatial kernel, and a linear kernel for the tangential part. Processing times were 1 hour using normal cycles and Sobolev normal kernel (2000 iterations, 2 s/iter) and 45 min with varifolds (2000 iterations, 1.5 s/iter). The matching is complex since the number of branching points is not necessarily the same for corresponding curves, and two curves to match can be really twisted from one to another. Moreover, the fact that a single deformation is required for the whole brain implies high local variations. In figures 4.16 and 4.17, we present the registration with normal cycles and Sobolev normal kernel. The visualization of this three dimensional configuration is not easy, but the end points and corresponding branching points are well matched when possible (we recall that there is not always corresponding branching points). Moreover, the registration driven by normal cycles allows complex local deformation (even though it is expensive) to reduce the data attachment term.

In figure 4.18 we present a zoom on two sulci to showcase the properties of a registration with normal cycles compared to a registration with varifolds. This specific example show all the benefit that one can expect from the metric on normal cycles. The natural consideration of the extremities and the corresponding points provide a much more convincing registration, even though this implies a deformation with high local variation. This is even more striking in the left sulci where the registration with varifold twists the main curve to match to a branch. On the contrary, with normal cycles the deformation is a good compromise, even though there is not the same number of branching points in the source and in the target.

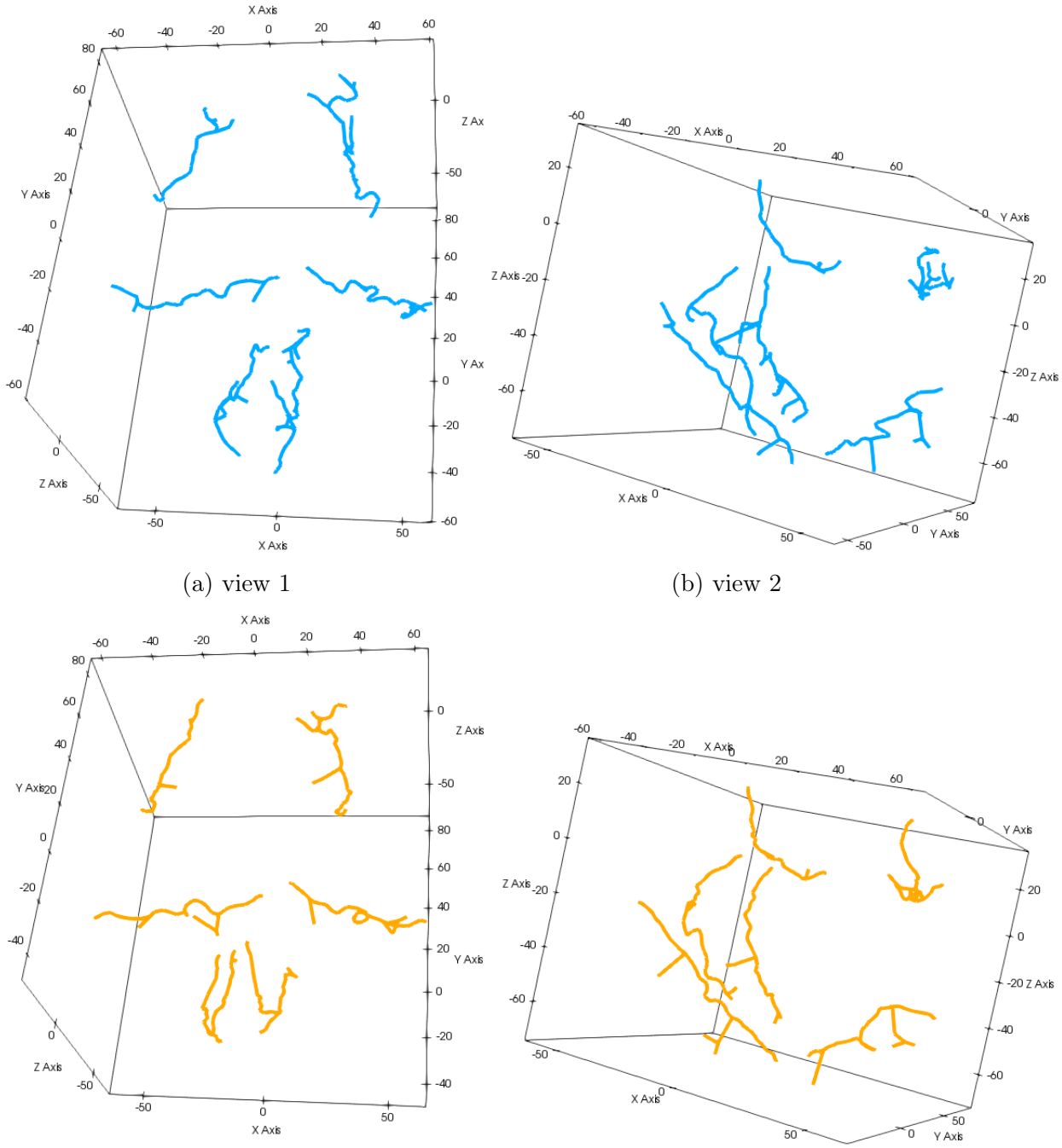

(a) view 1

(b) view 2

(c) view 1, target

(d) view 2, target

Figure 4.15: Two view of the brain sulci of two distinct subjects to be matched. Each individual has 6 sulci that are labelled. The target is in orange and the source in blue.

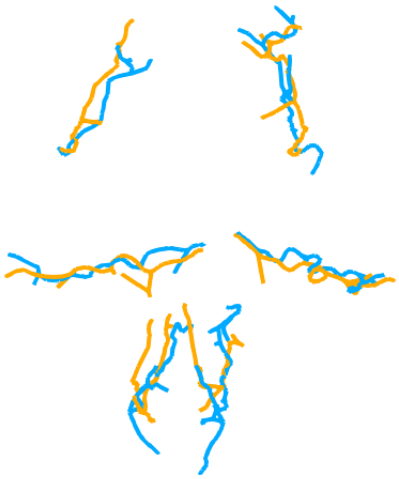

(a) view 1, $t = 0$

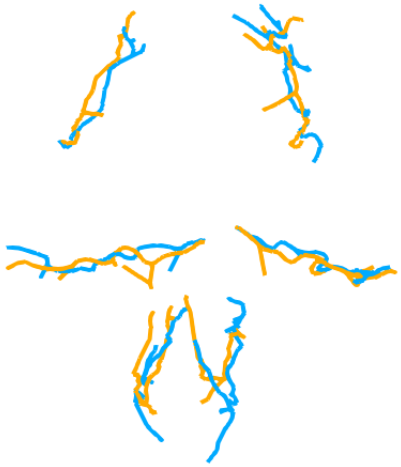

(b) view 1, $t = 1/3$

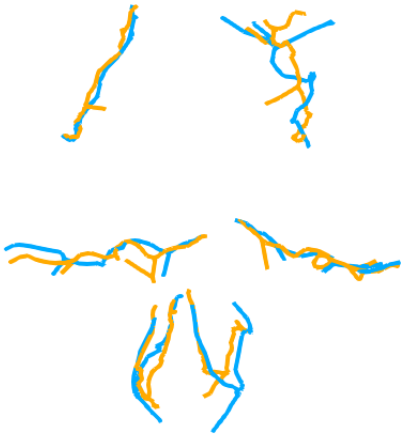

(c) view 1, $t = 2/3$

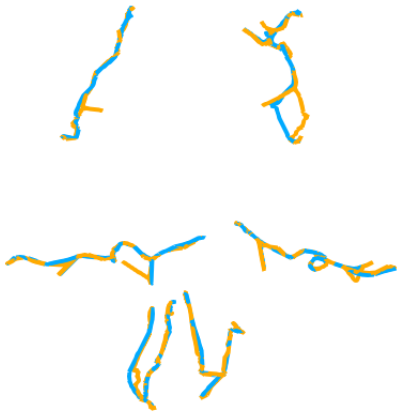

(d) view 1, $t = 1$

Figure 4.16: Registration of blue to orange brain sulci, view 1. The deformation kernel is a Cauchy kernel of width $\sigma_V = 20$. The data attachment term is normal cycles with Sobolev normal kernel of order 3 and Gaussian spatial kernel k_p with width $\sigma_W = 20$ for the first run and $\sigma_W = 5$ for the second run.

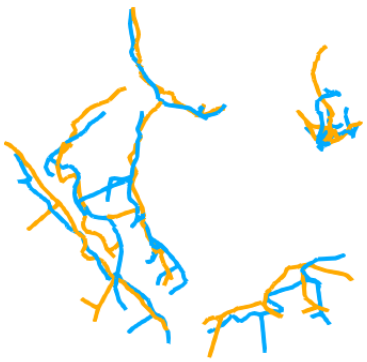

(a) view 2, $t = 0$

(b) view 2, $t = 1/3$

(c) view 2, $t = 2/3$

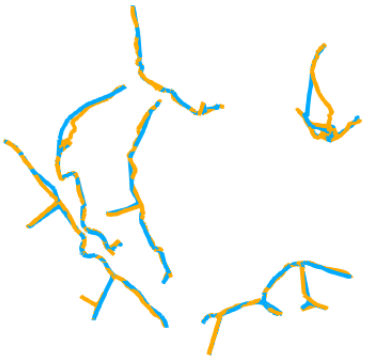

(d) view 2, $t = 1$

Figure 4.17: Registration of blue to orange brain sulci, view 2. The deformation kernel is a Cauchy kernel of width $\sigma_V = 20$. The data attachment term is normal cycles with Sobolev normal kernel of order 3 and Gaussian spatial kernel k_p with width $\sigma_W = 20$ for the first run and $\sigma_W = 5$ for the second run.

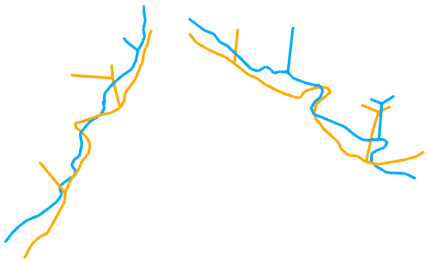

(a) Normal cycles, t = 0

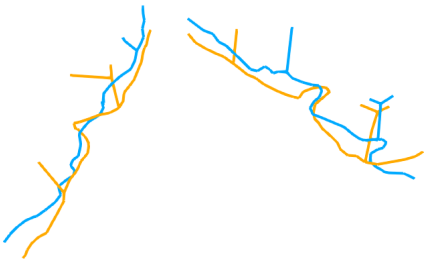

(b) Varifolds, t = 0

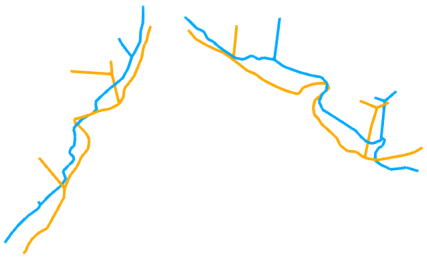

(c) Normal cycles, t = 1/3

(d) Varifolds, t = 1/3

(e) Normal cycles, t = 2/3

(f) Varifolds, t = 2/3

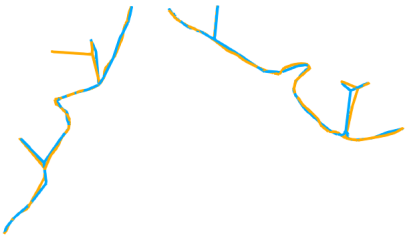

(g) Normal cycles, t = 1

(h) Varifolds, t = 1

Figure 4.18: Zoom of the registration on two sulci. Each column show the evolution of the deformation with time. In the left column, the registration with normal cycles and Sobolev normal kernel. In the right column, the registration with varifolds. One can observe that since normal cycles take into account the extremities, the matching is much more convincing. On the contrary, the metric on varifolds tends perform a matching between points that are close, even though this implies a poor registration for branches.

In conclusion we have seen that despite an increase of the calculation time, normal cycles improve the matching, especially for branching curves, or curves with end points. We must point out however that these conclusions hold for the particular examples of kernels we chose for the three methods : currents, varifolds and normal cycles. It will be interesting in future experiments to make comparisons with the use of other kernels, for example a gaussian kernel instead of a linear kernel for the varifold metric, as in [Charlier et al., 2015a], or other types of kernels for the spherical part in the normal cycle metric. Besides taking into account the curvature of the curves, we believe that another advantage of using normal cycles for the matching of such structures is the "connection cost". Since normal cycles consider currents associated with the normal bundle, the boundaries are also taken into account during the registration, and are enforced to match as well.

4.1.5 Surfaces Registration with Normal Cycles

Let us now move to the surface matching using LDDMM and kernel metrics on normal cycles. The aim of this section is to illustrate the properties of a matching with normal cycles, as well as some limitations. Using parallel computations, we are able to provide examples on real data (retina, hippocampi) with a large number of points (around 6000 for each shape).

The surface matching is made through the minimization procedure subsection 4.1.3. We used a geodesic shooting coupled with a quasi Newton Broyden Fletcher Goldfarb Shanno algorithm with limited memory (L-BFGS) [Liu and Nocedal, 1989]. The step in the descent direction is fixed by a Wolfe line search. For the numerical integrations, a Runge-Kutta (4,5) scheme is used (function ode45 in Matlab). The evaluations of the functional and its gradient, as well as the numerical integrations are the limiting part of the computational cost. In order to improve the computational cost, the convolution operations arising are done with parallel computing on a graphic card. The CUDA mex files using GPU are included in the MATLAB body program. The algorithm is run until convergence with a stopping criterion on the norm of the successive iterations, with a tolerance of 10^{-6}. This procedure allows us to perform matching of surfaces with up to 10 000 points in a reasonable time, which will be specified for each experimentation.

Notice that due to the increasing complexity of the model of normal cycles for surfaces, we are able to provide registration with the constant normal kernel only. For all the following matching, the geometric kernel k_p is a Gaussian kernel of width σ_W, k_n is a constant kernel as in section 3.5. The kernel K_V is a sum of 4 Gaussian kernels of decreasing sizes, in order to capture different features of the deformation. The trade-off parameter γ is fixed at 0.1 for all the experiments.

Synthetic data: illustration of the curvature properties

Registration of an ellipsoid to a duck. Let us start with the simple, yet interesting example of figure 4.19. We want to perform a matching between blue ellipsoid (the source) and the orange duck (the target). The orange duck contains 2000 points and the blue ellipsoid 10 000.

The registration is performed with normal cycles and varifolds. We chose a Gaussian kernel for the spatial kernel and a sum of 4 Gaussian kernels of decreasing size ($\sigma_V = 0.15, 0.075, 0.0375, 0.0185$) for the deformation kernel k_V. We recall that for normal cycles, we chose a constant normal kernel and for varifolds, a linear kernel on the Grassmanian. Two runs are performed, one at size $\sigma_W = 0.15$ and one at size $\sigma_W = 0.075$ for spatial kernel. The first run can be seen as an initialization step. For normal cycles, the run ended respectively at 23 and 33 iterations, for a total time of 4000 seconds (71s/it). For varifolds, the run ended respectively at 79 and 2 iterations, for a total time of 9330 seconds (114s/it, this experiment was made without any parallelization for varifolds). The registrations can be found in figures 4.20 and 4.21. As expected, the matching with normal cycles is more accurate that the one with varifolds. This appears clearly in the neighbourhood of regions

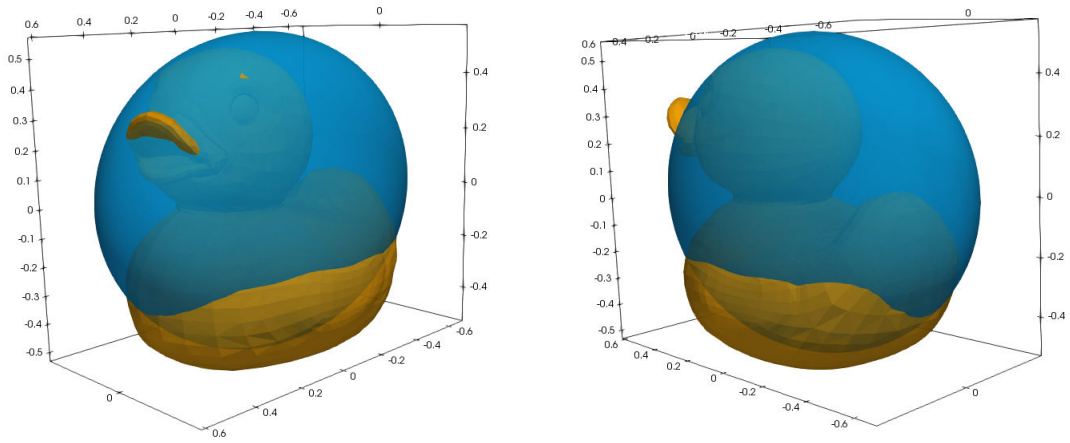

Figure 4.19: Two views of the matching problem of a blue ellipsoid to an orange duck.

with high curvature as the beak or the eyes. It is interesting to notice that even the coarse mesh of the duck appears in the deformed ellipsoid for normal cycles.

Registration of hippocampi. The second example is a matching of two hippocampus, of typical size $10 \times 20 \times 40$. Each shape is around 7000 points. Three runs at different geometric kernel sizes are performed (see Fig. 4.22). We can see the the final deformation matches well the two hippocampus, even the high curved regions of the shape.

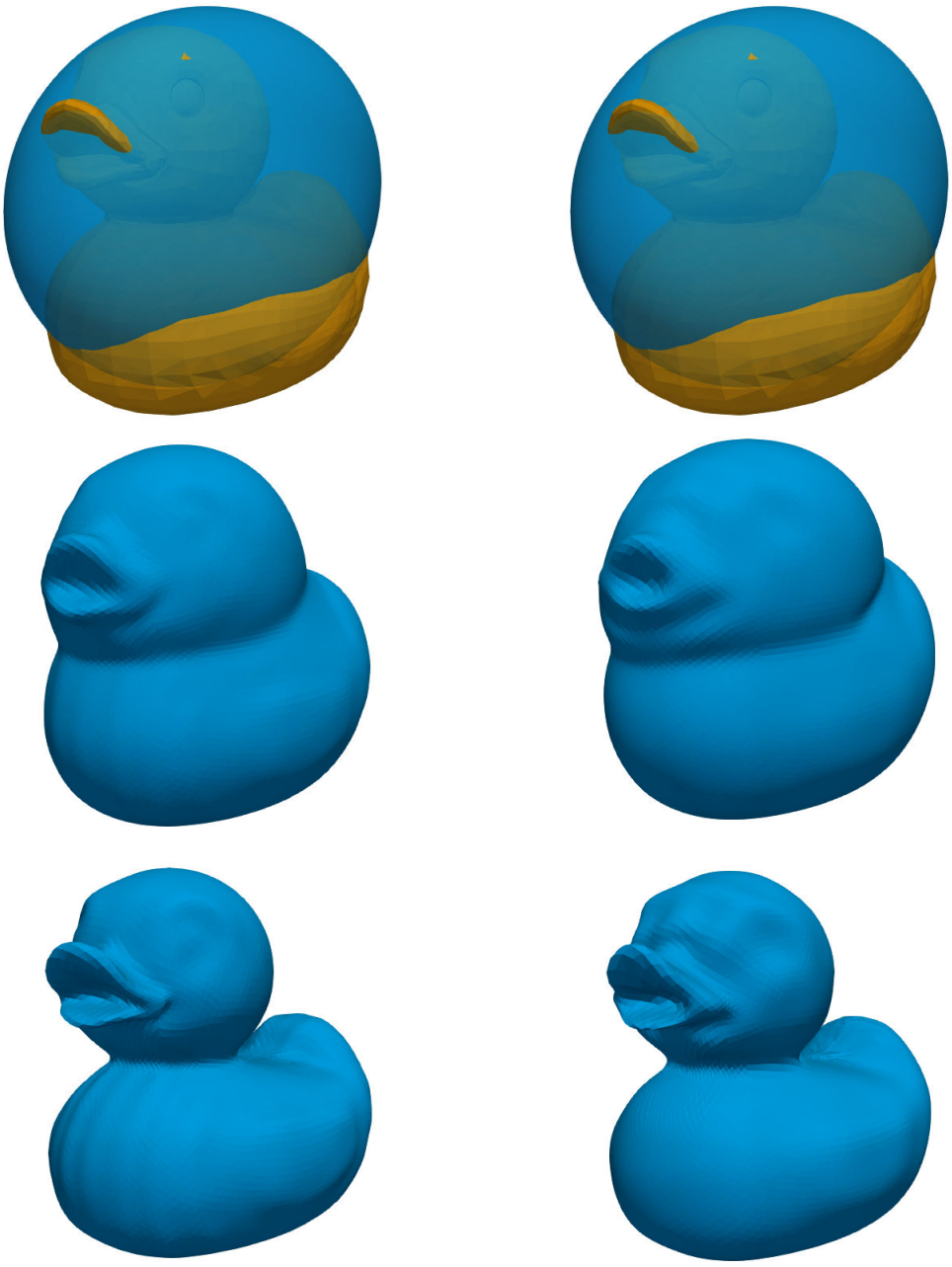

Figure 4.20: View 1. Registration of a blue ellipsoid to an orange duck. The left column represents the matching with normal cycles and the right column the one with varifolds. The registration with normal cycles is more accurate as it can be seen with the beak or the eyes. One can even notice that the coarse mesh of the duck appears in the deformed ellispoid.

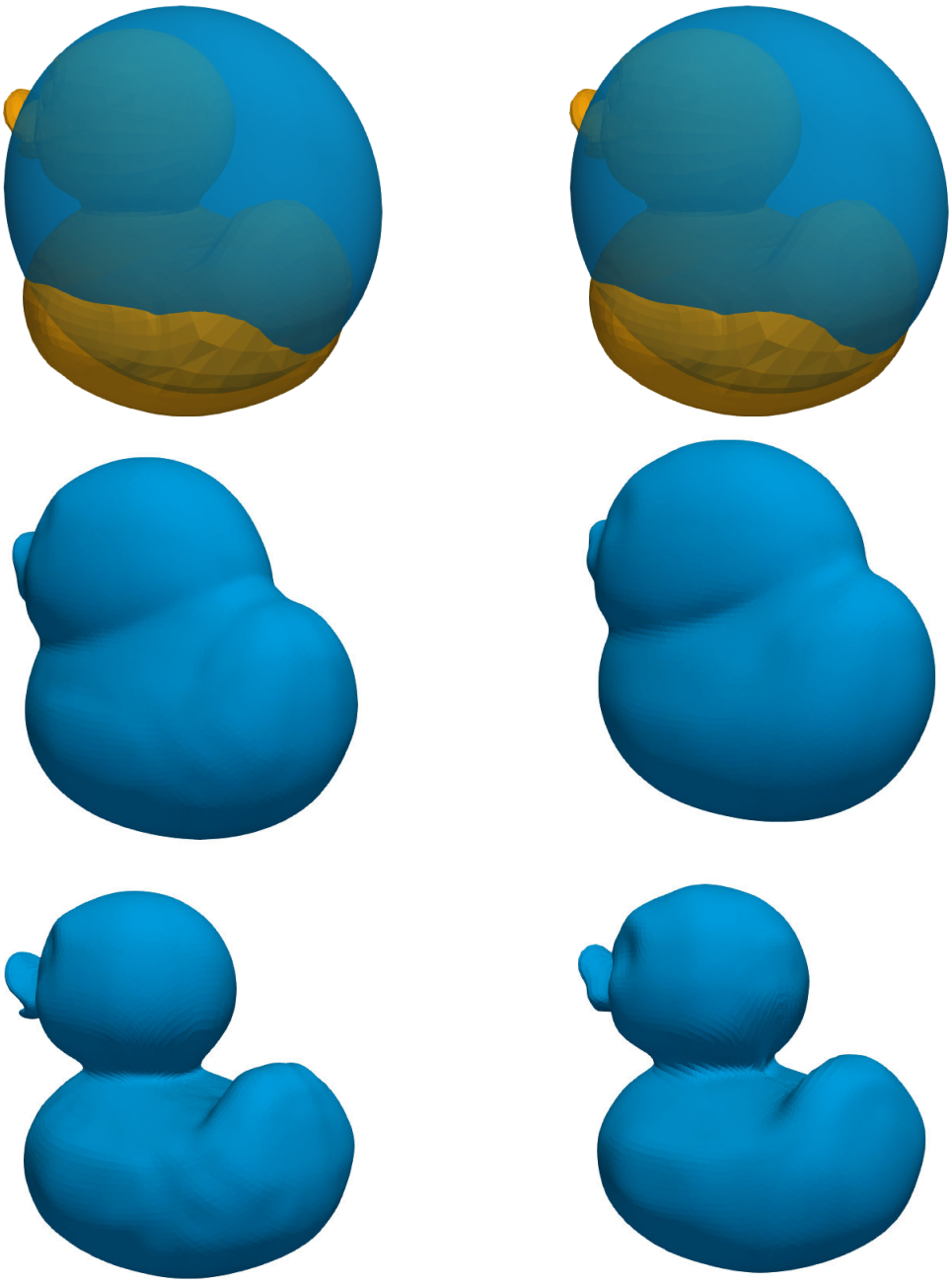

Figure 4.21: View 2. Registration of a blue ellipsoid to an orange duck. The left column represents the matching with normal cycles and the right column the one with varifolds. The registration with normal cycles is more accurate as it can be seen with the beak or the neck.

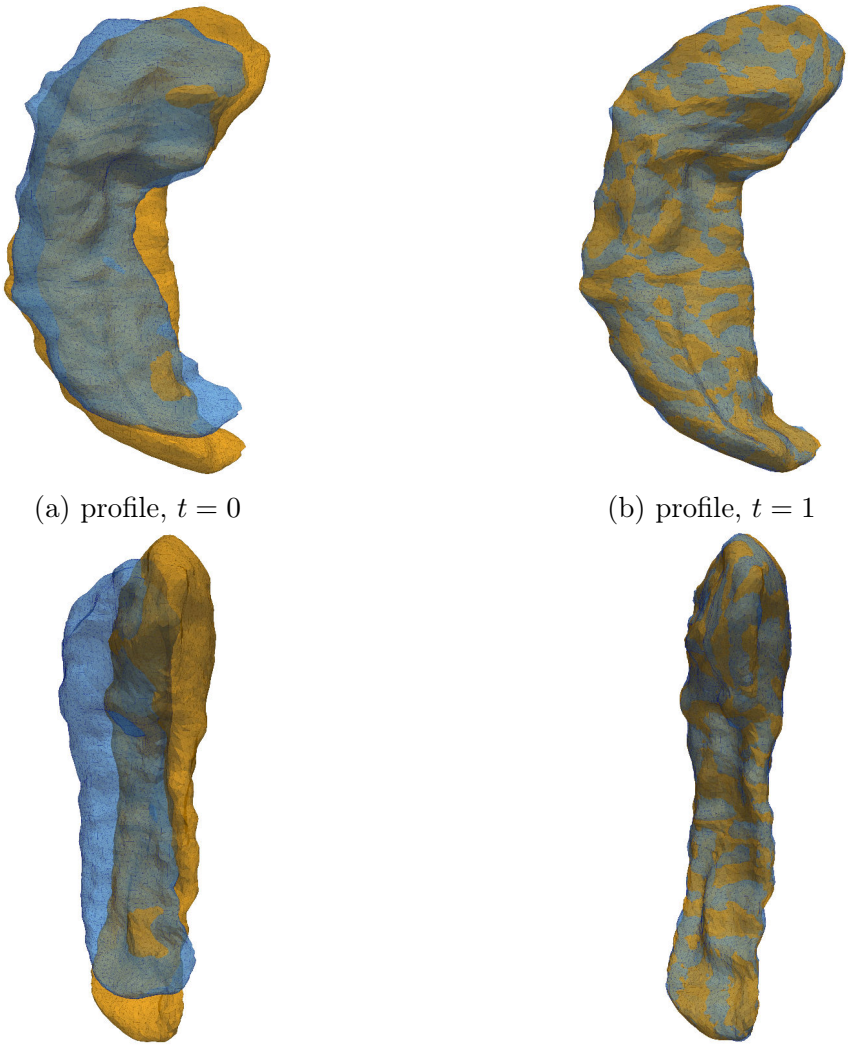

(a) profile, $t = 0$

(b) profile, $t = 1$

(c) face, $t = 0$

(d) face, $t = 1$

Figure 4.22: Two views (profile and face) at times $t = 0$ and $t = 1$ of the matching of two hippocampus with normal cycles. The target shape is in orange and the source in blue. Each shape has 6600 points. Three runs at different geometric kernel sizes are performed ($\sigma_W = 25, 10, 5$) and the kernel of deformation is a sum of Gaussian kernels with $\sigma_V = 10, 5, 2.5, 1.25$. Each run ended respectively at 62, 66 and 48 iterations for a total time of 4076 seconds (23 seconds per iteration).

Real data: retinas

The third data set was provided by B. Charlier, N. Charon and M.F. Beg is a set of retina layers from different subjects. Originally, each surface comes with a signal that represents the thickness of the retina layers at each vertex. In [Lee et al., 2017a], a statistical analysis of these functional shapes is made using atlas estimation in the framework of LDDMM and with a varifolds kernel metric. We refer to this article for the procedure of generation of this data set. In the following, we only use the geometrical information of the shapes to illustrate the properties of a matching with normal cycles. The difficulty of this example is to perform a matching that is convincing for the interior of the retina, as well as for the border. One should notice that the border has no real physical meaning but is the result of the data acquisition. The hole in the center of each retina corresponds to optical nerve. Even though these borders are not the interesting part for a medical application, they make the registration harder. We will see that the matching with normal cycles will incorporate the borders during the registration, resulting to a much smoother deformation.

The retina are surfaces of typical size 8×8mm. Each retina is sampled with approximately 5000 points. As for hippocampus, three runs are performed, with $\sigma_W = 0.8, 0.4, 0.2$ and the deformation kernel K_V is a sum of 4 Gaussian kernels, $\sigma_V = 2.4, 1.2, 0.6, 0.3$. All the details of the matching are in Fig. 4.23. The retinas have a border which will be seen as region with singularities for the kernel metric on normal cycles. This is not the case for the varifolds metric which makes the matching of the corresponding corners harder. The matching of the borders is better with normal cycles, and provides a much more regular deformation (see Fig. 4.23).

In the last example (Fig. 4.24), the two retinas are the result of an unsatisfactory segmentation . This leads to artifacts in each retina : two triangles for the source retina (in blue, Fig. 4.24) and only one for the target, in orange. We would like that during the matching, these artificial features are not taken into account. However, These are regions of high curvature and as we could expect, the kernel metric on normal cycles will make a correspondence between those points. As we can see in the second row of Fig. 4.24, the two triangles are crushed together, into one triangle, even though the cost of the resulting deformation is high. This example shows how sensitive to noise or artifacts normal cycles are. The data must be smooth and well segmented so that the matching works well.

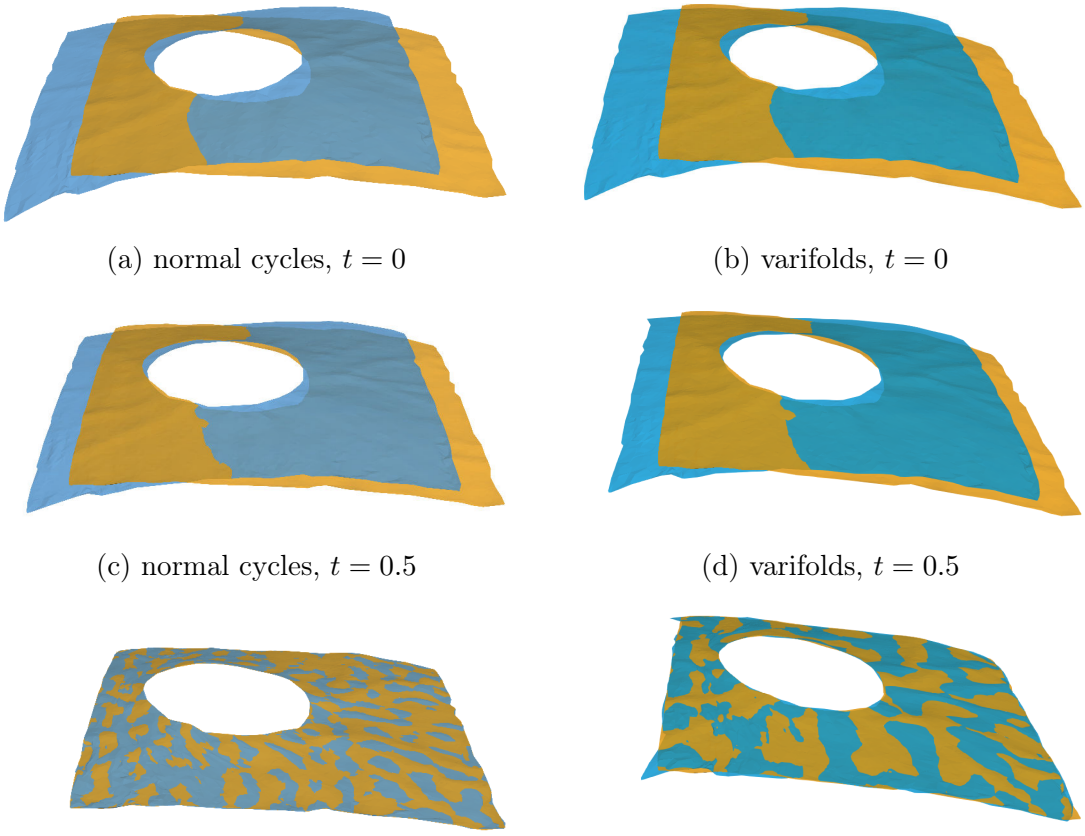

(a) normal cycles, $t = 0$

(b) varifolds, $t = 0$

(c) normal cycles, $t = 0.5$

(d) varifolds, $t = 0.5$

(e) normal cycles, $t = 1$

(f) varifolds, $t = 1$

Figure 4.23: Each column represents the matching of two retina with kernel metric on normal cycles (left) and varifolds (right). The target shape is in orange and the source shape is in blue. Each shape has 5000 points. For the varifolds metric, the geometric kernel is Gaussian. The kernel on the Grassmanian is chosen linear so that no additional parameter is involved. The same parameters are used for each data attachment term. Three runs at different geometric kernel sizes are performed ($\sigma_W = 0.8, 0.4, 0.2$). K_V is a sum of Gaussian kernels with $\sigma_V = 2.4, 1.2, 0.6, 0.3$. For normal cycles, each run ended respectively at 88, 297 and 5 iterations for a total time of 5487 seconds (14 seconds per iteration).

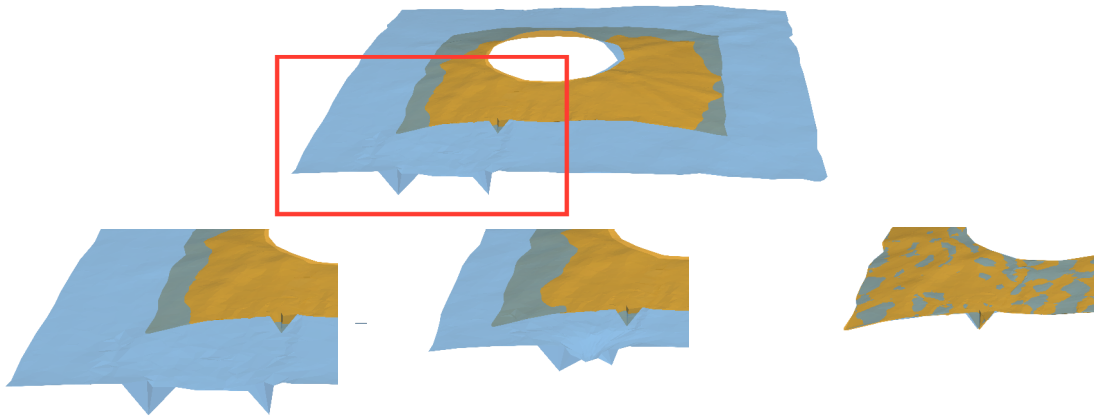

(a) $t = 0$ (b) $t = 0.5$ (c) $t = 1$

Figure 4.24: Matching of two retina with normal cycles : the target (in orange) and the source (in blue). Three runs at different geometric kernel sizes are performed ($\sigma_W = 0.8, 0.4, 0.2$). K_V is a sum of Gaussian kernels with $\sigma_V = 2.4, 1.2, 0.6, 0.3$. The first row shows the initial configuration. The second row shows the matching in the specific zone delimited by the red rectangle. The metric on normal cycles enforce the matching of corresponding high curvature points, which leads to the alignment of the two triangles into the single one of the target. Each run ended respectively at 211, 90 and 202 iterations for a total time of 8114 seconds (16 seconds per iteration).

4.2 Atlas Estimation with Normal Cycles

One of the goal of computational anatomy is the statistical analysis of the variability in a dataset of shapes. This is classically tackled with the estimation of a mean shape as well as the deformations that match the mean shape to each shape of the dataset. This estimation of both the mean shape and the deformations from the mean shape to the targets is called an *atlas*. The mean shape contains all the anatomical invariants across the dataset. The statistical analysis is then transferred to the study of the deformations, that can be reduced with the framework of LDDMM to the study of the initial momenta. Reducing the study to initial momenta has the major advantage to set the framework in the Euclidean space $(\mathbb{R}^d)^n$ where all the classical statistical tools are available. From there, an adequate analysis could quantify abnormalities across a dataset of shapes, but also describe the anatomical differences behind these quantified abnormalities. These tools aim to help the researchers and the doctors to find early biomarkers of a disease that would allow for a precocious diagnosis. Of course, for now this is a research field that necessitates a wide range of validations, but some works are noteworthy to mention. In [Durrleman et al., 2014], the authors propose a generic method to the statistical analysis of a collection of anatomical shape complexes. This method relies on the LDDMM framework with *control points* to encode the deformation (see [Durrleman et al., 2013, Durrleman et al., 2011b]) and they provide a classification between down syndrom subjects and control subjects, with potential anatomical

features that could have a discriminative power. In [Lee et al., 2017a] (see also [Charon and Trouvé, 2013], chapter 4 and [Charlier et al., 2015a]), the authors apply the framework of *functional shapes* with LDDMM to perform a statistical analysis of retinal optical coherence tomography images. A classification using a linear discriminant analysis on initial momenta to automatically classified glaucoma, suspects and healthy subjects across the dataset. Note that this work has been pushed forward in [Lee et al., 2017b].

In this section, we present some first results of atlas estimations with kernel metrics on normal cycles as data attachment term. Examples are shown on synthetic and real data, using the algorithm of hypertemplate that is recalled in subsection 4.2.1 and subsection 4.2.2. The estimated atlas on retina datasets shows an improvement on the quality of the obtained deformations and some hints on the consideration of curvatures with normal cycles are shown (subsection 4.2.4). For now, we have not performed a statistical analysis of the initial momenta and this is postponed to future work with relevant data.

4.2.1 Theoretical Framework

In the following, we will consider a set of N shapes (curves or surfaces) $X_1, \dots X_n$. We recall that we are set in the LDDMM framework, where a group of transformations G_V is generated with integration of time-varying vector fields living in a RKHS V. Let us start with the simple case where all the shapes live in the same orbit under the action of G_V: $X_i \in G_V.X_1 := \mathcal{X}$ for $i = 1, \dots, N$. The Riemannian metric on G_V provides a metric on $\mathcal{X}$ and the *Fréchet mean* is the natural extension of the well known Euclidean mean. The Fréchet mean $\overline{X}$ is the critical point of the square distances to each X_i, namely:

$$\overline{X} = \arg\min_{X \in \mathcal{X}} \sum_{i=1}^{N} d_{\mathcal{X}}(X_i, X)^2,$$

where $d_{\mathcal{X}}(X_i, X) = \inf_{\varphi \in G_V} d_{G_V}\big(\varphi.X, X_i\big)$. This means $\overline{X}$ comes with N deformations $(\varphi^i)_{1 \leq i \leq N}$ such that $\varphi^i(\overline{X}) = X_i$. In this setting, it is a well known result of Riemannian geometry that the Fréchet mean exists. Even though it is a good candidate for the mean shape, the assumption that the shapes live in the same orbit under the action of G_V is not relevant nor desirable. To relax this hypothesis, we allow for some residual:

$$X_i = \varphi^i(\overline{X}) + \varepsilon_i.$$

The quantification of the residual ε_i is of crucial importance for the atlas estimation and depends on the data attachment term that we choose. In common applications, this quantification is made using kernel metrics on shapes representations that we have seen in Chapter 2 and Chapter 3. The relaxed problem of estimating a mean

shape writes:

$$\min_{\substack{X \\ \varphi^1,\dots,\varphi^N \in G_V}} \gamma \sum_{i=1}^{N} d_{\mathcal{X}}(X, \varphi^i(X))^2 + \sum_{i=1}^{N} g\Big(\varphi^i(X), X_i\Big). \tag{4.8}$$

Remark 4.8. *All the classical result on Fréchet mean are usually in finite dimension. However, once discretized, the problem of atlas estimation leads back to this usual case.*

In our application, g will be a kernel metric on normal cycles: $g\Big(\varphi^i(X), X_i\Big) = \|N(\varphi^i(X)) - N(X_i)\|^2_{W'}$.

Remark 4.9. *The formulation* (4.8) *can be formally derived from a Maximum A Posteriory (MAP) as it has been detailed in [Durrleman, 2010], chapter 5. In this statistical setting, we introduce two priors: the first on the deformations, encoded with the optimal vector field $v_0 \in L^2_V$ with Gaussian density $p_{defo}(v_0) = \exp(-\|v_0\|^2_V / 2\sigma^2_V)$ and the other prior on the noise model on shape residuals: $p_r(\varepsilon_i) = \exp(-\|\varepsilon_i\|^2_{W'} / 2\sigma^2_W)$. Supposing that the residuals are i.i.d., we are looking for the template $\overline{X}$ that maximizes the probability of observing the shapes $(X_i)_{1\leq i\leq N}$ knowing the template $\overline{X}$: $\prod_{i=1}^N p\big(X_i|\overline{X}\big)$. With appropriate approximation, the minimization of the associated log-likelihood takes the form* (4.8)*. See [Durrleman, 2010], chapter 5, [Charon and Trouvé, 2013], chapter 4 for more details.*

Of course, this equation has to be considered cautiously since there is no precision on the space on which X lives. A nice approach to provide a sound mathematical framework is to consider that the possible templates live in a restricted yet large space, generated by a *hypertemplate*. This idea was introduced in [Ma et al., 2008, Ma et al., 2010]. Considering a shape X_0, called the hypertemplate, we restrict the problem as follow:

$$\min_{\substack{X \in G_{V_0}.X_0 \\ \varphi^1,\dots,\varphi_N \in G_V}} \gamma \sum_{i=1}^{N} d_{\mathcal{X}}(X, \varphi^i(X))^2 + \sum_{i=1}^{N} g\Big(\varphi^i(X), X_i\Big). \tag{4.9}$$

Notice that the group of deformations G_{V_0} needs not be the same as G_V. In order to have a mathematical well-posed setting as well as a closed form for the computations, we consider an additional cost in the functional: the hypertemplate not only generates the space $\mathcal{X}_0 = G_{V_0}.X_0$ but it is also the starting point for optimization:

$$\min_{\substack{X \in \mathcal{X}_0 \\ \varphi^1,\dots,\varphi^N \in G_V}} \gamma_0 d_{\mathcal{X}_0}(X_0, X)^2 + \gamma \sum_{i=1}^{N} d_{\mathcal{X}}(X, \varphi^i(X))^2 + \sum_{i=1}^{N} g\Big(\varphi^i(X), X_i\Big). \tag{4.10}$$

With the LDDMM framework, the previous minimization over G_{V_0} and G_V can be transferred to a minimization on the Hilbert spaces $L^2_{V_0}$ and L^2_V:

$$\min_{\substack{v^0\in L^2_{V_0}\\ v^1,\dots,v^N\in L^2_V}} J_{atlas}(v^0,v^1,\dots,v^N) := \gamma_0 \left\|v_0^0\right\|^2_{V_0} + \gamma \sum_{i=1}^N \left\|v_0^i\right\|^2_V + \sum_{i=1}^N g\Big(\varphi_1^{v^i}\circ\varphi_1^{v^0}(X), X_i\Big). \tag{4.11}$$

where we recall that optimal trajectories in G_V have constant velocities: $\|v_t\|^2_V = \|v_0\|^2_V$ and where $\frac{\partial \varphi_t^{v^i}}{\partial t} = v_t^i \circ \varphi_t^{v^i}$, $\varphi_0^{v^i} = \mathrm{Id}$. One should notice that the minimization of (4.11) provides both the template $\overline{X}$ ($\overline{X} = \varphi_1^{v^0}(X_0)$) and the deformations $\left(\varphi_1^{v^i}\right)_{1\leq i\leq N}$ from the template to the shapes $(X_i)_{1\leq i\leq N}$ of the datasets.

Theorem 4.10. *Suppose that $X_1,\dots,X_N$ are N compact sets in $\mathcal{U}_{PR}$ and assume that one has the embeddings $V, V_0 \hookrightarrow \mathcal{C}^3_0(\mathbb{R}^d,\mathbb{R}^d)$, and $W \hookrightarrow \Omega^{d-1}_{0,1}(\mathbb{R}^d\times S^{d-1})$. Then there exists a minimizer $(v_*^0, v_*^1,\dots,v_*^N) \in L^2_{V_0}\times (L^2_V)^N$ for the problem (4.11) of atlas estimation in the hypertemplate setting, with kernel metrics on normal cycles as data attachment term.*

Proof. The proof follows the one of theorem 4.2. From a minimizing sequence $(v_n^0, v_n^1,\dots,v_n^N)_{n\in\mathbb{N}} \in \left(L^2_{V_0}\times (L^2_V)^N\right)^{\mathbb{N}}$, we extract a subsequence that weakly converges to $(v_*^0, v_*^1,\dots,v_*^N)$. This is possible since the energy terms $\gamma_0\left\|v_0^0\right\|^2_{V_0} + \gamma\sum_{i=1}^N \left\|v_0^i\right\|^2_V$ guarantee that the sequence is bounded. Now we recall that $v\mapsto \|\varphi_1^v.N(C) - N(S)\|^2_{W'}$ is continuous for the weak convergence on L^2_V and lower semi-continuous. This property implies that $(v_*^0, v_*^1,\dots,v_*^N)$ is indeed a minimizer of (4.11). □

Once again, this theorem encompasses both the case of smooth submanifolds and the one of polyhedral shapes.

4.2.2 Atlas Estimation Algorithms for Discrete Shapes

As for registration problems, we approximate this continuous atlas estimation in the case of discrete shapes. The action of diffeomorphisms is restricted to the vertices of the shapes only, leaving the meshes structure unchanged, and we use the classical approximations on the metric on normal cycles that have been presented in (2.20), (2.21) and section 4.1. In this discrete setting, the geodesic equations on G_V reduced to the case of landmarks and the optimal paths are parametrized by initial momenta localized on the vertices of the source shape. For a set of shapes $X_1,\dots X_N$ with an initial hypertemplate X_0, we denote x^i the vertices of X_i for $i\in\{0,\dots,N\}$. Denoting $K_V(x,x)p = \left(\sum_{l=1}^n K_v(x_k,x_l)p_l\right)_{1\leq k\leq n}$ where n is the number of vertices of x and K_V the kernel of deformation, then we can write the approximated problem of atlas estimation in the discrete setting with kernel metrics on normal cycles:

$$\min_{p_0,\dots p_N\in(\mathbb{R}^d)^n} J(p_0,\dots,p_N) = \gamma_0 p_0^T K_{V_0}(x^0,x^0)p_0 + \gamma\sum_{i=1}^{N} p_i^T K_V(x^i,x^i)p_i + \sum_{i=1}^{N} g\big(\varphi^{p^i}(\overline{x}),x^i\big), \tag{4.12}$$

where:

$$\begin{cases} \overline{x} = \varphi^{p_0}(x^0) \\ g_i(\varphi^{p^i}(\overline{x}),x^i) = \left\| N(\overline{X}_{\varphi^{p_i}})^{approx} - N(X^i)^{approx} \right\|^2_{W'} \end{cases}$$

and where we recall that $N(\overline{X}_{\varphi^{p_i}})^{approx}$ corresponds to the approximated normal cycle of the mesh with vertices $\varphi^{p_i}(\overline{x})$ and with the same mesh structure as $\overline{X}$. Now that we have the discrete formulation, we detail the algorithm of atlas estimation. In the following, we denote $(x(1),p(1))$ the forward integration of the geodesic equation for landmarks:

$$\begin{aligned} \dot{x}(t) &= K_V(x(t),x(t))p(t) \\ \dot{p}(t) &= -\nabla_1 \langle p(t), K_V(x(t),x(t))p(t)\rangle \\ (x(0),p(0)) &= (x,p). \end{aligned}$$

Algorithm 3 Hypertemplate algorithm

Input: X_0 (hypertemplate initialization) with vertices x^0, $X_1,\dots,X_N$ shapes of the dataset with respective vertices $x^1,\dots x^N$.
Output:

$$\arg\min_{p_0,p_1,\dots,p_N} J(p_0,p_1,\dots,p_N) := \gamma_0 p_0^T K_{V_0}(x^0,x^0)p_0 + \gamma\sum_{i=1}^{N} p_i^T K_V(x^i,x^i)p_i + \sum_{i=1}^{N} g\big(\varphi^{p^i}(\overline{x}),x^i\big).$$

initialization: $p_0 = 0, p_1 = 0,\dots,p_N = 0$
while Convergence **do**
  Compute $(x_0(1) = \overline{x}, p_0(1))$, $(\overline{x}(1),p_i(1))_{1\le i\le N}$ through *forward integration* of (1.13) (with kernel K_{V_0} for X_0 and K_V for $(X_i)_{1\le i\le N}$.
  Compute $\nabla_{\overline{x}(1)} g(\overline{x}(1),x_i)$ for $i = 1\dots N$.
  Compute $\nabla_{p_i(0)} g(\overline{x}(1),x_i)$ for $i = 1\dots N$ through *backward integration* of (1.14).

  Compute $\nabla_{p_0(0)} J^g :=$ *backward integration* of (1.14) with kernel K_{V_0} starting with $\nabla_1 J := \sum_{i=1}^N \nabla_{p_i(0)} g(\overline{x}(1),x_i)$.
  Compute $\nabla_{p_0} J(p_0,p_1,\dots,p_N) = \gamma_0 K_v(x_0,x_0)p_0 + \nabla_{p_0} J^g$.
  Compute $\nabla_{p_i} J(p_0,p_1,\dots,p_N) = \gamma K_v(x_i,x_i)p_i + \nabla_{p_i} g(\overline{x}(1),x_i)$ for $i = 1,\dots,N$.

  $p_0 \leftarrow p_0 - \delta_0 \nabla_{p_0} J(p_0)$
  $p_i \leftarrow p_i - \delta \nabla_{p_i} J(p_0,p_1,\dots,p_N)$ for $i = 1,\dots,N$.
end while

As for registration, we use a quasi Newton Broyden Fletcher Goldfarb Shanno algorithm with limited memory (L-BFGS) [Liu and Nocedal, 1989] to minimize (4.12).

The step in the descent direction is fixed by a Wolfe line search. For the numerical integrations, a Runge-Kutta (4,5) scheme is used (function ode45 in Matlab). The convolution operations arising are done with parallel computing on a graphic card. The CUDA mex files using GPU are included in the MATLAB body program. The algorithm is run until convergence with a stopping criterion on the norm of the successive iterations, with a tolerance of 10^{-6}.

Remark 4.11. *Other template estimations are possible. For example, we could have minimized on the vertices of the template directly, i.e. we minimize the functional:*

$$\min_{\overline{x},p_1,\dots,p_N} J(\overline{x},p_1,\dots,p_N) := \gamma \sum_{i=1}^{N} p_i^T K_V(x^i,x^i)p_i + \sum_{i=1}^{N} g\big(\varphi^{p^i}(\overline{x}),x^i\big).$$

The gradient with respect to the vertices $\nabla_{\overline{x}} J$ is computed through backward integrations of (1.14) starting with $\Big(\nabla_{\overline{x}(1)} g\big(\overline{x}(1),x^i\big),0\Big)_{1\leq i\leq N}$. This procedure is also used in the community of LDDMM. If this estimation procedure seems more direct and less "initialization-dependant" than the hypertemplate setting, it still suffers from several drawbacks. First of all, we are not able yet to prove the existence of a minimizer in this framework. Moreover, the gradient $\nabla_{\overline{x}} J$ is a L^2-gradient and it is possible that the evolution of the template during the minimization procedure suffers from singularities (as folding for example). Thus, we need to regularize the gradient (e.g. with a Gaussian kernel). All this have been studied with more details in [Charon and Trouvé, 2013], chapter 4 and [Charlier et al., 2015a]. We have not investigated yet this template estimation in this manuscript, but it could definitely be a future work.

4.2.3 Curve Atlas Estimation

Atlas estimation of brain sulci: we find again the brain sulci studied in subsection 4.1.4. The database is composed of 6 brain sulci from 6 individuals (figure 4.25). One can see in figure 4.15 that the brain sulci fit in a bow of size 120mm × 120 mm × 80 mm. The atlas estimation is made with the hypertemplate algorithm, exposed in subsection 4.2.2. The hypertemplate is composed of 6 sulci from another subject that is not in the database. Note that this is not an optimal initialization since it introduces bias of the chose subject in the template estimation. We will evoke later other possibilities to chose the hypertemplate. We present in the following the results for atlas estimation with normal cycles and varifolds

The hypertemplate algorithm is run with the already seen L-BFGS procedure for the minimization, and with a geodesic shooting as explained in Algorithm 3. For the deformation kernel, we chose a Cauchy kernel of width $\sigma_V = 20$ both for the hypertemplate deformations (K_{V_0}) and for the template deformations (K_V). The spatial kernel k_p for normal cycles and varifolds is a Gaussian kernel with width σ_W. The normal kernel for normal cycles is a Sobolev kernel of order 3. For the varifolds, the kernel on the Grassmanian is chosen linear. Two runs are performed

Figure 4.25: The database of 6 brain sulci for 6 individuals.

for the minimization, one at coarse scale with $\sigma_W = 25$ and one at finer scale with width $\sigma_W = 5$. Each run are ended at 1000 iterations.

The total number of points for on subject is in average 300. For normal cycles, the total time for the atlas estimation was 20000 seconds (around 5 hours and 30 minutes, 10s/it). Note that this time can be reduced with parallel computing that we have not implemented yet for curves. For varifolds, it was 15000 seconds (4 hours and 10 minutes, 8.7s/it). The obtained template for normal cycles and varifolds are shown in figure 4.26.

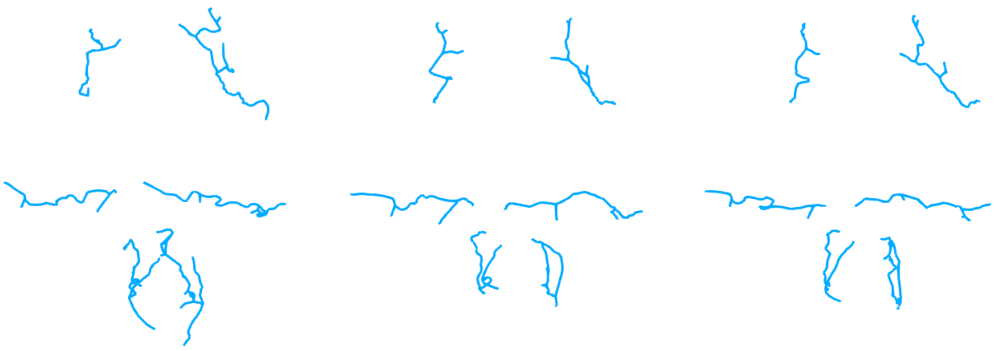

(a) Hypertemplate (initialization of the template) (b) Template obtained with normal cycles (c) Template obtained with varifolds

Figure 4.26: Template estimation from the dataset of figure 4.25 with normal cycles and varifolds as a data attachment term, starting with the hypertemplate on the left.The hypertemplate corresponds to a subject that is not in the database.

In figures 4.27 and 4.28, we show the registration from the estimated template (with normal cycles and with varifolds) to two chosen subjects, in order to illustrate the difference between the estimated atlas. The main difference lies in the consideration of the branching points with normal cycles. This implies that with normal cycles, the registration tries when possible to make a correspondence between the branches. For the metric on varifolds on the contrary, it is similar to make a correspondence between the branches or to twist one branch to match in the neighbourhood of a branching point. As one can observe in the middle sulci in figures 4.27 and 4.28, even though the cost of deformation is higher, the metric on normal cycles will enforce the registration of branching points, leading to a much more convincing matching. Note that this atlas estimation is hard since there is not the same number of branches in the template and in the subjects.

The template estimation could be improved by choosing an hypertemplate that is not a real individual subject. One could imaging a synthetic hypertemplate composed of segments with branching. Then we can take a close look at the deformation from the hypertemplate to the template: if one branch of the hypertemplate is crushed during the deformation, we can remove this branch from the hypertemplate and perform again the template estimation until a satisfactory template is found.

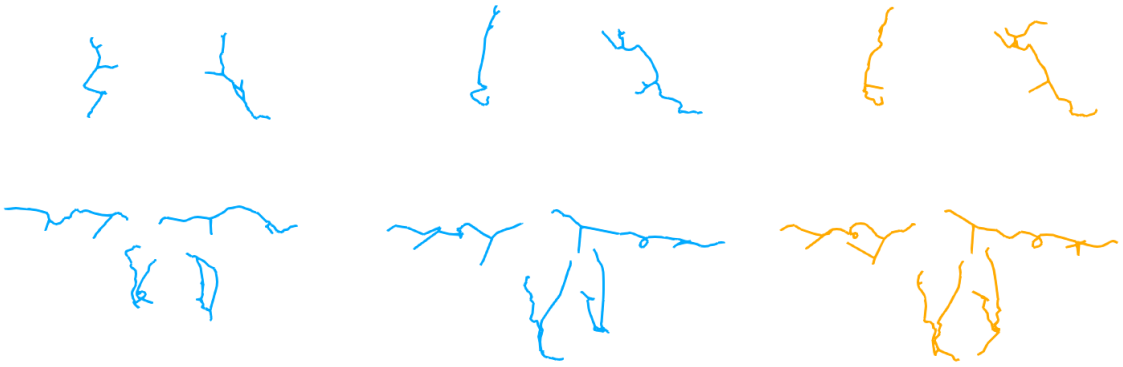

(a) Template estimated with normal cycles

(b) Shooting to the subject 1 with normal cycles

(c) Subject 1

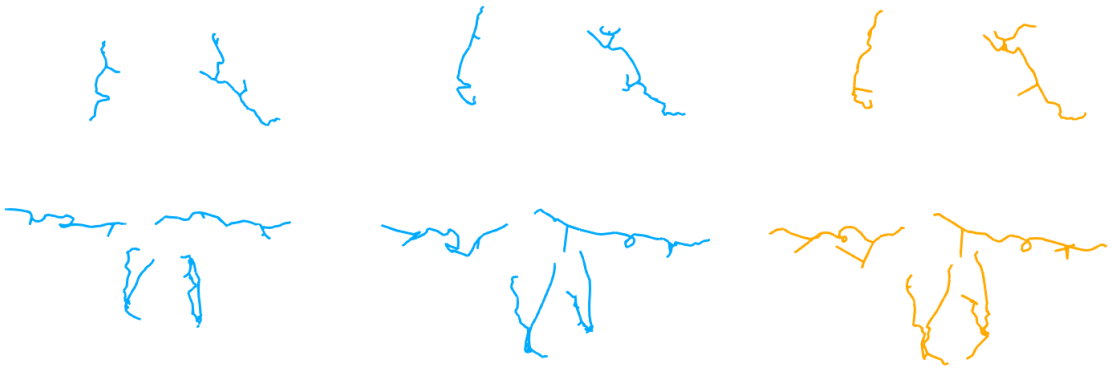

(d) Template estimated with varifolds

(e) Shooting to subject 1 with varifolds

(f) Subject 1

Figure 4.27: Shooting from the template to subject 1 with normal cycles (top row) and varifolds (bottom row). The main difference is observable is the middle sulci. The metric on normal cycles enforce the matching of branching points and extremities and the registration takes into account those features. On the contrary, with the metric on varifolds there is not such enforcing and it is similar to twist the sulci instead of making a correspondence between branches.

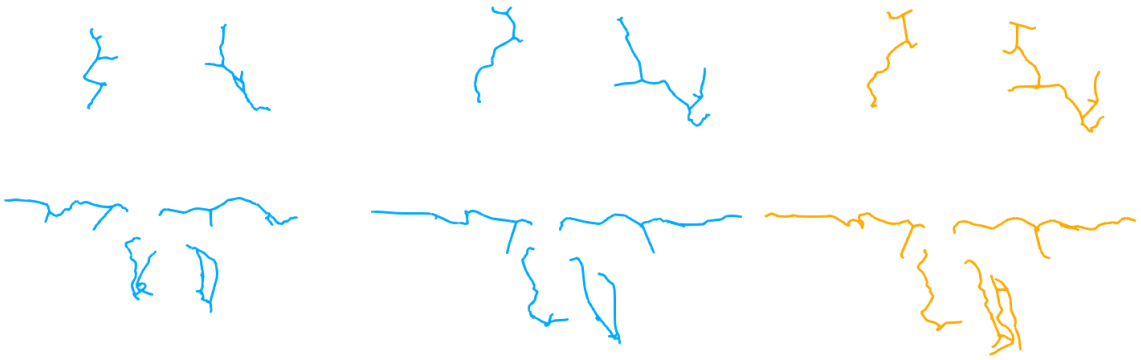

(a) Estimated template with normal cycles

(b) Shooting to subject 5 with normal cycles

(c) Subject 5

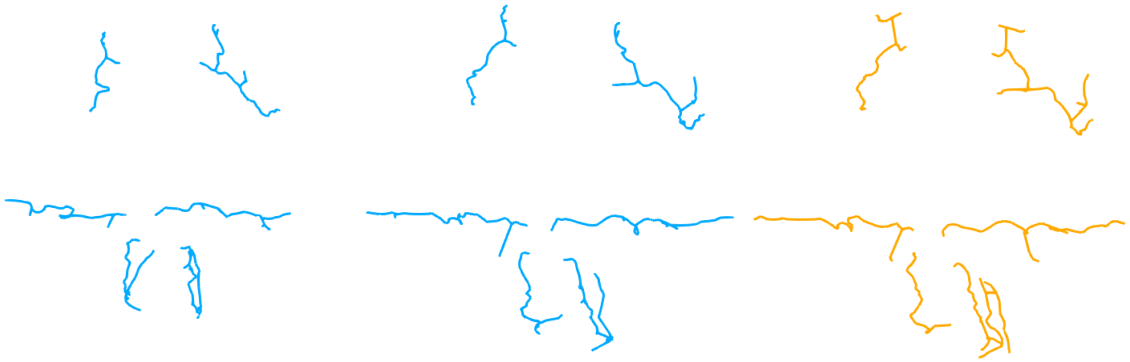

(d) Estimated template with varifolds

(e) Shooting to subject 5 with varifolds

(f) Subject 5

Figure 4.28: Shooting from the template to subject 5 with normal cycles (top row) and varifolds (bottom row). The main difference is observable is the middle sulci. The metric on normal cycles enforce the matching of branching points and extremities and the registration takes into account those features. On the contrary, with the metric on varifolds there is not such enforcing and it is similar to twist the sulci instead of making a correspondence between branches.

4.2.4 Surface Atlas Estimation

We present now some first results of atlas estimation with surfaces dataset and kernel metric on normal cycles, with constant normal kernel.

Atlas estimation of "Venus" dataset: The first dataset, provided by Nicolas Charon and Benjamin Charlier are 6 human-looking shapes, each shape containing around 2500 vertices fitting in a box of size $2 \times 2 \times 3$. The atlas estimation is made with Algorithm 3 and the metric on normal cycles with constant normal kernel. In figure 4.29, we have disposed the different subjects in orange and the initial hypertemplate in the center, in blue. Note that this disposition is only to ease the viewing, but the all the venus are in fact centered. In figure 4.30, we isolated the initial hypertemplate as well as an axis grid to visualize the scale of the features.

The minimization procedure is made with a deformation kernel K_V that is a sum of 4 Gaussian kernels of decreasing size $(0.8, 0.4, 0.2, 0.1)$. The deformation kernel of the hypertemplate is the same as K_V. The spatial kernel for the metric on normal cycles is a Gaussian kernel of width σ_W. Three runs are performed, with a decreasing size of σ_W: $\sigma_W = 1.5, 0.8, 0.4$. The two first runs can be seen as an improvement of the initialization and it captures different scales of the shapes during the atlas estimation. This atlas estimation has already been made with kernel metrics on varifolds in [Charon and Trouvé, 2013], chapter 4.

Each run is stopped at 100 iterations at most. The runs ended respectively at 100, 67 and 100 iterations, for a total time of 10812 seconds, i.e 3 hours (40.5 s/it). The results are shown in figure 4.31, figure 4.32 and figure 4.33. Figure 4.31 presents the shooting from the initial hypertemplate to the estimated template. The result is convincing, notably the rising of left arm that is an invariant of the dataset. figure 4.32 and figure 4.33 present two examples of registration from the template to one subject of the dataset. One can see that the matchings are very good.

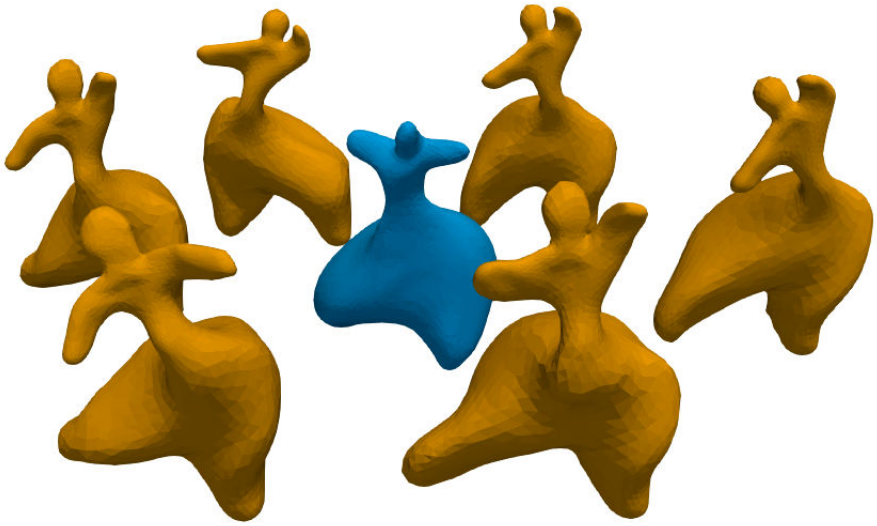

(a) $t = 0$

Figure 4.29: Dataset of 6 Venus and the blue hypertemplate (the initialization of the algorithm). Each venus contains 2500 points.

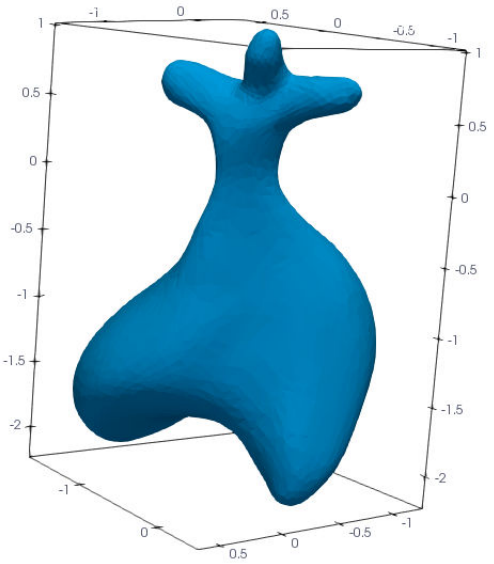

Figure 4.30: A closer look at the hypertemplate. It contains 3000 points.

(a) Hypertemplate ($t = 0$) (b) $t = 0.5$ (c) Template ($t = 1$)

Figure 4.31: Evolution of the hypertemplate's shooting with normal cycles and constant normal kernel as data attachment term. At time $t = 1$, we obtain the estimated template.

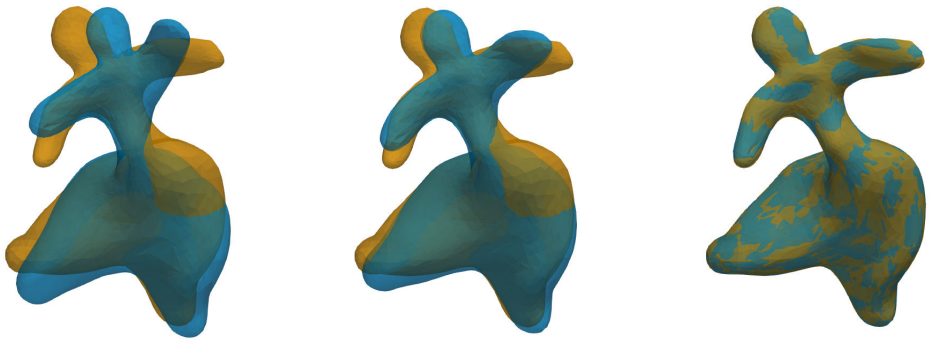

(a) $t = 0$ (b) $t = 0.5$ (c) $t = 1$

Figure 4.32: Shooting from the template to one subject.

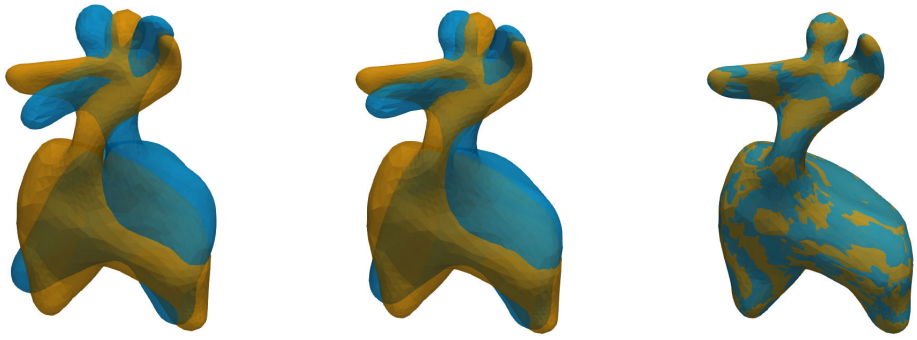

(a) $t = 0$ (b) $t = 0.5$ (c) $t = 1$

Figure 4.33: Shooting from the template to one subject.

Atlas estimation of a retina dataset: This second dataset is the same as subsection 4.1.5, provided by B. Charlier, N. Charon, and M.F. Beg. It provides more hint on the behaviour of the metric with normal cycles. In this dataset, we recall that the surfaces are retina layers, and that the borders (exterior or the hole in the center) distort considerably the registration with classical metrics on shapes (currents, varifolds). We have seen with the registration problem of subsection 4.1.5 that the metric on normal cycles improves greatly the registration, resulting in a much smoother deformation with a good matching of the borders. This observation will be similar for atlas estimation. In this experiment, we compare the result with the one obtained with the RKHS metric on varifolds.

We start with 6 retinas presented in figure 4.34. The hypertemplate is in blue in the center. We have chosen another retina of the dataset that is not one of the 6 in order to reduce the bias from this choice. Again, the disposition of figure 4.34 is only for a visualization purpose, and the data are in fact hole-centered. Moreover, for a better viewing in this manuscript, we multiply the x-scale of the representation by 2 (but not on the data!), which gives this more curved aspect.

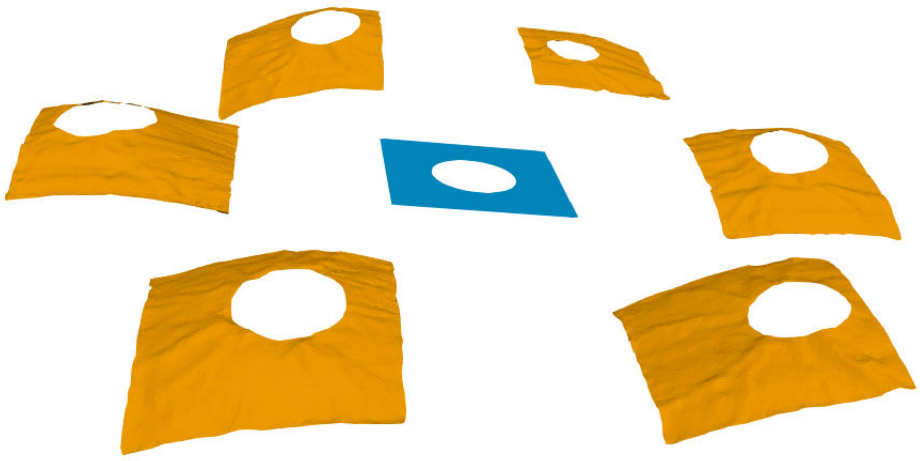

(a) $t = 0$

Figure 4.34: Dataset of 6 retinas and a blue hypertemplate. Each shape contains 5000 points.

The minimization procedure is made with a deformation kernel K_V that is a sum of 4 Gaussian kernels of decreasing size $(0.8, 0.4, 0.2, 0.1)$. The deformation kernel of the hypertemplate is the same as K_V. For varifolds and normal cycles, the spatial kernel is a Gaussian kernel of width σ_W. Three runs are performed, with a decreasing size of σ_W: $\sigma_W = 1.5, 0.8, 0.4$.

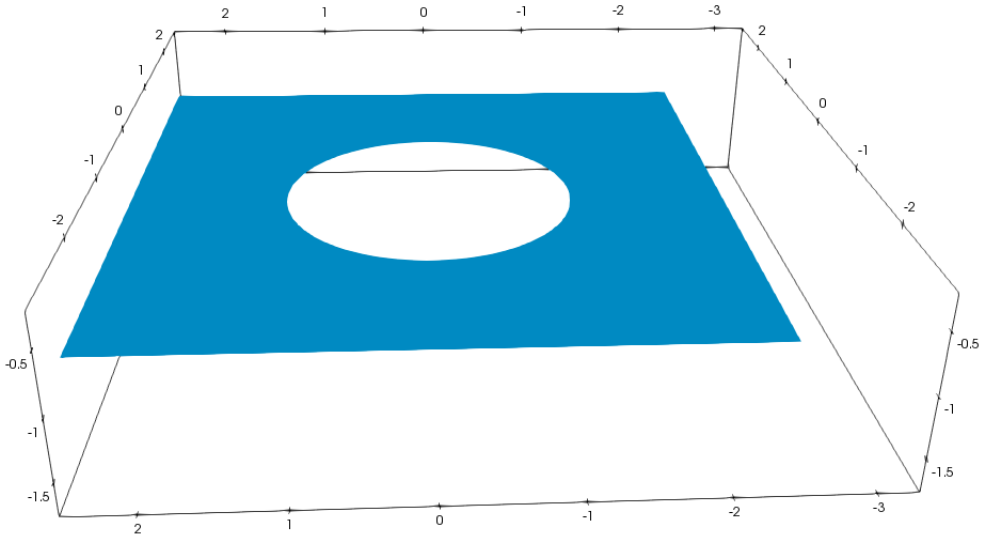

Figure 4.35: A closer look at the hypertemplate. It contains 5000 points

Each run is stopped at 100 iterations at most. For normal cycles, only the first run was effective and ended at 100 iterations (the second and third runs only had 2 iterations before converging) for a total time of 10656 seconds, i.e 3 hours (102 s/it). For the varifolds, only the first run was effective as well, and ended at 47 iterations, for a total time of 14766 seconds (300 s/it, notice that this comes from the fact that we did not parallelized the computations of the varifold metric, but theoretically the varifold metric is less complex that the normal cycles').

Figure 4.36 presents the shooting from the initial hypertemplate to the estimated template for normal cycles. Notice that the borders are smoothly deformed. This result is to compare with figure 4.37 where the border is strongly deformed, even though it does not correspond to any invariant feature of the dataset. It does not happen with normal cycles since the metric is sensitive to the borders. figure 4.38 and figure 4.39 present the registration from the template to one subject of the dataset respectively with normal cycles and varifolds. The nice estimation of the template provided by normal cycles allows for a much more convincing and regular registration than for varifolds.

Remark 4.12. *To overcome the difficulty of the border that arises with the varifold metrics, it has been proposed to enforce the matching by adding a current or varifold term associated with the curve ∂S of the shape S (i.e. a supplementary data attachment term) (see [Lee et al., 2017a], [Charon and Trouvé, 2013], chapter 4 and [Charlier et al., 2015a] for all the numerical considerations of the retinas atlas estimation with varifolds.). It is important to notice that for normal cycles, we have not made any supplementary assumptions, nor any numerical regularization or scaling*

of the gradient to obtain the template.

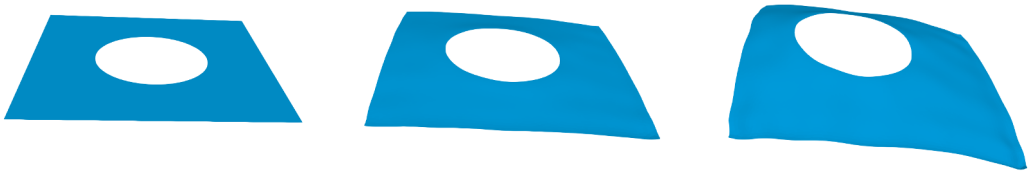

(a) Hypertemplate ($t = 0$) (b) $t = 0.5$ (c) template ($t = 1$)

Figure 4.36: Shooting from the hypertemplate to the estimated template with normal cycles

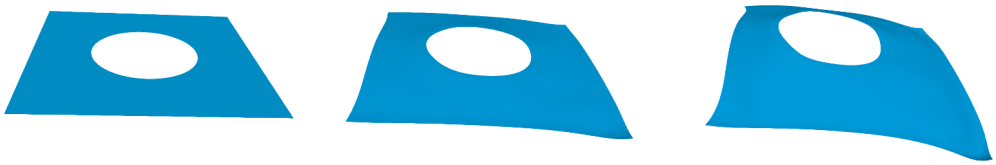

(a) Hypertemplate ($t = 0$) (b) $t = 0.5$ (c) Template ($t = 1$)

Figure 4.37: Shooting of the estimated template with varifold

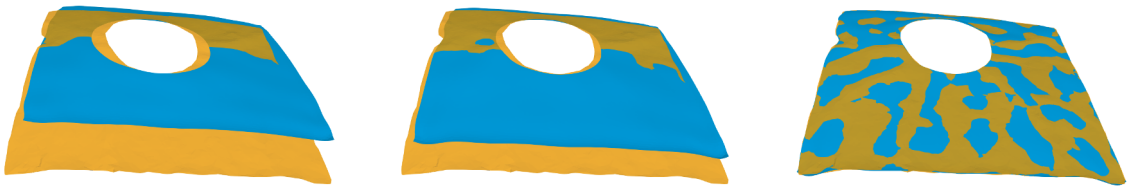

(a) $t = 0$ (b) $t = 0.5$ (c) $t = 1$

Figure 4.38: Shooting from the template to subject 6 (normal cycles)

Now, let consider the same dataset, but this time we add another retina that was the result of a bad segmentation (figure 4.40). One can observe that the new retina presents two triangles that are artefacts. We will see the influence of this subject in the template estimation.

The same parameters were chosen for the minimization procedure for normal cycles with constant normal kernel and for varifolds. The two first runs were stopped at 100 iterations, and the last run had only one iteration before convergence for a total of 201 iterations in 22188.9 sec, i.e. almost 6 hours (110 s/it). For the varifolds, only the first run was effective, with 69 iterations (i.e. the algorithm

(a) $t = 0$ (b) $t = 0.5$ (c) $t = 1$

Figure 4.39: Shooting from the template to subject 6 (varifolds)

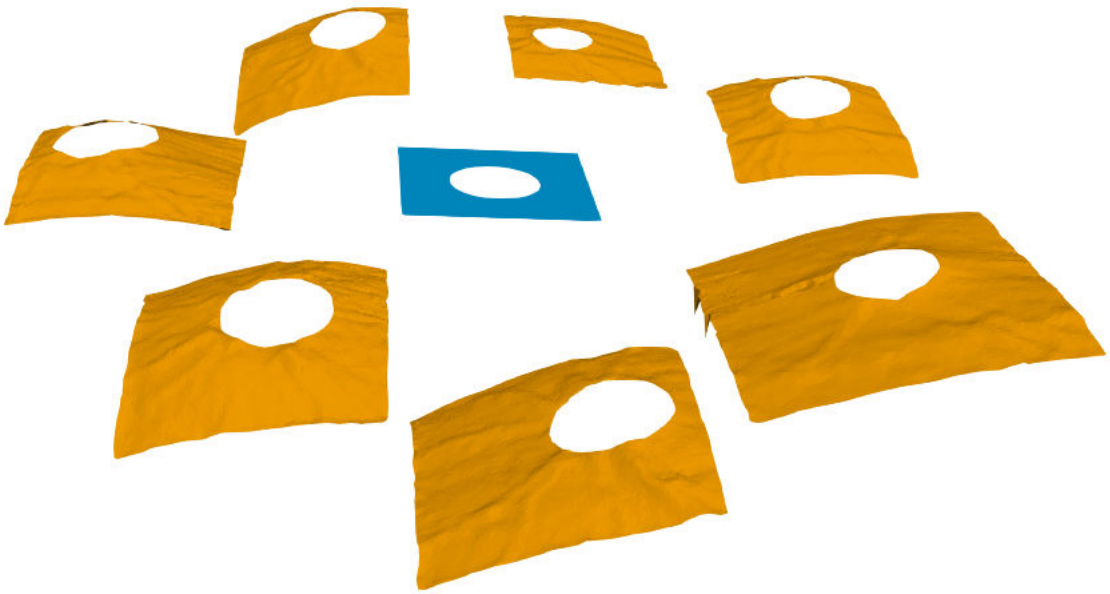

(a) $t = 0$

Figure 4.40: Dataset of 7 subjects and the blue hypertemplate.

stopped because it has converged), for a total time of 23000 seconds (334 s/it, again the time per iteration is high compared to the complexity of the varifolds due to the non-parallelization).

Figure 4.41 presents the shooting from the initial hypertemplate to the estimated template for normal cycles. Again, the borders are smoothly deformed. Moreover, one can notice the appearance of two little bumps located at the same position as the artefacts of the new retina. Even though these artefacts are small compared to the size of the spatial kernel, the metric on normal cycles sees them as region of high curvature and takes it into account during the atlas estimation. This result is to compare with the estimated template obtained with varifolds,figure 4.37, where we observe the same behaviour as for the previous atlas estimation (figure 4.37). In figure 4.43 we present the registration between the estimated template with normal cycles and the new retina with artefacts. Notice how the two little bumps of the template are matched to the two triangles. Onecan find the same registration with varifolds in figure 4.44. As expected, the metric on varifolds is insensitive to this artefacts and the matching does not take them into account. This shows how sensitive to noise or artefacts normal cycles are. Once again, it can be an advantage or a drawback depending on the kind of data we are working with. Any uncertainty on the data acquisition can have a major impact on the estimation.

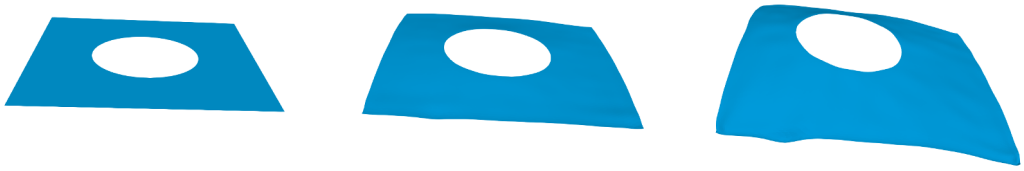

(a) Hypertemplate, $t = 0$ (b) $t = 0.5$ (c) Template ($t = 1$)

Figure 4.41: Evolution of the hypertemplate's shooting with normal cycles constant

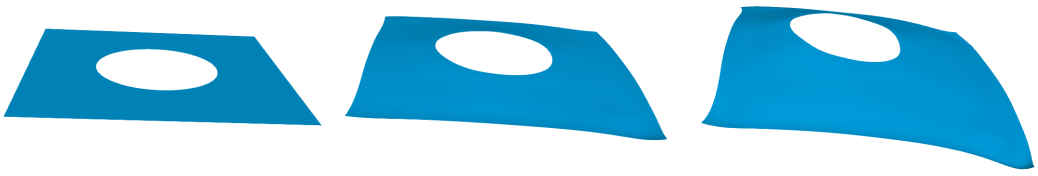

(a) Hypertemplate ($t = 0$) (b) $t = 0.5$ (c) Template ($t = 1$)

Figure 4.42: Evolution of the hypertemplate's shooting with varifolds

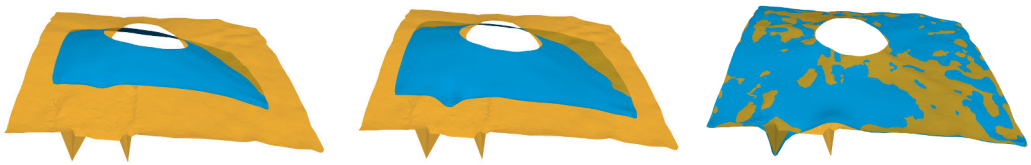

(a) $t = 0$ (b) $t = 0.5$ (c) $t = 1$

Figure 4.43: Shooting from the template to the subject 7 with normal cycles constant

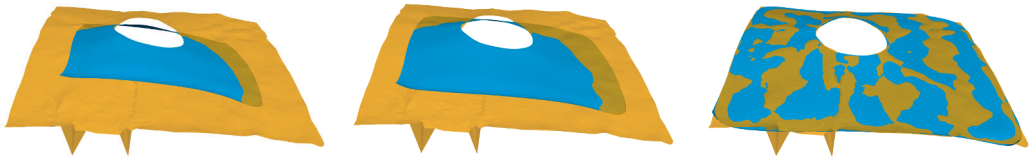

(a) $t = 0$ (b) $t = 0.5$ (c) $t = 1$

Figure 4.44: Shooting from the template to the subject 7 with varifolds

4.3 Conclusion

In this chapter, we have presented several examples of registrations and atlas estimations for curves and surfaces with different metrics on normal cycles and compared these results with the one obtained with varifolds. All these experiments draw a clear link between normal cycles and the curvature that is encoded depending on the metric. We have seen that the registration takes into account region of high curvatures as well as extremities, and that depending on the data, it allows for much smoother deformations. This is notably the case for retinas registrations and atlas estimation where the results are very convincing, including the borders. This is not the case with varifolds where an important amount of energy is spent on the corners for a result that is not physically relevant. However, this nice feature must be qualified: as we have seen again on the retina dataset, normal cycles are very sensitive to artefacts, and the slightest uncertainty on the data can have an important influence on the registration. This was an expected limitation since we cannot hope for a metric that is both sensitive to curvatures and extremities and insensitive to noise and artefacts.

An important future work that we have not made yet is a statistical analysis with the atlas estimation. In this chapter, we have provided atlas estimation for different dataset for a showcase purpose. However, it is of interest to provide a statistical analysis coupled with the atlas estimation for real dataset of shapes, and to compare this analysis to the one obtained with varifolds or currents. Doing so, we would see if the complexity of the normal cycles' model implies an improvement of the variability that is captured by the statistical analysis, and this would validate the introduction of this new model. Of course, this implies to find dataset for which the properties of registration seen in this chapter is interesting.

Conclusion

We present here an overview of the main contributions of the manuscript, as well as perspectives which would be interesting to investigate as a future work.

In this thesis, we focused on the design of a new dissimilarity metric between shapes, using kernel metrics on normal cycles. The aim was to provide a fully coherent framework that is also practicable in computational anatomy. The specifications for such a setting are multiple: a representation of shapes which encompasses both the continuous and the discrete case, with if possible a quantification of the information contained in the representation; the construction of a metric that is computable for discrete shapes and interpretable in a theoretical point of view.

Chapter 2 can be summed up with the following question: what are the properties of the representation of shapes with normal cycles? The contributions of this chapter are twofold. First of all, in section 2.4, we endeavour to show how to fit in a common framework normal cycles for smooth and discrete shapes. This is not immediate since normal cycles are defined at first for sets with positive reach. The additive property (2.15) allows to extend the definition to sets that are unions of sets with positive reach and an adapted decomposition of the normal bundle for meshes give an immediate description of the normal cycle for discrete shapes. Another contribution of this chapter is a precise overview of the curvature informations contained in a normal cycle in section 2.5. This part relies mostly on previous works [Federer, 1959, Zähle, 1987, Thäle, 2008], but we pushed further in this direction by introducing subspaces of differential forms, on which the infinity norm of a normal cycle is associated with unsigned curvatures.

To relate this work with previous ones, we can highlight section 2.6. We prove here that the varifold μ_X associated with a submanifold X can be interpreted as a projection of the normal cycle $N(X)$. If $N(X)$ encodes curvatures, we show that the projection loses all these informations and that a varifold is (in a sense that is specified in section 2.6) a "locally flattened" normal cycle. This is a first step to a unification of the different shapes representations (currents, varifolds and normal cycles) and it would be interesting as a future work to further investigate this link. We will come back to this consideration in the next paragraph.

The main contribution of Chapter 3 is the introduction of kernel metrics on normal cycles in section 3.3. These metrics allow for a dissimilarity measure between shapes that is both mathematically sound and numerically computable. The kernel

is chosen scalar and is a product of a spatial kernel k_p and a normal kernel k_n. If the choice of the spatial kernel is similar to what have been done for currents and varifolds, we had to choose the normal kernel. The main limitation for this choice was the requirement of an explicit discrete metric. Since the kernel metric involves integral over normal bundles, the computation may be intricate. For a simple constant kernel ($k_n(u,v) = 1$), we are able to provide explicit metric for discrete curves and surfaces, as well as their gradient. For the Sobolev kernel on the sphere or the linear kernel ($k_n(u,v) = \langle u, v\rangle$), which are more complex, we only have explicit metrics for discrete curves (section 3.7). Interestingly, even though the constant and the linear kernels may seem too simple at first, the associated metric on normal cycles still retrieve curvatures of the shapes. As it is shown in section 3.5, in the case of surfaces, the constant kernel encodes information linked with the mean curvature, and the linear kernel contains information linked to the Gaussian curvature. Thus, we do not get rid of all the curvatures with such kernels, and the complexification of the normal cycles model remains justified.

A promising avenue of research would be to link the metric on normal cycles and the projection of normal cycles on varifolds. To what extend do we retrieve usual metric on varifolds when projecting the metric on normal cycles? We can already observe that for the discrete part, the planar component of the scalar product on normal cycles can be interpreted as a varifold scalar product. It would be interesting to pursue this observation in the continuous case and maybe to explicit the obtained metric on varifold from the metric on normal cycles.

An application of this study could be close to the question of universality of the kernels that have been briefly tackled in section 3.4. We know that this property is not fulfilled with the constant or the linear normal kernel, resulting in a pseudo-distance on $\Omega_0^{d-1}(\mathbb{R}^d \times S^{d-1})'$ only. However, we do not want at any cost a real metric on $\Omega_0^{d-1}(\mathbb{R}^d \times S^{d-1})'$, but only that the distance on the normal cycles associated with shapes is a real distance, i.e. if $C \neq S$ are two shapes of $\mathbb{R}^d$, we want that $\|N(C) - N(S)\|_{W'} \neq 0$. This is a weaker result and we believe that it is true for constant and linear normal kernels. A way to prove this may be to make the most of the link between varifolds and normal cycles. Indeed it has been shown in [Charon and Trouvé, 2013], chapter 3, that kernel metrics on varifolds may provide metric on shapes, even when the property of universality is not fulfilled. It may be interesting to start with the metric on normal cycles with constant or linear normal kernel and study the projection of this metric to see if we retrieve a well known situation with varifolds.

In Chapter 4, we used this new dissimilarity measure for shapes registrations and atlas estimations. For the theoretical part, we proved the existence of a minimizer for the inexact registration problem with kernel metrics on normal cycles theorem 4.2 and theorem 4.10. For the applicative part, we implemented the evaluation of the kernel metric on normal cycles for curves and surfaces, as well as the gradient evaluation, and integrated it in the LDDMM numerical framework to provide first examples of registrations and atlas estimation (subsections 4.1.4, 4.1.5,

4.2.3 and 4.2.4). The complexity of the normal cycles model leads to an increasing calculation time for the computation of the metric. However, one should notice that the complexity remains within the same order, but more operations are needed at each step. Most of the computation time still comes from the LDDMM part (forward and backward integrations of the geodesic equations). To reduce the computation time, we parallelized the code, using GPU and mex files integrated on the Matlab body program. This allows for examples of registrations and atlas estimation with surfaces with up to 10 000 points in a reasonable time (for now, 30 minutes for a registration and 3 hours for a template estimation of 7 subjects).

We illustrated with numerous examples the properties of a registration with normal cycles. The first property that one can observe is that normal cycles provide more accurate matching, even when the size of the spatial kernel is large compared to the features to be matched. Moreover, the registration will favour the matching of corresponding high curvature regions. We can also highlight the fact that normal cycles take naturally into account the boundary of the shapes. This implies a good matching of the extremities or branching points for the curves, and a good matching of the boundary for surfaces. This implies also that normal cycles are sensitive to topological changes, as opposed to currents or varifolds. This may be a drawback if we have uncertainty on the data (for example a poor segmentation that creates artificial holes). However, we believe that this feature may be of interest on some data, as we showed for the retina dataset.

In subsection 4.2.4, we show first examples of atlas estimation. With the retina dataset figures 4.34 and 4.40, we see that normal cycles improve drastically the regularity of the deformations, as well as the accuracy of the matchings. And even though for an applicative purpose, the boundary of the retina are not relevant, we observe that varifolds provide a less regular deformation because a significant amount of energy is spent on the corners. We hope that this illustration may be a good indication for a future use on real medical data.

Of course, these are preliminary results. The estimated atlas had no other objective but to show the advantages and drawbacks of normal cycles. A first step after this thesis will be to perform a statistical analysis on the estimated atlas in the spirit of what have been done in [Charlier et al., 2015b, Lee et al., 2017a, Durrleman et al., 2014] among others. The idea is to use the Riemmanian framework provided by LDDMM, and to use statistical tools on the initial momenta of the deformations. These tools may be as simple as a Principal Component Analysis, to isolate the principal modes of the deformations, but they can be more complex (see again the previous references).

This manuscript paves the way for further applications of normal cycles. Among the future avenues of research we would like to highlight a few. First of all, an obvious future work is to develop the computation of the metric in the case of discrete surfaces for non constant k_n, at least for the linear normal kernel. This is of interest since we have already seen that the kernel metric with linear kernel encodes Gaussian curvature information of the surfaces. A normal kernel $k_n(u, v) =$

$1+\langle u, v\rangle$ would thus contains all the curvatures informations. However, the calculus remains intricate and this may lead to another approach: to find interesting compact approximation of the spherical part of a normal cycle. The approximations in the space of normal cycles are not as obvious as they are for currents or varifolds. Indeed, one of the requirements of an approximation of discrete shapes would be that it converges to a continuous version when the size of the mesh goes to zero. This is not the case for the spherical part of the normal cycles. For example, one could think of "spherical Dirac" to approximate the integration over the spherical part of the normal bundle. However, the spherical part above a vertex may remain unchanged when the size of the mesh goes to zero, preventing from any convergence result.

The question of approximation for the metric on normal cycles can be linked to the one of *jet particles* [Sommer et al., 2013, Jacobs and Sommer, 2014]. In these articles the authors develop (in the framework of LDDMM) compact higher order representations of the deformations. For example, they introduce first-order momenta whose geodesic equations involve the kernel of the RKHS V and its derivative, but also higher derivative. The interest of such representation is that it can encode locally affine transformation compared to zero-th order momenta that only contains local translations.

Usually, we do not encounter higher order momenta in registration algorithm because the approximation made on the data attachment term is at order 0: it depends only on the point of discretization x_k, and the action of diffeomorphisms is restricted to the vertices only. The order of approximation is conserved during the geodesic shooting, making the optimal momenta a linear combination of order 0 momenta. However, it is possible to use higher order approximation for the data attachment, involving $\varphi(x_k)$, but also $d\varphi(x_k)$ and $d^2\varphi(x_k)$. With such approximations, we naturally end up with higher order momenta. As we have seen in subsection 2.4.4, the action of a diffeomorphism φ on normal cycles involves φ, $d\varphi$ and $d^2\varphi$. Thus it seems natural to consider compact second order approximations of the metric on normal cycles. Such approximations would provide second order momentum distributions. The increasing complexity of this model could be counterbalanced by its higher order accuracy. This consideration definitely needs further investigation.

Another natural extension of the framework of normal cycles is the consideration of functional shapes. Functional shapes are geometrical data with a signal information as for example functional MRI. In [Charon and Trouvé, 2013, Charlier et al., 2015a], the authors introduce a framework for the shape representation of this new kind of data and apply it in [Lee et al., 2017b, Lee et al., 2017a] with retina where the signal is the thickness of the nerve fiber layer surface. The framework developed in these article relies on the representation of shapes with currents or varifolds. Since the theoretical ground is similar for normal cycles, one could almost straightforwardly transfer the geometrico-functional setting to normal cycles.

We have not tackled an interesting aspect of the metric on normal cycles: independently of the dimensionality of the considered shapes, the associated normal cycles live in the same space $\Omega_0^{d-1}(\mathbb{R}^d \times S^{d-1})'$. This could be used in application for the registration of mixed structures. One could think for example of surfaces with thin corner that become one dimensional. With normal cycles, this specific case is naturally taken into account.

It can also be applied for reconstruction of surfaces of curves from incomplete data. This problematic close to the one of volume reconstruction from slice (see for example [Bretin et al., 2017] where the authors set up a variational framework with a minimization of an energy associated with the volume to reconstruct an object from slices). In our case, one could imagine for example to start with points cloud, and to reconstruct the associated surface by matching an initial surface (a candidate guess) to the point clouds with the registration problem seen in Chapter 4. Of course, this depends critically on the choice of the normal kernel, and for now the constant normal kernel is not interesting on points cloud (in fact the associated metric vanishes). But once more complex kernels are available, this would be an interesting line of inquiry.

We believe also that kernel metrics on normal cycles can prove useful outside the LDDMM framework, in the spirit of [Cohen-Steiner and Morvan, 2003, Cohen-Steiner and Morvan, 2006, Chazal et al., 2008, Chazal et al., 2009], where the authors study the curvature information of a smooth surface that one could retrieve from a surface approximation using normal cycles. The advantage of our setting is that it provides a Hilbert space W' where all the representation of shapes lives, and it might be possible to obtain convergence rate of the approximation on W' and retrieve information on the curvatures convergence. Of course these are only guess for now, and we need to work further on this direction.

Lastly, and still outside the deformation analysis it would be interesting to use with benefit the cost of connection that appears with normal cycles. In fact, in the Hilbert space W', the cost of connection is quantified. Indeed, in W' difference between two segments unconnected but at distance 0 and the associated connected segment has a norm that is exactly the norm of a point. This property can be used as a detection of topology change and one could think of classification algorithms from the evaluations of distance inside a dataset of curves. Again, this first rough outline deserves a study on its own.

Appendix A

Kernel metrics on normal cycles for discrete shapes and different normal kernels

We derive here all the calculus for the kernel metrics in the case of discrete shapes (curves and surfaces in $\mathbb{R}^3$) with different normal kernel k_n: constant, linear and a scalar spatial kernel k_p. In all this appendix, we use the notations introduced in section 3.7.

A.1 Constant kernel

Let us start with the constant kernel, $k_n(u, v) = 1$.

A.1.1 Discrete curves

For C and S two unions of curves, we want to compute $\langle N(C), N(S)\rangle_{W'}$ where W is the RKHS generated with $k_n(u, v) = 1$.

$$\langle N(C), N(S)\rangle_{W'} = \left\langle N(C)^{cyl}, N(S)^{cyl}\right\rangle_{W'} + \left\langle N(C)^{sph}, N(S)^{sph}\right\rangle_{W'}$$

Using the expression of $\mathcal{K}_W N(C)$ obtained in (3.17) for the constant normal kernel, we immediately see that the scalar product between two discrete curves involves only spherical terms (indeed, $\mathcal{K}_W N(C) \in W_0^1$). This means that given the decomposition of the normal bundle for unions of segments (figure A.1), only the scalar spherical scalar product between spheres and half-spheres remains.

$$\begin{aligned}\langle N(C), N(S)\rangle_{W'} &= \left\langle N(C)^{sph}, N(S)^{sph}\right\rangle_{W'} \\ &= \sum_{i=1}^{N}\sum_{j=1}^{M}\Big\langle x_i \times \big(\text{sphere} - \sum \text{half sphere}\big), y_j \times \big(\text{sphere} - \sum \text{half sphere}\big)\Big\rangle_{W'}\end{aligned}$$

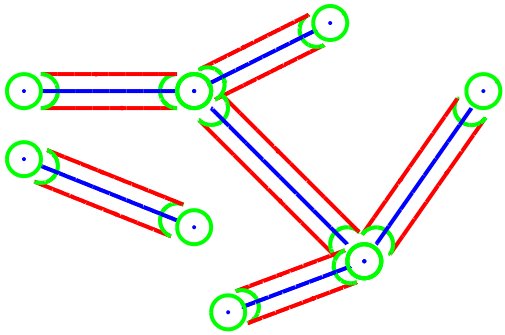

Figure A.1: Decomposition of the normal bundle of a union of segments. In green, the spherical part. For a given vertex, there is one associated sphere, and as many half spheres as the number of adjacent edges at this vertex.

(we recall that the half spheres are negatively oriented). The calculus with constant normal kernel are easy since it allows to decorrelate the integration over the spheres: if S_1 and S_2 are spheres or half spheres, with any spatial disposition, we have:

$$\begin{aligned}\langle x \times [S_1], y \times [S_2] \rangle_{W'} &= k_p(x,y) \int_{S_1} \int_{S_2} k_n(u,v) \, \langle \tau_{S_1}(u), \tau_{S_2}(v) \rangle \, d\mathscr{H}^2(u) d\mathscr{H}^2(v) \\ &= k_p(x,y) \int_{S_1} \int_{S_2} \langle u, v \rangle \, d\mathscr{H}^2(u) d\mathscr{H}^2(v) \\ &= k_p(x,y) \left\langle \int_{S_1} u d\mathscr{H}^2(u), \int_{S_2} v d\mathscr{H}^2(v) \right\rangle\end{aligned}$$

and one gets

$$\int_{S^2} u d\mathscr{H}^2(u) = 0, \int_{S^+_\alpha} u d\mathscr{H}^2(u) = \pi\alpha$$

where we recall that $S^+_\alpha = \left\{ u \in S^2 | \, \langle u, \alpha \rangle \geq 0 \right\}$ and $|\alpha| = 1$ is the half sphere spatially oriented with the vector α. Now we get for the scalar product of union of segments with constant normal kernel:

$$\langle N(C), N(S) \rangle_{W'} = \left\langle N(C)^{sph}, N(S)^{sph} \right\rangle_{W'} = \frac{\pi^2}{4} \sum_{i=1}^{N} \sum_{j=1}^{M} k_p(x_i, y_j) \, \langle A_i, B_j \rangle \quad \text{(A.1)}$$

where $A_i = \sum_k f^i_k / |f^i_k|$ is the sum of the normalized edges with x_i as vertex, and oriented outward from x_i. It encompasses the case of branching points with three or more edges with the same vertex x_i.

Gradient: The computation of the gradient with respect to a vertex x_{i_0} involves the gradient of the kernel $\nabla_1 k_p(x_{i_0}, y)$ and the gradient of the scalar product $\langle A_i, B_j \rangle$: $\nabla_{x_{i_0}} \langle A_i, B_j \rangle$. For the latter, if we consider $f_{ik} = x_k - x_i$ the edge linking the vertices k and i, one can compute explicitly $\nabla_{x_k} \langle f_{ik}/|f_{ik}|, B_j \rangle$:

$$\nabla_{x_k} \langle f_{ik}/|f_{ik}|, B_j \rangle = \frac{1}{|x_k - x_i|} p_{f_{ik}^\perp}(B_j)$$

where $p_{f_{ik}^\perp}$ is the orthogonal projection on f_{ik}, namely $p_{f_{ik}^\perp}(B_j) = B_j - \langle B_j, f_{ik}/|f_{ik}| \rangle \, f_{ik}/|f_{ik}|$. With these expressions, it is now possible to implement the computation of the gradient with respect to the vertices: for each vertex x_k, compute $\nabla_1 k_p(x_k, y_l)$ and $p_{f_{ik}^\perp}(B_j)$ for every edge f_{ik} that links x_k to another vertex.

A.1.2 Discrete surfaces

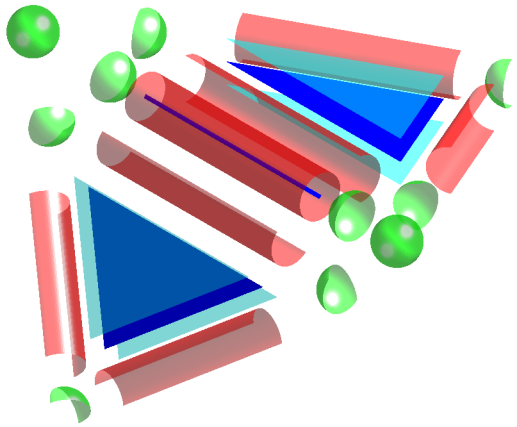

Figure A.2: Decomposition of the normal bundle for two triangles with a common edge. In this figure, the two normal bundle of the open triangles appear. Then, we add (only once) the normal bundle of the open edge (the red cylinder and the two green half spheres). Then we add (only once) the normal bundle of the vertices of the edge (the two green spheres).

For discrete surfaces, using (3.16) we see that above a regular part of the triangulation C, $\mathcal{K}_W N(C) \in W_1^2$ which means that $N(C)$ has a component in $(W_1^2)'$ only and thus that the planar part is not involved. The scalar product of normal cycles above vertices (i.e. the spherical scalar product) involves terms as:

$$\begin{aligned}
&k_p(x,y) \int_{S_1} \int_{S_2} k_n(u,v) \, \langle \tau_{\mathcal{N}_C}(x,u), \tau_{\mathcal{N}_C}(y,v) \rangle \, d\mathscr{H}^2(u) d\mathscr{H}^2(v) \\
&= k_p(x,y) \left\langle \int_{S_1} \underbrace{\tau_{\mathcal{N}_C}(x,u)}_{=u \text{ for the spherical part}} d\mathscr{H}^2(u), \int_{S_2} \tau_{\mathcal{N}_C}(y,v) d\mathscr{H}^2(v) \right\rangle \\
&= k_p(x,y) \left\langle \int_{S_1} u d\mathscr{H}^2(u), \int_{S_2} v d\mathscr{H}^2(v) \right\rangle
\end{aligned}$$

For the spherical part, we have already computed the scalar product with spheres and half spheres. If we focus on portion of sphere, one can show that if

$$S_1 = \left\{ \begin{pmatrix} s\theta_u c\varphi_u \\ s\theta_u s\varphi_u \\ c\theta_u \end{pmatrix} \middle| \theta_u \in [0,\pi],\ \varphi_u \in [0,\varphi_0] \right\}$$

is a portion of sphere, then $\int_{S_1} u d\mathscr{H}^2(u) = \pi \sin\left(\varphi_0/2\right) \begin{pmatrix} \cos(\varphi_0/2) \\ \sin(\varphi_0/2) \\ 0 \end{pmatrix}$. Now, taking into account the orientation, we have to compute for the spherical part:

$$\left\langle x \times \left([s.] - \sum [h.s] + \sum [p.s] \right), y \times \left([s.] - \sum [h.s] + \sum [p.s] \right) \right\rangle_{W'}$$

where s stands for sphere, $h.s$ for half sphere and $p.s$ for portion of spheres. In fact, one can show that for a given vertex, summing the contributions of the sphere, the half spheres (associated with the edges), and the portion of spheres (associated with the triangles), then the spherical part vanishes for a vertex that is not in the border. Moreover, we have the following equality:

$$\left\langle N(C)^{sph}, N(S)^{sph} \right\rangle_{W'} = \langle N(\partial C), N(\partial S) \rangle_{W'}$$

thus, the spherical part is exactly the scalar product of the curves associated with the border, scalar product that have been computed right above.

Now let us focus on the cylindrical part. As it has been said for discrete curves, the scalar product involving a cylinder is null, and thus, only the half cylinders remains. Consider thus the scalar product between two half cylinders. If we denote $HCyl_1 = [a,b] \times S^{\perp}_{b-a}$, $HCyl_2 = [c,d] \times S^{\perp}_{d-c}$ two half cylinders (where $S^{\perp +}_{b-a,\alpha} = \Big\{ u \in S^2 |\, \langle u, b-a \rangle = 0, \langle u, \alpha \rangle \geq 0 \Big\}$ is a half circle), we compute the scalar product in W' between these two half cylinders. With the approximations that we have made on normal cycles, the integration over the spatial part is replaced by a single evaluation of the spatial kernel k_p at the middle of the segment, and the integration over the spherical part is not approximated, this leads to:

$$\begin{aligned}
\langle HCyl_1, HCyl_2 \rangle_{W'} &= \int_{[a,b]} \int_{[c,d]} \int_{S^{\perp,+}_{b-a,\alpha}} \int_{S^{\perp}_{d-c,\beta},+} k_p(x,y) \left\langle \tau_{HCyl_1}(x,u), \tau_{HCyl_2}(y,v) \right\rangle d\mathscr{H}^2(x,u) s\mathscr{H}^2(y,v \\
&\simeq k_p\Big(\frac{a+b}{2}, \frac{c+d}{2}\Big) \langle b-a, d-c \rangle \\
&\times \int_{S^{\perp,+}_{b-a,\alpha}} \int_{S^{\perp}_{d-c,\beta},+} \left\langle \frac{b-a}{|b-a|} \times u, \frac{d-c}{|d-c|} \times v \right\rangle d\mathscr{H}^1(u) d\mathscr{H}^1(v) \\
&\simeq k_p\Big(\frac{a+b}{2}, \frac{c+d}{2}\Big) \langle b-a, d-c \rangle \\
&\times \left\langle \frac{b-a}{|b-a|} \times \int_{S^{\perp,+}_{b-a,\alpha}} u d\mathscr{H}^1(u), \frac{d-c}{|d-c|} \times \int_{S^{\perp}_{d-c,\beta},+} v d\mathscr{H}^1(v) \right\rangle \\
&\simeq \frac{\pi^2}{4} k_p\Big(\frac{a+b}{2}, \frac{c+d}{2}\Big) \langle b-a, d-c \rangle \left\langle \frac{b-a}{|b-a|} \times \alpha, \frac{d-c}{|d-c|} \times \beta \right\rangle
\end{aligned}$$

In a triangle T, $[a,b]$ corresponds to an edge and α corresponds to a unitary vector orthogonal to $[a,b]$, in the plane defined by the triangle and oriented in the interior of the triangle. Finally, if we consider two triangulations $\mathcal{T}$ and $\mathcal{T}'$, we have:

$$\begin{aligned}\langle N(\mathcal{T}), N(\mathcal{T}')\rangle_{W'} &= \left\langle N(\mathcal{T})^{cyl}, N(\mathcal{T}')^{cyl}\right\rangle_{W'} + \langle N(\partial\mathcal{T}), N(\partial\mathcal{T}')\rangle_{W'} \\ &= \frac{\pi^2}{4}\sum_{i=1}^{n_e}\sum_{j=1}^{m_e} k_p(c_i,d_j)\,\langle f_i, g_j\rangle \left\langle \sum_{\substack{T_i \text{ triangles}\\ \text{with edge } f_i}} n_{T_i,f_i}, \sum_{\substack{T'_j \text{ triangles}\\ \text{with edge } g_j}} n_{T'_j,g_j} \right\rangle \\ &\quad + \langle N(\partial\mathcal{T}), N(\partial\mathcal{T}')\rangle_{W'}\end{aligned} \tag{A.2}$$

where n_{T_i,f_i} is the normal vector of the triangle T_i such that $n_{T_i,f_i}\times f_i$ is oriented inward for the triangle T.

Gradient: The spherical part of the gradient has already been tackled for discrete curve. For the cylindrical part, we basically need to compute the gradient of terms that takes the form $k_p(c_i,d_j)\,\langle f_i,g_j\rangle\,\langle n_T, n_{T'}\rangle$.

$$\begin{aligned}\nabla_{x_k}\big(k_p(c_i,d_j)\,\langle f_i,g_j\rangle\,\langle n_T,n_{T'}\rangle\,\big) &= \nabla_{x_k}\big(k_p(c_i,d_j)\big)\,\langle f_i,g_j\rangle\,\langle n_T,n_{T'}\rangle \\ &\quad + k_p(c_i,d_j)\nabla_{x_k}\big(\,\langle f_i,g_j\rangle\,\big)\,\langle n_T,n_{T'}\rangle \\ &\quad + k_p(c_i,d_j)\,\langle f_i,g_j\rangle\,\nabla_{x_k}\big(\,\langle n_T,n_{T'}\rangle\,\big)\end{aligned}$$

Each term being easily computed. The only difficult part is $\nabla_{x_k}\big(\,\langle n_T,n_{T'}\rangle\,\big)$. For this, suppose that $n_T = \frac{(x_2-x_1)\times(x_3-x_2)}{|(x_2-x_1)\times(x_3-x_2)|}$ and that we want to compute $\nabla_1 n_T$. Using the fact that

$$d\big(u\mapsto\frac{u}{|u|}\big)(h) = \frac{1}{|u|}\big(h - \left\langle h, \frac{u}{|u|}\right\rangle\frac{u}{|u|}\big) = \frac{1}{|u|}p_{u^\perp}(h)$$

where $p_{u^\perp}$ is the orthogonal projection on $u^\perp$, then we have using chain rules for derivative:

$$\nabla_{x_1} n_T = -\frac{1}{|(x_2-x_1)\times(x_3-x_2)|}p_{n_T^\perp}(h\times(x_3-x_2)).$$

A.2 Linear kernel

In this section, we consider $k_n(u,v) = \langle u,v\rangle$.

A.2.1 Discrete curves

$$\langle N(C), N(S)\rangle_{W'} = \left\langle N(C)^{cyl}, N(S)^{cyl}\right\rangle_{W'} + \left\langle N(C)^{sph}, N(S)^{sph}\right\rangle_{W'}$$

Let start with the spherical part:

$$\begin{aligned}\langle x \times [S_1], y \times [S_2] \rangle_{W'} &= k_p(x,y) \int_{S_1} \int_{S_2} k_n(u,v) \langle \tau_{S_1}(u), \tau_{S_2}(v) \rangle \, d\mathscr{H}^2(u) d\mathscr{H}^2(v) \\ &= k_p(x,y) \int_{S_1} \int_{S_2} \langle u, v \rangle^2 \, d\mathscr{H}^2(u) d\mathscr{H}^2(v)\end{aligned}$$

Suppose that S_1 and S_2 are two half spheres. With the invariance to rotation, we can suppose that

$$S_1 = \left\{ \begin{pmatrix} s\theta_u c\varphi_u \\ s\theta_u s\varphi_u \\ c\theta_u \end{pmatrix} \middle| \theta_u \in [0,\pi], \varphi_u \in [0,\pi] \right\}, S_2 = \left\{ \begin{pmatrix} s\theta_v c\varphi_v \\ s\theta_v s\varphi_v \\ c\theta_v \end{pmatrix} \middle| \theta_v \in [0,\pi], \varphi_v \in [\varphi, \pi+\varphi] \right\}$$

The integration is thus explicit, and one can show that

$$\begin{aligned}\int_{S_1} \int_{S_2} \langle u, v \rangle^2 \, d\mathscr{H}^2(u) d\mathscr{H}^2(v) = \int_0^\pi \int_0^\pi \int_0^\pi \int_\varphi^{\varphi+\pi} &\left\langle \begin{pmatrix} s\theta_u c\varphi_u \\ s\theta_u s\varphi_u \\ c\theta_u \end{pmatrix}, \begin{pmatrix} s\theta_v c\varphi_v \\ s\theta_v s\varphi_v \\ c\theta_v \end{pmatrix} \right\rangle^2 \\ &\times \sin\theta_u \sin\theta_v d\varphi_u d\varphi_v d\theta_u d\theta_v \\ &= \frac{4\pi^2}{3}\end{aligned}$$

which is independent of any relative disposition of the half spheres. The same calculations leads to:

$$\int_{\text{sphere}} \int_{\text{sphere}} \langle u, v \rangle^2 \, d\mathscr{H}^2(u) d\mathscr{H}^2(v) = \frac{16\pi^2}{3}, \int_{\text{half-sphere}} \int_{\text{sphere}} \langle u, v \rangle^2 \, d\mathscr{H}^2(u) d\mathscr{H}^2(v) = \frac{8\pi^2}{3}$$

And thus we obtain for the spherical part, taking into account the positive orientation of the sphere and the negative orientation of the half spheres:

$$\left\langle N(C)^{sph}, N(S)^{sph} \right\rangle_{W'} = \frac{16\pi^2}{3} \sum_{k=1}^{N} \sum_{l=1}^{M} k_p(x_k, y_l) \left(1 - \frac{n_{x_k}}{2}\right) \left(1 - \frac{m_{y_l}}{2}\right)$$

Now, consider the cylindrical part. With the now usual approximations, we have:

$$\begin{aligned}\left\langle N(C)^{cyl}_{approx}, N(C)^{cyl}_{approx} \right\rangle_{W'} = &\sum_{i=1}^{n_e} \sum_{j=1}^{m_e} k_p(c_i, d_j) \langle f_i, g_j \rangle \\ &\times \int_{S^\perp_{f_i}} \int_{S^\perp_{g_j}} \langle u, v \rangle \langle u \wedge f_i/|f_i|, v \wedge g_j/|g_j| \rangle \, d\mathscr{H}^1(u) d\mathscr{H}^1(v).\end{aligned}$$

and again with rotational invariance, we can suppose that $f_i/|f_i| = (0,1,0)$ and $g_j/|g_j| = (-\sin\varphi_{ij}, \cos\varphi_{ij}, 0)$ where φ_{ij} is the angle between f_i and g_j. This means that

$$S_{f_i} = \left\{ \begin{pmatrix} s\theta_u c\varphi_u \\ s\theta_u s\varphi_u \\ c\theta_u \end{pmatrix} \middle| \theta_u \in [0,\pi], \varphi_u \in \{0,\pi\} \right\}, S_{g_j} = \left\{ \begin{pmatrix} s\theta_v c\varphi_v \\ s\theta_v s\varphi_v \\ c\theta_v \end{pmatrix} \middle| \theta_v \in [0,\pi], \varphi_v \in \{\varphi_{ij}, \pi+\varphi_{ij}\} \right\}$$

and thus we want to compute

$$\int_{S^\perp_{f_i}} \int_{S^\perp_{g_j}} \langle u, v \rangle \langle u \wedge f_i/|f_i|, v \wedge g_j/|g_j| \rangle \, d\mathscr{H}^1(u) d\mathscr{H}^1(v)$$

This last expression is explicit with the parametrization of $S^\perp_{f_i}$ and $S^\perp_{g_j}$, and one can show by developing

$$\int_{S^\perp_{f_i}} \int_{S^\perp_{g_j}} \langle u, v \rangle \langle u \wedge f_i/|f_i|, v \wedge g_j/|g_j| \rangle \, d\mathscr{H}^1(u) d\mathscr{H}^1(v) = \frac{\pi^2}{2} \cos \varphi_{ij}$$

and if we substitute this expression in the cylindrical scalar product, we get:

$$\begin{aligned} \left\langle N(C)^{cyl}_{approx}, N(C)^{cyl}_{approx} \right\rangle_{W'} &= \frac{\pi^2}{2} \sum_{i=1}^{n_e} \sum_{j=1}^{m_e} k_p(c_i, d_j) \langle f_i, g_j \rangle \cos \varphi_{ij} \\ &= \frac{\pi^2}{2} \sum_{i=1}^{n_e} \sum_{j=1}^{m_e} k_p(c_i, d_j) |f_i||g_j| \cos \varphi_{ij}^2 \end{aligned}$$

and for the total scalar product:

$$\begin{aligned} \langle N(C), N(S) \rangle_{W'} = &\frac{\pi^2}{2} \sum_{i=1}^{n_e} \sum_{j=1}^{m_e} k_p(c_i, s_j) |f_i||g_j| \cos^2 \varphi_{ij} \\ &+ \frac{16\pi^2}{3} \sum_{k=1}^{N} \sum_{l=1}^{M} k_p(x_k, y_l) \left(1 - \frac{n_{x_k}}{2}\right) \left(1 - \frac{m_{y_l}}{2}\right) \end{aligned}$$

where n_{x_k} (resp. m_{y_l}) is the number of segments with x_k as vertex (resp. y_l).

Gradient: The gradient of the spherical part is immediate since it depends only on $k_p(x_k, y_l)$. For the cylindrical part, the only non immediate part is the computation of $\nabla_{x_k} \cos \varphi_{ij}$. For this, we recall that $\cos \varphi_{ij} = \langle f_i/|f_i|, g_j/|g_j| \rangle$. If we suppose that $f_i = x_2 - x_1$ and compute $\nabla_{x_1} \cos \varphi_{ij}$, one gets again with the chain rules for derivative that has already been done in Appendix A.1.1:

$$\nabla_{x_1} \cos \varphi_{ij} = -\frac{1}{|x_2 - x_1|} p_{f_i^\perp}(g_j/|g_j|).$$

A.2.2 Discrete surfaces

With (3.19), only the spherical and planar part are involved. For the planar part, an immediate computation shows that the planar scalar product is exactly the one obtained with the varifold kernel metric with the linear kernel on Grassmanian, [Charon and Trouvé, 2013]:

$$\left\langle N(\tau)^{pln}, N(\tau')^{pln} \right\rangle_{W'} = 4 \sum_{i=1}^{N} \sum_{j=1}^{M} k_p(b_i, b'_j) \left|A_{T_i}\right| \left|A_{T'_j}\right| \left\langle n_{T_i}, n_{T_j} \right\rangle^2 .$$

However, the computation of the spherical part is more involved. The one involving spheres and half spheres have already been computed in Appendix A.2.1. Consider in full generality the scalar product between two portion of spheres S_1 and S_2, located at vertices x and y. Du to rotational invariance, we can suppose that

$$S_1 = \left\{ \begin{pmatrix} s\theta_u c\varphi_u \\ s\theta_u s\varphi_u \\ c\theta_u \end{pmatrix} \middle| \theta_u \in [0, \pi],\ \varphi_u \in [\varphi_0, \varphi_1] \right\}$$

$$\begin{aligned}
\langle x \times [S_1], y \times [S_2] \rangle_{W'} &= k_p(x,y) \int_{S_1} \int_{S_2} \langle u, v \rangle^2 \, d\mathscr{H}^2(u) d\mathscr{H}^2(v) \\
&= k_p(x,y) \int_{S_2} \int_{S_1} \left(s\theta_u s\theta_v c(\varphi_u - \varphi_v) + c\theta_u c\theta_v \right)^2 s\theta_u s\theta_v d\theta_u d\theta_v d\varphi_u d\varphi_v \\
&= k_p(x,y) \int_{S_1} \int_{S_2} \Big[s^3\theta_u s^3\theta_v c(\varphi_u - \varphi_v)^2 \\
&+ s\theta_u s\theta_v c^2\theta_u c^2\theta_v + 2 s^2\theta_u s^2\theta_v c\theta_u c\theta \\
&\times c(\varphi_u - \varphi_v) \Big] d\theta_u d\theta_v d\varphi_u d\varphi_v
\end{aligned}$$

Now we use the following equalities:

$$\int_0^\pi \sin^3\theta d\theta = 4/3, \quad \int_0^\pi \sin^2\theta \cos\theta d\theta = 0, \quad \int_0^\pi \sin\theta \cos^2\theta d\theta = 2/3,$$

and integrate first with respect to θ_u:

$$\begin{aligned}
\langle x \times [S_1], y \times [S_2] \rangle_{W'} &= 4/3 k_p(x,y) \int_{\varphi_0}^{\varphi_1+\varphi_0} \int_{S_2} s^3\theta_v c(\varphi_u - \varphi_v)^2 \\
&+ 2/3 k_p(x,y) \int_{\varphi_0}^{\varphi_1+\varphi_0} \int_{S_2} s\theta_v c^2\theta_v d\theta_u d\theta_v d\varphi_u d\varphi_v
\end{aligned}$$

then with respect to φ_u:

$$\begin{aligned}
\langle x \times [S_1], y \times [S_2] \rangle_{W'} &= 4/3 k_p(x,y) \int_{S_2} s^3\theta_v 1/4 \big[\sin(2(\varphi_1 + \varphi_0 - \varphi_v) - \sin(2(\varphi_0 - \varphi_v)) + \varphi_1 \big] d\theta_v d\varphi_v \\
&+ 2/3 k_p(x,y) \varphi_1 \int_{S_2} s\theta_v c^2\theta_v d\theta_u d\theta_v d\varphi_u d\varphi_v
\end{aligned}$$

Since $\sin(2(\varphi_1+\varphi_0-\varphi_v)-\sin(2(\varphi_0-\varphi_v)=2\sin\varphi_1\cos\big(2(\varphi_0-\varphi_v)+\varphi_1\big)$, we finally obtain:

$$\int_{S_1}\int_{S_2}\langle u,v\rangle^2\,d\mathscr{H}^2(u)d\mathscr{H}^2(v)=4/3\varphi_1\varphi_2+4/3\sin\varphi_1\int_{S_2}\sin^3(\theta_u)\cos\big(2(\varphi_v-\varphi_0-\varphi_1)\big)d\theta_v d\varphi_v.$$

One should notice that this situation encompasses the case of sphere and half sphere that has already been tackled for discrete curves. In this case, $\sin\varphi_1=0$ and we retrieve the product of the area of the considered spheres. For the second term, we cannot use any more assumptions on the position for S_2. For now, we are not able to compute this term, and we will consider a *truncated* version of this integral by neglecting this last term. Considering now two triangulated meshes $\mathcal{T}$ and $\mathcal{T}'$, we get:

$$\langle N(\mathcal{T})_{approx},N(\mathcal{T}')_{approx}\rangle_{W',trunc}=4\sum_{i=1}^{N}\sum_{j=1}^{M}k_p(b_i,b'_j)|\mathcal{A}_{T_i}||\mathcal{A}_{T'_j}|\left\langle n_{T_i},n_{T'_j}\right\rangle^2+\frac{1}{3}\sum_{k=1}^{N_v}\sum_{j=1}^{M_v}k_p(x_k,y_l)$$
$$\times\left[\pi(4-2n_{x_k}+2N_{x_k})-2\sum_{i=1}^{N_{x_k}}\varphi_{i,x_k}\right]\left[\pi(4-2m_{y_l}+2M_{y_l})-2\sum_{j=1}^{M_{y_l}}\varphi_{j,y_l}\right]$$

where n_{x_k} is the number of edges with vertex x_k and N_{x_k} is the number of triangles with vertex x_k, and φ_{i,x_k} is the angle at vertex x_k of the triangle i.

Gradient: We want to compute $\nabla_{x_k}\langle N(\mathcal{T})_{approx},N(\mathcal{T}')_{approx}\rangle_{W',trunc}$. This gradient involves quantities as $\nabla_1 k_p(x,y)$ that are easy to compute and implement. In the following we focus on the computation of $\nabla_{x_k}|\mathcal{A}_{T_i}||\mathcal{A}_{T'_j}|\left\langle n_{T_i},n_{T'_j}\right\rangle^2$ and $\nabla_{x_k}\varphi_{i,x_l}$. We can suppose that T has x_1,x_2,x_3 for vertices and that $n_T=\frac{(x_2-x_1)\times(x_3-x_2)}{|(x_2-x_1)\times(x_3-x_2)|}$. Noticing that $|\mathcal{A}_T|\langle n_T,n_{T'}\rangle^2=\left\langle\frac{(x_2-x_1)\times(x_3-x_2)}{\sqrt{|(x_2-x_1)\times(x_3-x_2)|}},n_{T'}\right\rangle^2$, we have

$$\nabla_{x_1}\left\langle\frac{(x_2-x_1)\times(x_3-x_2)}{\sqrt{|(x_2-x_1)\times(x_3-x_2)|}},n_{T'}\right\rangle^2=2\left\langle\frac{(x_2-x_1)\times(x_3-x_2)}{\sqrt{|(x_2-x_1)\times(x_3-x_2)|}},n_{T'}\right\rangle$$
$$\times\nabla_{x_1}\left(\left\langle\frac{(x_2-x_1)\times(x_3-x_2)}{\sqrt{|(x_2-x_1)\times(x_3-x_2)|}},n_{T'}\right\rangle\right)$$

Since

$$d\left(u\mapsto\frac{u}{\sqrt{|u|}}\right)(h)=\frac{1}{\sqrt{|u|}}\Big(h-\frac{1}{2}\left\langle\frac{u}{|u|},h\right\rangle\frac{u}{|u|}\Big)$$

then, using the chains rule for the derivative, we get:

$$\nabla_{x_1}\left\langle \frac{(x_2-x_1)\times(x_3-x_2)}{\sqrt{|(x_2-x_1)\times(x_3-x_2)|}}, n_{T'}\right\rangle = -\frac{1}{\sqrt{|(x_2-x_1)\times(x_3-x_2)|}} \times\left(n_{T'}\times(x_3-x_2)-\frac{1}{2}\langle n_{T'}\times(x_3-x_2), n_T\rangle\, n_T\right)$$

For $\nabla_{x_1}\varphi_{i,x_l}$, we consider the triangle T with vertices x_1, x_2, x_3 and $e_{12} = \frac{x_2-x_1}{|x_2-x_1|}$, $e_{13} = \frac{x_3-x_1}{|x_3-x_1|}$. We recall that $\varphi_{T,1} = \arccos\Big(\langle e_{12}, e_{13}\rangle\Big)$. Using the chains rule for derivative, we obtain:

$$\begin{aligned}\nabla_{x_2}\varphi_{T,1} &= \frac{-1}{\sqrt{1-\langle e_{12}, e_{13}\rangle^2}}\frac{1}{|x_2-x_1|}p_{e_{12}^\perp}(e_{13})\\ &= \frac{-1}{|\sin\varphi_{T,1}|}\sin\varphi_{T,1}\frac{e_{12}^\perp}{|x_2-x_1|}\\ &= \frac{-e_{12}^\perp}{|x_2-x_1|}\end{aligned}$$

where $e_{12}^\perp$ is the normalized orthogonal vector of e_{12} in the plane of the triangle such that $\langle e_{12}^\perp, e_{13}\rangle \geq 0$. With similar notations, we have

$$\nabla_{x_3}\varphi_{T,1} = \frac{-e_{13}^\perp}{|x_3-x_1|}$$

and since $\varphi_{T,1}+\varphi_{T,2}+\varphi_{T,3} = \pi$, $\nabla_{x_1}\varphi_{T,1} = -\nabla_{x_2}\varphi_{T,1} - \nabla_{x_3}\varphi_{T,1}$.

This gives all the necessary quantities to implement the gradient $\nabla_{x_k}\langle N(\mathcal{T})_{approx}, N(\mathcal{T}')_{approx}\rangle_{W',trunc}$.

A.3 Sobolev kernel

The computation of the metric on normal cycles for discrete curves and Sobolev normal kernel is postponed to the next two appendices.

Appendix B

Spherical Harmonics

The sphericals harmonics are eigenvectors of the spherical Laplacian. In the same spirit as Fourier expansion, spherical harmonics are useful to expand a function on the sphere since they form an orthonormal basis of the Hilbert space $L^2(S^2)$. This basis encodes spatial frequencies on the latitude and the longitude : the first spherical harmonics describe low spatial variation on the sphere, and the more we expand a function on this basis, the more details about the spatial frequencies of this function we get.

Spherical harmonics will be useful in this paper to explicit the normal kernel : since the RKHS we chose on the sphere is a Sobolev Hilbert space, it can be expressed as the RKHS defined by an operator $L_V = (\mathrm{Id} - \Delta)^s$, and the normal kernel will have an explicit expansion.

A scalar function on the unit sphere can be seen as a function of two variables θ, φ, where $\theta \in [0, \pi]$ is the polar angle and $\varphi \in [0, 2\pi]$ the azimuthal angle (see B.1)

There are $2l + 1$ spherical harmonics of order l, denoted $(Y_{l,m})_{-l \leq m \leq l}$ and satisfying the equations

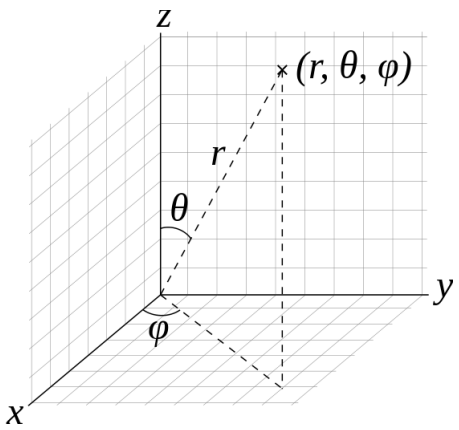

Figure B.1: Spherical coordinates, $\varphi \in [0, 2\pi]$ and $\theta \in [0, \pi]$

$$\begin{cases} -\Delta_{S^2} Y_{l,m}(\theta,\varphi) = l(l+1) Y_{l,m}(\theta,\varphi) \\ -\dfrac{\partial Y_{l,m}}{\partial \varphi} = m Y_{l,m}(\theta,\varphi) \end{cases} \tag{B.1}$$

The $(Y_{l,m})_{\substack{l\geq 0 \\ -l\leq m\leq l}}$ form an orthonormal basis of $L^2(S^2)$, endowed with its usual scalar product. Thus, any $f \in L^2(S^2)$ can be written

$$f = \sum_{l\geq 0} \sum_{m=-l}^{l} \alpha_{l,m} Y_{l,m}$$

where the limit is in L^2. We have explicit expression of the spherical harmonics with the Legendre polynomials . We will rather use the real spherical harmonics :

$$\begin{cases} Y_{l0}(\theta,\varphi) = \sqrt{\dfrac{2l+1}{4\pi}} P_l(\cos\theta) \\ Y^c_{lm}(\theta,\varphi) = \sqrt{\dfrac{2l+1}{2\pi}\dfrac{(l-m)!}{(l+m)!}} P_l^m(\cos\theta)\cos(m\varphi) \\ Y^s_{lm}(\theta,\varphi) = \sqrt{\dfrac{2l+1}{2\pi}\dfrac{(l-m)!}{(l+m)!}} P_l^m(\cos\theta)\sin(m\varphi) \end{cases} \tag{B.2}$$

$$\begin{aligned} P_l(x) &= \frac{1}{2^l l!}\frac{d^l}{dx^l}(x^2-1)^l \\ &= \sum_{\frac{l}{2}\leq k\leq l} (-1)^{l-k} \frac{(2k-1)!!}{(l-k)!(2k-l)!2^{l-k}} x^{2k-l} \end{aligned}$$

and

$$\begin{aligned} P_l^m(x) &= (-1)^m (1-x^2)^{m/2} \frac{d^m}{dx^m} P_l(x) \\ &= (-1)^{l+m}(1-x^2)^{m/2} \sum_{\frac{m+l}{2}\leq k\leq l} (-1)^k \frac{(2k-1)!!}{(l-k)!(2k-(m+l))!2^{l-k}} x^{2k-(m+l)} \end{aligned}$$

with $(2n+1)!! = 1*3*\cdots*(2n+1)$ et $(2n)!! = 2*4*\cdots*2n$.

Appendix C

Annexes

C.1 Some Notations

$$a_{kl} := \int_0^\pi \sin^k\theta \cos^l\theta d\theta = \frac{l-1}{k+1} a_{k+2,l-2}$$

We get obviously with induction :

$$a_{kl} = \begin{cases} 0 & \text{if } l \text{ is odd} \\ \dfrac{2(k-1)!!(l-1)!!(k+l-1)!!}{(k+l)!} & \text{if } l \text{ is even and } k \text{ odd} \\ \dfrac{(l-1)!!(k-1)!!}{(k+l-1)!!} \dfrac{(k+l)!}{(k+l)!!^2}\pi & \text{if } k, l \text{ are even} \end{cases}$$

With these notations, we have :

$$\begin{aligned} D_{l,0,i,j} &= \sqrt{\frac{2l+1}{4\pi}} \int_0^\pi P_l(\cos\theta) \sin^i\theta \cos^j\theta d\theta \\ &= \sqrt{\frac{2l+1}{4\pi}} \sum_{l/2 \le k \le l} (-1)^{l-k} \frac{(2k-1)!!}{(l-k)!(2k-l)!2^{l-k}} a_{i,2k-l+j} \end{aligned}$$

et

$$\begin{aligned} D_{l,m,i,j} &= \sqrt{\frac{2l+1}{2\pi}\frac{(l-m)!}{(l+m)!}}\int_0^\pi P_{lm}(\cos\theta)\sin^i\theta\cos^j\theta d\theta \\ &= \sqrt{\frac{2l+1}{2\pi}\frac{(l-m)!}{(l+m)!}} \\ &\times \sum_{\frac{m+l}{2}\leq k\leq l}\frac{(-1)^{k+l+m}(2k-1)!!}{(l-k)!(2k-(m+l))!2^{l-k}}\int_0^\pi \sin^{m+i}\theta\cos^{2k-m-l+j}\theta d\theta \\ &= \sqrt{\frac{2l+1}{2\pi}\frac{(l-m)!}{(l+m)!}}\sum_{\frac{m+l}{2}\leq k\leq l}\frac{(-1)^{k+l+m}(2k-1)!!}{(l-k)!(2k-(m+l))!2^{l-k}}a_{m+i,2k-m-l+j} \end{aligned} \tag{C.1}$$

C.2 Computing the scalar product between cylindrical parts 3.24

We compute here the approximate scalar product between the cylindrical parts of two segments, C_1 and S_1. $C_1 = [c_0, c_1]$ and $S_1 = [s_0, s_1]$. We use the same notations as in 2.4.3 If we denote $\alpha = \frac{c_1-c_0}{\|c_1-c_0\|}$ and $\beta = \frac{s_1-s_0}{\|s_1-s_0\|}$ (notice that for every $x \in C_1$, $y \in S_1$, $\tau_{C_1}(x) = \alpha$ and $\tau_{S_1}(y) = \beta$) we have :

$$\left\langle N(C_1)^{cyl}_{approx}, N(S_1)^{cyl}_{approx}\right\rangle_{W'} = \left\langle \delta_{\frac{c_0+c_1}{2},\alpha^\perp}, \delta_{\frac{s_0+s_1}{2},\beta^\perp}\right\rangle_{W'}$$

and we can sum up the scalar product :

$$\begin{aligned} \left\langle N(C_1)^{cyl}_{approx}, N(S_1)^{cyl}_{approx}\right\rangle &= \left\{k_p\left(\frac{c_0+c_1}{2}, \frac{s_0+s_1}{2}\right)\langle c_1-c_0, s_1-s_0\rangle\right\} \\ &\times \left\{\int_{S^\perp_\alpha}\int_{S^\perp_\beta} k_n(u,v)\left\langle \tau_{S^\perp_\alpha}(u), \tau_{S^\perp_\beta}(v)\right\rangle d\mathcal{H}^1(u)d\mathcal{H}^1(v)\right\} \end{aligned} \tag{C.2}$$

The first factor necessitate only the evaluation of the point kernel at the middle of the segments. The second factor is more involved : we will use the expansion on spherical harmonics of the normal kernel developed in **??**.

A first and very important remark is the future use of the invariance of the normal kernel under a rotation. This means that, if $u, v \in S^2$, $k_n(u,v)$ depends *only* of the relative position of u and v. And by invariance of the kernel, we can suppose that $\alpha = (1,0,0)$ and $\beta = (\cos\varphi, \sin\varphi, 0)$ where $\varphi \in [0,\pi]$ is the unoriented angle between α and β (the notations were defined in B.1). We will now formulate the integral with the parametrization of the sphere (φ, θ). One should be cautious that the tangent vector $\tau_C(x)$ should have a coherent orientation with α and u, i.e. $\tau_{S^\perp_\alpha}(u) = -\alpha\wedge u$, with $u = \begin{pmatrix}\sin\theta_u\cos\varphi_u\\ \sin\theta_u\sin\varphi_u\\ \cos\theta_u\end{pmatrix}$, et $\tau_{S^\perp_\beta}(v) = -\beta\wedge v$, avec $\beta = \begin{pmatrix}\cos\varphi_v\\ \sin\varphi_v\\ 0\end{pmatrix}$.

u should describe all $S_\alpha^\perp$, which means $\varphi_u = \pm\frac{\pi}{2}$, $\theta_u \in [0,\pi]$ and v should describe all $S_\beta^\perp$, which means $\varphi_v = \pm\frac{\pi}{2} + \varphi$, $\theta_v \in [0,\pi]$. Then, we get

$$\left\langle N(C_1)^{cyl}_{approx}, N(S_1)^{cyl}_{approx} \right\rangle_{W'} = k_p\left(\frac{c_0+c_1}{2}, \frac{s_0+s_1}{2}\right)\langle c_1 - c_0, s_1 - s_0\rangle$$
$$\sum_{\varphi_u = \pm\frac{\pi}{2}} \sum_{\substack{\varphi_v \\ = \varphi \pm \frac{\pi}{2}}} \int_0^\pi \int_0^\pi k_n(u,v)(\cos\varphi\cos\theta_v\cos\theta_u + \sin\theta_u\sin\varphi_u\sin\theta_v\sin(\varphi_v - \varphi))d\theta_u d\theta_v \tag{C.3}$$

Developing k_n in spherical harmonics and regrouping the terms gets :

$$\begin{aligned}\left\langle N(C_1)^{cyl}_{approx}, N(S_1)^{cyl}_{approx} \right\rangle_{W'} = k_p\left(\frac{c_0+c_1}{2}, \frac{s_0+s_1}{2}\right)\langle c_1 - c_0, s_1 - s_0\rangle \sum_{\varphi_u = \pm\frac{\pi}{2}} \sum_{\substack{\varphi_v \\ = \varphi \pm \frac{\pi}{2}}} \\ \sum_{l\geq 0}\frac{1}{\lambda_l}\left\{\int_0^\pi Y_{l0}(x)\cos\theta_u d\theta_u \int_0^\pi Y_{l0}(y)\cos\theta_v d\theta_v \cos\varphi\right. \\ + \int_0^\pi Y_{l0}(x)\sin\theta_u d\theta_u \int_0^\pi Y_{l0}(y)\sin\theta_v d\theta_v \sin\varphi_u \sin(\varphi_v - \varphi) \\ + \sum_{m=1}^{l}\int_0^\pi Y^c_{lm}(x)\cos\theta_u d\theta_u \int_0^\pi Y^c_{lm}(y)\cos\theta_v d\theta_v \cos\varphi \\ + \int_0^\pi Y^c_{lm}(x)\sin\theta_u d\theta_u \int_0^\pi Y^c_{lm}(y)\sin\theta_v d\theta_v \sin\varphi_u \sin(\varphi_v - \varphi) \\ + \sum_{m=1}^{l}\int_0^\pi Y^s_{lm}(x)\cos\theta_u d\theta_u \int_0^\pi Y^s_{lm}(y)\cos\theta_v d\theta_v \cos\varphi \\ \left. + \int_0^\pi Y^s_{lm}(x)\sin\theta_u d\theta_u \int_0^\pi Y^s_{lm}(y)\sin\theta_v d\theta_v \sin\varphi_u \sin(\varphi_v - \varphi)\right\}\end{aligned}$$

Using the notations of C.1, we get :

$$\begin{aligned}\left\langle N(C_1)^{cyl}_{approx}, N(S_1)^{cyl}_{approx} \right\rangle_{W'} = k_p\left(\frac{c_0+c_1}{2}, \frac{s_0+s_1}{2}\right)\langle c_1 - c_0, s_1 - s_0\rangle \sum_{\varphi_u = \pm\frac{\pi}{2}} \sum_{\substack{\varphi_v \\ = \varphi \pm \frac{\pi}{2}}} \\ \sum_{l\geq 0}\frac{1}{\lambda_l}\left\{D^2_{l,0,0,1}\cos\varphi + D^2_{l,0,1,0}\sin\varphi_u\sin(\varphi_v - \varphi)\right. \\ + \sum_{m=1}^{l} D^2_{l,m,0,1}\cos\varphi\cos(m(\varphi_u - \varphi_v)) \\ \left. + \sum_{m=1}^{l} D^2_{l,m,1,0}\cos(m(\varphi_u - \varphi_v))\sin\varphi_u\sin(\varphi_v - \varphi)\right\}\end{aligned}$$

Since

$$\sum_{\varphi_u \in \{\pm\frac{\pi}{2}\}} \sum_{\varphi_v \in \{\varphi \pm \frac{\pi}{2}\}} \cos\varphi\cos(m(\varphi_u - \varphi_v)) = \begin{cases} 0 & \text{if } m \text{ odd} \\ 4\cos\varphi\cos(m\varphi) & \text{if } m \text{ even}\end{cases}$$

and

$$\sum_{\varphi_u \in \{\pm\frac{\pi}{2}\}} \sum_{\varphi_v \in \{\varphi \pm \frac{\pi}{2}\}} \sin\varphi_u \sin(\varphi_v - \varphi)\cos(m(\varphi_u - \varphi_v)) = \begin{cases} 0 & \text{if } m \text{ even} \\ 4\cos(m\varphi) & \text{if } m \text{ odd} \end{cases}$$

We gather the terms and get

$$\begin{aligned} \left\langle N(C_1)^{cyl}_{approx}, N(S_1)^{cyl}_{approx} \right\rangle_{W'} = k_p &\left(\frac{c_0 + c_1}{2}, \frac{s_0 + s_1}{2} \right) \langle c_1 - c_0, s_1 - s_0 \rangle \\ &\times \sum_{l \geq 0} \frac{1}{\lambda_l} \{ (4D^2_{l,0,0,1} + 2D^2_{l,2,0,1} + 4D^2_{l,1,1,0}) \cos\varphi \\ &+ \sum_{\substack{m=3 \\ m \text{ odd}}}^{l} \left[4D^2_{l,m,1,0} + 2D^2_{l,m-1,0,1} + 2D^2_{l,m+1,0,1} \right] \cos(m\varphi) \} \end{aligned}$$

Interverting the summation symbols, we obtain

$$\begin{aligned} \left\langle N(C_1)^{cyl}_{approx}, N(S_1)^{cyl}_{approx} \right\rangle_{W'} = k_p &\left(\frac{c_0 + c_1}{2}, \frac{s_0 + s_1}{2} \right) \\ &\times \langle c_1 - c_0, s_1 - s_0 \rangle \sum_{m \geq 0} a_m \cos(m\varphi) \end{aligned} \tag{C.4}$$

with

$$\begin{cases} a_1 = \sum_{l \geq 0} \frac{1}{\lambda_l} (4D^2_{l,0,0,1} + 2D^2_{l,2,0,1} + 4D^2_{l,1,1,0}) \\ a_{2m-1} = \sum_{l \geq 2m-1} \frac{1}{\lambda_l} (4D^2_{l,2m-1,1,0} + 2D^2_{l,2m-2,0,1} + 2D^2_{l,2m,0,1}) \\ a_{2m} = 0 \end{cases}$$

C.3 Computing the scalar product between the spherical parts

This computation is somehow similar to the previous one. However, one should be cautious at the different terms involved in the computation. As seen in **??**, there are different objects in the spherical scalar product : the half sphere, associated with the extremities of the segments, and the sphere, associated with the vertices. Thus the scalar product involves cross term. We begin with the scalar product between two spheres, i.e. the normal cycles associated with isolated vertices a and b. One should be cautious when parametrizing the integral, as the volume element on the sphere is non trivial.

$$\begin{aligned} \langle N(\{a\}), N(\{b\}) \rangle_{W'} =& k_p(a,b) \int_0^{2\pi} \int_0^{\pi} \\ &\left\{ \int_0^{2\pi} \int_0^{\pi} k_n(u,v)(\sin\theta_u \sin\theta_v \cos(\varphi_u - \varphi_v) + \cos\theta_u \cos\theta_v) \sin\theta_v d\varphi_v d\theta_v \right\} \sin\theta_u d\varphi_u d\theta_u \end{aligned}$$

With an expansion on spherical harmonics of k_n :

$$\begin{aligned}
\langle N(\{a\}), N(\{b\})\rangle_{W'} = k_p(a,b)\int_0^{2\pi}\int_0^{\pi}\Bigg\{\int_0^{2\pi}\int_0^{\pi}\sum_{l\geq 0}\frac{1}{\lambda_l}\big(Y_{l0}(x)Y_{l0}(y) \\
+\sum_{m=1}^{l} Y^c_{lm}(x)Y^c_{lm}(y)+Y^s_{lm}(x)Y^s_{lm}(y)\big) \\
\times\big(\sin\theta_u\sin\theta_v\cos(\varphi_u-\varphi_v)+\cos\theta_u\cos\theta_v\big)\sin\theta_v d\theta_v d\varphi_v\Bigg\}\sin\theta_u d\theta_u d\varphi_u \\
= k_p(a,b)\sum_{l\geq 0}\frac{1}{\lambda_l}\big(4\pi^2 D^2_{l,0,1,1} \\
+\int_0^{2\pi}\int_0^{\pi} Y^c_{l,1}(x)\sin^2\theta_u d\theta_u\int_0^{2\pi}\int_0^{\pi} Y^c_{l,1}(y)\sin^2\theta_v\cos(\varphi_u-\varphi_v)d\varphi_u d\theta_v d\varphi_v \\
+\underbrace{\int_0^{2\pi}\int_0^{\pi} Y^c_{l,1}(x)\sin\theta_u\cos\theta_u d\theta_u\int_0^{2\pi}\int_0^{\pi} Y^c_{l,1}(y)\sin\theta_v\cos\theta_v d\varphi_u d\theta_v d\varphi_v}_{=0} \\
+\int_0^{2\pi}\int_0^{\pi} Y^s_{l,1}(x)\sin^2\theta_u d\theta_u\int_0^{2\pi}\int_0^{\pi} Y^s_{l,1}(y)\sin^2\theta_v\cos(\varphi_u-\varphi_v)d\varphi_u d\theta_v d\varphi_v \\
+\underbrace{\int_0^{2\pi}\int_0^{\pi} Y^s_{l,1}(x)\sin\theta_u\cos\theta_u d\theta_u\int_0^{2\pi}\int_0^{\pi} Y^s_{l,1}(y)\sin\theta_v\cos\theta_v d\varphi_u d\theta_v d\varphi_v}_{=0}\big)
\end{aligned}$$

The integral of the variables φ_u et φ_v cancels all the other terms:

$$\int_0^{2\pi}\int_0^{2\pi}\cos(m\varphi_u)\cos(m\varphi_v)\cos(\varphi_u-\varphi_v)d\varphi_u d\varphi_v = 0,\ \ \forall m\geq 2$$

and for $m=1$,

$$\begin{aligned}
&\int_0^{2\pi}\int_0^{2\pi}\cos(\varphi_u)\cos(\varphi_v)\cos(\varphi_u-\varphi_v)d\varphi_u d\varphi_v = \pi\int_0^{2\pi}\cos^2\varphi_v d\varphi_v = \pi^2\\
&=\int_0^{2\pi}\int_0^{2\pi}\sin(\varphi_u)\sin(\varphi_v)\cos(\varphi_u-\varphi_v)d\varphi_u d\varphi_v
\end{aligned}$$

With the same calculus as in C.2 we get :

$$\langle N(\{a\}), N(\{b\})\rangle_{W'} = k_p(a,b)\sum_{l\geq 0}\frac{1}{\lambda_l}\big(4\pi^2 D^2_{l,0,1,1}+2\pi^2 D^2_{l,1,2,0}\big) \tag{C.5}$$

The scalar product between a half-sphere S^+_α at point a, and a sphere follows the exact same calculus and we get :

$$\big\langle[\{a\}\times S^+_\alpha], N(\{b\})\big\rangle_{W'} = k_p(a,b)\sum_{l\geq 0}\frac{\pi}{\lambda_l}\big(2\pi D^2_{l,0,1,1}+\pi D^2_{l,1,2,0}\big) \tag{C.6}$$

For the scalar product between two half spheres, S_α^+ and S_β^+ at point a and b :

$$\left\langle [\{a\} \times S_\alpha^+], [\{b\} \times S_\beta^+] \right\rangle_{W'} = k_p(a,b) I(\alpha,\beta)$$

where

$$I(\alpha,\beta) = \int_0^\pi \int_{-\frac{\pi}{2}}^{\frac{\pi}{2}} \Big\{ \int_0^\pi \int_{\varphi-\frac{\pi}{2}}^{\varphi+\frac{\pi}{2}} k_n(u,v)(\sin\theta_u \sin\theta_v \cos(\varphi_u - \varphi_v) + \cos\theta_u \cos\theta_v) \sin\theta_v d\varphi_v d\theta_v \Big\} \sin\theta_u d\varphi_u d\theta_u$$

Again, with an expansion on spherical harmonics :

$$I(\alpha,\beta) = \sum_{l\geq 0} \frac{1}{\lambda_l} \int_{-\frac{\pi}{2}}^{\frac{\pi}{2}} \int_0^\pi \int_{\varphi-\frac{\pi}{2}}^{\varphi+\frac{\pi}{2}} \int_0^\pi \Big(Y_{l0}(x) Y_{l0}(y) + \sum_{m=1}^{l} Y_{lm}(x) Y_{lm}(y) \Big) [\sin\theta_u \sin\theta_v \cos(\varphi_u - \varphi_v) + \cos\theta_u \cos\theta_v] \sin\theta_v \sin\theta_u d\theta_v d\varphi_v d\theta_u d\varphi_u$$

Integration on θ_u and θ_v gets (with notations of C.1) :

$$I(\alpha,\beta) = \sum_{l\geq 0} \frac{1}{\lambda_l} \Bigg\{ D_{l,0,2,0}^2 \underbrace{\int_{\frac{-\pi}{2}}^{\frac{\pi}{2}} \int_{\varphi-\frac{\pi}{2}}^{\varphi+\frac{\pi}{2}} \cos(\varphi_u - \varphi_v) d\varphi_v d\varphi_u}_{=4\cos\varphi} + \pi^2 D_{l,0,1,1}^2$$
$$+ \sum_{m=1}^{l} D_{l,m,1,1}^2 \int_{-\frac{\pi}{2}}^{\frac{\pi}{2}} \int_{\varphi-\frac{\pi}{2}}^{\varphi+\frac{\pi}{2}} \big(\cos(m\varphi_u)\cos(m\varphi_v) + \sin(m\varphi_u)\sin(m\varphi_v) \big) d\varphi_v d\varphi_u$$
$$+ \sum_{m=1}^{l} D_{l,m,2,0}^2 \int_{-\frac{\pi}{2}}^{\frac{\pi}{2}} \int_{\varphi-\frac{\pi}{2}}^{\varphi+\frac{\pi}{2}} \big(\cos(m\varphi_u)\cos(m\varphi_v) + \sin(m\varphi_u)\sin(m\varphi_v) \big) \cos(\varphi_u - \varphi_v) d\varphi_v d\varphi_u \Bigg\}$$

$$I(\alpha,\beta) = \sum_{l\geq 0} \frac{1}{\lambda_l} \Bigg\{ 4D_{l,0,2,0}^2 \cos\varphi + \pi^2 D_{l,0,1,1}^2 + \frac{\pi^2}{2} D_{l,1,2,0}^2 + \sum_{\substack{m=1 \\ m \text{ odd}}}^{l} \frac{4D_{l,m,1,1}^2}{m^2} \cos(m\varphi)$$
$$+ \sum_{\substack{m=1 \\ m \text{ even}}}^{l} D_{l,m,2,0}^2 \left[\frac{2}{(m-1)^2} \cos((m-1)\varphi) + \frac{2}{(m+1)^2} \cos((m+1)\varphi) \right] \Bigg\}$$

We can write :

$$I(\alpha,\beta) = \sum_{l\geq 0} \frac{1}{\lambda_l} \sum_{m=0}^{l} a_{l,m} \cos(m\varphi)$$
$$= \sum_{m\geq 0} \left(\sum_{l\geq m} a_{l,m} \right) \cos(m\varphi)$$

So

$$\left\langle [\{a\} \times S_\alpha^+], [\{b\} \times S_\beta^+] \right\rangle_{W'} = k_p(a,b) \sum_{m \geq 0} b_m \cos(m\varphi) \tag{C.7}$$

where $b_m = \sum_{l \geq m} a_{l,m}$ with

$$\begin{cases} b_0 = \displaystyle\sum_{l \geq 0} \frac{\pi^2 D^2_{l,0,1,1}}{\lambda_l} + \sum_{l \geq 1} \frac{\pi^2}{2\lambda_l} D^2_{l,1,2,0} \\ b_1 = \displaystyle\sum_{l \geq 0} \frac{4D^2_{l+1,1,1,1}}{\lambda_{l+1}} + \frac{4D^2_{l,0,2,0}}{\lambda_l} + \frac{2D^2_{l+2,2,2,0}}{\lambda_{l+2}} \\ b_m = \displaystyle\frac{1}{m^2} \sum_{l \geq m} \frac{4D^2_{l,m,1,1}}{\lambda_l} + \frac{2D^2_{l-1,m-1,2,0}}{\lambda_{l-1}} + \frac{2D^2_{l+1,m+1,2,0}}{\lambda_{l+1}} \quad \text{if } m \text{ odd }, m > 1 \\ b_m = 0 \quad \text{if } m \text{ even }, m > 0 \end{cases}$$

C.4 Computing the Gradient of the Norm Associated with a Kernel Metric on Normal Cycles

Here, we compute in the discrete case the gradient of the cylindrical part of the kernel metric on normal cycles.

$$\begin{aligned} A^{cyl}(C_1, C_2) &:= \left\| N(C_1)^{cyl} - N(C_2)^{cyl} \right\|^2 \\ &= \left\| N(C_1)^{cyl} \right\|^2 + \left\| N(C_2)^{cyl} \right\|^2 - 2 \left\langle N(C_1)^{cyl}, N(C_2)^{cyl} \right\rangle \end{aligned}$$

If we keep the same notations as in the previous appendixes, with

$$\theta_{ij} = \arccos\left(\left\langle \frac{f_i}{|f_i|}, \frac{f_j}{|f_j|} \right\rangle \right)$$

, we have (by composing the differentiation) :

$$\partial_{x_k} A^{cyl} = \sum_{i=1}^{n} \partial_{p_i} A^{cyl} \circ \partial_{x_k} p_i + \partial_{x_{f_i^1}} A^{cyl} \circ \partial_{x_k} x_{f_i^1} + \partial_{x_{f_i^2}} A^{cyl} \circ \partial_{x_k} x_{f_i^2}$$

with

$$\begin{aligned} \partial_{p_i} A^{cyl} = &\sum_{j=1}^{n} (\partial_1 k_p(p_i, p_j) + \partial_2 k_p(p_j, p_i)) \langle f_i, f_j \rangle \sum_{m \geq 0} a_m \cos(m\theta_{ij}) \\ &- 2 \sum_{j=1}^{m} \partial_1 k_p(p_i, q_j) \langle f_i, g_j \rangle \sum_{m \geq 0} a_m \cos(m\varphi_{ij}) \end{aligned}$$

$$\partial_{f_i^2} A^{cyl} = 2\left(\sum_{j=1}^{n} k_p(p_i,p_j)\sum_{m\geq 0} a_m\cos(m\theta_{ij})f_j - \sum_{j=1}^{m} k_p(p_i,q_j)\sum_{m\geq 0} a_m\cos(m\varphi_{ij})g_j\right)$$
$$+ 2\left(\sum_{j=1}^{n} k_p(p_i,p_j)\langle f_i,f_j\rangle \sum_{m\geq 0}\delta_{i\neq j}\frac{m\sin(m\theta_{ij})}{|\sin(\theta_{ij})|}\frac{1}{|f_j|}\left(\frac{f_j}{|f_i|} - \left\langle\frac{f_i}{|f_i|},\frac{f_j}{|f_i|}\right\rangle\frac{f_i}{|f_i|}\right)\right.$$
$$\left. - \sum_{j=1}^{m} k_p(p_i,q_j)\langle f_i,g_j\rangle\sum_{m\geq 0} a_m\frac{m\sin(m\varphi_{ij})}{|\sin(\varphi_{ij})|}\frac{1}{|g_j|}\left(\frac{g_j}{|f_i|} - \left\langle\frac{f_i}{|f_i|},\frac{g_j}{|f_i|}\right\rangle\frac{f_i}{|f_i|}\right)\right)$$

here, we use :

$$\begin{aligned}\partial_{f_i^2}\cos(m\varphi_{ij}) &= \frac{m\sin(m\varphi_{ij})}{|\sin(\varphi_{ij})|}\nabla_{f_i^2}\left\langle\frac{f_i}{|f_i|},\frac{g_j}{|g_j|}\right\rangle\\ &= \frac{m\sin(m\varphi_{ij})}{|\sin(\varphi_{ij})|}\frac{1}{|f_i|}\left(\frac{g_j}{|g_j|} - \left\langle\frac{f_i}{|f_i|},\frac{g_j}{|g_j|}\right\rangle\frac{f_i}{|f_i|}\right)\\ &= \frac{m\sin(m\varphi_{ij})}{|\sin(\varphi_{ij})|}\frac{1}{|f_i|}p_{f_i^\perp}\frac{g_j}{|g_j|}\end{aligned}$$

with $p_{f_i^\perp}$ is the orthogonal projection on $f_i^\perp$, and

$$\begin{cases}\partial_{x_k} p_i = \dfrac{1}{2}\left(\delta_{\{k=f_i^1\}} + \delta_{\{k=f_i^2\}}\right)\mathrm{Id}\\ \partial_{x_k} x_{f_i^1} = \delta_{\{k=f_i^1\}}\mathrm{Id}\end{cases}$$

Then, we get for the gradient of A^{cyl} :

$$\begin{aligned}\nabla A^{cyl}((x_k)_{1\leq k\leq N}) = \Bigg[&\sum_{i=1}^{n}\left(\sum_{j=1}^{n}(\nabla_1 k_p(p_i,p_j) + \nabla_2 k_p(p_j,p_i))\langle f_i,f_j\rangle\sum_{m\geq 0}\alpha_m\cos(m\theta_{ij})\right.\\ &\left. -2\sum_{j=1}^{m}\nabla_1 k_p(p_i,q_j)\langle f_i,g_j\rangle\sum_{m\geq 0}a_m\cos(m\varphi_{ij})\right)\frac{1}{2}(\delta_{\{k=f_i^1\}} + \delta_{\{k=f_i^2\}})\\ &+ 2\sum_{i=1}^{n}\left(\sum_{j=1}^{n}k_p(p_i,p_j)\sum_{m\geq 0}a_m\cos(m\theta_{ij})f_j - \sum_{j=1}^{m}k_p(p_i,q_j)\sum_{m\geq 0}a_m\cos(m\varphi_{ij})g_j\right)\\ &\times(\delta_{\{k=f_i^2\}} - \delta_{\{k=f_i^1\}})\\ &+ 2\sum_{i=1}^{n}\left(\sum_{j=1}^{n}k_p(p_i,p_j)\langle f_i,f_j\rangle\sum_{m\geq 0}\delta_{i\neq j}a_m\frac{m\sin(m\theta_{ij})}{|\sin(\theta_{ij})|}\frac{1}{|f_i|}p_{f_i^\perp}\frac{f_j}{|f_j|}\right.\\ &\left. - \sum_{j=1}^{m}k_p(p_i,q_j)\langle f_i,g_j\rangle\sum_{m\geq 0}a_m\frac{m\sin(m\varphi_{ij})}{|\sin(\varphi_{ij})|}\frac{1}{|f_i|}p_{f_i^\perp}\frac{g_j}{|g_j|}\right)\\ &\times(\delta_{\{k=f_i^2\}} - \delta_{\{k=f_i^1\}})\Bigg]_{1\leq k\leq N}\end{aligned}$$

One can check that $\nabla A^{cyl}((x_k)_{1\leq k\leq N}) \in (\mathbb{R}^3)^N$

With the same type of calculus, that we do not detail here, we get also the gradient for the spherical part :

$$
\begin{aligned}
\nabla A^{sph}((x_k)_{1\leq k\leq N}) = \Bigg(& \sum_{l=1}^{N} (\nabla_1 k_p(x_k, x_l) + \nabla_2 k_p(x_l, x_k)) \Bigg[\left(1 - \frac{n_{x_k} + n_{x_l}}{2}\right) K \\
& + \sum_{i=1}^{n}\sum_{j=1}^{m} (\delta_{\{k=f_i^1\}} - \delta_{\{k=f_i^2\}})(\delta_{\{l=f_j^1\}} - \delta_{\{l=f_j^2\}}) \sum_{m\geq 0} b_m \cos(m\theta_{ij}) \Bigg] \\
& - 2\sum_{l=1}^{M} \nabla_1 k_p(x_k, y_l) \Bigg[\left(1 - \frac{n_{x_k} + n_{y_l}}{2}\right) K \\
& + \sum_{i=1}^{n}\sum_{j=1}^{m} (\delta_{\{k=f_i^1\}} - \delta_{\{k=f_i^2\}})(\delta_{\{l=g_j^1\}} - \delta_{\{l=g_j^2\}}) \sum_{m\geq 0} b_m \cos(m\varphi_{ij}) \Bigg] \\
& + 2 \sum_{\substack{s \text{ vertex} \\ \text{linked to } k}} \sum_{l=1}^{N} k_p(x_s, x_l) \sum_{i=1}^{n}\sum_{j=1}^{m} (2\delta_{k=s} - 1)(\delta_{\{l=f_j^2\}} - \delta_{\{l=f_j^1\}})(\delta_{\{s=f_i^1\}} + \delta_{\{s=f_i^2\}}) \\
& \quad \times \sum_{m\geq 1} b_m \frac{m\sin(m\theta_{ij})}{|\sin(\theta_{ij})|} \frac{1}{|f_i|} p_{f_i^\perp} \frac{g_j}{|g_j|} \\
& - 2 \sum_{\substack{s \text{ vertex} \\ \text{linked to } k}} \sum_{l=1}^{M} k_p(x_s, y_l) \sum_{i=1}^{n}\sum_{j=1}^{m} (2\delta_{k=s} - 1)(\delta_{\{l=g_j^2\}} - \delta_{\{l=g_j^1\}})(\delta_{\{s=f_i^1\}} + \delta_{\{s=f_i^2\}}) \\
& \quad \times \sum_{m\geq 0} b_m \frac{m\sin(m\varphi_{ij})}{|\sin(\varphi_{ij})|} \frac{1}{|f_i|} p_{f_i^\perp} \frac{g_j}{|g_j|} \Bigg)_{1\leq k\leq N}
\end{aligned}
$$

Bibliography

[Allard, 1972] Allard, W. (1972). On the first variation of a varifold. *Annals of Mathematics*, 95(3). 19, 50, 61, 62, 63, 64

[Almgren, 1966] Almgren, F. (1966). *Plateau's Problem: An Invitation to Varifold Geometry*. Mathematical Library. 50

[Arguillère, 2014] Arguillère, S. (2014). *Géométrie sous-riemannienne en dimension infinie et applications à l'analyse mathématique des formes*. PhD thesis, Université Pierre et Marie Curie. 47

[Arguillère et al., 2015] Arguillère, S., Trélat, E., Trouvé, A., and Younès, L. (2015). Shape deformation analysis from the optimal control viewpoint. *Journal de Mathématiques Pures et Appliquées*, 104(1):139 – 178. 18, 28, 47, 140, 141

[Arnold, 1989] Arnold, V. I. (1989). Mathematical methods of classical mechanics. 39, 43

[Aronszajn, 1950] Aronszajn, N. (1950). Theory of reproducing kernels. *Transactions of the American Mathematical Society*, 68:337–404. 100, 103, 105, 113

[Arsigny et al., 2006a] Arsigny, V., Commowick, O., Pennec, X., and Ayache, N. (2006a). *A Log-Euclidean Framework for Statistics on Diffeomorphisms*, pages 924–931. Springer Berlin Heidelberg, Berlin, Heidelberg. 46

[Arsigny et al., 2006b] Arsigny, V., Fillard, P., Pennec, X., and Ayache, N. (2006b). Log-euclidean metrics for fast and simple calculus on diffusion tensors. *Magnetic Resonance in Medicine*, 56(2):411–421. 46

[Atkinson and Han, 2012] Atkinson, K. and Han, W. (2012). *Spherical Harmonics and Approximation on the Unit Sphere : an Introduction*. Springer. 113, 114

[Auzias et al., 2011] Auzias, G., Colliot, O., Glaunes, J. A., Perrot, M., Mangin, J. F., Trouve, A., and Baillet, S. (2011). Diffeomorphic brain registration under exhaustive sulcal constraints. *IEEE Transactions on Medical Imaging*, 30(6):1214–1227. 160

[Bauer et al., 2013] Bauer, M., Bruveris, M., and Michor, P. W. (2013). Overview of the Geometries of Shape Spaces and Diffeomorphism Groups. *ArXiv e-prints*. 37, 38, 41

[Bazen and Gerez, 2003] Bazen, A. M. and Gerez, S. H. (2003). Fingerprint matching by thin-plate spline modelling of elastic deformations. *Pattern Recognition*, 36(8):1859–1867. 39

[Beg et al., 2005] Beg, M. F., Miller, M. I., Trouvé, A., and Younes, L. (2005). Computing Large Deformation Metric Mappings via Geodesic Flows of Diffeomorphisms. *International Journal of Computer Vision*, 61(2):139–157. 19, 32, 40, 46

[Bernig, 2003] Bernig, A. (2003). On some aspects of curvature. 84

[Bookstein, 1989] Bookstein, F. L. (1989). Principal Warps: Thin-Plate Splines and the Decomposition of Deformations. *IEEE Transactions on Pattern Analysis and Machine Intelligence*, 11(6):567–585. 38

[Bretin et al., 2017] Bretin, E., Dayrens, F., and Masnou, S. (2017). Volume reconstruction from slices. 197

[Brézis, 2011] Brézis, H. (2011). *Functional analysis, Sobolev spaces and partial differential equations*. Universitext. Springer. 106, 108, 114, 117

[Bruveris and Vialard, 2014] Bruveris, M. and Vialard, F.-X. (2014). On Completeness of Groups of Diffeomorphisms. *ArXiv e-prints*. 41

[Buet, 2014] Buet, B. (2014). *Approximation de surfaces par des varifolds discrets : représentation, courbure, rectifiabilité.* PhD thesis, Université Claude Bernard Lyon 1. 62, 64

[Buet et al., 2015] Buet, B., Leonardi, G. P., and Masnou, S. (2015). *Discrete Varifolds: A Unified Framework for Discrete Approximations of Surfaces and Mean Curvature*, pages 513–524. Springer International Publishing, Cham. 92, 124

[Carmeli et al., 2008] Carmeli, C., De Vito, E., Toigo, A., and Umanitï¿½, V. (2008). Vector valued reproducing kernel Hilbert spaces and universality. *arXiv:0807.1659 [math]*. 112, 117

[Charlier et al., 2014] Charlier, B., Charon, N., and Trouvé, A. (2014). The fshape framework for the variability analysis of functional shapes. *preprint*.

[Charlier et al., 2015a] Charlier, B., Charon, N., and Trouvé, A. (2015a). The fshape framework for the variability analysis of functional shapes. *Foundations of Computational Mathematics*, pages 1–71. 17, 136, 165, 174, 178, 187, 196

[Charlier et al., 2015b] Charlier, B., Nardi, G., and Trouvé, A. (2015b). The matching problem between functional shapes via a BV-penalty term: a gamma-convergence result. *arXiv:1503.07685 [math]*. arXiv: 1503.07685. 29, 30, 124, 195

[Charon, 2013] Charon, N. (2013). *Analysis of geometric and functionnal shapes with extension of currents. Application to registration and atlas estimation.* PhD thesis, École Normale Supérieure de Cachan. 20, 21, 24, 29, 45, 50, 100, 111, 112, 142

[Charon and Trouvé, 2013] Charon, N. and Trouvé, A. (2013). The varifold representation of nonoriented shapes for diffeomorphic registration. *SIAM J. Imaging Sciences*, 6(4):2547–2580. 60, 61, 101, 111, 117, 174, 175, 178, 183, 187, 194, 196, 206

[Chazal et al., 2008] Chazal, F., Cohen-Steiner, D., Lieutier, A., and Thibert, B. (2008). Stability of curvature measures. *CoRR*, abs/0812.1390. 25, 197

[Chazal et al., 2009] Chazal, F., Cohen-Steiner, D., Lieutier, A., and Thibert, B. (2009). Stability of Curvature Measures. *Computer Graphics Forum*. 93, 197

[Christensen et al., 1996] Christensen, G. E., Rabbitt, R. D., and Miller, M. I. (1996). Deformable templates using large deformation kinematics. *IEEE Transactions on Image Processing*, 5(10):1435–1447. 17, 39

[Cohen-Steiner and Morvan, 2003] Cohen-Steiner, D. and Morvan, J.-M. (2003). Restricted Delaunay Triangulations And Normal Cycle. *SoCG'03*. 25, 72, 92, 93, 123, 124, 197

[Cohen-Steiner and Morvan, 2006] Cohen-Steiner, D. and Morvan, J.-M. (2006). Second fundamental measure of geometric sets and local approximation of curvatures. *J. Differential Geom.*, 74(3):363–394. 93, 197

[Csernansky et al., 2005] Csernansky, J., Wang, L., Swank, J., Miller, J., Gado, M., McKeel, D., Miller, M., and Morris, J. (2005). Preclinical detection of alzheimer's disease: hippocampal shape and volume predict dementia onset in the elderly. *NeuroImage*, 25(3):783 – 792. 17

[Csernansky et al., 2004] Csernansky, J. G., Wang, L., Joshi, S. C., Ratnanather, J. T., and Miller, M. I. (2004). Computational anatomy and neuropsychiatric disease: probabilistic assessment of variation and statistical inference of group difference, hemispheric asymmetry, and time-dependent change. *NeuroImage*, 23(Supplement 1):S56 – S68. Mathematics in Brain Imaging. 17

[Duchon, 1976] Duchon, J. (1976). Interpolation des fonctions de deux variables suivant le principe de la flexion des plaques minces. *Revue française d'automatique, informatique, recherche opérationnelle. Analyse numérique*, 10(R3):5–12. 38

[Duchon, 1977] Duchon, J. (1977). *Splines minimizing rotation-invariant seminorms in Sobolev spaces*, pages 85–100. Springer Berlin Heidelberg, Berlin, Heidelberg. 38

[Dupuis et al., 1998] Dupuis, P., Grenander, U., and Miller, M. I. (1998). Variational problems on flows of diffeomorphisms for image matching. *Quarterly of applied mathematics*, pages 587–600. 17, 39, 40

[Durrleman, 2010] Durrleman, S. (2010). *Statistical models of currents for measuring the variability of anatomical curves, surfaces and their evolution.* PhD thesis, Université Nice - Sophia Antipolis. 20, 45, 50, 100, 175

[Durrleman et al., 2013] Durrleman, S., Allassonnière, S., and Joshi, S. (2013). Sparse adaptive parameterization of variability in image ensembles. *International Journal of Computer Vision*, 101(1):161–183. 17, 29, 173

[Durrleman et al., 2011a] Durrleman, S., Fillard, P., Pennec, X., TrouvÃ©, A., and Ayache, N. (2011a). Registration, atlas estimation and variability analysis of

white matter fiber bundles modeled as currents. *NeuroImage*, 55(3):1073 – 1090. 17

[Durrleman et al., 2014] Durrleman, S., Prastawa, M., Charon, N., Korenberg, J. R., Joshi, S., Gerig, G., and Trouvé, A. (2014). Morphometry of anatomical shape complexes with dense deformations and sparse parameters. *NeuroImage*, 101:35–49. 17, 47, 173, 195

[Durrleman et al., 2011b] Durrleman, S., Prastawa, M., Gerig, G., and Joshi, S. (2011b). Optimal data-driven sparse parameterization of diffeomorphisms for population analysis. In *Information Processing in Medical Imaging*, pages 123–134. Springer. 173

[Federer, 1959] Federer, H. (1959). Curvature measures. *Trans. Amer. Maths. Soc.*, 93. 23, 50, 64, 66, 67, 84, 193

[Federer, 1969] Federer, H. (1969). *Geometric Measure Theory*. Springer. 20, 50, 54, 55, 56, 57, 70, 123

[Federer and Fleming, 1960] Federer, H. and Fleming, W. (1960). Normal and integral currents. *Annals of Mathematics*, 72:458–520. 19, 20, 50, 56

[Fleming, 1966] Fleming, W. (1966). Flat chains over a finite coefficient group. *Transactions of the American Mathematical Society*, 121:160–186. 57

[Fu, 1991] Fu, J. H. (1991). Convergence of curvatures in secant approximations. *Journal of Differentiel Geometry*, 37. 122

[Fu, 1994] Fu, J. H. (1994). Curvatures Measures of Subanalytic Sets. *American Journal of Mathemtics*, 116. 123

[Gallier, 2013] Gallier, J. (2013). *Notes on Spherical Harmonics and Linear Representations of Lie Groups*. 117

[Glaunès, 2005] Glaunès, J. (2005). *Transport par difféomorphismes de points, de mesures et de courants pour la comparaison de formes et l'anatomie numérique.* PhD thesis, Université Paris 13. 17, 20, 24, 25, 42, 45, 46, 50, 100, 101, 105, 109, 124, 138, 139

[Grenander and Miller, 1998] Grenander, U. and Miller, M. I. (1998). Computational anatomy: An emerging discipline. *Q. Appl. Math.*, LVI(4):617–694. 15, 17, 29, 32, 36

[Helm et al., 2006] Helm, P. A., Younes, L., Beg, M. F., Ennis, D. B., Leclercq, C., Faris, O. P., McVeigh, E., Kass, D., Miller, M. I., and Winslow, R. L. (2006). Evidence of structural remodeling in the dyssynchronous failing heart. *Circulation Research*, 98(1):125–132. 17

[Jacobs and Sommer, 2014] Jacobs, H. and Sommer, S. (2014). Higher-order spatial accuracy in diffeomorphic image registration. 1:447–484. 196

[Joshi and Miller, 2000] Joshi, S. C. and Miller, M. I. (2000). Landmark matching via large deformation diffeomorphisms. *IEEE Transactions on Image Processing*, 9(8):1357–1370. 19

[Kendall, 1984] Kendall, D. G. (1984). Shape manifolds, procrustean metrics, and complex projective spaces. *Bulletin of the London Mathematical Society*, 16(2):81–121. 34, 35

[Lee et al., 2017a] Lee, S., Charon, N., Charlier, B., Popuri, K., Lebed, E., Sarunic, M. V., Trouvé, A., and Beg, M. F. (2017a). Atlas-based shape analysis and classification of retinal optical coherence tomography images using the functional shape (fshape) framework. *Medical Image Analysis*, 35:570–581. 17, 171, 174, 187, 195, 196

[Lee et al., 2017b] Lee, S., Heisler, M. L., Popuri, K., Charon, N., Charlier, B., Trouvé, A., Mackenzie, P. J., Sarunic, M. V., and Beg, M. F. (2017b). Age and glaucoma-related characteristics in retinal nerve fiber layer and choroid: Localized morphometrics and visualization using functional shapes registration. *Frontiers in Neuroscience*, 11. 17, 29, 174, 196

[Liu and Nocedal, 1989] Liu, D. C. and Nocedal, J. (1989). On the limited memory BFGS method for large scale optimization. *Mathematical Programming*, 45(1-3):503–528. 141, 166, 177

[Ma et al., 2008] Ma, J., Miller, M. I., Trouvé, A., and Younes, L. (2008). Bayesian template estimation in computational anatomy. *NeuroImage*, 42(1):252–261. 136, 175

[Ma et al., 2010] Ma, J., Miller, M. I., and Younes, L. (2010). A bayesian generative model for surface template estimation. *Journal of Biomedical Imaging*, 2010:16. 136, 175

[Mansi et al., 2011] Mansi, T., Voigt, I., Leonardi, B., Pennec, X., Durrleman, S., Sermesant, M., Delingette, H., Taylor, A. M., Boudjemline, Y., Pongiglione, G., and Ayache, N. (2011). A statistical model for quantification and prediction of cardiac remodelling: Application to tetralogy of fallot. *IEEE Transactions on Medical Imaging*, 30(9):1605–1616. 17

[Meinguet, 1979] Meinguet, J. (1979). Multivariate interpolation at arbitrary points made simple. *Zeitschrift für angewandte Mathematik und Physik ZAMP*, 30(2):292–304. 38

[Meinguet, 1984] Meinguet, J. (1984). *Surface Spline Interpolation: Basic Theory and Computational Aspects*, pages 127–142. Springer Netherlands, Dordrecht. 38

[Mercer, 1909] Mercer, J. (1909). Functions of positive and negative type, and their connection with the theory of integral equations. *Philosophical Transactions of the Royal Society of London A: Mathematical, Physical and Engineering Sciences*, 209(441-458):415–446. 100

[Meyer et al., 2003] Meyer, M., Desbrun, M., Schröder, P., and Barr, A. H. (2003). *Discrete Differential-Geometry Operators for Triangulated 2-Manifolds*, pages 35–57. Springer Berlin Heidelberg, Berlin, Heidelberg. 92

[Micchelli et al., 2006] Micchelli, C. A., Xu, Y., and Zhang, H. (2006). Universal kernels. *Journal of Machine Learning Research*, 7:2651–2667. 117

[Micheli and Glaunès, 2014] Micheli, M. and Glaunès, J. A. (2014). Matrix-valued kernels for shape deformation analysis. *Geometry, Imaging and Computing*, 1(1):57–139. 42, 101, 102, 103, 105, 114

[Miller et al., 2006] Miller, M. I., Trouvé, A., and Younes, L. (2006). Geodesic Shooting for Computational Anatomy. *Journal of Mathematical Imaging and Vision*, 24(2):209–228. 32, 42, 46, 47, 140, 141

[Morvan, 2008] Morvan, J.-M. (2008). *generalized curvatures*. Springer. 25, 83, 84, 93, 123

[Pennec, 2006] Pennec, X. (2006). Intrinsic statistics on riemannian manifolds: Basic tools for geometric measurements. *Journal of Mathematical Imaging and Vision*, 25(1):127–154. 17, 18

[Petitjean, 2002] Petitjean, S. (2002). A survey of methods for recovering quadrics in triangle meshes. *ACM Comput. Surv.*, 34(2):211–262. 92

[Qiu et al., 2008] Qiu, A., Younes, L., Miller, M. I., and Csernansky, J. G. (2008). Parallel transport in diffeomorphisms distinguishes the time-dependent pattern of hippocampal surface deformation due to healthy aging and the dementia of the alzheimer's type. *NeuroImage*, 40(1):68 – 76. 17

[Rado, 1943] Rado, T. (1943). What is the area of a surface? *The American Mathematical Monthly*, 50(3):139–141. 122

[Rataj and Zähle, 2001] Rataj, J. and Zähle, M. (2001). Curvatures and currents for unions of sets with positive reach, ii. *Annals of Global Analysis and Geometry*, 20(1):1–21. 24, 73, 74

[Roussillon and Glaunès, 2016] Roussillon, P. and Glaunès, J. (2016). Kernel metrics on normal cycles and application to curve matching. *SIAM J. Imaging Sciences*, 9:1991–2038. 29

[Roussillon and Glaunès, 2017] Roussillon, P. and Glaunès, J. (2017). Surface matching using normal cycles. To appear in GSI'17: Geometric Science Information, 2017, Paris. 29

[Roussillon and Glaunès, 2015] Roussillon, P. and Glaunès, J. A. (2015). Kernel Metrics on Normal Cycles and Application to Curve Matching. In *MFCA 2015 : 5th MICCAI workshop on Mathematical Foundations of Computational Anatomy*, Munich, Germany. 29

[Sharon and Mumford, 2006] Sharon, E. and Mumford, D. (2006). 2d-shape analysis using conformal mapping. *International Journal of Computer Vision*, 70(1):55–75. 39

[Sommer et al., 2013] Sommer, S., Nielsen, M., Darkner, S., and Pennec, X. (2013). Higher-order momentum distributions and locally affine lddmm registration. *SIAM Journal on Imaging Sciences*, 6(1):341–367. 196

[Sprengel et al., 1996] Sprengel, R., Rohr, K., and Stiehl, H. (1996). Thin-plate spline approximation for image registration. In *Proceedings of the 18th Annual*

International Conference of the IEEE Engineering in Medicine and Biology Society, 1996. Bridging Disciplines for Biomedicine, volume 3, pages 1190–1191 vol.3. 39

[Steiner, 1840] Steiner, J. (1840). über parallele flächen. *Monatsbericht der Akademie der Wissenchaften zu Berlin*, pages 114–118. 23

[Tang et al., 2014] Tang, X., Holland, D., Dale, A. M., Younes, L., Miller, M. I., and for the Alzheimer's Disease Neuroimaging Initiative (2014). Shape abnormalities of subcortical and ventricular structures in mild cognitive impairment and alzheimer's disease: Detecting, quantifying, and predicting. *Human Brain Mapping*, 35(8):3701–3725. 17

[US Dept of the Interior Fish and Wildlife Service, 1953] US Dept of the Interior Fish and Wildlife Service (1953). Fishes of the gulf of maine. 142

[Thäle, 2008] Thäle, C. (2008). 50 years sets with positive reach, a survey. *Surveys in Mathematics and its Applications*, 3. 73, 74, 193

[Thirion, 1998] Thirion, J.-P. (1998). Image matching as a diffusion process: an analogy with maxwell's demons. *Medical image analysis*, 2(3):243–260. 39

[Thompson, 1917] Thompson, D. (1917). *On Growth and Forms*. ? 15, 29

[Trouvé, 1995] Trouvé, A. (1995). An infinite dimensional group approach for physics based models in patterns recognition. preprint. 17, 39, 40

[Trouvé, 1998] Trouvé, A. (1998). Diffeomorphisms groups and pattern matching in image analysis. *International Journal of Computer Vision*, 28(3):213–221. 17, 39

[Trouvé and Younes, 2011] Trouvé, A. and Younes, L. (2011). *Shape Spaces*, pages 1309–1362. Springer New York, New York, NY. 38

[Vaillant and Glaunès, 2005] Vaillant, M. and Glaunès, J. (2005). Surface Matching via Currents. In Christensen, G. E. and Sonka, M., editors, *Information Processing in Medical Imaging*, number 3565 in Lecture Notes in Computer Science, pages 381–392. Springer Berlin Heidelberg. 20, 24, 25, 109

[Vercauteren et al., 2009] Vercauteren, T., Pennec, X., Perchant, A., and Ayache, N. (2009). Diffeomorphic demons: Efficient non-parametric image registration. *NeuroImage*, 45(1):S61–S72. 39

[Wang et al., 2007] Wang, L., Beg, F., Ratnanather, T., Ceritoglu, C., Younes, L., Morris, J. C., Csernansky, J. G., and Miller, M. I. (2007). Large deformation diffeomorphism and momentum based hippocampal shape discrimination in dementia of the alzheimer type. *IEEE Transactions on Medical Imaging*, 26(4):462–470. 17

[Werther, 2003] Werther, T. (2003). *Optimal Interpolation in Semi-Hilbert Spaces*. PhD thesis, Institut für Mathematik der Universität Wien. 117

[Weyl, 1939] Weyl, H. (1939). On the volume of tubes. *Amer. J. Ma*, pages 461–472. 23

[Wintgen, 1982] Wintgen (1982). Normal cycle and integral curvature for polyhedra in Riemannian manifolds. *Differential Geometry*. 64

[Younès, 2010] Younès, L. (2010). *Shapes and Diffeomorphisms*. Springer. 17, 37, 40

[Zähle, 1986] Zähle, M. (1986). Integral and current representation of Federer's curvature measure. *Arch. Maths.*, 23:557–567. 24, 30, 50, 64, 65, 68, 69, 84

[Zähle, 1987] Zähle, M. (1987). Curvatures and currents for unions of set with positive reach. *Geometriae Dedicata*, 23:155–171. 24, 65, 73, 74, 84, 123, 193